POSTERIOR CORTICAL ATROPHY: A NEUROPSYCHOLOGICAL AND NEUROIMAGING STUDY.

SUBMITTED TO UNIVERSITY COLLEGE LONDON

FOR THE DEGREE OF

DOCTOR OF PHILOSOPHY

MANJA LEHMANN

INSTITUTE OF NEUROLOGY, UNIVERSITY COLLEGE LONDON

2011

DECLARATION STATEMENT

I, Manja Lehmann, confirm that the work presented in this thesis is my own. Where information has been derived from other sources, I confirm that this has been indicated in the thesis.

Manja Lehmann

ABSTRACT

This thesis investigates the neuroimaging and neuropsychological characteristics of Posterior Cortical Atrophy (PCA) which is most often caused by Alzheimer's disease (AD) pathology. Posterior cortical atrophy describes a predominantly posterior pattern of atrophy and cognitive deficits. PCA has been poorly characterized and is likely to have been under-recognized. Using magnetic resonance imaging (MRI), patterns of cortical thickness were assessed in patients with pathologically-confirmed AD and different clinical presentations during life (including amnestic, visual and behavioural phenotypes). In addition to atrophy in the medial temporal lobe, tissue loss in posterior regions is indicative of AD pathology. Since medial temporal lobe atrophy is not specific to AD, posterior atrophy may aid distinction between AD and other dementias. Using easily-applied visual rating scales for medial temporal and posterior atrophy in patients with pathologically-confirmed AD and frontotemporal lobar degeneration (FTLD), it was shown that posterior atrophy ratings improve classification accuracy of AD from FTLD and controls.

Cross-sectional and longitudinal image analysis techniques were used to characterize atrophy patterns in PCA compared with controls and typical amnestic AD. Whilst the cross-sectional analysis revealed differential patterns of tissue loss in these two groups, with PCA showing greatest atrophy in posterior parietal regions, and typical AD predominantly in medial temporal lobe regions, longitudinal results showed that at five years disease duration, both PCA and typical AD had global grey matter loss and cortical thinning compared with controls.

The nature of visual deficits in PCA was assessed by administering detailed neuropsychological tests. The behavioural data showed that visual deficits were not uniformly affected in PCA, with considerable heterogeneity of visual impairments shown. Cortical thickness measures were used to assess atrophy patterns in PCA patients with predominant space versus object perception impairments, revealing overlap in cortical thinning patterns between these two PCA subgroups.

In summary this thesis investigates the common and differential atrophy patterns of atypical AD presentations as well as the degree of heterogeneity of deficits which exist within the PCA presentation.

TABLE OF CONTENTS

TABLE OF FIGURES

APPENDIX FIGURES

TABLE OF TABLES

AIMS OF THIS THESIS

The Problem

Alzheimer's disease (AD) is one of the leading public health issues of our time. With ageing populations, the number of patients with degenerative dementias such as AD will rise dramatically, estimated to affect 81.1 million people worldwide by 2040. AD is characterized by specific pathological changes which are often accompanied by atrophy that can be measured non-invasively using a variety of structural imaging techniques. Structural imaging methods have become widely used tools which assist diagnosis. Whilst most AD patients present with memory complaints and atrophy mainly in the medial temporal lobes, a number of studies have demonstrated significant heterogeneity in the clinical presentations of AD. In addition to the typical amnestic presentation in AD, atypical non-amnestic phenotypes including early aphasic or behavioural variants have been highlighted. Other patients may present with visuospatial, visuoperceptual, praxis, calculation, and spelling difficulties which implicate early parietal and occipital lobe involvement. The posterior pattern of atrophy with which these presentations are associated has led to the term posterior cortical atrophy (PCA). Atypical variants of AD have until recently been under-recognized and have been poorly studied. Studying atypical variants of AD is crucial in order to identify the biological factors and processes that drive the heterogeneity of phenotypes in AD, and may lead to a better understanding of AD as whole.

Aims

1) To assess patterns of cortical thickness in patients with pathologically-confirmed AD who had typical and atypical clinical presentations during life, and in patients with Frontotemporal Lobar Degeneration (FTLD).

2) To develop a visual rating scale for posterior atrophy and assess its reliability and clinical utility in pathologically-confirmed AD and FTLD patients.

3) To assess cross-sectional and longitudinal patterns of cortical thickness and grey matter loss in well-characterized individuals with PCA, and compare these with typical, amnestic AD and healthy controls.

4) To investigate the nature of visual deficits in PCA. Specifically, the aim was to characterize basic visual processing deficits in PCA, and to assess associations of higher-order visual processing deficits with basic visual processing impairments.

5) To assess patterns of cortical thickness in PCA patients with predominant object and space perception deficits.

1.INTRODUCTION

1.1 Chapter introduction

Dementia is one of the leading public health issues of our time: it has a great effect on the quality of life for the patient and the caregivers and it places heavy demands on health care systems. The most common cause of dementia in people over the age of 65 years is Alzheimer's disease (AD) (Hebert et al., 2003). The greatest risk factor for dementia is advancing age, with the prevalence of developing AD increasing exponentially over the age of 65 years, affecting up to 20% of those over the age of 80 years (Jorm and Jolley, 1998). With ageing populations, the number of patients with degenerative dementias such as AD will rise dramatically, estimated to affect 81 million people worldwide by 2040 (Ferri et al., 2005).

Few causes of dementia are currently treatable. Whilst early diagnosis is important now for patients and families, in the future an early and accurate diagnosis may become crucial since a) new disease-modifying drugs are currently being developed, some of which are in phase III clinical trials, and b) potential therapeutic agents may have their greatest efficacy when administered in the early stages of the disease before extensive cognitive deficits develop. Furthermore, potential therapeutic drugs are likely to be pathology-specific, making accurate diagnoses essential to prevent those without the targeted pathology being given potentially harmful and unnecessary medications.

Structural neuroimaging techniques have become widely used tools which assist diagnosis through the exclusion of other treatable causes, the discrimination of neurodegeneration from normal ageing, and differentiating between degenerative diseases (e.g. Likeman et al., 2005). As such, structural imaging is included in diagnostic guidelines for both Europe (Hort et al., 2010; Waldemar et al., 2007) and the US (Knopman et al., 2001). Imaging has also been shown to predict conversion to dementia in individuals who are worried about their memory and cognition (for a review see Fennema-Notestine et al., 2009). Finally, serial neuroimaging can be used to track disease progression and may provide a good outcome measure for the efficacy of therapeutic drugs.

In recent years, a number of studies have demonstrated significant heterogeneity in the clinical presentations of AD. In addition to the typical amnestic presentation in AD, atypical non-amnestic phenotypes including early aphasic and visual problems have been highlighted. Increasing the clinical and scientific community's knowledge of these atypical variants is important in order to identify the biological factors which promote or protect against pathological changes in different brain regions. Furthermore, understanding atypical forms of AD and the factors driving the heterogeneity in AD may

lead to a better understanding of AD as a whole, and will improve the support, care and education that can be given to the patients, carers and healthcare professionals. This chapter describes the clinical, pathological, epidemiological, genetic and neuropsychological characteristics of the main dementias assessed in this thesis.

1.2 Dementia

Dementia can be defined as an acquired deficit involving multiple domains of cognitive function, including memory in the presence of normal consciousness, and sufficient to impact normal activities of daily living (Rossor, 1993). Whilst the most common pathological disease causing dementia is AD, other non-AD pathological processes have been identified, including frontotemporal lobar degeneration (FTLD), vascular dementia (VaD), dementia with Lewy Bodies (DLB), corticobasal degeneration (CBD), and Creutzfeld Jakob disease (CJD). Clinical distinction between these different diseases can often be problematic and some pathologies can be found together. This thesis focuses on AD and its atypical presentations as well as some diseases which are difficult to differentiate from AD.

1.2.1 Alzheimer's disease

1.2.1.1 Pathology

AD is characterized by two neuropathological hallmarks: extracellular deposits of amyloid (Aβ plaques) and intracellular neurofibrillary tangles (Braak and Braak, 1991). Progression of pathology has been described with neurofibrillary tangles first seen in the trans-entorhinal cortex and then in the hippocampus (Arnold et al., 1991; Braak and Braak, 1995). In contrast, amyloid deposition is first seen in the basal portions of the isocortex of temporal, parietal and occipital lobes, whereas the hippocampus remains relatively devoid of amyloid (Braak and Braak, 1991). In addition to these pathological protein deposits, AD pathology can exist alongside other pathologies including DLB and vascular disease (Jellinger and Attems, 2005; Jellinger and Attems, 2008). AD is characterized by a marked loss of neurons and synapses in many areas of the central nervous system, particularly in areas such as the basal forebrain and hippocampus. This neuronal loss is accompanied by gross atrophy: an example of atrophy in the medial temporal lobe typically found in AD is shown in Figure 1.1 (left).

1.2.1.2 Epidemiology and genetic risk factors

Whilst the vast majority of the AD population are elderly, there is a proportion of people who get AD earlier in life. Studies therefore often distinguish between early- and late-onset AD typically defined arbitrarily as age at onset before and after 65 years, respectively. Most research studies in AD focus on younger old persons (age <80 years). The association between AD pathology and dementia is stronger in younger old persons than in older old persons (Savva et al., 2009) suggesting that additional factors

may determine the clinical expression of dementia in the oldest old. These findings also suggest that it is important to take age into account when assessing the effects of interventional treatments against dementia.

A small proportion of the early-onset patients (0.5% according to www.molgen.ua.ac.be/ADMutations) carry an autosomal dominant mutation causing a predictable age of onset which is closely related to the ages of onset of other family members. These individuals are referred to as familial AD patients. Familial AD has been associated with mutations in the amyloid precursor protein (APP), presenilin 1 (PSEN1) and presenilin 2 (PSEN2) genes (Campion et al., 1999).

However, in the majority of AD patients the disease is sporadic. One of the most important genetic risk factors for developing sporadic AD is the presence of an apolipoprotein E (ApoE) ε4 allele (Okuizumi et al., 1994). The presence of a single ε4 allele increases the lifetime risk of AD by 2-4-fold relative to the more common ε3 allele (Meyer et al., 1998). Over recent years, evidence has suggested that the presence or absence of an ε4 allele may also influence the pattern of atrophy and the associated clinical phenotype in AD, with regions in the medial temporal lobe being more affected in ε4-carriers than non-carriers (Gutierrez-Galve et al., 2009; Hashimoto et al., 2001). This is in accordance with studies showing that the presence of ε4 is particularly associated with greater memory impairment (Marra et al., 2004; Snowden et al., 2007b). ApoE ε4 has also been shown to be associated with an earlier onset of disease and possibly a more aggressive disease course (Cosentino et al., 2008; Okuizumi et al., 1994; Saunders et al., 1993).

1.2.1.3 Clinical diagnostic criteria for sporadic AD

AD is most commonly characterized by an insidious onset of memory impairment which progresses to involve multiple cognitive domains (McKhann et al., 1984). This amnestic presentation is in accordance with histopathological evidence for early medial temporal lobe involvement described above. The NINCDS-ADRDA criteria (see Appendix 1) offer three categories of diagnostic certainty for AD: i) definite AD, which can only be established by post-mortem or biopsy examination; ii) probable AD, which is made upon fulfilment of a certain set of criteria established by clinical and neuropsychological examination, and iii) possible AD when there is an atypical onset, presentation or progression, without a known aetiology, and absence of co-morbid diseases capable of producing dementia (McKhann et al., 1984). Since the publication of the NINCDS-ADRDA criteria in 1984, a better understanding of the underlying disease processes in AD has led to efforts to develop more sophisticated criteria which take other biomarkers into account. Recently proposed research criteria move diagnosis of AD earlier in the disease course by removing the need for subjects to have impairments of multiple

cognitive domains and utilizing one or more biomarkers (Dubois et al., 2007). According to these criteria a diagnosis of AD can be made when a patient presents with memory impairment and has supportive evidence of one of the following: medial temporal lobe atrophy from structural imaging, reduced glucose metabolism in bilateral temporal parietal regions on positron emission tomography (PET), or markers of pathology including evidence of amyloid deposition using either PET imaging (Klunk et al., 2004) or reduced amyloid and increased tau levels obtained from a cerebrospinal fluid (CSF) sample (Dubois et al., 2007).

Whilst the majority of AD patients typically present with an amnestic presentation, 'atypical' forms of AD in which memory is not the primary deficit (Galton et al., 2000) have until recently been under-recognized and have been poorly studied. Some of these patients may present with marked behavioural features and are often referred to as 'frontal-variant AD' (Johnson et al., 1999; Taylor et al., 2008), whilst others have a predominantly language presentation which often has features of logopenic progressive aphasia (LPA) (Gorno-Tempini et al., 2008). Yet others may present with visuospatial, visuoperceptual, praxis, calculation, and spelling difficulties which implicate early parietal and occipital lobe involvement (Benson et al., 1988; Cogan, 1985; Ross et al., 1996). The posterior pattern of atrophy with which these presentations are associated has led to the term posterior cortical atrophy (PCA). An example of the posterior atrophy pattern in a patient with PCA is illustrated in Figure 1.1. Growing efforts to characterize the clinical manifestation of AD has led to the realization that focal, non-amnestic phenotypes of AD represent a much higher proportion of cases than previously recognized, and these atypical presentations will likely be included in new consensus criteria for AD that are currently being formulated (http://www.alz.org/research/diagnostic_criteria/overview.asp, see also Dubois et al., 2010).

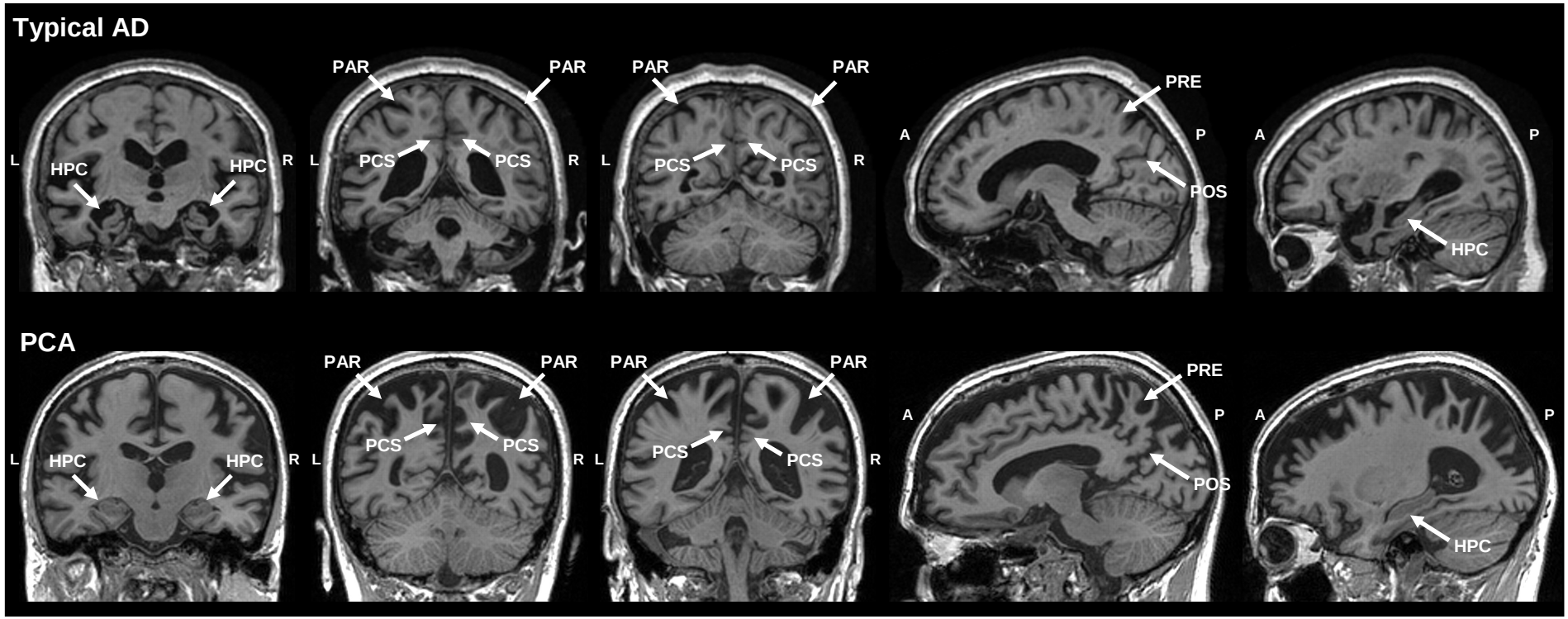

Figure 1.1: Patterns of atrophy in typical amnestic AD and PCA. Shown are structural MRI scans, coronal and sagittal views, of a typical, amnestic AD patient (top) showing prominent medial temporal lobe atrophy in the absence of prominent posterior atrophy, and a PCA patient (bottom) showing atrophy in posterior regions in the absence of marked medial temporal lobe atrophy. HPC - hippocampus, PAR - parietal lobe, PCS - posterior cingulate sulcus, PRE - precuneus, POS - parieto-occipital sulcus, L - left hemisphere, R - right hemisphere, A - anterior, P - posterior.

1.2.2 Posterior Cortical Atrophy (PCA)

1.2.2.1 Nosology

Individuals with PCA typically show a progressive and relatively selective decline in visual processing skills and other posterior functions. The term PCA was first introduced by Benson (1988) who reported five patients with predominant deficits in higher-order visual processing and neuronal loss in parieto-occipital areas (on computed tomography and magnetic resonance images, see section 2.2) (Benson et al., 1988). Other early studies have focussed mainly on the clinical and neuroimaging characteristics of PCA (Cogan, 1985; De Renzi, 1986). Subsequent histopathological studies identified AD as the most common underlying pathology which includes the presence of amyloid plaques and neurofibrillary tangles. PCA is therefore often considered a variant of AD and is also referred to as 'biparietal' or 'visual' variant AD (e.g. Bokde et al., 2001; Galton et al., 2000; Levine et al., 1993; Ross et al., 1996; Schott et al., 2006). However, PCA has been associated with other, non-AD pathologies, which has led to suggestions for PCA to be considered a distinct nosological entity with its own diagnostic criteria (Mendez et al., 2002; Tang-Wai and Mapstone, 2006). Other studies suggest that PCA should be considered as a point on a continuum of phenotypic variation in AD (Stopford et al., 2007).

Questions remain over whether PCA should be considered a unitary clinico-anatomical syndrome or rather a collection of related but distinct syndromic subtypes. Extrapolating from basic neuroscientific evidence of distinct cortical streams which process different types of visual information (Goodale and Milner, 1992; Ungerleider and Mishkin, 1982), it has been suggested that separate parietal (dorsal) and occipito-temporal (ventral) forms of PCA exist (Ross et al., 1996). A third, primary visual (striate cortex; caudal) form of PCA has also been proposed (Galton et al., 2000). However, these claims are largely based on findings from single case reports. The most detailed neuropsychological study of PCA to date found evidence of object perception deficits, faces and colours in a proportion of the patients tested, but overall the pattern of impairments was suggestive of greater impairment of the dorsal than ventral visual processing streams as no pure ventral stream syndrome was detected (McMonagle et al., 2006).

1.2.2.2 Epidemiology

The exact prevalence and incidence of PCA are currently unknown and any figure is likely to be an underestimate because of poor general knowledge of the syndrome's existence. However, in a study by Snowden et al. it was shown that 5% of 523 patients with AD presenting to a single specialist cognitive disorders centre had a visual presentation (also labelled posterior cortical atrophy) (Snowden et al., 2007b). Age at onset tends to be earlier in PCA (van der Flier et al., 2010), with studies reporting disease onsets in patients' mid 50s and early 60s (e.g. McMonagle et al., 2006; Mendez

et al., 2002) although a wide distribution has been described (40-86 years; Tang-Wai et al., 2004). In terms of gender distribution, some studies have reported no difference in the prevalence between the genders (e.g. McMonagle et al., 2006; Mendez et al., 2002; Renner et al., 2004), whereas others have reported an over-representation of women (e.g. Snowden et al., 2007b; Tang-Wai et al., 2004).

1.2.2.3 Genetics

Remarkably, to date, there have been no studies reporting an autosomal dominant inheritance pattern in PCA. Although 11 patients in a study by Tang-Wai et al. had a family history of dementia, none of those family members had a posterior cortical syndrome (Tang-Wai et al., 2004). Furthermore, there is no significant difference in the number of patients with a positive family history of dementia in PCA compared with typical AD (Mendez et al., 2002; Tang-Wai et al., 2004). Nonetheless there does seem to be an important modulating effect of genetic factors. Studies assessing ApoE in PCA have reported significant differences between the ApoE status of patients with posterior cortical presentations of AD and amnestic AD (see Table 1.1, Schott et al., 2006; Snowden et al., 2007b). Schott et al. described 20% of biparietal AD patients (PCA) were ApoE ε4-positive (which corresponds to an ε4-allele frequency of 10%), which was significantly lower compared with a typical AD group of who 86% were ε4-positive (ε4-allele frequency 52%). However, subject numbers were relatively small in this study (10 PCA). A larger study by Snowden et al. examined the relationship between cognitive profile and ApoE status in 302 patients with typical or atypical AD (Snowden et al., 2007b), and revealed that 30% of patients with a visual presentation were ε4-positive. This was significantly lower than the proportion of ε4 allele carriers in AD patients with an amnestic presentation (defined as severe memory impairments in absence of other cognitive dysfunctions, 82%) and patients with a memory/semantic presentation (defined as symptoms of memory loss and semantic memory impairment, 80%). Conversely, presence of the ε4 allele in the visual AD group did not differ to a population of 756 healthy individuals from the same region (27%, Pendleton et al., 2002). Since this study did not report the number of PCA and typical AD patients for whom ApoE data were available, ApoE ε4 allele frequencies cannot be determined at this stage.

Other studies, however, have reported no significant difference in ApoE between PCA and typical AD (Table 1.1, Mendez et al., 2002; Tang-Wai et al., 2004). Mendez et al. reported ε4 allele frequency of 25% in 8 PCA patients, with none of the patients having two ε4 alleles (50% were ε4-positive). These were compared with an AD cohort described in Saunders et al. who reported ApoE ε4 allele frequency of 40% in 176 autopsy-proven sporadic AD patients (Saunders et al., 1993). Tang-Wai et al. reported ε4 allele frequency of 26% in a group of 27 PCA patients (48% were ε4-positive). Only one patient was ε4-homozygous. These were compared with the ApoE ε4 prevalence of

AD patients described in Farrer et al., who reported an ε4 allele frequency of 37% (Caucasian AD patients, Farrer et al., 1997). Farrer et al. also report ε4 allele frequency of 14% for Caucasian control subjects. Discrepancies in the findings obtained in these studies may reflect differences in factors such as inclusion criteria used to define PCA and typical AD, and age at onset. Studies using larger sample sizes are required to obtain more conclusive results.

Table 1.1: Overview prevalence of ApoE ε4 in PCA, AD and controls. Shown are data from 4 studies that have reported ApoE ε4 frequency in PCA, and compared these with typical (or sporadic) AD and controls.

Study	PCA					AD					Controls		
	Total N	**Age at onset**	**N with ApoE**	**ε4 frequency**	**ε4 positive**	**N**	**Age at onset** [§]	**N with ApoE**	**ε4 frequency**	**ε4 positive**	**N**	**ε4 frequency**	**ε4 positive**
Tang-Wai et al. 2004	40	60.5 (8.9) [§]	27	26%	48%	5107 [†]	-	5107	37%	59%	6262 [†]	14%	26%
Mendez et al. 2002	15	58.2(5.1) [§]	8	25%	50%	176 [‡]	-	176	40%	-	-	-	-
Snowden et al. 2007 *	24	58.0 (4.0) [§]	-	-	30%	321	58.0 (4.0)	-	-	82% [¥]	767 [¶]	14%	27%
Schott et al. 2006 *	10	56.1 (4.1)	10	10%	20%	29	65.6 (6.9)	29	52%	86%	-	-	-

* reported significant difference in ApoE ε4 between PCA and AD

[†] Farrer et al. 1997

[‡] Saunders et al. 1993

[¶] Pendleton et al. 2002

[§] for whole PCA group, age at onset for subset of patients with ApoE unknown

[¥] amnestic AD; proportion ε4-positive in memory/semantic AD group = 80%

1.2.2.4 Pathology

Pathological studies have shown that AD is the most common underlying cause of PCA (Alladi et al., 2007; Galton et al., 2000; Hof et al., 1989; Hof et al., 1990; Renner et al., 2004; Tang-Wai et al., 2004). However, a small number of cases are attributable to other aetiologies such as CBD (Renner et al., 2004; Tang-Wai et al., 2003a), DLB (Renner et al., 2004; Tang-Wai et al., 2003b), prion disease (including CJD and familial fatal insomnia; Renner et al., 2004; Victoroff et al., 1994), and subcortical gliosis (Victoroff et al., 1994). These studies provide first insights into the prevalence of the different pathologies in PCA. For example, Renner et al. reported pathological data of 27 PCA patients of whom 13 (48%) had AD, 2 (7%) had CBD, 1 (4%) had DLB, 1 (4%) had CJD and 2 (7%) had prion disease (Renner et al., 2004). Tang-Wai et al. reported 7/9 (78%) PCA patients had AD pathology, whereas the remaining 2 (22%) had CBD (Tang-Wai et al., 2004).

Although the patterns of the distribution of pathology have been shown to be different in PCA compared with typical AD, the exact pattern of the pathological changes revealed by these studies is inconsistent and based on very small numbers of cases. Some studies have demonstrated differences in both plaques and neurofibrillary tangles between PCA and typical AD (Hof et al., 1997; Levine et al., 1993; Ross et al., 1996), whereas others have found no differences in the plaque distribution (Renner et al., 2004; Tang-Wai et al., 2004). For example, Levine et al. reported the pathological findings of 1 PCA patient who showed greatest density of senile plaques and neurofibrillary tangles in occipitoparietal regions, and lowest density in frontal lobe regions (Levine et al., 1993). Hof et al. reported similar findings with plaques and tangles found predominantly in primary visual and visual association areas around the occipito-parieto-temporal junction, whereas frontal regions such as the prefrontal cortex showed very low densities of pathological changes (Hof et al., 1993; Hof et al., 1997). In contrast, Tang-Wai et al. compared pathological changes in 9 PCA patients with 30 typical AD patients. The PCA group showed significantly higher density of neurofibrillary tangles in visual and visual association cortices and fewer tangles and senile plaques in the hippocampus and subiculum. However, density of senile plaques in other cortical areas was comparable in both groups (Tang-Wai et al., 2004). Reasons for the discrepant findings in these autopsy studies are unclear, however, differences in inclusion criteria and demographical characteristics (such as age and disease severity) as well as differences in the methods used to quantify the pathological changes (such as different staining techniques, and discrimination between diffuse and neuritic plaques) may have contributed. Studies assessing CSF biomarkers ($A\beta_{1-42}$, T-tau and P-tau_{181}) have reported similar concentrations in PCA compared with AD (Baumann et al., 2010; de Souza et al., 2011), supporting previous reports that PCA is often associated with underlying AD pathology.

1.2.2.5 Proposed diagnostic features

Two sets of diagnostic criteria have been proposed and are frequently used in research studies (Mendez et al., 2002; Tang-Wai et al., 2004, Appendix 2). Core features for a diagnosis of PCA include: (i) insidious onset and gradual progression; (ii) presentation of visual deficits in the absence of ocular disease; (iii) relatively preserved episodic memory, verbal fluency and personal insight; (iv) presence of symptoms including visual agnosia, simultanagnosia, optic ataxia, ocular apraxia, dyspraxia and environmental disorientation; and (v) absence of stroke or tumour. Supportive features include alexia, ideomotor apraxia, agraphia, acalculia, onset before the age of 65 years and neuroimaging evidence of posterior cortical atrophy or hypoperfusion.

1.2.2.6 Neuropsychological features

PCA is characterized by a number of different neuropsychological deficits, the most frequently cited ones are visuospatial and visuoperceptual deficits, including alexia and neglect, as well as features of Balint's syndrome (simultanagnosia, oculomotor apraxia, optic ataxia, environmental agnosia) and Gerstmann's syndrome (acalculia, agraphia, finger agnosia, left/right disorientation) (Andrade et al., 2010; Charles and Hillis, 2005; McMonagle et al., 2006; Mendez et al., 2002; Renner et al., 2004; Tang-Wai et al., 2004; Whitwell et al., 2007a). It should be noted that, whilst terms such as Balint's and Gerstmann's syndrome are still frequently used in the literature, these syndromes are often inconsistently defined and tested, and patients often show additional symptoms, limiting their diagnostic utility in PCA.

The most detailed neuropsychological study of 19 PCA patients to date by McMonagle et al. suggests that of the symptoms mentioned above, agraphia, alexia, simultanagnosia and optic ataxia are the most consistently identified features (McMonagle et al., 2006). Additional features reported in this study included agnosia for objects, faces and colours, though interestingly no pure ventral stream syndrome was detected, suggesting greater impairment of the dorsal stream in the PCA patients in this study. However, a clear distinction between patients with predominantly parietal deficits and impairments of basic visual processing skills has been shown (e.g. figure-ground discrimination, shape discrimination, visual crowding; Crutch and Warrington, 2007), with atrophy predominantly affecting the striate and extrastriate cortices (e.g. Galton et al., 2000). Overall, the visual deficits commonly reported in PCA have predictable consequences on performance on more general neuropsychological tests such as IQ (performance IQ is often up to 30-40 points lower than verbal IQ scores) and constructional tasks (e.g. Rey figure copy and clock drawing). Longitudinal studies have shown that anterograde memory and frontal lobe functions as well as linguistic skills, which are sometimes strikingly preserved in the earlier stages of the disease, gradually deteriorate in some patients as they progress to a more global dementia state (e.g.

Levine et al., 1993; McMonagle et al., 2006) making their cognitive phenotype ultimately virtually indistinguishable from that found in typical AD (DellaSala et al., 1996).

1.2.3 Frontotemporal lobar degeneration (FTLD)

A number of important other non-AD pathological processes cause dementia. FTLD, although less prevalent, is almost as common as AD below the age of 65 years (Harvey et al., 2003; Ratnavalli et al., 2002) and can be difficult to distinguish from AD at any age especially in early disease stages. There is great heterogeneity in the clinical, genetic and pathological phenotypes in FTLD (for a review see Seelaar et al., 2010b).

1.2.3.1 Pathology

Pathologically, FTLD is rather heterogeneous. It can be divided into two major subtypes: FTLD with tau-positive inclusions (FTLD-tau), and FTLD with ubiquitin-positive and TDP-43-positive, but tau-negative inclusions (FTLD-TDP) (Mackenzie et al., 2010). FTLD-tau includes patients with microtubule-associated protein tau (MAPT) mutations, Pick's disease, progressive supranuclear palsy (PSP), CBD, argyrophilic grain disease and multiple system tauopathy with dementia (Mackenzie et al., 2010). MAPT mutations are associated with different types of tau inclusions (Pick bodies, neurofibrillar tangles and pretangles) in the frontal and temporal cortex, hippocampus and subcortical nuclei, and sometimes in midbrain, brainstem, cerebellum and spinal cord (van Swieten and Spillantini, 2007).

FTLD-TDP is characterized by ubiquitin-positive inclusions that have the TDP-43 protein as major constituent (Neumann et al., 2006). FTLD-TDP is further divided into four different subtypes (Mackenzie et al., 2006) according to the morphology and distribution of the inclusions and correspond, to some extent, to the clinical phenotype (see 1.2.3.2): semantic dementia is strongly associated with abundant dystrophic neuritis; FTD-MND is characterized by numerous neuronal cytoplasmatic inclusions in both superficial and deep cortical laminae; progranulin (GRN) mutations are associated with cytoplasmatic inclusions, dystrophic neurites and neuronal intranuclear inclusions; and valosin containing protein (VCP) mutations are characterised by numerous intranuclear and infrequent number of neuronal cytoplasmatic inclusions and dystrophic neurites (Cairns et al., 2007). It remains unclear what differences in underlying pathophysiology determine the distinction between these TDP-43 subtypes.

Recently, a small number of FTLD cases with ubiquitin-positive, TDP-43 negative pathology have been reported to show immunoreactivity with the FUS antibody (Neumann et al., 2009a; Seelaar et al., 2010a). The FUS protein contains 526 amino acids and is as a nuclear protein involved in DNA repair and the regulation of RNA splicing (Vance et al., 2009). FTLD-FUS cases are characterised by a young age at

onset, a behavioural FTD (bvFTD) phenotype (see 1.2.3.2), a negative family history and caudate atrophy on MRI (Josephs et al., 2010; Seelaar et al., 2010a). FUS-positive inclusions are also found in patients with neuronal filament inclusion disease (NIFID) (Neumann et al., 2009b). NIFID patients most commonly present with bvFTD symptoms, a negative family history and pyramidal and/or extrapyramidal movement symptoms (Neumann et al., 2009b). Finally, cases have been described with ubiquitin-positive, TDP-43 and FUS-negative inclusions, termed FTLD-UPS. Most of the FTLD-UPS cases carry a CHMP2B mutation (Holm et al., 2009) but there are a few without CHMP2B mutations (Urwin et al., 2010).

1.2.3.2 Clinical presentations

FTLD comprises three prototypical clinical syndromes: frontotemporal dementia (FTD) or behavioural variant FTD (bvFTD), progressive non-fluent aphasia (PNFA), and semantic dementia (SemD). PNFA and SemD are also collectively referred to as primary progressive aphasia (PPA). BvFTD affects predominantly the frontal and anterior temporal lobes (Figure 1.2A) and presents with prominent behavioural and personality changes, followed by disturbances of executive functions, language and memory (Neary and Snowden, 1996; Snowden et al., 2007a). PNFA is associated with atrophy predominantly of areas around the left perisylvian fissure (Figure 1.2B) and is characterized by difficulty in speech production with agrammatism and apraxia of speech in the presence of relative preservation of comprehension (Neary et al., 1998). SemD usually presents with fluent aphasia and severely impaired comprehension and naming (Hodges and Patterson, 2007; Snowden et al., 2007a). Neuroimaging reveals atrophy predominantly in the left anterior temporal lobe, particularly the temporal pole, entorhinal cortex and fusiform gyrus (Figure 1.2C; Chan et al., 2001b; Galton et al., 2001; Rosen et al., 2002). A further syndrome has been described in which patients show predominant atrophy in the right temporal lobe (Figure 1.2D), and mainly behavioural symptoms as well as memory loss, topographical disorientation and prosopagnosia (Chan et al., 2009; Evans et al., 1995; Thompson et al., 2003).

1.3 Chapter conclusions

Dementia is a major and growing socioeconomic and public health problem. The most common disease which causes dementia is AD. AD can be difficult to distinguish clinically from other pathologies such as FTLD, especially in the early stages. Therefore methods which aid distinction of AD from non-AD pathologies are important. AD typically presents with episodic memory impairment leading to decline in multiple domains. An atypical variant is PCA which involves initial visual and parietal impairments which eventually lead to generalized cognitive decline.

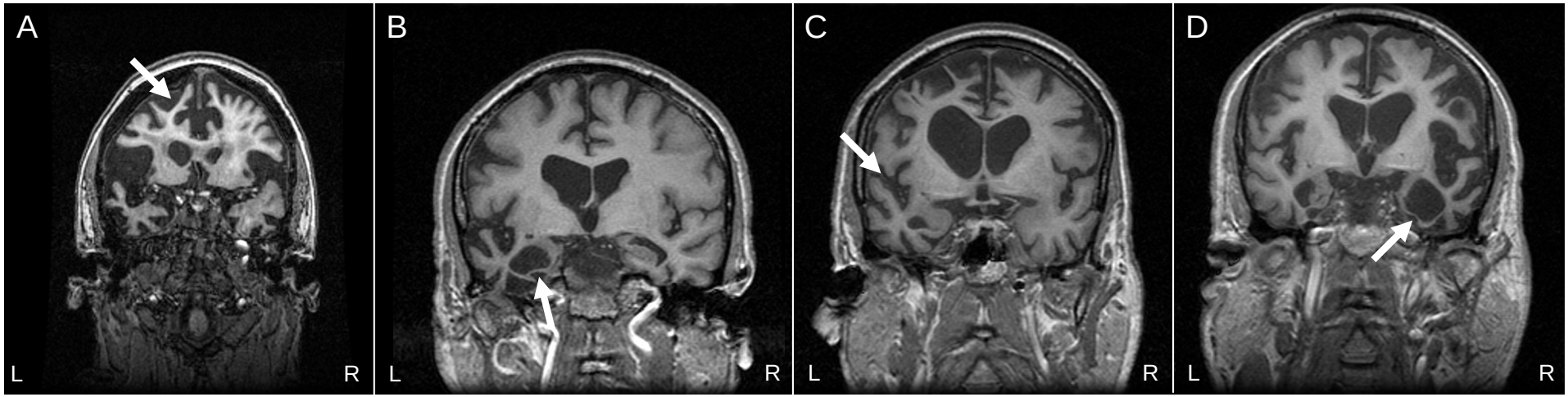

Figure 1.2: Patterns of atrophy in bvFTD, SemD, PNFA and right temporal lobe FTD. Presented are structural MRI scans of patients with **A)** bvFTD showing predominant frontal atrophy, **B)** SemD showing prominent left temporal lobe atrophy, **C)** PNFA showing atrophy in the left perisylvian fissure, and **D)** in right temporal FTD showing predominant atrophy in the right temporal lobe.

2.IMAGING IN DEMENTIA

2.1 Chapter introduction

Whilst a definitive diagnosis of AD can only be made with histopathological data, pathological changes are often accompanied by atrophy which can be measured non-invasively using a variety of structural imaging techniques. What this reveals about AD and PCA in particular will be the focus of this thesis. Therefore this chapter will mainly describe structural imaging methods, but for completeness a brief description of other imaging techniques, such as functional imaging, which reveal additional biological changes or deficits in the AD brain will be included. After describing the main tools available to measure structural and functional characteristics of the brain, this chapter will demonstrate how these have been used to characterize normal ageing, AD, PCA and FTLD.

2.2 Structural imaging techniques

Structural imaging, such as computed tomography (CT) or magnetic resonance imaging (MRI), allows non-invasive visualization of brain anatomy. In dementia, pathological changes result in neuronal loss which may be visualized as macroscopic atrophy using such imaging techniques. Although CT is relatively cheap and widely available, low image contrast makes it a less useful technique to assess atrophy, in particular for research purposes. However, CT can be used for patients for whom MRI is contraindicated, such as those with pacemakers. MRI is a technique which produces high-resolution and contrast images and which has become increasingly available in clinical practice. By using different pulse sequences and by changing the imaging parameters, different image contrasts can be achieved, such as T1, T2 and proton density, which relate to specific tissue characteristics. Figure 2.1 provides an overview of commonly used MRI sequences. In the studies described in this thesis only T1-weighted images were used. MRI-based patterns of atrophy are useful diagnostic markers and serial MRI can be used to assess disease progression. Atrophy patterns have been shown to correlate well with cognitive deficits (e.g. Fox et al., 1999; Mungas et al., 2005; Ridha et al., 2008), and correspond to areas with greatest tangle deposition at post-mortem (Vemuri et al., 2008; Whitwell et al., 2008b).

CT	T1	FLAIR	T2	PD
	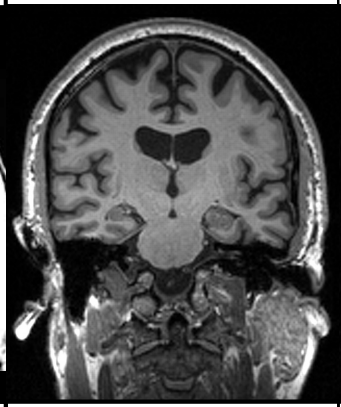	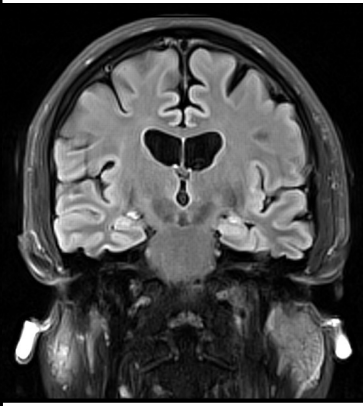	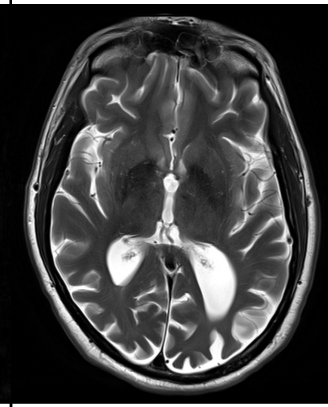	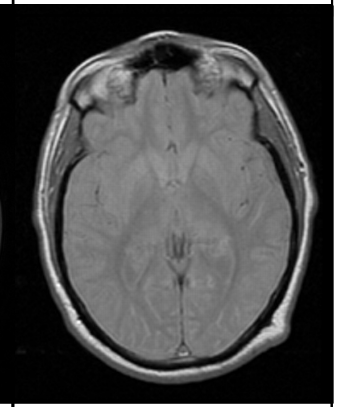
Computed tomography CT scanning produces images on which CSF appears dark, and brain tissue brighter. It is often used to assess atrophy, and to detect infarction, tumours, calcifications, haemorrhages and bone trauma.	**T1-weighted scans** T1-weighted images have similar applications and a similar appearance as CT images, but has a better grey/white matter contrast (with grey matter appearing darker than white matter).	**Fluid Attenuated Inversion Recovery (FLAIR)** FLAIR is an inversion recovery technique that nulls fluids. For example, it can be used to suppress CSF in order to bring out periventricular hyperintense lesions, such as multiple sclerosis plaques.	**T2-weighted scans** In T2-weighted images fat, water and fluid appear bright. These are useful to pick up oedema as collections of abnormal fluid are bright against the darker normal tissue.	**Proton density (PD)** PD scans measure the proton concentration in a structure. They are used to assess periventricular and subcortical lesions such as inflammatory damage, microinfarcts, and arteriosclerotic white matter lesions.

Figure 2.1: Overview of CT, T1, FLAIR, T2 and PD images. Shown are examples for each type of scanning sequence and a brief description of their main application.

2.2.1 Cross-sectional image analysis

2.2.1.1 Visual assessment

In a clinical setting CT and MR images are most commonly assessed by visual inspection by a radiologist. Atrophy is typically evaluated using MR-based T1-weighted images. Tissue damage such as vascular lesions or microbleeds is better investigated using T2-weighted images and FLAIR (fluid attenuated inversion recovery, Figure 2.1). Although visual assessment has been shown to be useful in differential diagnosis, co-existing pathologies (e.g. AD and vascular dementia) or overlap in the atrophy patterns of different diseases (e.g. AD, DLB and normal ageing), especially in the early stages of the disease, makes accurate radiological diagnosis using brain atrophy patterns problematic. To allow a more systematic method of assessment, visual rating scales have been developed such as the Scheltens scale which measures the degree of atrophy in the medial temporal lobe: an area affected early by AD pathology and atrophy (Scheltens et al., 1992, chapter 3, section 3.5.3.1.1). This scale has good intra- and inter-rater reliabilities, and has been shown to discriminate well between AD and healthy controls, and predict the conversion from mild cognitive impairment (MCI) to AD (Korf et al., 2004; Scheltens et al., 1992; Scheltens et al., 1995). A study by Wattjes et al. further showed that MTA can also be applied to CT as well as T1-weighted MRI (Wattjes et al., 2009). Other scales have been developed to assess global atrophy (Scheltens et al., 1997), and white matter changes (Wahlund et al., 2001). These scales are easy to apply, require minimal training and have been validated extensively. They therefore represent a convenient way of assessing atrophy patterns and other pathologies and may aid differential diagnosis in a clinical setting.

2.2.1.2 Manual delineation of brain structures

Currently the gold standard for measuring and quantifying atrophy in regions of interest (ROI) is by manual delineation. A number of protocols have been developed to delineate and determine the volumes of different regions, particularly for regions in the medial temporal lobe owing to its early and disproportionate involvement in AD (see Figure 2.2 for an example of manual delineations of temporal lobe regions). A number of protocols have been developed to delineate the hippocampus (Jack, Jr., 1994; Killiany et al., 1993; Pantel et al., 2000; Pruessner et al., 2000; Watson et al., 1992); a more extensive list of available protocols can be found on http://www.hippocampal-protocol.net/site/sops_protocols.html. Protocols have also been developed to segment the amygdala (Basso et al., 2006; Morey et al., 2009; Whitwell et al., 2005b), entorhinal cortex (Du et al., 2003; Insausti et al., 1998). Manual delineation protocols have also been developed for the cingulate gyrus and its subsections (Jones et al., 2006), and total intracranial volume (TIV) (Whitwell et al., 2001). A number of studies using manual volumetric data have shown greater atrophy in AD compared with healthy controls in regions of the medial temporal lobe, in particular in the hippocampus, entorhinal cortex,

amygdala, and parahippocampus (e.g. Basso et al., 2006; Chan et al., 2001b; Jack, Jr. et al., 1992; Juottonen et al., 1998; Teipel et al., 2006). Manual volumes of medial temporal lobe structures have further been shown to predict conversion from MCI to AD (e.g. Fox and Schott, 2004; Jack et al., 1999; Rusinek et al., 2004). However, manual delineation is time-consuming, labour-intensive, and subject to operator error. It is therefore less suitable as a routine diagnostic tool in a clinical setting.

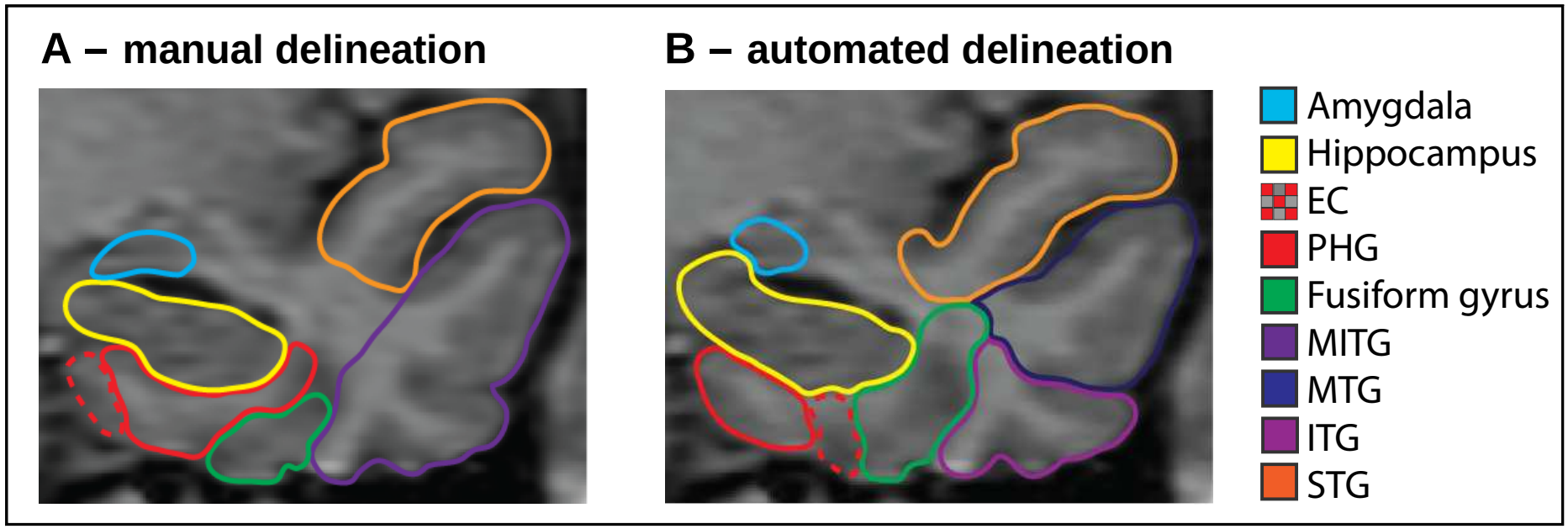

Figure 2.2: Schematic illustration of individual regions of the left temporal lobe of a control subject. A) Regions produced by manual delineation (adapted from Chan et al., 2001b), **B)** Regions obtained from an automated technique (FreeSurfer) (Lehmann et al., 2010). EC - entorhinal cortex, PHG - parahippocampal gyrus, MITG - medial-inferior temporal gyrus, MTG - medial temporal gyrus, ITG - inferior temporal gyrus, STG - superior temporal gyrus.

2.2.1.3 Automated techniques

With improving MRI quality, semi-automated and automated segmentation tools including the use of 'brain atlases' (template images with specific regions outlined) have been developed and are increasingly used to conduct not only ROI analyses, but also whole brain analyses which are not biased to a set of regions chosen *a priori*. Unlike relatively laborious manual delineation approaches, these techniques also have the advantage of being more reliable and potentially reducing operator time. There are online resources such as www.idoimaging.com which provide comprehensive and continuously updated overviews of current tools.

2.2.1.3.1 Between-subject registration

Many automated techniques require between-subject registration in order to achieve correspondence. A number of registration algorithms have been developed varying in their complexity and accuracy. Linear registration describes techniques where the same set of parameters is applied to all image voxels, for example to transform them onto a standard template. A rigid body registration applies translations and rotations in each of the x, y and z directions. This type of linear registration is referred to as having six degrees of freedom (dof). It is also possible to add scaling factors, increasing the degrees of freedom to nine. Finally, a 12 dof, or affine registration, includes shears in addition to the previous transformations. In contrast, non-linear registration describes a process in which the registration parameters are allowed to vary throughout the image (see Figure 2.3). This allows a more accurate matching of gyral anatomy by providing more freedom to warp one image onto another. There are a variety of different non-linear matching procedures. For example, there are high-dimensional mapping techniques which aim to achieve an exact match between two images, eliminating morphological differences between scans. In theory any shape can be warped into another, but it is important that solutions are biologically plausible, so that the topology of brain tissue is maintained. This type of non-linear matching algorithm is generally based on a physical model, which includes some type of constraint to limit 'unlikely' deformations. One example is the fluid registration (see chapter 7, section 7.2.5) where deformations are confined by the properties of a viscous compressible fluid.

The choice of registration algorithm depends on the question being addressed. All registration techniques result in images being in correspondence to a greater or lesser extent, i.e. one point on one image corresponds to a particular point on the other image. Theoretically these two points represent the same type of tissue in each scan although the correspondence is limited by the chosen algorithm. Note that the term 'spatial normalisation' refers to the mapping of a single subject's brain image into a standard space. This is commonly performed for both manual and automated procedures to ensure that all subjects and images are processed in the same stereotactic space and

that subsequent procedures are not affected by differences in head orientation and positioning.

2.2.1.3.2 Brain atlases / templates

Brain templates combined with atlases have two main uses: they can be used in order to obtain spatial correspondence between subjects within the atlas space or they can be used to delineate regions within native space of the region using a process of image registration and region propagation (see section 2.2.1.3.1). Originally atlases were derived from single subjects, such as the Montreal Neurological Institute (MNI)-single subject T1-volume used in AAL (Automatic Anatomical Labeling, Tzourio-Mazoyer et al., 2002), or even single hemispheres such as the Talairach atlas brain (Talairach and Tournoux, 1988). However more recent atlases represent an average of multiple subjects or a library of subjects, with the advantage that they incorporate greater between subject variability. For example the brain atlas developed by Hammers et al. comprises 20 subjects and provides labels for a number of regions including temporal lobe structures, which can be used to propagate regions onto new subjects (Hammers et al., 2003). It should be noted, however, that the majority of brain atlases have the disadvantage that they represent labels which can be used to label regions on an MRI scan. Most of them do not represent tools which can perform automatic segmentations. Other software packages such as FSL (FMRIB Software Library) (Smith et al., 2004) are fully automated but only provide segmentations of a limited number of structures.

2.2.1.3.3 Voxel-based morphometry

Voxel-based morphometry (VBM) is a neuroimaging analysis technique that allows investigation of focal differences in brain anatomy between subject groups using statistical parametric mapping (SPM) (Ashburner and Friston, 2000, http://www.fil.ion.ucl.ac.uk/spm). It typically uses T1-weigthed volumetric MRI scans and performs statistical tests to compare scans from different groups on a voxel by voxel basis throughout the whole image. It represents an ‘unbiased’ method which is not dependent on *a priori* assumptions about which regions may be affected in a disease. VBM involves a number of processing steps including: i) spatial normalisation; ii) segmentation of the images into different tissue compartments (i.e. grey matter, white matter, CSF) with analysis typically being performed separately on each tissue class; iii) modulation which adjusts the image for the warping necessary during the spatial normalisation step in order for the resulting image to again represent volume; and iv) smoothing at each voxel in order for the value at a given voxel to become a weighted average of the surrounding voxels. The methods have been described in much detail by Ashburner and Friston (Ashburner and Friston, 2000). The spatial normalisation step ensures that all the subjects’ data are transformed into the same stereotactic space. It is

generally achieved by registering each image onto the International Consortium for Brain Mapping (ICBM) Montreal Neurological Institute (MNI) template image (Mazziotta et al., 1995). Recently, DARTEL (SPM8; Wellcome Trust Centre for Neuroimaging, London, United Kingdom), a fast diffeomorphic registration algorithm, has been developed for use with VBM (Ashburner, 2007). This involves creating a mean image of all images taken, which serves as a subject-specific template. Subsequently, whole-brain images of individual subjects are normalized to the template, modulated, and smoothed. DARTEL has been shown to improve registration and provide precise and accurate localization of structural damage and functional overlays (Takahashi et al., 2010). Parametric statistical analysis is then performed on the smoothed images at every voxel with the tests normally used being t-tests. This generates maps showing all voxels that show differences in tissue intensities (commonly interpreted as differences in volumes) between groups at a certain, user-selected, p value. Because the statistical tests involve the comparison of a very large number of voxels, it is important to correct for multiple comparisons to reduce the occurrence of false positives.

Whilst VBM has been widely used in neuroimaging research due to the fact that it is relatively quick and easy to apply, there are also certain limitations that need to be considered when using VBM and interpreting the results. First, VBM is greatly affected by variability which can reduce sensitivity for detecting group differences. Variability between individuals can be caused by heterogeneity within the sample as well as errors introduced by the preprocessing steps. For example, the power to detect a difference in a particular region is particularly dependent on the accuracy of the normalisation (Bookstein, 2001). VBM does not differentiate between changes in tissue content and local misregistration of images. This may be a particular problem for small structures such as the amygdala or hippocampus that not only have a complex shape but may also be highly variable between subjects (Good et al., 2002). Normalisation, however, has improved with the introduction of DARTEL. Variability and normalisation errors can also produce false negatives, which represents a further limitation of VBM. Whilst the presence of false positives (i.e. the rejection of a true null hypothesis) can, to some extent, be controlled for by using multiple comparison corrections, the occurrence of false negatives (i.e. the failure to reject a false null hypothesis) cannot be controlled for in VBM, and needs to be considered when interpreting the results. This means that if no difference was found between two groups in a certain brain region, this does not mean that there is no difference, but rather that no difference was detected using the current method.

Furthermore, the segmentation step provides an additional source of error. The misclassification of tissue is especially likely in atrophic brains, because there is a greater potential for partial volume effects between grey matter and CSF, and because

tissue pathology may be associated with reduced grey/white matter contrast (Good et al., 2002). Errors in segmentation can also occur due to the displacement of tissue. This is a particular problem in subcortical grey matter structures surrounding the ventricles, which can shift due to enlargement of the ventricular system. However, it should be noted that segmentations have greatly improved with the introduction of the unified segmentation model in SPM5, which combines image registration, tissue classification, and bias correction within the same generative model (Ashburner and Friston, 2005). Finally, the smoothing step involves a trade-off: whereas high levels of smoothing increase the ability of VBM to detect grey matter differences by reducing the variance, excess smoothing diminishes its ability to accurately localize change.

There are often significant variations across studies in the VBM preprocessing steps, the size of the smoothing kernel, and in the level of significance applied, making it difficult to compare results directly across studies. It is essential, therefore, that parameter choice is documented, as outlined in the paper by Ridgway et al. (Ridgway et al., 2008).

2.2.1.3.4 Surface-based techniques

An alternative method to investigate anatomical differences between groups is by using surface-based methods. These techniques are used to construct and analyse surfaces that represent structural boundaries within the brain. As such, they differ from voxel-based techniques which analyse image properties at a voxel by voxel level. Whilst some of the processing steps are similar to those in VBM, there are also fundamental differences. Typically surface-based methods involve: i) brain segmentation which produces boundaries between grey and white matter; and white matter and CSF; ii) generation of corresponding surfaces by using a meshing algorithm; and iii) mapping of the surfaces to a unit sphere to achieve between-subject correspondence. Once the brain surfaces are in the same space and the gyri and sulci are well matched, a number of different variables can be assessed, which include measuring the distance between different surfaces, known as cortical thickness, sulcal depth, and also some local or global measures of area and curvature (e.g. gyrification). Cortical thickness measures have been extensively used in dementia research and a number of algorithms have been developed for this type of analysis (Dale et al., 1999; Lerch et al., 2005; MacDonald et al., 2000; Thompson et al., 2001). One of these tools which is widely used and is freely available from the web is FreeSurfer (Dale et al., 1999; Fischl et al., 1999, http://surfer.nmr.mgh.harvard.edu/fswiki).

FreeSurfer allows a large number of different analyses, including the measuring of different morphometric properties of the brain such as cortical thickness, regional volumes (see Figure 2.2 for an example of temporal lobe regions obtained by FreeSurfer) and surface areas. The cortical surface stream of FreeSurfer involves the

following steps: registration to the Talairach atlas space, intensity normalisation, skull stripping, segmentation of white matter, and tessellation of the grey/white matter boundary, inflation of the folded surface tessellation patterns and automatic topology correction. This surface is then used as the starting point for a deformable surface algorithm to find the grey/white and grey/CSF surfaces. This method uses both intensity and continuity information from the surfaces in the deformation procedures to produce representations of cortical thickness, calculated as the closest distance from the grey/white boundary to the grey/CSF boundary at each vertex on the tessellated surface.

A cortical surface-based atlas has been defined based on average folding patterns mapped to a sphere. Surfaces from individuals can be aligned with this atlas with a high-dimensional nonlinear registration algorithm. The registration is based on aligning the cortical folding patterns and so directly aligns the anatomy instead of image intensities. The spherical atlas naturally forms a coordinate system in which point-to-point correspondence between subjects can be achieved. This coordinate system can then be used to create group maps.

FreeSurfer further allows the extraction of subcortical volumes obtained from the volume-based stream (which is different to the surface-based stream described above). The stream consists of several stages (Fischl et al., 2002): the first stage is an affine registration with Talairach space specifically designed to be insensitive to pathology and to maximize the accuracy of the final segmentation (this is different to that used in the surface-based stream). This is followed by an initial volumetric labelling and intensity correction. A high dimensional nonlinear volumetric alignment to the Talairach atlas is then performed. After the preprocessing, labels are transferred onto the volume. Both the cortical and the subcortical labelling use the same basic algorithm. The final segmentation is based on both a subject-independent probabilistic atlas and subject-specific measured values. The atlas is built from a training set, i.e., a set of subjects whose brains (surfaces or volumes) have been labelled by hand. These labels are then mapped into a common space (Talairach space for volumes and spherical space for surfaces) to achieve point-to-point correspondence for all subjects.

Whilst techniques such as FreeSurfer have the advantage of being fully automated, they are also highly dependent on good image quality (i.e. good grey/white matter contrast). Poor image quality may cause the algorithm to either fail or to produce unsatisfactory results which may motivate further manual intervention, reducing the advantage of this method being an automated procedure. Furthermore, techniques such as FreeSurfer are also prone to fail in the presence of severe atrophy. This has been demonstrated in SemD patients who often show great atrophy in the left temporal lobe (Lehmann et al.,

2010). Finally, unless segmentation protocols are similar across methods and studies, regions obtained by manual and automated methods can vary greatly, which makes comparisons between studies using manual and automated regions more difficult (see section 2.2.1.4).

2.2.1.3.5 Machine-learning algorithms

Classification algorithms are increasingly used to test whether specific imaging features can differentiate between different types of dementia. In neuroimaging research, machine-learning algorithms such as support vector machines (SVM, Vapnik, 1995; Vapnik, 1998) have been used to conduct such classification analyses. The standard SVM is a non-probabilistic binary linear classifier. It typically involves training a set of example inputs (e.g. scans of different subjects), with each input being defined as belonging to one of two categories (e.g. different groups). For each subsequent input the SVM predicts whether the subject is more likely to fall into one group or the other.

In studies which assess whether subjects belong to one disease group or another, the SVM essentially represents these subjects as points (based on imaging features) in an n-dimensional space. The SVM then identifies the optimal separating hyperplane in this space such that subjects from each group lie as far as possible from the hyperplane on opposite sides. Once the hyperplane has been defined, scores can be generated by projecting the point (i.e. the subject) onto the normal of the hyperplane. The direction of the normal can be visualized as an image, showing the relative weights and signs of vertices' contributions to the classifier scores.

For small group analyses, where an example set to train the SVM is not available, the classifier can be trained using a leave-one-out loop (Wilson et al., 2009). By leaving each scan in turn entirely out of the training procedure, an unbiased estimation of generalisation accuracy is ensured.

SVMs are increasingly used in imaging studies to test the ability of a certain imaging measure to distinguish between subject groups. Since new scans can be tested against trained data sets and can in turn be categorized as members of a particular clinical group (e.g. AD), it has been suggested that SVMs have the potential to become valuable diagnostic tools in the future (Kloppel et al., 2008). SVMs have the advantage that they generalize well to new data sets, and generalize across image sets from different centres (Kloppel et al., 2008). This is very important as it could facilitate the generation and use of SVMs for rarer forms of dementia (such as PCA and LPA) using scans from multiple imaging sites.

Whilst some patients may be differentiated relatively easily from controls using less intensive methods (e.g. using paper and pencil tests), these might be less specific in milder patients that only have very subtle cognitive impairments. Furthermore, SVMs may be used to differentiate disorders that show overlapping clinical symptoms and atrophy patterns, but differ in their neuropathological characteristics, such as AD and FTLD (see chapter 4). Unlike methods that include expert-dependent hippocampal tracing (2.2.1.2), SVMs are fully automated and can use all the information in a brain scan. The fact that SVMs are automated eliminates observer/experimenter bias, generates reproducible results with the same image set and makes the method much less labour-intensive. These are important characteristics for a method proposed for clinical use.

Although the processing and preparation of a training dataset can be relatively time consuming, this may not necessarily be a limiting factor. First, this represents computer processing time without user interaction. Secondly, once a training dataset is prepared, spatial normalisation and classification of any new scan can be performed within minutes. Finally, the time required is likely to shorten further with increasing computing speeds.

2.2.1.4 Differences between manual and automated methods

Automated segmentation methods are increasingly used owing to the need for segmentation of large datasets which include thousands of scans. Studies which compare different segmentation algorithms are of increasing importance since inaccuracy of segmentation methodologies can lead to reduced power of a study to detect anatomical changes. For example, a recent study by Clark et al. showed that the choice of segmentation algorithm had the largest impact on variability, whereas the choice of pulse sequence had the second largest impact. It further showed that the classification of grey matter is the most variable, and that the optimal segmentation protocol may differ across tissue types (Clark et al., 2006). In particular segmentation methods which exhibit disease-related or atrophy-related biases can lead to overestimates or underestimates in subject group differences. However, studies which compare automated techniques with “gold standard” manual techniques or other automated techniques are often hampered by the lack of standardisation of segmentation protocols across laboratories on which methods are based. This is naturally unproblematic for laboratories where the techniques being compared have been developed, but for techniques to demonstrate wider utility, use at different centres is required. Therefore, in addition to traditional voxel overlap analyses which may be confounded by differences in protocols, studies which investigate whether patterns of atrophy in specific diseases are replicated across techniques are useful.

A small number of studies have focused on the comparison of different segmentation methods. In the FreeSurfer validation paper by Fischl et al., segmentation accuracy of FreeSurfer compared with manual delineations was assessed in seven healthy volunteers for two temporal lobe structures (hippocampus and amygdala), and other brain structures including the caudate, putamen, thalamus and ventricles, showing that FreeSurfer is comparable in accuracy to manual methods (Fischl et al., 2002). A study by Morey et al. compared FreeSurfer and FSL segmentations of the hippocampus and amygdala with manually delineated regions using 3T MRI scans of 20 healthy subjects (Morey et al., 2009). This study found relatively good correlations and agreements of volumes produced by FreeSurfer and manual methods, and overall greater voxel overlap and smaller volume differences of FreeSurfer regions compared with manual delineations than regions produced by FSL compared with manual methods. The percent volume overlap (Dice coefficient) between FreeSurfer and manual segmentations of the hippocampus was above 81%.

In a study by Lehmann et al., eight temporal lobe structures in each hemisphere and ventricles were delineated using FreeSurfer and compared with manual segmentations in 10 control, 10 AD, and 10 SemD subjects (Lehmann et al., 2010). The study revealed differences in segmentation protocols between FreeSurfer and manual methods, including the exclusion of the temporal stem white matter in the manual segmentation which affected volumes of most temporal lobe regions (Figure 2.2). Another difference was the exclusion of the hippocampal tail in the manual hippocampal segmentations, and the inclusion of the cerebellum in the manual whole brain segmentations. Finally, differences in ventricular segmentations were observed, with manually segmented ventricles including the posterior horns of the ventricles which are not consistently included in the FreeSurfer ventricle segmentation. These differences in protocol led to differences in absolute volumes and overlap ratios between the methods, making the evaluation of segmentation accuracy of these methods problematic. However, despite differences in protocol and volumes, both methods showed similar atrophy patterns in the patient groups compared with controls, and similar right-left differences, suggesting that both methods distinguish between the three groups with similar accuracies. Other studies have focused on assessing the patterns of regional volume differences in different diseases. Hippocampal volumes produced by FreeSurfer were compared with manual measurements in patients with chronic major depressive disorder and healthy controls (Tae et al., 2008). FreeSurfer showed good agreement with manual method regarding hippocampal volumes; however, in the right hippocampus in particular volumes produced by FreeSurfer were greatly larger than those obtained from manual method.

Other studies have compared different automated techniques with each other. Klauschen et al. compared FSL, SPM5 and FreeSurfer using a set of simulated MRI data of 10 healthy brains obtained from BrainWeb (resembling ~1.5 T), and a set of real 1.5 T MRI data of 9 healthy volunteers (Klauschen et al., 2009). They showed that volumetric accuracy for grey and white matter was similar in SPM5 and FSL, and better than in FreeSurfer. FSL showed the highest stability for white, and FreeSurfer for grey matter for the simulated data set. Another study compared VBM with region-of-interest (ROI) measurements of temporal lobe structures in 10 AD patients and 10 SemD patients (Good et al., 2002). It was shown that VBM detects a general trend of atrophy similar to that of expertly labelled ROI measurements in both disease groups; however, they also found discrepancies in the ranking of severity and in the significance of volume reductions that were more marked in AD.

2.2.2 Longitudinal image analysis

Longitudinal image analysis can be used to assess the progression of tissue loss over time. It involves the comparison of two scans taken at different time points from the same subject. Each subject therefore acts as his/her own control, which can reduce between-subject variability in morphology. A number of different methods are available to quantify the change between different time points and most techniques rely on some form of within subject registration.

2.2.2.1 Within-subject image registration

One of the key steps for the majority of more recent longitudinal processing methods is the aligning of scans from different time points so that they are in the same spatial framework. However, in dementia, atrophy complicates matters since tissue is lost and replaced by fluid which makes very accurate tissue correspondence problematic for linear registration since this type of registration is only able to match the linear differences between the images (rotations, translations, scaling and shears), and the way in which the brain atrophies over time is not linear. The remaining lack of correspondence following linear registration (see difference image in Figure 2.3) is a mixture of atrophy and non-linear imaging artefacts. Following linear registration, changes in brain volume can be easier to visualise. This easy visualisation can be clinically useful since establishing whether a disease is progressing in a patient may be crucial in making an accurate diagnosis. The benefits of linearly co-registering two scans has been demonstrated in a study by Barnes et al. which showed that co-registration of two serial scans may improve visual diagnosis in dementia (Barnes et al., 2010).

2.2.2.2 Measuring change in volume and cortical thickness

A number of techniques have been developed to study longitudinal changes in specific structures and across the whole brain. Widely used methods to quantify changes over time in whole brain volume are the boundary-shift integral (BSI) (Freeborough and Fox, 1997) and SIENA (Structural Image Evaluation using Normalisation of Atrophy, Smith et al., 2001; Smith et al., 2002). Both techniques rely on pairs of images spatially matched using linear registration. The BSI determines the total volume through which the boundaries of the brain (or any given cerebral structure) have moved (Figure 2.3). It therefore measures volume change directly from voxel intensities. The original BSI algorithm has recently been improved by applying tissue-specific intensity normalisation and automated BSI parameters selection to improve consistency over time and between scanners (KN-BSI, Leung et al., 2010). The BSI method has been applied to measure whole brain atrophy in a range of neurological disorders including AD (Schott et al., 2005), FTLD (Knopman et al., 2009), multiple sclerosis (Anderson et al., 2007), Huntington's disease (Henley et al., 2006), and PSP (Paviour et al., 2006) and it is also used as an outcome measure in clinical trials of AD (Fox et al., 2005; Salloway et al., 2009). SIENA involves a slightly different quantification approach but gives highly correlated results compared with BSI (Smith et al., 2002). Such changes in volume are often represented as annualised percent changes compared with baseline volume which allows for the fact that people have differing initial brain volumes.

Another method which is used to assess volumetric changes in grey matter, white matter, and CSF over time across the whole brain is non-linear registration based techniques which quantify change on a voxel-wise basis determined by the deformation field required to match the images. One such technique is the fluid registration method (Freeborough and Fox, 1998). This technique takes the linearly registered paired images and registers these using a non-linear (fluid) algorithm which is based on a physical model of a compressible viscous fluid resulting in accurate tissue correspondence. The deformations required to achieve this non-linear registration can be stored and these represent how much and where the images needed to be warped in order to obtain accurate correspondence. This deformation field can be visualized as voxel-compression maps which show regions that contract and expand over time (Figure 2.3). Fluid registration can be used to illustrate structural changes in individual subjects (an example is shown in Appendix 3), and it can be used in combination with VBM to assess volume changes in specific tissue types that are statistically significant, and compare these between subject groups.

Finally, changes in cortical thickness can be measured and quantified using FreeSurfer (section 2.2.1.3.4) which has a longitudinal processing stream incorporated (http://surfer.nmr.mgh.harvard.edu/fswiki/LongitudinalProcessing). The longitudinal

stream involves the creation of a template brain using both time points, which represents a rough estimation of the segmentation and surface reconstruction. This template brain is then used to initiate the real segmentation and surface reconstruction of both time points. This procedure ensures that there is no bias towards any one time point.

2.2.3 Diffusion tensor imaging (DTI)

DTI is a relatively novel technique that allows the measurement of the diffusion of water in brain tissue, which gives information about the structural integrity of white matter. From DTI, white matter tracts throughout the brain can be identified (tractography) and such methods are useful in assessing connections and how these may be disrupted in different types of disease.

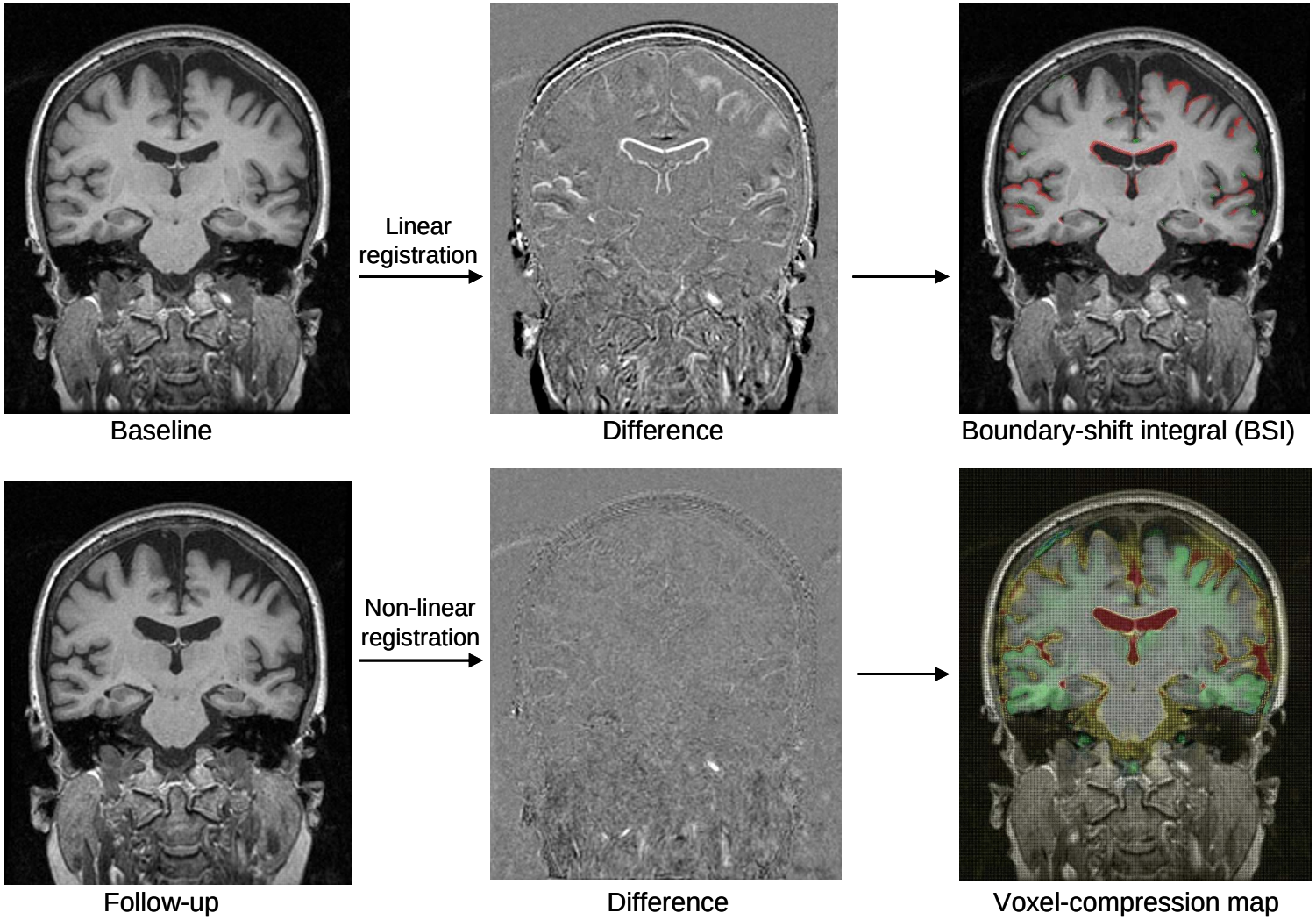

Figure 2.3: Structural T1 and difference images as well as examples of outcome measures for linear and non-linear registration. Shown are a baseline and a follow-up scan of a patient with PCA (left), difference images resulting from linear and linear plus non-linear registration of the repeat scan to the baseline (middle), and examples of outcome measures, namely BSI and voxel-compression map derived from linear and non-linear registration respectively (right).

2.3 Functional image analysis

Functional imaging techniques are useful in measuring physiological activities within the brain, including changes in metabolism, blood flow or the chemical composition of certain substances in the brain. Techniques most commonly used in dementia research include single photon emission computerised tomography (SPECT), positron emission tomography (PET), and functional MRI (fMRI). Since the focus of this thesis is on structural imaging, these functional methods will only be described briefly.

2.3.1 Techniques measuring metabolic changes

Because metabolic changes have been suggested to coincide or even precede structural changes, measuring these changes does not only provide valuable insights into the underlying pathophysiological processes but may also aid early diagnosis. SPECT is a non-invasive technique which uses gamma rays to produce 3D images of the brain. It requires the injection of gamma-emitting radioisotopes into the bloodstream of the subject. Brain metabolism can also be studied using PET, which is a non-invasive tomographic method for imaging the regional distribution of radioactive tracers. The most commonly used tracer is labelled glucose, [18F]fluorodeoxyglucose (FDG), which provides qualitative and quantitative estimates of the cerebral metabolic rate of glucose, an index of synaptic functioning and density (Pellerin and Magistretti, 1994; Rocher et al., 2003). PET provides very similar information as SPECT, and typically produces higher-resolution images.

2.3.2 Functional MRI (fMRI)

Functional MRI (fMRI) measures the haemodynamic response (i.e. change in blood flow) in the brain, from which inferences about the neural activity in the brain can be drawn. Historically, it has mainly been used to measure activation during performance of cognitive tasks, however, more recently it is increasingly used to assess brain activity during resting state and therefore provides useful information about the functional connectivity of networks in the brain (Greicius et al., 2003).

2.4 Imaging pathology

Imaging of pathological markers in the brain provides the opportunity to visualize and quantify the evolution of pathology *in vivo*. The first amyloid imaging agent developed to be used in humans was ^{18}fluoro-labelled1,1-dicyano-2-[6-(dimethylamino)-2-naphthalenyl]propene (FDDNP), which is a fluorinated derivative of a non-specific cell membrane dye (Agdeppa et al., 2001). FDDNP binds in vitro to amyloid conformations of Aβ, as well as to tau and prion protein (Agdeppa et al., 2001; Bresjanac et al., 2003). Elevated FDDNP-uptake in one patient who came to autopsy matched regions with significant plaque and tangle pathology (Small et al., 2006). The most widely used amyloid marker, and one which appears to have superior amyloid detection, is 11C-labelled [N-methyl]-2-(4'-methylaminophenyl)-6-hydroxybenzothiazole, or short Pittsburgh Compound-B (PIB) (Klunk et al., 2004). PIB binds

specifically to extracellular and intravascular fibrillar Aβ deposits. Post-mortem studies have shown that elevated regional PIB signal during life strongly correlates with *in vitro* measures of Aβ pathology (both plaques and vascular amyloid) found at autopsy (Bacskai et al., 2007; Ikonomovic et al., 2008). A number of other amyloid imaging tracers have been subsequently developed, which include F18 ligands (for review see Rabinovici and Jagust, 2009).

2.5 Clinical application of imaging techniques

2.5.1 Normal ageing

The brain changes structurally throughout life: normal ageing, in the absence of a neurodegenerative process, is associated with structural changes in the brain (Fox and Schott, 2004). Since patterns of atrophy in AD and other dementias are typically compared with those in a healthy control group, it is important to understand the structural changes associated with normal ageing. A number of different image analysis techniques, including visual assessment, volumetric and surface-based methods, have been used to study atrophy patterns in healthy older controls.

Early cross-sectional CT and MRI studies showed a reduction in whole brain volume and an increase in ventricular volume with advancing age (Coffey et al., 1992; Pfefferbaum et al., 1994). Studies using manual and automated imaging techniques measuring changes in volume and cortical thickness on MRI have consistently demonstrated enlargement of the ventricles as well as atrophy in temporal, parietal and frontal regions (e.g. Allen et al., 2005; Good et al., 2001; Raz et al., 2004; Resnick et al., 2000; Salat et al., 2004). Longitudinal studies have further suggested that atrophy rates accelerate with advancing age (Fjell et al., 2009; Scahill et al., 2003), with some regions (in particular in dorsal frontal and parietal association areas) showing a particularly strong non-linear association with age (Sowell et al., 2003). Annualised whole brain atrophy rates have been reported to increase gradually from 0.2% per year at age of 30-50 to 0.5% at age 75-80 years (Jack, Jr. et al., 2004; Resnick et al., 2003; Scahill et al., 2003; Schott et al., 2003; Silbert et al., 2003; Wang et al., 2002). Similarly, hippocampal atrophy rates increase from around 0.1-0.2% a year in apparently healthy control subjects aged 30-50, to around 0.8% in subjects in their mid-70s, rising further to 1.5-2% a year at an age of 80-90 in subjects who do not have a diagnosis of dementia (Fox and Schott, 2004; Jack, Jr. et al., 2000; Schott et al., 2003). Whilst the association of pathological changes with age attenuates in the very old, cerebral atrophy was shown to maintain a relationship with age in younger old persons with dementia (75 years of age) and older old persons with dementia (95 years of age, Savva et al., 2009).

Interestingly, studies measuring amyloid deposition in healthy controls using PIB-PET have reported around 20% of older control subjects being PIB-positive (Aizenstein et al., 2008; Rowe et al., 2007, mean age 74 and 73 years respectively), which means that there is a

certain proportion of cognitively normal older subjects showing levels of amyloid deposition similar to that found in AD. The question of whether these subjects represent very early stages of AD is unclear.

2.5.2 Alzheimer's disease

Neuroimaging techniques have been used extensively to study AD. One of the main objectives of these studies is the identification of atrophy patterns which are typical for AD, and which may therefore aid the differentiation of AD from other dementias and normal ageing. Atrophy in the medial temporal lobe has been shown to occur early in the disease which is in accordance with pathological and cognitive features of AD (early studies include Ball et al., 1985; Fox et al., 1996b; Jack, Jr. et al., 1997; Lehericy et al., 1994). Atrophy in the medial temporal lobe, in particular in the hippocampus, has been shown to be a good marker to distinguish AD from normal ageing. For example, visual assessment using Scheltens scale has been shown to discriminate well between AD and healthy controls (Scheltens et al., 1992). It also correlates well with manual delineations of medial temporal lobe structures (Bresciani et al., 2005; Scheltens et al., 1992; Wahlund et al., 2000) and has been shown to predict conversion from MCI to AD (Korf et al., 2004).

The predictive power of atrophy in structures of the medial temporal lobe, in particular in the hippocampus, has been supported by manual volumetric studies (Jack et al., 1999; Rusinek et al., 2004). However, since the region showing earliest tau accumulation is the entorhinal cortex (Arnold et al., 1991; Braak and Braak, 1991), it has been suggested that atrophy of this region may be a better marker of conversion to AD. Hippocampal and entorhinal volume loss have been shown to have similar accuracies for discriminating AD from controls and both measures together were shown to improve discrimination accuracy, suggesting that AD is characterized by atrophy in both these regions (Juottonen et al., 1999). However, the diagnostic benefits of atrophy in the entorhinal cortex are attenuated by the higher variability of the manual volumetric measures of this region due to differences in the manual delineation protocols used in imaging studies (Du et al., 2001; Xu et al., 2000). Manually obtained regions of the entorhinal cortex have also been shown to differ to those obtained by automated methods such as FreeSurfer (Lehmann et al., 2010, Figure 2.2). Overall, a number of other manual volumetric investigations have revealed a consistent pattern of regions showing greater atrophy in AD compared with healthy controls; these include the hippocampus, entorhinal cortex, amygdala, and parahippocampus (e.g. Basso et al., 2006; Chan et al., 2001c; Jack, Jr. et al., 1992; Juottonen et al., 1998; Teipel et al., 2006), as well as cingulate gyrus (Barnes et al., 2007a; Jones et al., 2006; Killiany et al., 2000). Whole brain losses are an early feature too (Fox et al., 1996a; Ridha et al., 2006). With disease progression, atrophy typically spreads from focal temporal lobe regions to cortical areas (Fox et al., 1996b; Scahill et al., 2002).

Studies using VBM support these findings, showing significant grey matter loss mainly in the medial temporal lobe, but also in the posterior cingulate gyrus, precuneus, insula, temporal-parietal association cortex and prefrontal gyrus in AD (Baron et al., 2001; Boxer et al., 2003; Good et al., 2002; Karas et al., 2004). A number of studies assessing patterns of cortical thickness have also demonstrated cortical thinning predominantly in temporal and parietal regions in AD when compared with healthy controls (Du et al., 2007; Lerch et al., 2005; Richards et al., 2009). Cortical thinning in these areas has also been shown to separate AD groups from controls (Lerch et al., 2008).

Longitudinal volumetric studies have given further insights into the progression of atrophy patterns in AD. Studies have demonstrated whole brain atrophy rates of around 2% per year in AD which is several times higher than that found in healthy controls (0.2-0.5% per year depending on age, Bradley et al., 2002; Evans et al., 2010; Fox and Freeborough, 1997; Jack, Jr. et al., 2005; O'Brien et al., 2001; Wang et al., 2002). Measures of whole brain atrophy rate have been used as an outcome measure in clinical trials of therapies targeted at AD pathology (Fox et al., 2005; Salloway et al., 2009). Whole brain atrophy has been shown to be non-linear, with atrophy rates gradually increasing as the disease progresses (Chan et al., 2003). Ventricular expansion has also been shown to be a non-specific marker of progression, with studies demonstrating annual expansion rates between 4-8% (of baseline ventricular volume) in AD (Jack, Jr. et al., 2004; Schott et al., 2005; Whitwell et al., 2007b). Atrophy rates for the hippocampus have been found between 4-7% per year (Barnes et al., 2009 (meta-analysis); Cardenas et al., 2003; Du et al., 2004; Hashimoto et al., 2005; Jack, Jr. et al., 1998; Jack, Jr. et al., 2000), whereas atrophy rates for the entorhinal cortex tend to be a little higher, around 7-9% per year (Cardenas et al., 2003; Du et al., 2004; Schott et al., 2003).

An increasing number of studies in AD report atrophy in posterior regions such as precuneus and posterior cingulate gyrus (Barnes et al., 2007a; Frisoni et al., 2007; Galton et al., 2000). Atrophy in posterior regions may be particularly prominent in early-onset AD (Frisoni et al., 2007; Ishii et al., 2005a; Shiino et al., 2008). Amyloid deposition is seen in posterior regions very early in AD (e.g. Devanand et al., 2010; Kemppainen et al., 2007; Klunk et al., 2004). The FDNNP-PET-tracer, which binds to both tangles and plaques, shows increased uptake in AD compared with controls in the entorhinal, inferior temporal and frontal cortices, but also in parietal and secondary visual cortex regions (Shin et al., 2010).

Recent studies using fMRI have provided new insights into the functional connectivity of different brain regions. There is increasing evidence that the regions typically affected in AD overlap with a network of regions active during resting state which is referred to as the ‘default-mode network’ (Greicius et al., 2003). The default-mode network represents a network of regions which show co-ordinated low frequency fluctuations and elevated activity

during resting state (Buckner et al., 2008; Raichle et al., 2001). The key regions associated with the default-mode network are the medial temporal lobe, lateral parietal regions, precuneus, extending into posterior cingulate and retrosplenial cortices as well as medial and lateral frontal regions. The same regions that are activated at rest appear to be suppressed during various cognitive tasks, including the encoding of new memories (Pihlajamaki et al., 2008). There is also evidence that failure to suppress activity in some of the core default-mode regions is associated with unsuccessful encoding and poor performance in subsequent memory tests in cognitively normal young and old subjects (Grady et al., 2006; Miller et al., 2008; Otten and Rugg, 2001). Future studies should provide valuable insights into how functional networks are affected in different phenotypical presentations of AD.

2.5.3 PCA

As the term PCA suggests, the syndrome is associated with tissue loss primarily of the occipital, parietal and temporo-occipital cortices. Whilst the neuroimaging signature of PCA may often be evident from clinical inspection of structural MR images (e.g. DellaSala et al., 1996; Galton et al., 2000; Mendez et al., 2002, Figure 1.1), image analysis tools can be useful in localizing and quantifying the patterns of atrophy in these patients. To date only one study has used VBM to assess patterns of grey matter atrophy in PCA, and compared these with healthy controls and typical AD (Whitwell et al., 2007a). This study revealed distinct patterns of grey matter loss in both the PCA and typical AD group compared with controls, however, the direct comparison between PCA and typical AD did not show any statistically significant differences after multiple comparison correction. Differential patterns of cortical thickness between PCA and typical AD, as well as longitudinal changes in grey matter volume and cortical thickness in PCA have previously not been investigated.

There have been a greater number of group-based functional imaging studies than structural imaging in PCA. Data from functional imaging studies using SPECT and FDG-PET are often consistent with structural changes in occipitoparietal areas (e.g. Aharon-Peretz et al., 1999; Cohen et al., 2010; Goethals and Santens, 2001; Nestor et al., 2003; Pietrini et al., 1996). Using SPECT, Ross et al. showed hypoperfusion in 4 PCA patients mainly in the bilateral parietal lobe (Ross et al., 1996). Using FDG-PET, Freedman et al. showed strikingly asymmetric hypometabolism with areas in the left hemisphere showing greater reductions than in the right (Freedman et al., 1991). The area showing greatest reduction in glucose metabolism (50%) was shown to be the left occipital lobe. Wakai et al. showed reduced metabolism mainly in dorsal regions, also asymmetric (Wakai et al., 1994). In addition to posterior regions, FDG-PET has revealed specific areas of hypometabolism in the frontal eye fields bilaterally which may occur secondary to loss of input from occipitoparietal regions and underpin ocular apraxia in PCA (Nestor et al., 2003).

To date only a very limited number of studies have assessed patterns of amyloid deposition using PIB-PET in PCA. Two single case studies have reported increased Aβ accumulation predominantly in the occipital and parietal lobes (Kambe et al., 2010; Tenovuo et al., 2008). Ng et al. further showed greater Aβ deposition in the occipital lobe in a single PCA patient compared with 10 typical AD subjects (Ng et al., 2007). Only one study has compared PIB uptake in a group of PCA patients (N=12) with a group of typical AD (N=14) (Rosenbloom et al., 2010). Interestingly, there was no evidence of a significant difference in amyloid deposition between PCA and typical AD, with both groups showing diffuse PIB uptake throughout frontal, temporoparietal and occipital cortex. However, this study may not have been powered to detect significant differences in the direct comparison.

New image analysis tools such as DTI have been applied to investigate atrophy in the white matter tracts in PCA. Yoshida et al. applied DTI to 1 PCA patient and compared it with 5 typical AD patients (Yoshida et al., 2004). The fractional anisotropy (FA) index was lower in the splenium (posterior end) of the corpus callosum than the genu (anterior end) in the PCA patient, whereas the typical AD group showed the reversed pattern. The PCA patient further showed reduced anisotropy and fiber volume in the splenium compared with typical AD. These findings may suggest that the splenium of the corpus callosum degenerates secondarily as a result of the neuronal degeneration of the temporal, parietal and occipital cortices. A more recent longitudinal DTI study by Duning et al. assessed the progression of white matter changes in 1 PCA patient over a period of 15 months, and compared the FA and volumetric changes with 1 typical AD patient and 65 healthy controls (Duning et al., 2009). The PCA patient showed reductions in FA mainly in the occipital lobe in the early stages of the disease which, with disease progression, tended to align with the FA ratios of the typical AD patient, involving increasingly regions in the parietal lobe. These results may suggest that PCA begins as a distinct clinical syndrome with its later course turning into a final pathway shared with typical AD.

2.5.4 FTLD

Clinically, the distinction between patients with AD and FTLD pathology is often challenging since there is considerable overlap in both the clinical symptoms and the cognitive domains impaired (Hodges et al., 2004; McKhann et al., 1984; Neary et al., 1998; Siri et al., 2001). Cross-sectional structural MRI studies have revealed characteristic patterns of atrophy in different FTLD phenotypes, mainly affecting temporal and frontal lobe regions (e.g. Grossman et al., 2004; Rosen et al., 2002; Whitwell et al., 2005a). Delineation of temporal lobe structures has been shown to provide an effective tool to discriminate between AD and FTLD phenotypes (Chan et al., 2001b; Galton et al., 2001; Laakso et al., 2000, Figure 2.2). Longitudinal studies in SemD have suggested that patients who present with predominantly left-sided temporal lobe atrophy develop clinical and structural features of right temporal lobe damage as the disease evolves (Chan et al., 2001c; Diehl-Schmid et al., 2006; Seeley et al.,

2005). In patients with disease duration of around 4 years, the right temporal lobe has further been shown to atrophy more rapidly than left temporal lobe regions (Rohrer et al., 2008). Whole brain volume loss as measured using the BSI has been shown to be between 1-3% per year, whereas ventricular expansion was shown to be between 6-12% per year (Gordon et al., 2010; Knopman et al., 2009; Whitwell et al., 2008a). Both whole brain and ventricular BSI measures produced feasible sample size estimates for detecting meaningful treatment effects, suggesting that these semi-automated methods might be useful biomarkers to assess progression in FTLD (Gordon et al., 2010).

Automated methods such as VBM measuring grey matter and cortical thickness have also been shown to aid the distinction between AD and FTLD (e.g. Du et al., 2007; Gee et al., 2003; Grossman et al., 2004; Kitagaki et al., 1998). However, because medial temporal lobe atrophy is also a hallmark of AD, a division based on MRI is problematic, leading to misdiagnoses. For example, a post-mortem study revealed that 32% of patients diagnosed with a language subtype of FTLD (i.e. PNFA, SemD) had AD pathology (Knibb et al., 2006). Information about metabolic and pathological changes in these groups as measured using FDG-PET and PIB-PET, respectively, may aid clinical distinction from AD (Drzezga et al., 2008; Foster et al., 2007; Rabinovici et al., 2007).

2.6 Chapter conclusions

Structural image analysis is a valuable tool to exclude treatable causes of cognitive deficits and to aid diagnosis. Quantification of structural changes using serial imaging is a powerful and objective measure of disease progression and as such can be useful in both diagnosis and in clinical trials. Other forms of imaging give complementary information regarding function and pathology in the brain. These methods have been used to describe changes in the brain owing to normal ageing as well as the natural history of AD, PCA and other neurodegenerative diseases such as FTLD.

3.METHODS OVERVIEW

3.1 Chapter introduction

This chapter provides a general overview of the subjects and the methods used in the experiments presented in this thesis. Deviations from the procedures described here as well as relevant additional details are provided in the corresponding chapters.

3.2 Subjects

3.2.1 Healthy controls

Neurologically healthy subjects without family history of dementia were recruited as controls. These were mostly spouses of affected or at-risk study participants; a small number of normal volunteers were also included. Typically individuals had a detailed history taken and underwent neurological and brief neuropsychological examination which includes the Mini-Mental State Examination (MMSE) (Folstein et al., 1975). If there was no evidence to suggest cognitive problems and no contraindications to MRI, subjects underwent MR scanning. The spouses of study subjects were usually assessed and scanned on the same day as their partners.

3.2.2 Patients

All clinically affected subjects had attended the Specialist Cognitive Disorders Clinic at the National Hospital for Neurology and Neurosurgery, Queen Square, London, UK. This is a secondary/tertiary referral centre and consequently these individuals tend to represent younger patients and those in whom there is more diagnostic uncertainty. The subjects recruited from the clinic included patients with sporadic AD (including typical, amnestic cases), PCA patients, and FTLD subjects. All patients underwent full clinical and neuropsychological assessment as well as imaging.

3.2.3 Pathologically-proven cases

Some patients agreed to a post-mortem to obtain confirmation of the underlying pathology and disease, and to contribute to research. These cases are very valuable since pathological confirmation is still regarded as the only way to obtain a definite diagnosis of disease. Additionally, some patients had a brain biopsy taken to determine the cause of disease; this usually involves the right (or non-dominant) frontal lobe. Brain biopsy cases are more likely to be younger individuals with dementia where a treatable cause (e.g. vasculitis) is considered.

Whilst including post-mortem confirmed cases in research studies has the great advantage of having a definite confirmation of the underlying pathology in each subject, it may also introduce a bias in that patients may be more atypical and have an earlier onset of disease than patients that did not go to post-mortem and that are typically seen in memory clinics and

referral centres. Therefore, for all studies that included pathologically-confirmed subjects in this thesis, patient notes were reviewed to assess the ante-mortem clinical diagnosis of each subject, ensuring that patients who were included as 'typical amnestic AD' patients did indeed have a typical amnestic presentation during life.

All subjects have given written informed consent and the Local Ethics Research Committee had given approval of all studies detailed in this thesis.

3.3 Clinical assessment

All subjects attending the Specialist Cognitive Disorders Clinic undergo comprehensive diagnostic evaluation. A full history is taken from the patient and (usually separately) from a close informant. A full clinical assessment is performed, which typically includes:

1) Detailed neuropsychology in order to establish the nature and severity of any cognitive deficits.

2) Standard screening blood tests to exclude other treatable causes of cognitive problems such as impaired renal or liver function, B12 and thyroid function.

3) EEG to exclude seizures, or identify patterns indicative of a particular type of dementia.

4) Neuroimaging, typically MRI, in order to exclude other treatable causes such as tumours and subdural haematomas and assess patterns of atrophy and vascular disease.

In addition to the routinely administered assessments above, patients may also undergo:

1) Genetic testing: In affected individuals with an age at onset or family history suggestive of an autosomal dominant inheritance, screening for known genetic mutations (AD or FTLD as appropriate) may be undertaken. In at risk cases where individuals have a known mutation in their family, genetic testing may be offered to determine whether the subject is carrying the mutation. This is supported by a genetic counselling service.

2) Lumbar puncture and CSF analysis: This investigation may be used to detect evidence of inflammation and to measure neuron-specific proteins (tau and Aβ1-42).

3.4 Patient inclusion criteria

All PCA and typical, amnestic AD patients included in research studies described in this thesis had to fulfil a number of stringent inclusion criteria based on performance on specific neuropsychological tests. These are designed to minimize the overlap between these two groups whilst excluding suspected non-AD pathologies where possible.

3.4.1 PCA

Individuals were only included in the PCA group if clinical assessment and investigation did not suggest a non-AD dementia (e.g. DLB, CBD) and if they also fulfilled the following behavioural criteria: i) relatively preserved episodic memory (>5th percentile on a Recognition Memory Test; Warrington, 1984; Warrington, 1996) and ii) neuropsychological deficits (<5th

percentile) in at least two of the following four tests of posterior functions: 1) object perception (VOSP (Visual Object and Space Perception Battery) Object Decision test; Warrington and James, 1991, Appendix 4); 2) space perception (VOSP Number Location test, Appendix 4); 3) calculation (Graded Difficulty Arithmetic test; Jackson and Warrington, 1986) and 4) spelling (Graded Difficulty Spelling test; Baxter and Warrington, 1994). In addition to these neuropsychological criteria, all PCA patients fulfilled the clinical criteria proposed by Mendez et al. and Tang-Wai et al., summarized in chapter 1 (section 1.2.2.5), and Appendix 2 (Mendez et al., 2002; Tang-Wai et al., 2004). It should be noted that, whilst all PCA patients had to fulfil the above criteria at some stage in their clinical history, at the time of experimental investigations some PCA patients may have progressed to a more global pattern of impairment including memory impairment.

3.4.2 Typical, amnestic AD

Typical AD patients had to fulfil NINCDS-ADRDA criteria for probable AD with recently proposed revisions (Dubois et al., 2007; McKhann et al., 1984), and had to have a history suggestive of an amnestic presentation. Those individuals with typical AD who were included for comparisons with PCA also had to demonstrate significant episodic memory impairment (<5th percentile on verbal and visual Recognition Memory Tests; Warrington, 1984; Warrington, 1996).

3.5 Imaging

3.5.1 MRI acquisition

The majority of scans were acquired on a 1.5T Signa MRI scanner (General Electric, Milwaukee, Wisconsin, USA) using a spoiled gradient echo (SPGR) technique. Scans typically included a sagittal T1-weighted scout sequence, an axial dual-echo sequence (T2-weighted and proton-density weighted) and a T1-weighted volumetric image (124 contiguous 1.5mm slices). A small number of scans were acquired on a Siemens Trio TIM 3T scanner using a magnetization-prepared rapid acquisition with gradient echo (MPRAGE) sequence. Imaging parameters varied according to study, details of which are given in Appendix 5.

3.5.2 Image processing software

Digitised images were transferred to a Linux workstation. A number of different software packages and programs were used for image and statistical analyses.

3.5.2.1 MIDAS

The MIDAS (Medical Information Display and Analysis System) software (Freeborough et al., 1996; Freeborough et al., 1997) allows simultaneous multiplanar display of 3D imaging data. Brain structures, including whole brain (Freeborough et al., 1997) and ventricles, can be delineated using both semi-automated and manual procedures. The whole brain

segmentation tool is semi-automated and uses interactive thresholding, together with a series of erosions and dilations, to separate brain from non-brain-tissue such as scalp and dura. The simultaneous display of orthogonal views allows the operator to outline structures on one view (e.g. coronal view) whilst the segmentation is updated in real time in other views (e.g. sagittal and axial). Different types of registration (linear and non-linear), as described in chapter 2 (sections 2.2.1.3.1 and 2.2.2.1), can be implemented within MIDAS over regions of interest such as whole brain. Quantification of volumes and change in volumes of specific structures can be performed using MIDAS.

3.5.2.2 MATLAB

Matlab (matrix laboratory) is a high-level language and interactive computing environment developed by MathWorks (Sherborn, Massachusetts). It allows matrix manipulations, plotting of functions and data, implementation of algorithms, creation of user interfaces, and interfacing with programs written in other languages. Software packages used in this thesis which were implemented in Matlab include SPM (section 3.5.3.2.1) and SurfStat (section 3.5.4.2.2).

3.5.3 Image analysis techniques

3.5.3.1 Visual rating scales

Visual rating scales are a convenient way of assessing atrophy patterns and may aid differential diagnosis in a clinical setting. Two different scales were used in this thesis: Scheltens scale to assess medial temporal lobe atrophy (MTA) (Scheltens et al., 1992) and a novel scale assessing posterior atrophy (PA) which was developed by Esther Koedam (VU Medical Centre, Amsterdam) and me.

3.5.3.1.1 Medial temporal lobe atrophy (MTA) scale

Visual ratings of MTA using Scheltens scale (Scheltens et al., 1992) are typically performed on T1-weighted images viewed in the coronal plane. The MTA scale rates atrophy on a 5-point scale (Figure 3.1): 0 = absent, 1 = minimal, 2 = mild, 3 = moderate and 4 = severe, based on the width of the choroid fissure, the height of the hippocampus, and the width of the temporal horn. Separate scores for the left and right hemispheres are acquired.

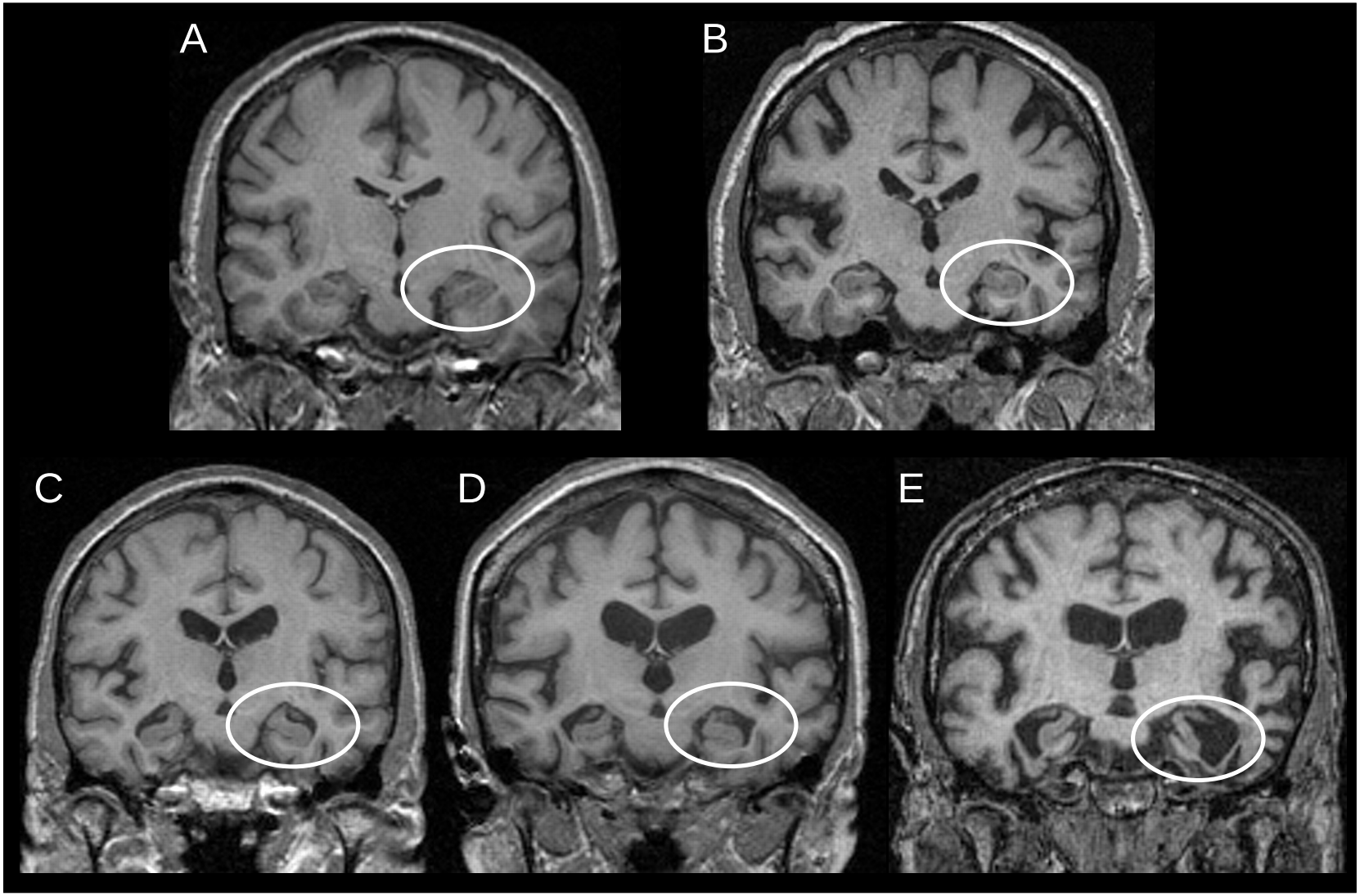

Figure 3.1: Scheltens scale of medial temporal lobe atrophy. This 5-point scale rates the degree of atrophy in the medial temporal lobes based on the height of the hippocampal formation and the width of the choroid fissure and the temporal horn (circled region): **A)** grade 0=no atrophy; **B)** grade 1=minimal atrophy; **C)** grade 2=mild atrophy; **D)** grade 3=moderate atrophy; **E)** grade 4=severe atrophy.

3.5.3.1.2 Posterior atrophy (PA) scale

The PA scale was developed in conjunction with Esther Koedam (Amsterdam) and is described in detail in chapter 5, section 5.2. In brief, PA was scored on T1-weighted images viewed in the sagittal, axial and coronal planes. Separate scores for the left and right hemispheres were obtained. The 4-point scale (0 = no atrophy, 1 = mild widening of the sulci without evident volume loss of the gyri, 2 = substantial widening of the sulci and volume loss of the gyri, grade 3 = severe end-stage atrophy) includes the posterior cingulate sulcus, precuneus, parietal-occipital sulcus and parietal lobe. An overall score was given based on the presence of atrophy in all these regions. When there was a difference between scores in the different planes (e.g. score 1 for the sagittal view and score 2 for the axial view), the highest score was given.

3.5.3.2 Image processing for voxel or vertex-wise whole brain analyses

3.5.3.2.1 VBM

VBM analyses were performed using either SPM version 5 or 8 (specified in corresponding chapters). Images were first converted to NIFTI (http://nifti.nimh.nih.gov) format and rigidly reoriented to standard space (ICBM template). The reoriented scans were then segmented into grey and white matter using a unified model (Ashburner and Friston, 2005). Default values were used for bias regularization (0.0001) and full-width at half-maximum (FWHM) cut-off (60 mm). The resulting grey and white matter segments of all subjects were then imported for use with DARTEL (Ashburner, 2007) which iteratively registered the segments to an evolving estimate of their group-wise average. The segments were then normalized using the DARTEL transformations, modulated to account for local volume changes, and finally smoothed with a 6mm FWHM kernel. The smoothed modulated DARTEL-imported segments were then used for the analysis. Note that the procedure of using DARTEL-imported segments is described as an 'alternative approach' in the SPM8 manual (www.fil.ion.ucl.ac.uk/spm/doc/manual.pdf). It differs to the more standard approach of normalising all images to MNI space. In this thesis, coordinates extracted of specific clusters therefore represent DARTEL coordinates which were converted to MNI coordinates as specified in the corresponding chapters.

3.5.3.2.2 FreeSurfer

Cortical thickness analyses were performed using version 4.0.3, 4.1.0, 4.3.0 or 4.5.0 (the particular version is specified where used). An overview of bug fixes, new features and remaining issues for each version can be found on http://surfer.nmr.mgh.harvard.edu/fswiki/ReleaseNotes. One important fix concerns changes to the longitudinal stream in version 4.5.0. Improvements to the longitudinal stream include

the creation of a template brain using all time points which is used to initiate the actual surface reconstructions for each time, avoiding bias towards any one time point (chapter 2, section 2.2.2.2).

Image processing in FreeSurfer involved the following steps: intensity normalisation, skull stripping, segmentation of white matter, and tessellation of the grey/white matter boundary, inflation of the folded surface tessellation patterns and automatic topology correction. This surface was then used as the starting point for a deformable surface algorithm to find the grey/white and grey/CSF surfaces. This method uses both intensity and continuity information from the surfaces in the deformation procedures to produce representations of cortical thickness, calculated as the closest distance from the grey/white boundary to the grey/CSF boundary at each vertex on the tessellated surface. Thickness measures were mapped to the inflated surface of each subject's brain reconstruction, allowing visualization of data across the entire cortical surface. All images were aligned to a common surface template using a high-resolution surface-based averaging technique that aligned cortical folding patterns. Cortical thickness was smoothed with a 20mm FWHM surface-based Gaussian kernel to reduce local variations in the measurements for further analysis.

In all FreeSurfer analyses described in this thesis, two modifications to the standard FreeSurfer processing stream were undertaken. First, a different skull stripping algorithm was applied which used a brain mask which was locally generated by a semi-automated segmentation procedure within MIDAS (section 3.5.2.1, Freeborough et al., 1997). Secondly, the white matter mask was modified by adding the ventricle segmentations from the FreeSurfer volume processing stream to improve the ventricle regions and limit the misclassification of CSF.

All images were carefully visually inspected to ensure accurate identification of the grey/white matter boundary and the pial surface. Most scans underwent manual editing involving the addition of control points as well as changes to the white matter segmentations and the brain masks, as suggested on http://surfer.nmr.mgh.harvard.edu/fswiki/FsTutorial/Troubleshooting. Whilst manual editing may have introduced a bias into the results, all edits were performed before group differences were examined. However, the editing process resulted in improved grey matter segmentations as determined by visual inspection. To the best of my knowledge, there is, to date, no study that has systematically evaluated potential biases and effects of manual editing on the results obtained by FreeSurfer. It should further be noted that rerunning the longitudinal cortical analysis (chapter 7) using unedited scans produced very similar results to those presented in this thesis. Further details on how much editing was performed in each study are given in corresponding chapters.

3.5.4 Statistical models and software

3.5.4.1 Stata

Most statistical analyses in this thesis were conducted in STATA (Stata Corporation, College Station, TX, USA). STATA is a standard statistical package used for performing basic statistical analyses and producing graphs. Version 10 (Intercooled) was used for the majority of statistical analyses in this thesis. Demographical univariate group differences were analysed using t-tests and ANOVAs for continuous variables and χ^2 tests for categorical data unless specified.

3.5.4.2 Voxel and vertex-wise analyses

3.5.4.2.1 VBM statistical analysis

For the analysis, an explicit mask was applied to include only voxels for which the intensity was at least 0.1 in at least 80% of the images. This was preferred to the default 'absolute thresholding' mask option in SPM which would exclude any voxels for which one or more images had a value of less than 0.1 and therefore perhaps be unduly influenced by a single very atrophic or poorly registered scan (Ridgway et al., 2009). Results are displayed as overlays on a study-specific template which was created by normalizing all native space images using the DARTEL transformations and calculating the average of the warped brain images. A general linear model was typically used as described below.

3.5.4.2.2 FreeSurfer statistical analysis

Cortical thickness data from FreeSurfer were analysed and visualized using a Matlab toolbox called SurfStat (http://www.math.mcgill.ca/keith/surfstat). This is a freely available tool downloadable from the web which can be used for the statistical analysis of univariate and multivariate surface and volumetric data. Again, a general linear model was typically used as described below.

3.5.4.2.3 General linear model (GLM)

Imaging data were typically analysed using a general linear model (GLM). A GLM is a statistical linear model which can be expressed as follows: $Y = b*x + \varepsilon$, where Y is a matrix with series of multivariate measurements, x is a matrix that might be a design matrix, b is a matrix containing parameters that are usually to be estimated and ε is a matrix containing errors or noise.

In the studies described in this thesis, GLMs were performed on a vertex-by-vertex or voxel-by-voxel level. Atrophy A (i.e. volume or thickness) is typically modelled as a function of

group, controlling for specific co-variates, such as age, gender and TIV. For example, a GLM to compare two groups adjusting for age, gender and TIV looks as follows: $A = \beta_1 group_1 + \beta_2 group_2 + \beta_3 age + \beta_4 gender + \beta_5 TIV + \varepsilon$. The contrasts of interest were then calculated using t-tests (two-tailed for FreeSurfer, one-tailed for VBM) between the estimates of the group parameters, e.g. β_1 and β_2 to compare $group_1$ with $group_2$. The specific models used in each study are described in the corresponding chapters.

3.5.4.2.4 Difference maps

Differences between groups are visualized as difference maps. For FreeSurfer analyses, statistically-significant differences are presented as p-maps, whereas for VBM data statistically-significant differences are shown as t-maps. Corrections for multiple comparisons were made to control the false discovery rate (FDR) at a 0.05 level of significance (Genovese et al., 2002). In addition to statistical difference maps, data are also visualized as effect size maps, showing either percent differences or raw differences in mm for cortical thickness data, and correlation coefficients for VBM data. The type of map used in each study is described in the methods section in each chapter.

3.5.4.2.5 Multiple comparison correction

In the studies described in this thesis, FDR correction is the main method used to correct for multiple comparisons. Originally, familywise error (FWE) correction was widely used in neuroimaging studies and was the default technique within SPM. Whilst highly powered studies with multiple scans per subject such as fMRI are able to tolerate this harsh level of correction, structural studies using VBM often show no significance with FWE and numerous early studies resorted to reporting uncorrected data. FDR was introduced by Genovese et al. as an alternative family-wise error procedure (Genovese et al., 2002); FDR procedures are more sensitive because they do not control the false positive rate but the false discovery rate. The false discovery rate is the proportion of tests declared significant that have been falsely declared significant. Whilst FDR correction is widely used to correct for multiple comparisons in neuroimaging studies, recently limitations of this method have been highlighted (Chumbley et al., 2010; Chumbley and Friston, 2009). The problem of conventional FDR procedures is that they regard SPMs as a collection of discrete tests, i.e. inference using false discovery rate treats each voxel as a separate feature. However, when using SPM, inferences are made about a topological feature or clusters above a certain threshold, and not about each voxel in that cluster. This is why usually only clusters are reported, most commonly in terms of their maximum value and location. Conventional FDR procedures control the false discovery rate of voxels, whereas it is more appropriate to control the false discovery rate of features. An alternative correction method has been proposed that controls the false discovery rate of topological features as opposed to voxels. In other words, the FDR procedure can be applied

to the null distribution of features such as cluster-volume or peak height (Chumbley et al., 2010).

3.5.4.2.6 Support vector machine

For classification analyses using volume or thickness data, a linear support vector machine (SVM, chapter 2, section 2.2.1.3.5) was used (Vapnik, 1995; Vapnik, 1998), implemented with LIBSVM version 2.89 (Chang and Lin, 2001) under MATLAB (version 7.2.0). In this thesis, outputs from specific analyses using T1-weighted MR images were used as input into the SVM. More specifically, for SVM analyses in which cortical thickness was used, all vertices were included except the medial wall as defined by FreeSurfer's Desikan parcellation atlas (Desikan et al., 2006). For the classification analyses using longitudinal data (chapter 7), only the grey matter voxel-compression maps (see 7.2.6) were used for the VBM SVM analysis, whereas differences in cortical thickness between two time points (again excluding the medial wall) were used for the FreeSurfer SVM analysis. The C-SVM formulation was used, employing a two-level nested cross-validation to optimize the misclassification penalty parameter C using a leave-one-out procedure within the main leave-one-out loop (Wilson et al., 2009). This ensures an unbiased estimation of generalisation accuracy by leaving each scan in turn entirely out of the training procedure.

4. PATTERNS OF CORTICAL THICKNESS IN PATHOLOGICALLY-CONFIRMED TYPICAL AND ATYPICAL AD AND FTLD

4.1 Chapter introduction

Clinically, patients with AD and FTLD pathology may be difficult to differentiate because of overlapping symptoms (chapter 1, section 1.2) In particular 'atypical' forms of AD showing marked behavioural features ('frontal-variant AD') (Johnson et al., 1999; Taylor et al., 2008) or predominant language deficits (LPA) (Gorno-Tempini et al., 2008) can be difficult to distinguish from patients with FTLD pathology.

A number of studies have used MRI to assess brain atrophy in these disorders (chapter 2, section 2.5). These patterns of atrophy may aid diagnosis; an *in vivo* atrophy 'signature' may predict the underlying pathology (Likeman et al., 2005). In many research studies, however, pathological confirmation is lacking and 'clinically diagnosed' patients are included. Clinical prediction of histopathology is inevitably imperfect; more importantly there is a risk of circularity. Clinically diagnosed subjects may reflect 'typical' presentations of these diseases as the purpose of clinical criteria is to describe the most typical presentations to reduce misdiagnosis.

In this chapter, the term frontotemporal dementia (FTD) refers to the clinical (frontotemporal) syndrome including both behavioural and language variants, whereas FTLD refers to the confirmation of tau- or ubiquitin-positive pathology. Furthermore, the term 'typical AD' refers to patients with a typical amnestic presentation of AD and underlying AD pathology, whereas 'atypical' AD in this study refers to patients with AD pathology but who had a clinical diagnosis of either FTD or PCA. Within this group, the term AD-FTD refers to those patients who presented with FTD symptoms (behavioural or language deficits) and yet had underlying AD pathology at autopsy.

Atrophy patterns were investigated in patients with pathology confirmation including atypical and typical clinical presentations of AD and FTLD. Non-amnestic presentations of AD were incorporated including language and behavioural presentations which are more likely to overlap with FTLD in terms of atrophy. The aim of this study was to assess the commonality of cortical thickness patterns between patients with AD pathology who presented with either typical amnestic deficits or atypical non-amnestic deficits during life. Patients clinically diagnosed as FTD were further investigated to assess whether there were differences in cortical atrophy patterns between those who were subsequently found to have AD pathology and those with FTLD pathology.

4.2 Methods

4.2.1 Subjects

62 patients were initially selected from a database of pathologically-confirmed cases: 32 individuals with a pathological diagnosis of AD and 30 subjects with pathologically-confirmed FTLD who had undergone volumetric MR imaging as part of their diagnostic work-up. Twenty-five healthy controls that had undergone MRI assessment were also included. Some of these patients have been included in previous imaging studies (Barnes et al., 2007a; Kloppel et al., 2008; Rohrer et al., 2009). Subjects with mixed AD and DLB pathology were excluded.

The clinical notes were retrospectively reviewed by a clinician to determine the clinical ante-mortem presentation of each patient. Based on this, pathologically-confirmed AD subjects were divided into typical and atypical AD. Typical AD patients were defined as those who presented with amnestic deficits during life and had been diagnosed ante-mortem with AD according to NINCDS-ADRDA criteria (McKhann et al., 1984). In contrast, atypical AD patients presented predominantly with language, behavioural or visuoperceptual and visuospatial deficits (Figure 4.1). After image processing, 11 subjects were excluded (see below). The study therefore included 28 AD patients, 23 with FTLD, and 25 controls: the demographics of the 76 subjects included are summarized in Table 4.1. Of the 11 typical AD subjects, 10 had post-mortem and 1 had brain biopsy confirmation. Of the 17 atypical AD subjects, 12 had post-mortem confirmation and 5 had biopsy confirmation. This group consisted of 9 patients who had a clinical diagnosis of PPA, 6 patients with PCA, and 2 patients with bvFTD (Figure 4.1). Of the 23 pathologically-confirmed FTLD subjects, 20 had post-mortem confirmation and 3 had brain biopsy. The FTLD group comprised 10 tau-positive patients (5 bvFTD, 4 PNFA, 1 atypical SemD) and 13 tau-negative, ubiquitin-positive patients (10 SemD and 3 bvFTD). All FTLD subjects had been clinically-diagnosed with FTD (Neary et al., 1998).

4.2.2 MRI acquisition

Images were acquired as described in chapter 3 (section 3.5.1) and Appendix 5.

4.2.3 Image processing

Cortical thickness measurements were made using FreeSurfer version 4.0.3 (chapter 3, section 3.5.3.2.2). All images were visually inspected and on average edited and re-run three times. At this stage, as mentioned above, four individuals with AD and seven with FTLD were excluded due to poor image quality causing poor segmentations.

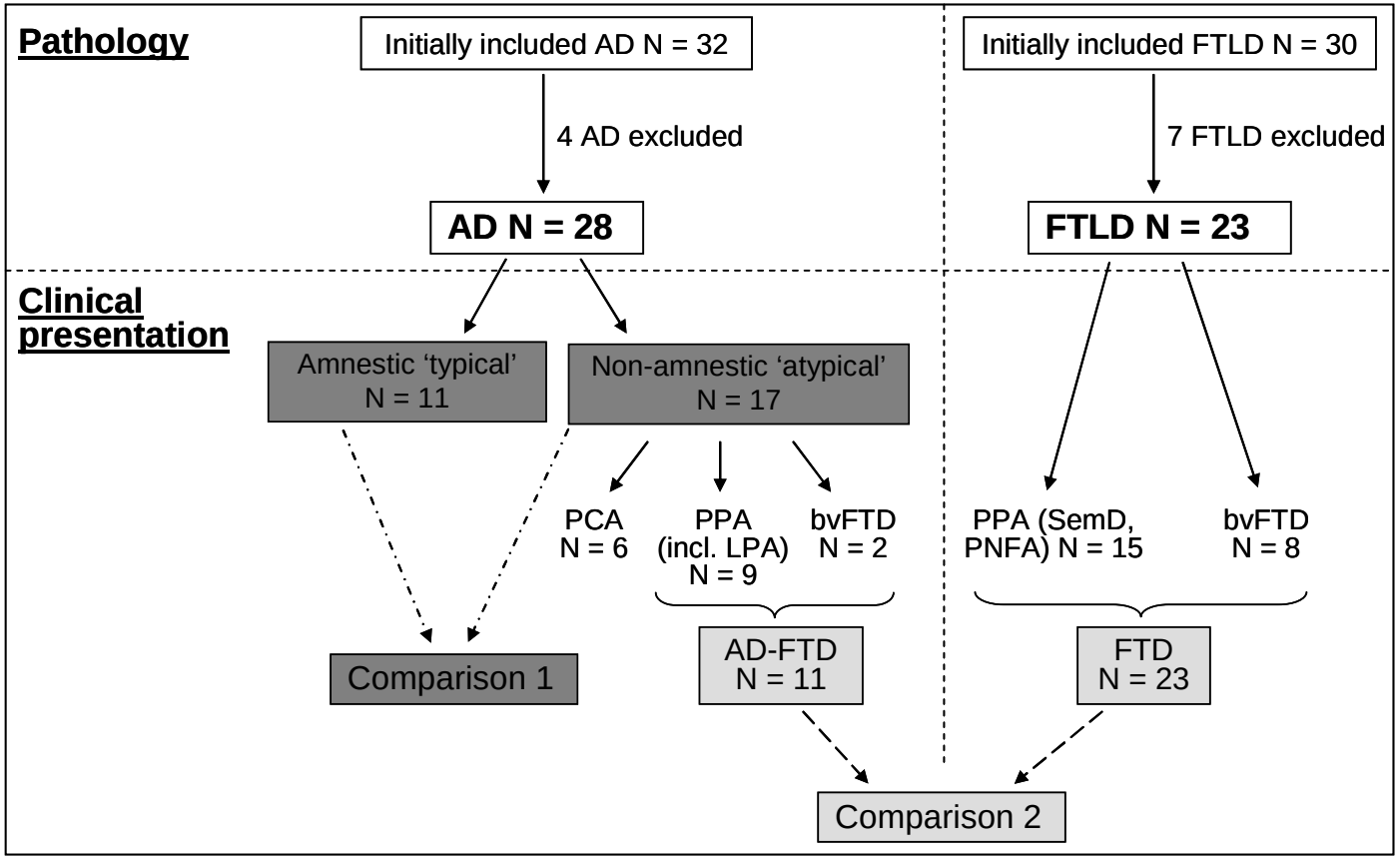

Figure 4.1: Overview groups and comparisons. Comparison 1 assessed differences in cortical thickness between patients with underlying AD pathology but different clinical presentations ('typical' amnestic vs. 'atypical' non-amnestic), whereas comparison 2 assessed differences in cortical thickness between patients with a clinic presentation of FTD and underlying AD pathology (AD-FTD) vs. FTD patients with FTLD pathology (FTD).

4.2.4 Statistical analysis

Regional cortical thickness variations between the patient groups and the control group were assessed using a vertex-by-vertex GLM (chapter 3, section 3.5.4.2.3). Cortical thickness (C) was modelled as a function of group, controlling for age (mean-centred), gender and scanner by their inclusion as covariates. Separate models were used for the two comparisons of interest.

Comparison 1 assessed cortical thickness in typical and atypical AD, and was modelled $C = \beta_1$ (controls) + β_2 (typical AD) + β_3 (atypical AD) + β_4 age + β_5 gender + β_6 scanner + ε, contrasting β_1 vs. β_2 (controls vs. typical AD), β_1 vs. β_3 (controls vs. atypical AD), and β_2 vs. β_3 (typical AD vs. atypical AD; see Figure 4.1). Contrasts were calculated using two-tailed t-tests.

Comparison 2 assessed cortical thickness in AD-FTD (including the clinically diagnosed PPA and bvFTD patients with AD pathology) vs. FTLD, and was modelled $C = \beta_1$ (controls) + β_2 (AD-FTD) + β_3 (FTLD) + β_4 age + β_5 gender + β_6 scanner + ε, contrasting β_1 vs. β_2 (controls vs. AD-FTD), β_1 vs. β_3 (controls vs. FTLD), and β_2 vs. β_3 (AD-FTD vs. FTLD, see Figure 4.1). Maps were produced showing percentage differences in average cortical thickness and statistically significant differences with FDR correction at $p<0.05$. Intersection maps highlight regions where the two patient groups commonly showed differences compared with controls.

4.2.5 Support vector machine (SVM)

Images were analysed using an SVM as described in chapter 3 (section 3.5.4.2.6). The same scans as in the vertex-wise statistical comparisons described above were used for this analysis. The comparison of interest was the classification of the FTLD and AD-FTD groups (which relates to comparison 2 described above, see Figure 4.1), i.e. assessing how well patients with a clinical diagnosis of FTD who were subsequently found to have either AD or FTLD pathology can be classified into their respective group.

4.3 Results

4.3.1 Subjects

No significant differences across groups were found for gender, disease duration and time to death (Table 4.1). Age difference across all groups was not significant, however, the atypical AD group was significantly younger than controls and the typical AD group ($p<0.05$). MMSE scores were significantly different across groups ($p<0.001$), driven by statistically significant differences between patient groups and controls ($p<0.001$), as well as significantly higher MMSE scores in the FTLD group compared with typical and atypical AD ($p<0.001$ and $p<0.01$ respectively).

Table 4.1: Subject demographics.

	N	Gender [§ NS]	Age in years at scan [¶ NS]	MMSE at scan [¶ ¥ *]	Disease duration at scan [¶ NS]	Time to death from scan [¶ NS†]	Scanner			
		% male	mean (SD)	mean (SD)	mean (SD)	mean (SD)	a	b	c	d
Controls	**25**	**68%**	**64.2 (9.4)**	**29.3 (0.9)**	**-**	**-**	**6**	**15**	**0**	**4**
Typical AD	**11**	**73%**	**68.0 (10.5)**	**14.4 (7.0)**	**3.6 (2.3)**	**3.8 (2.7)**	**4**	**7**	**0**	**0**
Atypical AD	**17**	**53%**	**59.2 (6.5)**	**17.7 (6.9)**	**3.7 (1.5)**	**4.7 (1.7)**	**0**	**14**	**3**	**0**
PPA	9	67%	58.6 (6.9)	16.6 (7.1)	3.8 (1.2)	3.5 (1.3)	0	7	2	0
PCA	6	33%	60.2 (7.5)	22.2 (4.3)	3.4 (2.2)	6.0 (0.9)	0	5	1	0
bvFTD	2	50%	59.0 (1.4)	9.5 (0.7)	4.4 (1.0)	6.6	0	2	0	0
FTLD	**23**	**57%**	**62.5 (10.1)**	**23.4 (5.6)**	**4.3 (2.1)**	**6.0 (3.4)**	**0**	**18**	**2**	**3**
SemD	11	55%	65.9 (6.0)	22.2 (5.6)	4.3 (2.4)	8.0 (3.0)	0	7	1	3
bvFTD	8	50%	58.3 (14.2)	22.7 (5.1)	4.3 (2.3)	3.6 (2.3)	0	7	1	0
PNFA	4	75%	62.8 (6.9)	27.7 (1.2)	4.4 (0.7)	4.0 (2.6)	0	4	0	0

[§] Fisher's exact test; [¶] ANOVA; * $p<0.001$; [†] available in 10 typical AD, 13 atypical AD (7PPA, 5 PCA, 1bvFTD), and 21 FTLD (11SemD, 7bvFTD, 3PNFA); [¥] available in 12 controls, all typical and atypical AD, and 20 FTLD (10 SemD, 7 bvFTD, 3 PNFA); a, b, c, d - different 1.5T GE scanners (Appendix 5); NS = not significant

4.3.2 Comparison 1: typical vs. atypical AD

Compared with controls, typical AD showed lower thickness across the cortex, with the most prominent reduction bilaterally in the medial and posterior temporal regions, posterior cingulate gyrus, and frontal lobe regions (Figure 4.2A). The atypical AD group showed reduced cortical thickness bilaterally in the medial temporal lobe, posterior cingulate gyrus, precuneus, posterior parietal lobe, and frontal pole compared with controls (Figure 4.2B). The intersection map shows areas of reduced cortical thickness common to both typical and atypical AD compared with controls (Figure 4.2C) bilaterally in the medial temporal lobe, posterior cingulate gyrus, precuneus, posterior parietal lobe, and frontal pole.

The direct comparison of typical and atypical AD showed lower cortical thickness predominantly in the left posterior temporal lobe and left occipital lobe in the typical AD group compared with atypical AD (Figure 4.3A). However, this difference was reduced when including disease duration as covariate, and disappeared completely when correcting for MMSE. No regions were found to be significantly thinner in the atypical AD group compared with typical AD. However, the percent difference maps indicate trends towards lower cortical thickness bilaterally in the precuneus and superior parietal lobe in the atypical compared with typical AD group (Figure 4.3B).

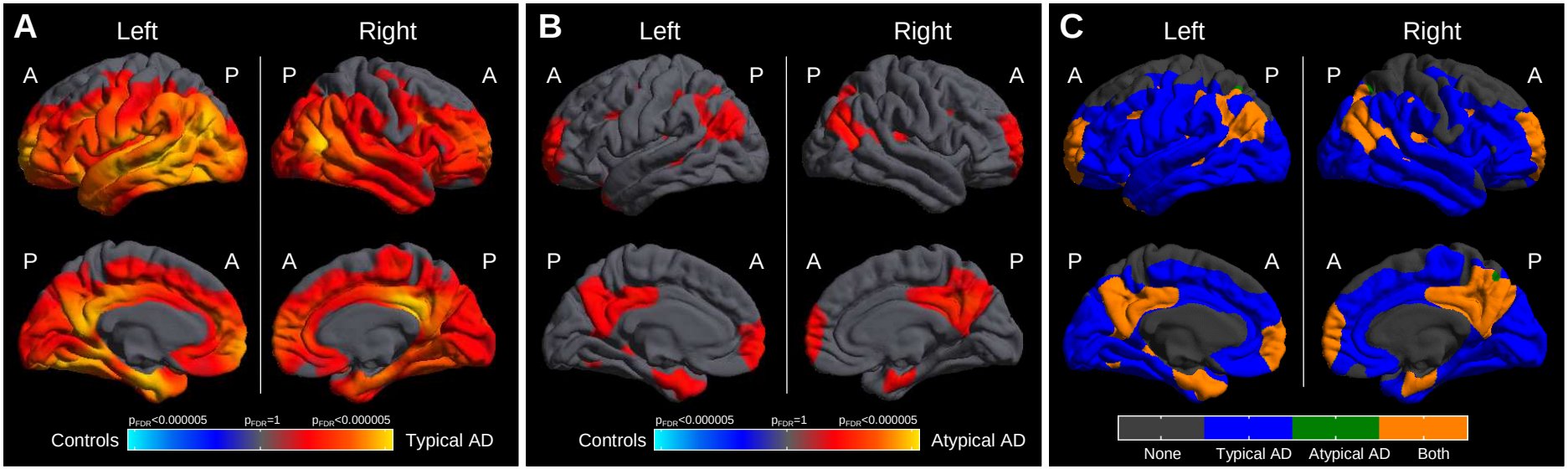

Figure 4.2: Differences and similarities in reduced cortical thickness in typical and atypical AD compared with controls. The figure shows differences in cortical thickness between **A)** typical AD and controls, and **B)** atypical AD and controls. The colour scale represents FDR-corrected p values thresholded at a 0.05 significance level. Red and yellow represent lower cortical thickness in the patient group, whereas blue represents lower cortical thickness in the control group. **C)** Intersection map showing regional differences in cortical thickness between typical AD and controls, and atypical AD and controls. Blue represents areas which are reduced in the typical AD group only, green represents regions which are reduced in atypical AD only, and orange shows areas which are reduced in both typical and atypical AD compared with controls.

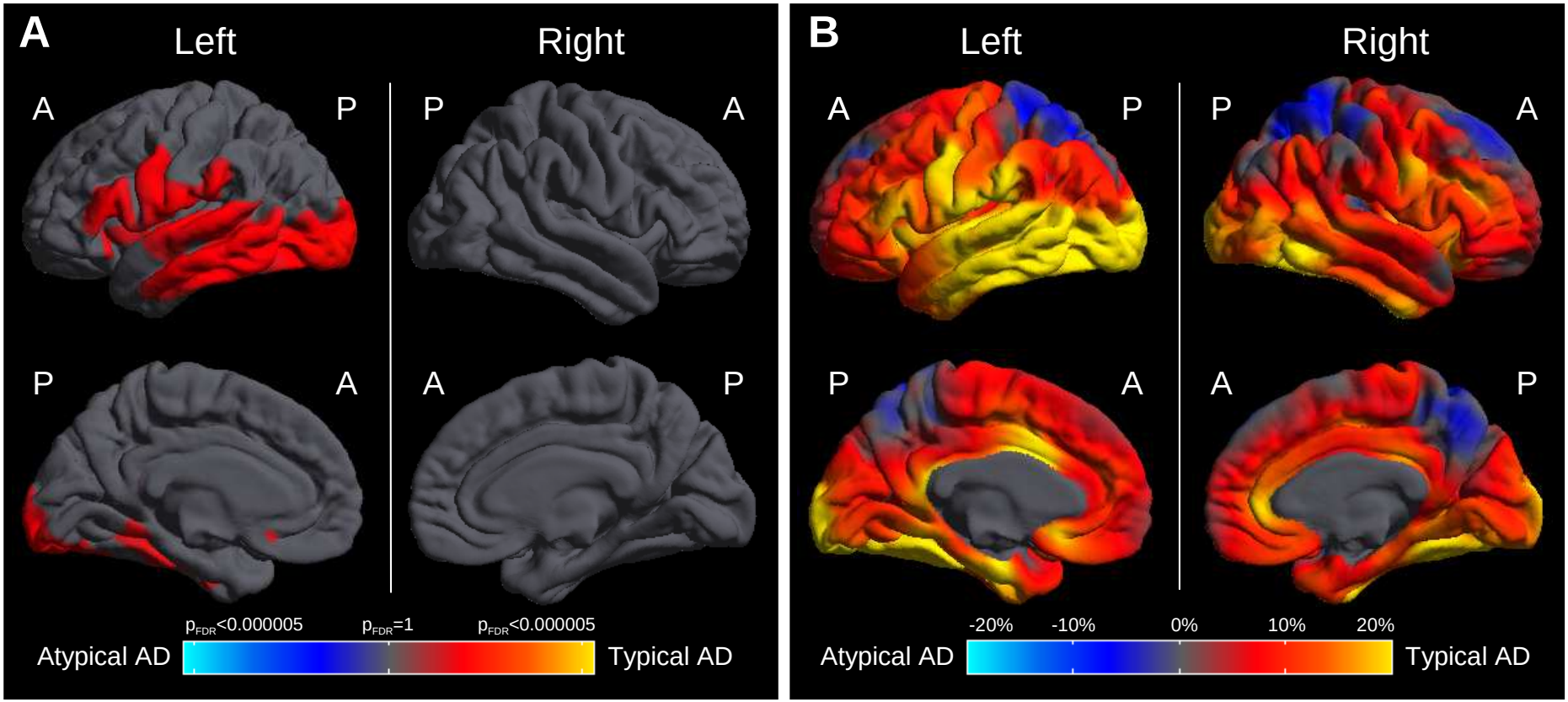

Figure 4.3: Differences in reduced cortical thickness between typical and atypical AD. Differences in cortical thickness between typical and atypical AD are shown as **A)** statistical difference map, and **B)** percent difference map. The colour scale of the statistical difference map represents FDR-corrected p values thresholded at a 0.05 significance level whereas the colour bar for percent difference represents magnitude of cortical thickness group difference expressed as a percentage of mean thickness across both groups (adjusted for age, gender and scanner). Red and yellow represent lower cortical thickness in the typical AD group, whereas blue represents lower cortical thickness in the atypical AD group.

4.3.3 Comparison 2: AD-FTD vs. FTLD

Compared with controls, AD-FTD patients showed lower cortical thickness in the left superior temporal lobe, as well as bilaterally in the posterior cingulate gyrus, precuneus, left posterior parietal lobe and bilateral frontal pole (Figure 4.4A). The FTLD group showed widespread thinning with the most prominent reductions found bilaterally in the anterior temporal lobe (Figure 4.4B). The intersection map reveals regions in which both AD-FTD and FTLD show reduced cortical thickness compared with controls which include the bilateral posterior cingulate gyrus, left superior temporal lobe and left medial temporal lobe (Figure 4.4C).

Differences in cortical thickness between AD-FTD and FTLD in a direct comparison did not reach statistical significance after FDR correction. However, percent difference maps show tendencies of reduced thickness bilaterally in the anterior temporal lobe and frontal lobe regions in the FTLD group compared with AD-FTD, whereas the AD-FTD group showed lower cortical thickness in left posterior parietal regions, bilaterally in the precuneus, posterior cingulate gyrus and, perhaps surprisingly, frontal pole compared with FTLD (Figure 4.5A).

The classification analysis of AD-FTD vs. FTLD produced a classification accuracy of 79.4% with 95% confidence intervals [62.1%, 91.3%]. Of the AD-FTD patients 54.5% [23.4%, 83.3%] were correctly classified (sensitivity), whereas 91.3% [72.0%, 98.9%] of the FTLD patients were correctly classified (specificity). The area under the receiver operating characteristic (ROC) curve is 0.87 (Figure 4.6). Areas in which reduced cortical thickness contributed most to the classification of AD-FTD were shown bilaterally in the posterior cingulate gyrus, posterior parietal lobe, precuneus, medial temporal lobe, and frontal pole (Figure 4.5B). In contrast, regions which contributed most towards a classification of FTLD were shown bilaterally in frontal lobe regions and the lateral temporal lobe.

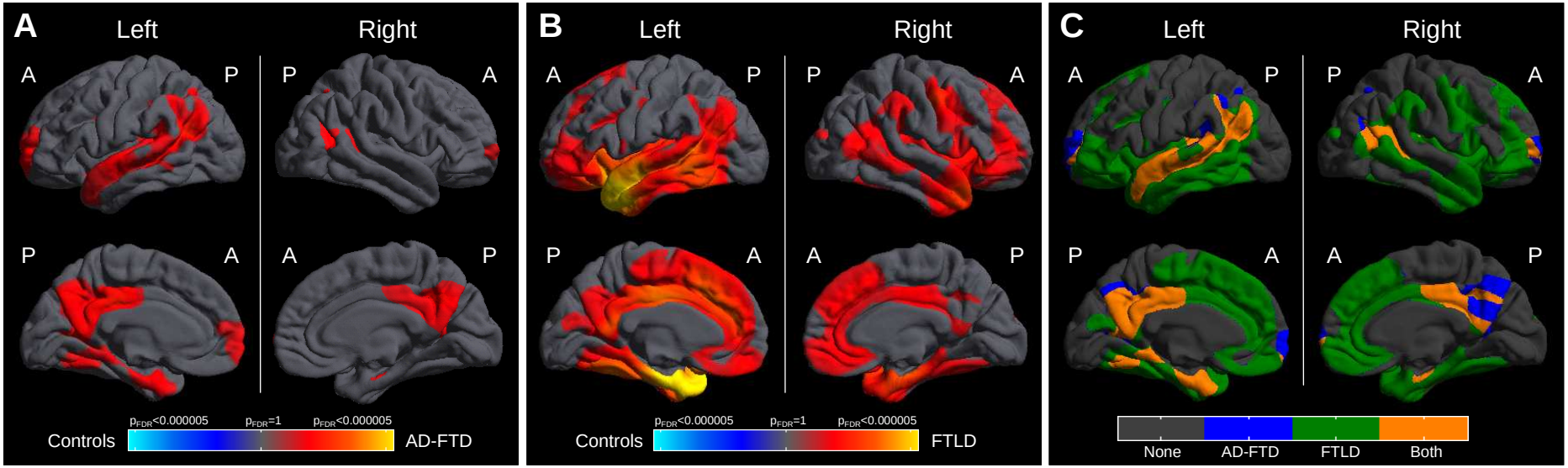

Figure 4.4: Differences and similarities in reduced cortical thickness in AD-FTD and FTLD compared with controls. Differences in cortical thickness are shown between **A)** AD-FTD and controls, and **B)** FTLD and controls. The colour scale represents FDR-corrected p values thresholded at a 0.05 significance level. Red and yellow represent lower cortical thickness in the patient group, whereas blue represents lower cortical thickness in the controls. **C)** Intersection map showing regional differences in cortical thickness between AD-FTD and controls, and FTLD and controls. Blue represents areas which are reduced in the AD-FTD group only, green represents regions which are reduced in FTLD only, and orange shows areas which are reduced in both AD-FTD and FTLD compared with controls.

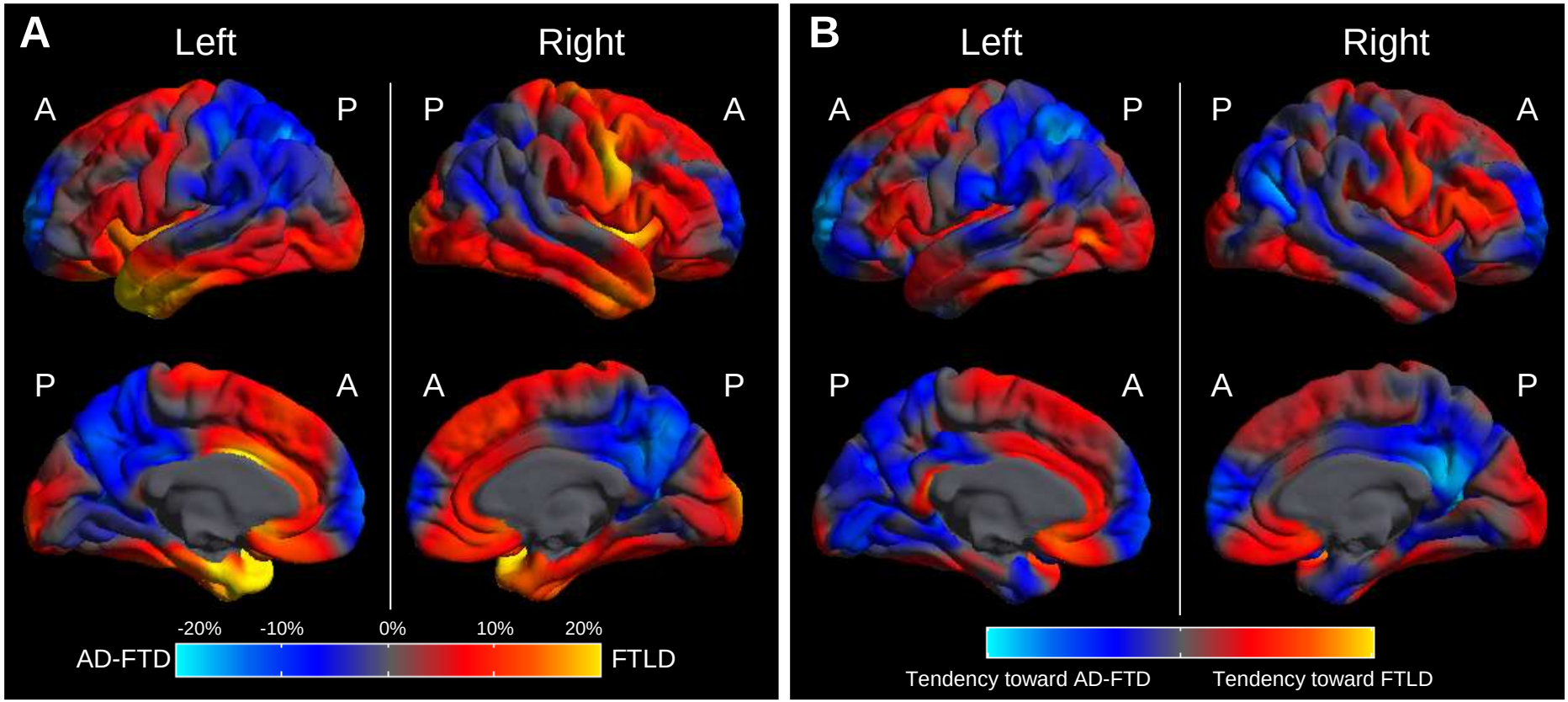

Figure 4.5: Differences in reduced cortical thickness between AD-FTD and FTLD. A) Regional differences in cortical thickness between AD-FTD and FTLD shown as percent difference map. The colour bar represents magnitude of cortical thickness group difference expressed as a percentage of mean thickness of both groups (adjusted for age, gender and scanner). Red and yellow represent lower cortical thickness in the FTLD group, whereas blue represents lower cortical thickness in the AD-FTD group. **B)** Classification map showing regions that were most influential in making a classification between AD-FTD and FTLD. Red represents areas where low cortical thickness indicates FTLD, whereas blue shows areas where lower cortical thickness indicates AD-FTD.

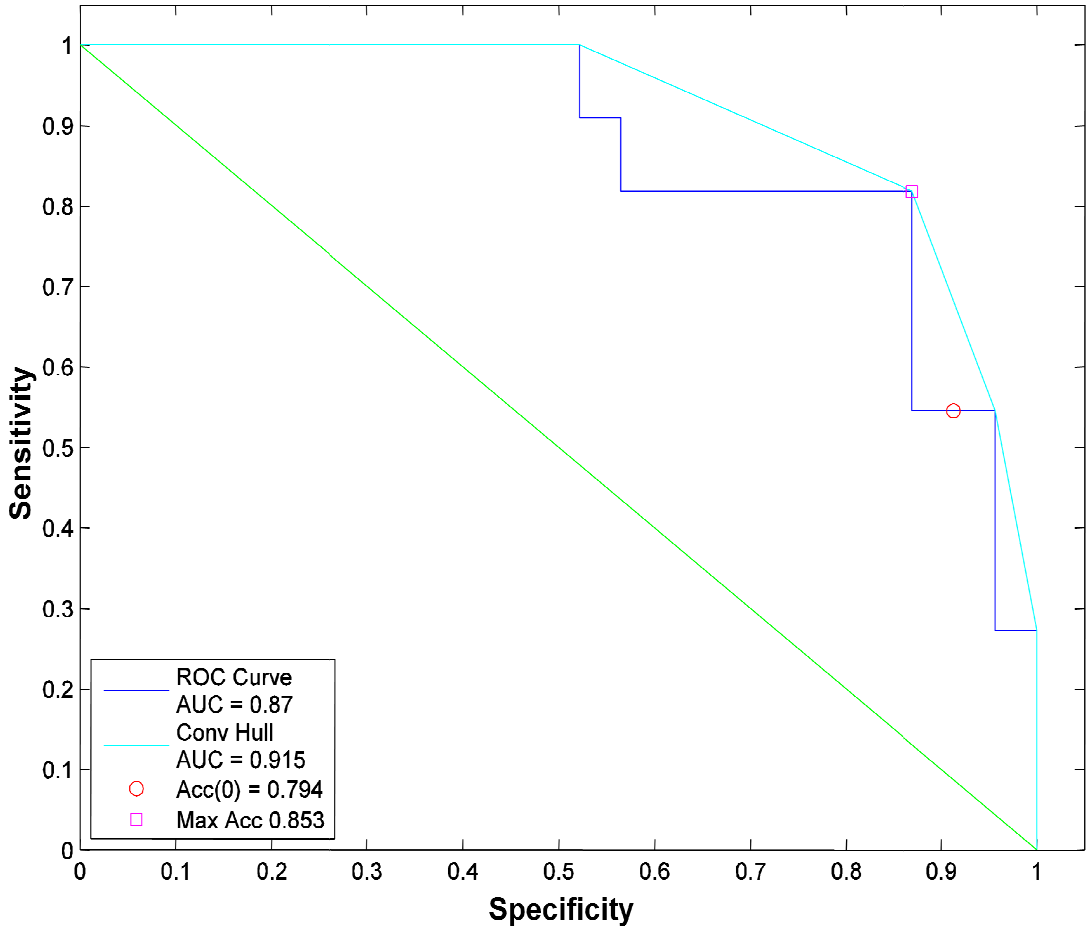

Figure 4.6: ROC curve for classification of AD-FTD vs. FTLD. Shown is the trade-off between sensitivity and specificity. The ROC curve is plotted by varying the decision threshold. The low sensitivity reported in the results arises from unbalanced group numbers, which allow high accuracy from high specificity. The ROC curve shows that relatively high sensitivity and specificity are simultaneously achievable if the threshold is altered. AUC - area under the curve, acc - accuracy.

4.4 Discussion

This study describes the patterns of cortical thinning in pathologically-confirmed AD and FTLD. Patients with AD pathology and a typical amnestic presentation during life showed reduced cortical thickness bilaterally in the medial temporal lobe, posterior cingulate gyrus, precuneus, posterior parietal regions, and frontal lobe. The association of an amnestic presentation of AD with medial temporal lobe atrophy was expected (Du et al., 2007; Ridha et al., 2006; Teipel et al., 2006). The finding of prominent thinning in the posterior cingulate cortex and precuneus concurs with increasing recognition that atrophy as well as hypometabolism in these regions is characteristic of AD (Barnes et al., 2007a; Mosconi, 2005; see also chapter 2, section 2.5.2). However, frontal pole involvement was less expected.

A similar pattern of cortical thinning, compared with controls, was found in patients with AD pathology who had a different ante-mortem clinical diagnosis; however, thinning was less widespread, perhaps reflecting the mix of 'focal' presentations of AD in this group. A direct comparison between these two patient groups revealed greater loss in left posterior temporal lobe and left occipital lobe regions in the typical AD group compared with atypical AD. The fact that this difference is diminished after correcting for disease duration and MMSE may suggest that these differences simply reflect severity differences. However, mean disease duration was almost identical between groups. Disease progression in typical and atypical forms of AD may vary which means that disease duration is not a very accurate marker of disease severity. MMSE is also an imperfect indicator of disease severity in dementias with different cognitive profiles, and the high mean MMSE in atypical AD subjects is largely driven by the PCA subjects included.

The intersection analysis illustrates the commonality of cortical thinning in typical and atypical AD. Cortical thickness was reduced in both the typical and atypical AD groups, compared with controls, bilaterally in the medial temporal lobe, posterior cingulate gyrus, precuneus, posterior parietal lobe and frontal pole. Cortical thinning in these regions appears to indicate the presence of AD pathology irrespective of clinical presentation. Cortical thinning in the medial temporal lobe in typical and atypical AD is consistent with the presence of memory deficits at the time of scan in both groups. Our general AD-specific findings are in accordance with previous imaging studies which investigated differences in cortical thickness (Du et al., 2007; Lerch et al., 2005) and grey matter volume using VBM (Baron et al., 2001; Busatto et al., 2003) in typical forms of AD.

A strong involvement of the posterior cingulate gyrus in AD has been shown in a number of structural (Barnes et al., 2007a; Baron et al., 2001; Boxer et al., 2003; Jones et al., 2006) and functional imaging studies (Lustig et al., 2003). Most functional imaging studies (PET, SPECT and fMRI) have reported reduced activity in this region in early stages of the disease (Johnson et al., 1998; Matsuda, 2001; Minoshima et al., 1997). The regions showing reduced cortical thickness in pathologically-confirmed AD patients in our study are consistent with those associated with the 'default mode' network (Greicius et al., 2004). Our finding adds to the growing number of studies suggesting that functional imaging findings are not as dissociated from atrophy as was once thought; temporal associations, however, remain unclear (Villain et al., 2008).

The involvement of the frontal lobe in AD, and more specifically of the prefrontal cortex and frontal pole, remains controversial. A number of studies have shown reduced cortical thickness (Du et al., 2007; Lerch et al., 2005) and grey matter volumes (Baron et al., 2001; Busatto et al., 2003; Davatzikos et al., 2008) in this region. However, a number of studies

have failed to show involvement of any frontal areas (Whitwell and Jack, Jr., 2005). The current study, with the advantage of pathology confirmation, does support frontal pole atrophy in AD. There is always the theoretical possibility that this could be an artefact of the analysis technique, however, after careful visual inspection of this area in each subject we could not see any signal drop off or any kind of fault in the FreeSurfer surfaces which would explain reduced cortical thickness in this region.

The second subject group comparison revealed that patients with AD pathology and a clinical diagnosis of FTD during life (either behavioural or language variant) had a thinner cortex in the medial temporal lobe, posterior parietal regions, posterior cingulate gyrus and frontal pole than patients with FTLD pathology. In contrast, patients with FTLD pathology showed reduced cortical thickness predominantly in anterior temporal and frontal lobe regions. The highly significant reduction in the anterior temporal lobe in the FTLD group is possibly driven by the high proportion of semantic dementia patients in this group who are known to have marked atrophy in this region (Boxer et al., 2003; Chan et al., 2001b; Rosen et al., 2002). The patterns of cortical thinning observed in the FTLD group are consistent with previous histopathological and volumetric MRI studies (Broe et al., 2003; Grossman et al., 2004; Rosen et al., 2002; Whitwell et al., 2005a).

Although differences in the direct comparison between AD-FTD and FTLD did not reach statistical significance, tendencies of cortical thinning as shown in the percent difference maps are consistent with the patterns observed in the control comparisons. Thinner cortex in the posterior cingulate gyrus, parietal lobe and frontal pole suggests the presence of AD pathology, whereas cortical thinning in the anterior temporal lobe and frontal lobe regions suggests the presence of FTLD pathology. Our classification algorithm showed that subjects could be correctly classified on the basis of the scans alone in 79% of cases despite having had similar (FTD) clinical diagnoses in life. The ROC curve illustrates that although the original sensitivity is relatively low, this is probably driven by the imbalance in subject numbers between the two groups. The high area under the curve reveals that the classifier performs well, and a more favourable balance of sensitivity and specificity could be obtained by altering the threshold. The pattern of cortical thinning shown to separate the two patient groups best was consistent with that observed in the direct comparison between AD-FTD and FTLD.

One strength of this study is that all AD and FTLD cases had pathological confirmation. This is particularly important considering that accuracies for the clinical diagnosis of AD can vary between 60-90% (Brayne et al., 2009; Jellinger, 2006). Consequently, a number of individuals included in studies of AD will inevitably have a different type of pathology. A post-mortem study further revealed 30% of patients diagnosed with a language subtype of FTLD had AD pathology (Knibb et al., 2006). It is noteworthy, however, that the inclusion of only

pathologically-confirmed cases inevitably limits subject numbers, reducing the power to detect differences between disease groups. Furthermore, the fact that patients went to post-mortem might suggest a more atypical presentation, even in the typical amnestic AD patients. However, all patient notes were reviewed confirming a typical clinical phenotype in these cases. The young onset of these post-mortem proven cases may mean that results are less generalisable to an older AD population in that older-onset typical AD cases naturally have more years for ageing processes to occur and may have increased co-morbidities and pathologies (e.g. white matter disease). Pathology confirmation was not obtained for the whole control group and it may be that some controls had a neurological condition but were asymptomatic. This is, however, unlikely and would only have reduced the ability to detect differences.

Another limitation is the variety in image acquisition which has been shown to affect thickness measures (Han et al., 2006). Analyses were therefore adjusted for scanner type. It should also be noted that there was an imbalance in scanner type between groups, with scanner 'A' being present only in the control and typical AD group. However, excluding subjects imaged using scanner 'A' from the analyses gave very similar results. Our groups were matched for disease duration, but not for disease severity as measured by MMSE. As expected, MMSE scores varied significantly between individual groups owing to the weighting of questions towards memory and orientation.

4.5 Chapter conclusion

In summary, this chapter describes patterns of cortical thickness in patients with AD pathology but different clinical presentations. Common areas of lower cortical thickness were found in patients with AD pathology despite different clinical symptoms. These areas included the medial temporal lobe, posterior cingulate gyrus, precuneus, posterior parietal cortex and frontal pole. In contrast, lower cortical thickness in the anterior temporal lobe and frontal lobe regions is indicative of the presence of FTLD pathology in patients with a clinical presentation of FTD. Furthermore, patients with a frontal presentation during life and AD pathology at post-mortem show lower cortical thickness in posterior regions than patients with FTLD pathology. These findings suggest that atrophy in posterior regions of the brain might be indicative of the presence of AD pathology irrespective of clinical syndrome. Assessing atrophy in posterior regions might therefore aid the distinction between AD and FTLD. This finding provides a motivation for developing methods of assessing posterior atrophy that could be applied relatively simply to the individual patient's scan. The next chapter will present a tool with which posterior atrophy can be easily assessed in a clinical setting.

5. POSTERIOR CEREBRAL ATROPHY IN THE ABSENCE OF MEDIAL TEMPORAL LOBE ATROPHY IN PATHOLOGICALLY-CONFIRMED AD

5.1 Chapter introduction

The presence of medial temporal lobe atrophy is an important hallmark of AD (Basso et al., 2006; Fox and Schott, 2004; Teipel et al., 2006; see also chapter 2, section 2.5.2). New AD research diagnostic criteria (Dubois et al., 2007) propose that the presence of memory loss together with medial temporal lobe atrophy on MRI are sufficient to make a diagnosis of prodromal AD. However, atrophy in the medial temporal lobe is also present in FTLD and normal ageing (Chan et al., 2001b; Fjell et al., 2009; Frisoni et al., 1996; Galton et al., 2001). The previous chapter, together with a number of other studies, emphasize the presence of atrophy in posterior areas of the brain such as precuneus and posterior cingulate gyrus in AD (Jones et al., 2006; Karas et al., 2007). Atrophy in these regions has further been suggested to be more of a feature of early-onset AD (EOAD) than late-onset AD (LOAD) (Frisoni et al., 2007; Ishii et al., 2005a; Shiino et al., 2008), and conversely medial temporal atrophy may be a less sensitive marker of AD in younger patients.

Since quantitative volumetric measurements are not yet available for routine clinical use, visual rating scales are increasingly used to assess global atrophy (Scheltens et al., 1997), MTA (Scheltens et al., 1992), and white matter changes (Wahlund et al., 2001). The MTA scale (chapter 3, section 3.5.3.1.1) has been shown to discriminate well between AD and healthy controls, and to predict the conversion from MCI to AD (Korf et al., 2004; Scheltens et al., 1992; Scheltens et al., 1995). We have recently developed a visual rating scale for posterior atrophy (PA), which includes the posterior cingulate gyrus, precuneus and parietal lobes.

This chapter first describes the development and validation of the PA scale which was conducted in collaboration with the VU Medical Centre in Amsterdam. It then describes a study in which MTA and PA ratings were assessed in pathologically-confirmed AD and FTLD patients. This study aimed i) to assess the inter- and intra-rater agreement of the MTA and PA scale in a large cohort of pathologically-proven AD and FTLD patients, and controls; ii) to investigate associations of visual rating scores with manual volumetric measures, iii) to assess the utility of MTA and PA scales in distinguishing between pathologically-confirmed AD and controls as well as FTLD which may be misdiagnosed as AD; and iv) to assess the discriminatory ability of visual ratings according to age at onset.

5.2 Development and validation of the PA rating scale

5.2.1 Development of the PA scale

MRI scans of 25 patients with probable AD were selected from the VU Medical Centre Amsterdam database, and were used to determine posterior regions that were most affected in AD. The same areas were then assessed in 10 control subjects to determine whether these regions are more affected in AD and therefore are likely to represent atrophy. Based on these findings the following anatomical regions were selected: the posterior cingulate sulcus, precuneus, parieto-occipital sulcus and the cortex of the parietal lobes.

The PA scale rates atrophy on a 4-point scale (Figure 5.1): grade 0 represents closed posterior cingulate and parieto-occipital sulci and closed sulci of the parietal lobes and precuneus; grade 1 includes a mild widening of the posterior cingulate and parieto-occipital sulci, with mild atrophy in the parietal lobes and precuneus; grade 2 represents substantial widening of the posterior cingulate and parieto-occipital sulci, with marked atrophy in the parietal lobes and precuneus; and grade 3 represents end-stage atrophy with evident widening of the posterior cingulate and parieto-occipital sulci and knife-blade atrophy in the parietal lobes and precuneus. When there was a difference between scores in the different planes (e.g. score 1 for the sagittal view and score 2 for the axial view), the highest score was given.

PA was scored on T1-weighted images viewed in the sagittal, axial and coronal planes. Separate scores for the left and right hemispheres were obtained. The following anatomical features were rated in the three different planes:

a) Sagittal plane: Evaluation of widening of the posterior cingulate and parieto-occipital sulci, and atrophy in the precuneus in the paramedian-sagittal plane.

b) Axial plane: Evaluation of widening of the posterior cingulate sulcus and sulcal dilatation in the parietal lobes.

c) Coronal plane: Evaluation of widening of the posterior cingulate and parietal sulci.

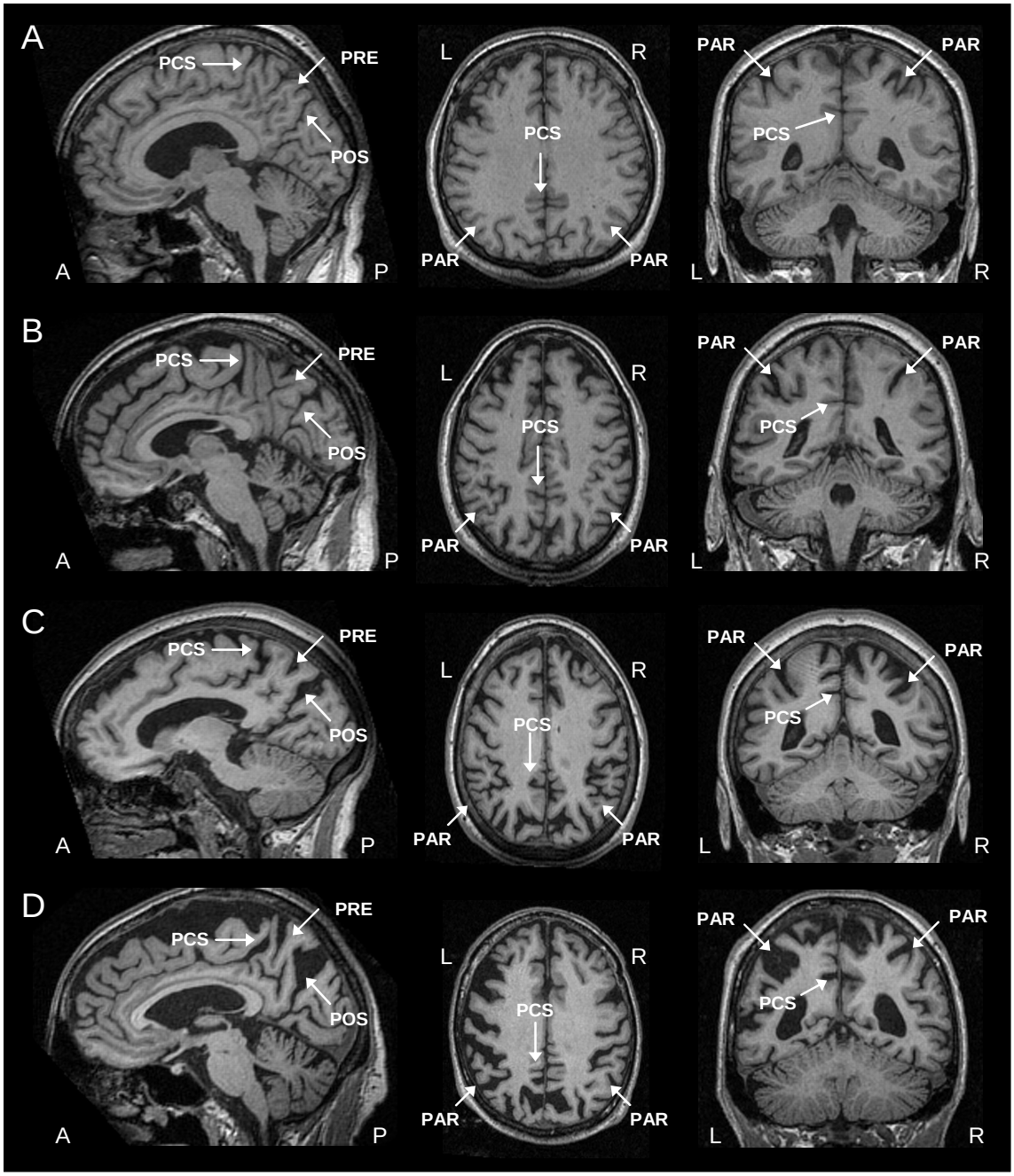

Figure 5.1: **Posterior visual rating scale.** T1-weighted sagittal, axial and coronal images as examples for each grade of the PA scale. **A)** grade 0=no atrophy; **B)** grade 1=minimal atrophy, **C)** grade 2=moderate atrophy; and **D)** grade 3=severe atrophy. PCS - posterior cingulate sulcus, PRE - precuneus, PAR - parietal lobe, POS - parieto-occipital sulcus. L - left hemisphere, R - right hemisphere, A - anterior, P - posterior.

5.2.2 Validation of the PA scale

5.2.2.1 Subjects and analysis

118 subjects were selected from the VU Medical Centre Amsterdam database based on their clinical diagnosis. The selection included 60 AD patients, 20 age-matched patients with other dementias (10 FTLD and 10 DLB patients) and 38 age-matched patients with subjective memory complaints but no cognitive impairment (acting as the control group in this study). All patients underwent a standard battery of investigations including a patient and informant-based medical history, physical and neurological examination including the MMSE and MR imaging. The clinical diagnosis of probable AD, FTLD and DLB was made according to current diagnostic criteria (McKeith et al., 1996; McKhann et al., 1984; Neary et al., 1998), based purely on clinical characteristics. MR imaging was performed on a 3T MR scanner (Signa HDxt, General Electric, Milwaukee) using a sagittal T1-weighted 3D fast spoiled gradient echo (FSPGR) sequence. PA as well as MTA ratings were obtained in all 118 subjects by three different raters (Esther Koedam, Mike Wattjes, and myself). All raters were blinded to clinical diagnosis. Twenty-nine MRI scans were rated twice by two raters. Inter- and intra-rater agreement was calculated using quadratically weighted kappas (Cohen, 1968). Linear regression was used to assess relationships between PA rating scores and age and MMSE score. PA and MTA ratings were dichotomized into normal and abnormal, with a mean score (left and right hemisphere) of >1 being considered abnormal.

5.2.2.2 Results

Intra-rater kappa scores (determined in 29 scans for two raters) were 0.93 (rater 1) and 0.95 (rater 2). Inter-rater agreement (determined in 118 scans for three raters) was best between rater 1 and rater 2 (kappa=0.84), followed by agreement between rater 2 and 3 (kappa=0.70) and lowest between rater 1 and rater 3 (kappa=0.65). The average weighted kappa value for inter-rater agreement was 0.73.

Mean scores for the PA rating scale were significantly higher in the AD group (mean=1.6; SD=0.9) compared with controls (mean=0.6; SD=0.7, $p<0.01$) and other dementias (mean=0.8; SD=0.8, $p<0.01$). PA scores did not differ between other dementias and controls. There was no evidence of a significant association of PA ratings with age, however, a strong relationship was found with MMSE score ($p<0.01$).

28% of AD patients had prominent PA (scores>1) without evident MTA (score≤1), whereas only 15% had prominent MTA without marked PA. Twenty-seven percent of the AD patients had only minimal MTA and PA. Most controls (88%) and patients with other dementias (i.e. FTLD and DLB, 45%) had normal scores for MTA and PA.

5.2.2.3 Conclusion

This study revealed good intra- and inter-rater agreement for the PA scale. The AD group showed higher PA scores compared with controls and patients with other dementias, suggesting that the PA scale may be useful for discriminating AD from normal ageing and other neurodegenerative diseases. Whilst this study provided first insights into the reproducibility and validity of the new PA scale, it is only with pathologically-proven cases that one can be sure of the predictive value of different atrophy measures such as MTA or PA ratings in different types of dementia. The following study was conducted to validate the PA scale in pathologically-confirmed AD and FTLD subjects, and to assess its clinical utility to distinguish between AD and FTLD as well as normal ageing.

5.3 Visual ratings in pathologically-confirmed AD and FTLD

5.3.1 Subjects

Patients were selected retrospectively from a database (Dementia Research Centre) of pathologically- and genetically-confirmed subjects. This identified 152 subjects who had undergone volumetric MR imaging (see Figure 5.2): 62 patients with 'definite' AD (55 pathologically- and 7 genetically confirmed) according to NINCDS-ADRDA criteria (McKhann et al., 1984, Appendix 1) and 40 patients with FTLD (all pathologically-confirmed). 50 healthy age- and gender-matched controls were also included. Demographics are presented in Table 5.1. 44% of the control subjects, 45% of the AD and 50% of the FTLD patients were included in the study described in the previous chapter. The clinical notes were retrospectively reviewed by a clinician to determine whether the clinical presentation was predominantly an amnestic, behavioural, language presentation or a PCA syndrome.

5.3.2 MRI acquisition and processing

Images were acquired as described in chapter 3 (section 3.5.1) and Appendix 5. All scans were spatially-normalized into MNI 305 atlas space (Mazziotta et al., 1995) with a six dof registration.

5.3.3 Regional volumes in subset of subjects

Manual delineations of the hippocampus and posterior cingulate gyrus had been obtained in a subset of 38 subjects (11 controls, 19 AD, 8 FTLD, matched for age and gender) as part of a previous study (Barnes et al., 2007a). Demographic details as well as manual delineation protocols are described in Barnes et al. (2007a). Volumes in mm^3 were measured and analysed separately for the left and right hemisphere. TIVs were also available for the same subjects derived according to a previously described protocol (Whitwell et al., 2001).

5.3.4 Rating scales

All scans were assessed by two raters (Esther Koedam and myself) blind to diagnoses. MTA and PA were rated as described in sections 3.5.3.1.1 and 5.2.1 respectively, once by each rater for the whole cohort (152 subjects), and twice for the subset of 38 subjects for which there were cingulate and hippocampal volumes available.

5.3.5 Statistical analysis

A flowchart showing which subjects were used for the different parts of the analysis is presented in Figure 5.2.

5.3.5.1 Inter- and intra-rater reliability

Inter-rater reliability between the two raters for the MTA and PA scales was assessed using scores from the whole cohort of 152 subjects whereas intra-rater reliability for both scales was assessed in the subset of 38 subjects. Reliability was measured using quadratically weighted kappas (Cohen, 1968). Bias-corrected and accelerated 95% bootstrap confidence intervals (CI) for kappa were found using 10,000 bootstrap samples.

5.3.5.2 Anatomical correlates

Relationships between volumes and rating scores were assessed by calculating mean volumes (in mm^3) and standard deviations (SDs) of hippocampal volumes per MTA grade, and posterior cingulate gyrus volumes per PA grade. Ratings of both raters were averaged, resulting in half grades (i.e. 0.5, 1.5 etc). In order to ensure reasonable subject numbers for each grade, volumes were averaged for grades 0 and 0.5; 1 and 1.5; 2 and 2.5, and all ≥3. Furthermore, MTA and PA scores were dichotomized into normal and abnormal scores, with a score of >1 being considered abnormal. Mean volumes for normal and abnormal scores as well as percent differences in volumes between normal and abnormal scores are presented. Differences between grades were further assessed statistically by using ordinal logistic regression with the rating score (MTA and PA) as dependent variable and corresponding volume (hippocampal and posterior cingulate gyrus) as independent variable, adjusting for age, gender and TIV.

5.3.5.3 Group comparisons

MTA and PA ratings scores were first analysed in pathologically-confirmed sporadic AD (N=44) and compared with pathologically-confirmed sporadic FTLD (N=27) and controls (see Figure 5.2). In order to assess the effect of age at onset on visual ratings, the sporadic AD group was then split into pathologically-confirmed EOAD (age at onset <65, N=33) and pathologically-confirmed LOAD (age at onset ≥65years, N=11), and compared with younger (N=33) and older controls (N=14), matched for age at time of scan and gender to the EOAD and LOAD groups, respectively. Differences between early and late-onset FTLD patients

were not examined since the number of late-onset FTLD patients was too small (N=4) to conduct a meaningful comparison

5.3.5.3.1 Atrophy patterns

Mean scores and SDs of MTA and PA ratings were calculated and differences in scores between groups were assessed using a Mann-Whitney / Wilcoxon rank-sum test. MTA and PA scores were further dichotomized into normal and abnormal, with a score of >1 being considered abnormal. Ratings of both raters were averaged.

5.3.5.3.2 Classification analysis and added value

In order to assess the diagnostic accuracy of the MTA and PA scales for discriminating between groups, areas under the ROC, denoted AUC, were estimated. The AUC measures the ability of a score to discriminate between groups, and ranges from 0.5 (no predictive value) to 1 (perfect discrimination). The added value of MTA and PA was assessed by combining MTA and PA in a logistic regression model. Differences in AUCs between combined and single rating scales are reported as well as 95% Wald-type CIs (1,000 bootstrap samples) and p-values based on a z-test of the difference in AUCs, using the bootstrap standard error. This was performed with the user-written Stata command comproc (Janes et al., 2009). These analyses were also based on the average of ratings from two raters.

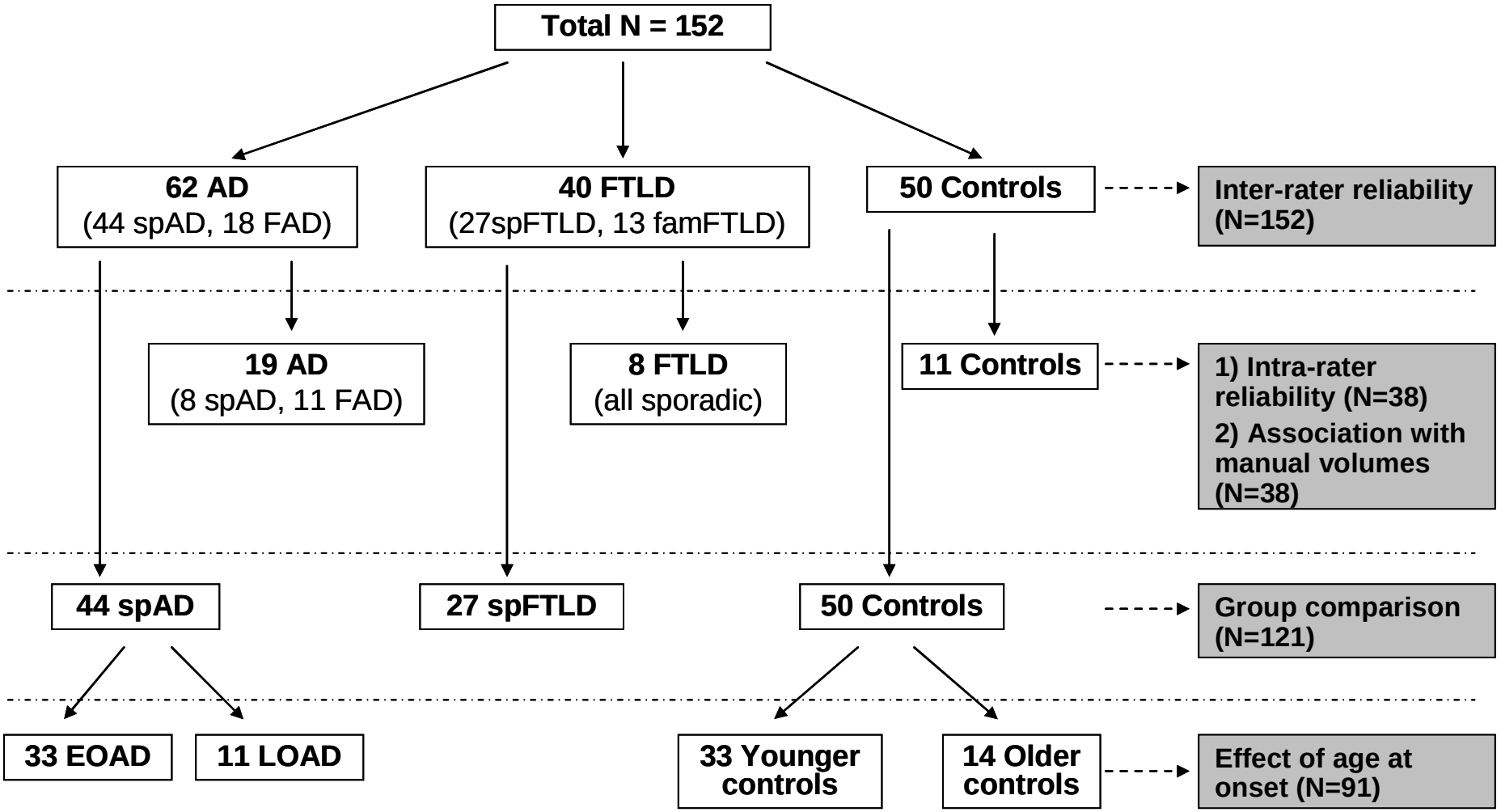

Figure 5.2: Overview of subject groups included in each analysis. FAD and spAD - familial and sporadic Alzheimer's disease; famFTLD and spFTLD - familial and sporadic Frontotemporal lobar degeneration; EOAD and LOAD - early- and late-onset Alzheimer's disease.

5.4 Results

5.4.1 Subjects

Subject demographics are presented in Table 5.1. Of the 62 AD patients, 48 had a post-mortem confirmation of AD, 7 had had a brain biopsy, and 7 had diagnostic genetic testing. The AD group consisted of 44 sporadic cases, and 18 familial cases. All sporadic AD patients had pathological confirmation of disease. Of the 44 sporadic AD cases, 19 patients had a typical amnestic presentation during life, whereas 10 had a PCA syndrome, 9 had a language presentation, and 4 had a behavioural presentation. There were insufficient clinical details to determine the presenting clinical features for 2 subjects. Furthermore, of the 44 sporadic cases, 33 patients had an age at onset <65 years (EOAD), whereas 11 had an age at onset of ≥65 years (LOAD). All of the familial AD subjects had an amnestic presentation during life. Of the 18 familial AD subjects, 11 had both genetic testing and post-mortem confirmation of disease, and 7 had a genetic diagnosis only. The familial AD cohort comprised 9 individuals with a Presenilin 1 mutation and 8 with an amyloid precursor protein (APP) gene. One individual had pathologically confirmed AD but screened negative for mutations currently known to cause familial AD. As she had a strong family history suggesting autosomal dominant inheritance of AD and a very young age at symptom onset of 36, this subject was included in the familial cohort.

Of the 40 FTLD patients included in this study, 36 had post-mortem confirmation of FTLD, and 4 had a brain biopsy. Twenty of the FTLD cases had a behavioural syndrome during life, and 20 had a language presentation. Twenty-seven patients were sporadic cases, whereas 13 had a family history of FTLD. Of the 27 sporadic cases, 9 were tau-positive (Pick's pathology) and 18 were tau-negative (13 TDP1, 3 ubiquitin-positive with unknown TDP status, 1 with neuronal intermediate filament inclusion disease (NIFID), and 1 with DLDH). 23 had an age at onset <65 years, and 4 had an age at onset of ≥65 years. Of the 13 familial cases, 7 were tau-positive and 6 were ubiquitin-positive (5 TDP43-positive and 1 TDP43-negative). Seven familial patients had a microtubule-associated protein tau (MAPT) mutation, 3 had a progranulin (PGRN) mutation, and in 3 subjects with a history suggestive of FTLD a genetic mutation was not identified.

There was no evidence of differences across the three main groups (controls, AD, FTLD) for age and gender, and for the FTLD and AD groups no significant difference in distribution of sporadic and familial cases, age at disease onset, disease duration, or time to death (Table 5.1). However, the AD subjects had a lower MMSE than the FTLD group ($p<0.001$). Scanner distribution was not significantly different between AD and FTLD ($p=0.3$), however, the controls had a greater number of scans on scanner 'A' ($p=0.002$).

There was no significant difference in age and gender between EOAD (mean age (SD): 58.8 (6.6) years, 61% male) and younger controls (mean age (SD): 56.5 (7.4) years, 58% male). Similarly, there was no evidence of a significant difference in age or gender between LOAD (mean age (SD): 73.0 (5.4) years, 64% male) and older controls (mean age (SD): 72.7 (5.0) years, 64% male). The EOAD and LOAD groups had a mean MMSE score of 16.7 and 19.1, respectively (p=0.5), and a mean disease duration of 4.2 years and 2.8 years, respectively (p=0.02).

Table 5.1: Subject demographics.

	Controls	AD	FTLD	p
N	50	62	40	N/A
Age in years, mean (SD)	59.7 (11.3)	58.2 (10.6)	59.2 (8.9)	0.7 ¶
Gender male / female	29 / 21	34 / 28	26 / 14	0.6 §
Sporadic / familial	N/A	44 / 18	27 / 13	0.8 §
MMSE, mean (SD) ±	29.1 (1.1)	17.2 (6.8)	22.9 (5.2)	<0.0001 ¶
Age at onset in years, mean (SD)	N/A	54.2 (10.8)	55.0 (8.7)	0.7 ¶
Disease duration in years, mean (SD) ‡	N/A	3.9 (2.9)	4.2 (2.1)	0.6 ¶
Time to death in years, mean (SD) †	N/A	5.6 (2.8)	6.4 (3.3)	0.2 ¶
Scanner A / B / C / D	14 / 27 / 8 / 1	7 / 37 / 15 / 3	1 / 26 / 9 / 4	0.002 §

± available in: 15 controls, 53 AD, 28 FTLD; ‡ time between first symptoms (onset) and scan; † time between scan and death, available in: 53 AD and 35 FTLD; ¶ ANOVA; § Fischer's exact test; A, B, C, D: different 1.5T scanners (Appendix 5); N/A - not applicable

5.4.2 Inter- and intra-rater reliability

Both the MTA and PA scales had good inter- and intra-rater reliability. Inter-rater kappa scores for the MTA scale were 0.88 for left, 0.86 for right, and 0.91 for mean of both hemisphere scores (Table 5.2). Inter-rater kappa scores for the PA scale were 0.83 for left, 0.82 for right, and 0.84 for mean of left and right hemisphere scores. Intra-rater kappa scores ranged from 0.83 to 0.91 for the MTA, and from 0.87 to 0.89 for the PA scale.

Table 5.2: Inter- and intrarater kappa scores for MTA and PA scale.

Scale	Side	Inter-rater (N=152)	Intra-rater (N=38)	
			EK	ML
MTA	LH	0.88 (0.84, 0.92)	0.90 (0.84, 0.96)	0.91 (0.84, 0.96)
	RH	0.86 (0.80, 0.90)	0.87 (0.77, 0.94)	0.83 (0.71, 0.92)
	Mean LH&RH	0.91 (0.87, 0.93)	0.90 (0.83, 0.95)	0.90 (0.83, 0.95)
PA	LH	0.83 (0.76, 0.88)	0.88 (0.77, 0.96)	0.88 (0.74, 0.96)
	RH	0.82 (0.75, 0.87)	0.88 (0.78, 0.95)	0.87 (0.74, 0.95)
	Mean LH&RH	0.84 (0.77, 0.89)	0.89 (0.79, 0.95)	0.88 (0.76, 0.96)

5.4.3 Anatomical correlates

Higher MTA scores were associated with smaller hippocampal volumes (Table 5.3, Figure 5.3) which differed significantly across all MTA grades in both hemispheres (p=0.001). A similar relationship was found for posterior cingulate gyrus volumes and grades of the PA scale in the right hemisphere (p=0.004), however, not in the left hemisphere (p=0.3).

Table 5.3: Manual volumes per rating scale grade. Shown are hippocampal volumes per MTA grade, and volumes of the posterior cingulate gyrus per PA grade.

	Hpc volumes per MTA grade				PCG volumes per PA grade			
	LH		RH		LH		RH	
Grade ‡	**N**	**Mean (SD)**	**N**	**Mean (SD)**	**N**	**Mean (SD)**	**N**	**Mean (SD)**
0 & 0.5	19	2598 (534)	18	2732 (544)	18	2449 (685)	17	2809 (459)
1 & 1.5	9	2182 (403)	12	2419 (290)	14	2197 (818)	13	2591 (798)
2 & 2.5	5	1892 (196)	7	2115 (707)	6	2021 (520)	8	1900 (540)
≥ 3	5	1985 (526)	1	1488 (0)	0	-	0	-

Mean volumes and SDs are shown in mm^3; ‡ mean of grades from two raters; Hpc - Hippocampus, PCG - posterior cingulate gyrus; LH - left hemisphere, RH - right hemisphere

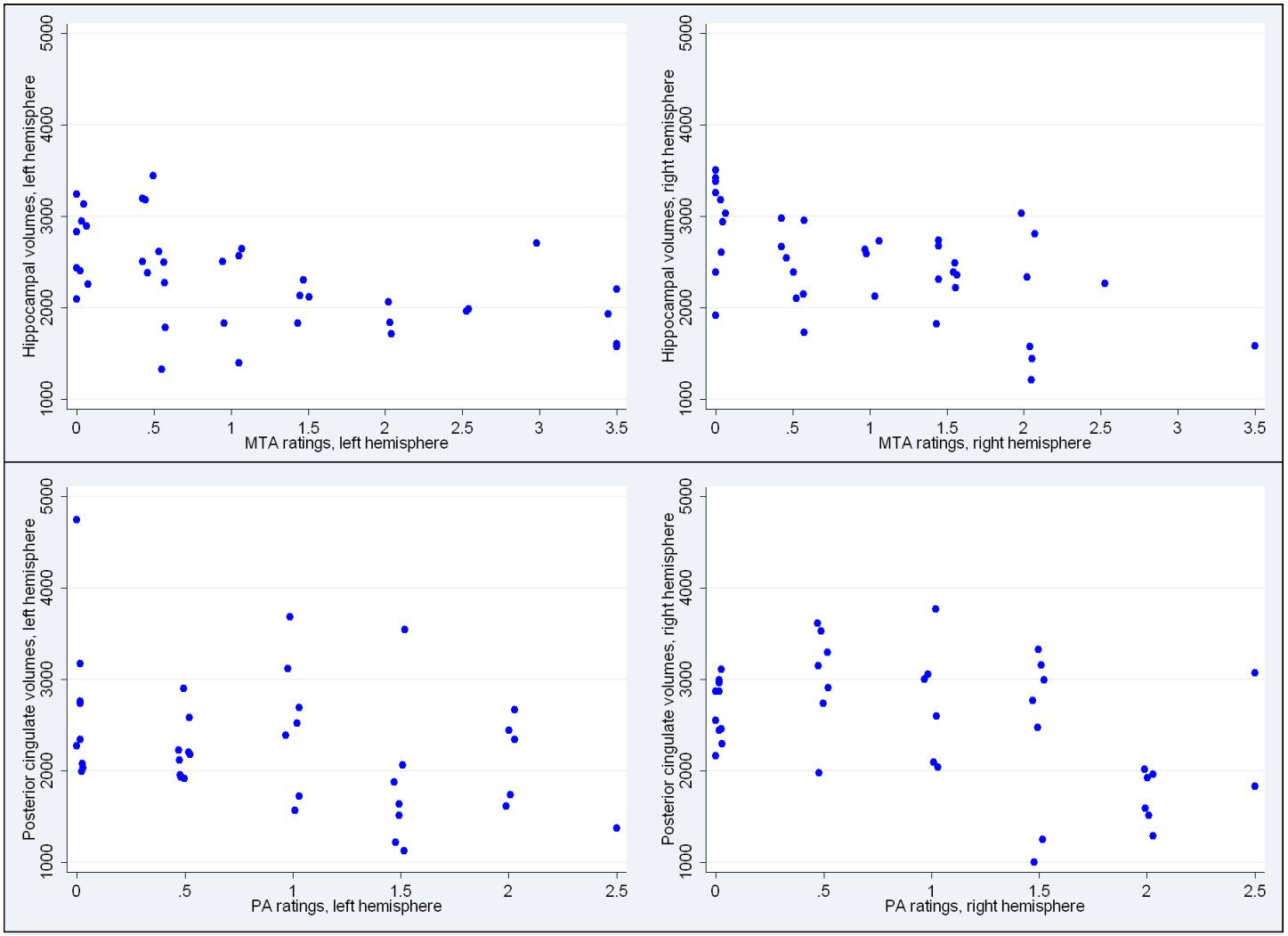

Figure 5.3: Scatter plots illustrating volumes per rating scale grade. Shown are hippocampal volumes per MTA rating (top), and posterior cingulate gyrus volumes per PA rating (bottom), for left and right hemispheres.

Mean hippocampal volume for subjects with abnormal MTA scores (>1) was 21.0% lower than for those with normal MTA scores in the left hemisphere (1992mm^3 versus 2520mm^3), and 17.5% lower in the right hemisphere (2214mm^3 versus 2685mm^3). Similarly, dichotomizing PA scores into normal and abnormal, mean posterior cingulate gyrus volume of subjects with abnormal PA scores was 21.7% lower than for those with normal PA ratings in the left (1936mm^3 versus 2471mm^3), and 23.3% lower in the right hemisphere (2149mm^3 versus 2800mm^3).

5.4.4 Visual ratings in AD and FTLD

5.4.4.1 Atrophy patterns

MTA ratings were significantly greater in the FTLD group compared with controls ($p<0.0001$) and AD ($p=0.002$ for left hemisphere; $p=0.03$ for mean left and right, Table 5.4). MTA ratings were also significantly higher in the AD group compared with controls ($p<0.0001$). Ratings for the PA scale were greater in the AD group compared with controls ($p<0.001$) and FTLD ($p=0.004$ for right hemisphere; $p=0.02$ for mean left and right). PA ratings were also significantly higher in the FTLD group compared with controls in the left hemisphere ($p=0.03$). The MTA/PA ratio was around 0.5 in the control group, 1 in the AD group and 2 in the FTLD group.

Table 5.4: Rating scores for controls, AD and FTLD. Means and SDs of MTA and PA scores are shown for each group, as well as p values for differences between groups.

Scale	Side	Controls (N=50)	AD (N=44)	FTLD (N=27)	Controls vs. AD	Controls vs. FTLD	AD vs. FTLD
		Mean (SD)	Mean (SD)	Mean (SD)	p	p	p
MTA	LH	0.44 (0.58)	1.43 (1.08)	2.37 (1.13)	<0.0001	<0.0001	0.002
	RH	0.37 (0.56)	1.24 (0.98)	1.37 (1.00)	<0.0001	<0.0001	0.7
	Mean LH&RH	0.41 (0.53)	1.34 (0.95)	1.87 (0.89)	<0.0001	<0.0001	0.03
PA	LH	0.77 (0.64)	1.40 (0.83)	1.13 (0.67)	0.0002	0.03	0.2
	RH	0.77 (0.68)	1.45 (0.81)	0.91 (0.65)	0.0001	0.3	0.004
	Mean LH&RH	0.77 (0.62)	1.43 (0.77)	1.02 (0.62)	0.0001	0.1	0.02

LH - left hemisphere, RH - right hemisphere

Dichotomizing MTA and PA scores into normal and abnormal revealed different patterns of atrophy in each group (Table 5.5). The majority (72%) of the control subjects had normal atrophy scores (i.e. normal MTA and PA), 30% of the AD patients had PA in the absence of abnormal MTA (i.e. abnormal PA, normal MTA), whereas only 7% of the FTLD group had abnormal PA score and normal MTA. 63% of the FTLD patients had a normal PA with an abnormal MTA score. The demographical data for the four different AD subgroups (Table 5.6) further show that the PA only AD group is younger in age than AD subjects with MTA only, however, this difference was not statistically significant.

Table 5.5: Atrophy patterns in controls, AD and FTLD. Shown are proportion of subjects in percent who had no atrophy, MTA only, PA only, and both MTA and PA, based upon a cut-off score of >1 for the PA and MTA visual rating scales.

	Controls	**AD**	**FTLD**
No atrophy	72%	18%	4%
MTA only	6%	18%	63%
PA only	18%	30%	7%
MTA & PA	4%	34%	26%

Table 5.6: Demographics of AD patients according to atrophy pattern.

	No atrophy	**MTA only**	**PA only**	**MTA & PA**	**p value**
N	8	8	13	15	-
Age, mean (SD) in years	63.3 (5.5)	66.7 (11.6)	60.6 (7.0)	61.0 (10.0)	0.3
Gender % male	63%	75%	46%	67%	0.6
MMSE, mean (SD) †	16.8 (6.7)	18.8 (6.3)	17.0 (6.1)	15.9 (7.9)	0.8
Age at onset, mean (SD) in years	58.4 (3.6)	63.4 (12.2)	56.9 (6.9)	57.6 (10.2)	0.3

5.4.4.2 Classification analysis

Whilst discrimination abilities for separating AD from control subjects were good for both MTA and PA scales (0.80 and 0.74, respectively, for mean left and right), they improved significantly when both scales were combined (0.87 mean left and right, Table 5.7). In contrast, adding the PA to the MTA scale did not improve accuracy for separating FTLD from controls (p=0.4). For the discrimination between AD and FTLD, combining both scales improved classification accuracy to 0.73 (mean left and right). The greatest improvement was found in the right hemisphere, where adding the PA to the MTA scale significantly increased accuracy to 0.72 (p=0.02).

Table 5.7: Classification analysis for AD, FTLD and controls. AUCs for classification of controls, AD and FTLD, for single and combined rating scales, as well as differences in AUCs between combined and single rating scales, 95% CI and p values.

Group	**Side**	**MTA**	**PA**	**MTA & PA**	**Adding PA to MTA**		**Adding MTA to PA**	
		AUC	AUC	AUC	Difference (95% CI)	p	Difference (95% CI)	p
C vs. AD	LH	0.77	0.72	0.86	0.08 [0.01, 0.16]	0.02	0.14 [0.05, 0.23]	0.002
	RH	0.76	0.74	0.83	0.06 [0.00, 0.16]	0.07	0.09 [0.02, 0.16]	0.01
	Mean LH&RH	0.80	0.74	0.87	0.07 [0.01, 0.14]	0.03	0.13 [0.04, 0.22]	0.004
C vs. FTLD	LH	0.92	0.65	0.92	0.00 [-0.02, 0.02]	1.0	0.28 [0.15, 0.40]	<0.001
	RH	0.81	0.57	0.80	-0.01 [-0.04, 0.03]	0.7	0.23 [0.08, 0.39]	0.003
	Mean LH&RH	0.93	0.61	0.92	-0.01 [-0.03, 0.01]	0.4	0.30 [0.17, 0.44]	<0.001
AD vs. FTLD	LH	0.72	0.60	0.74	0.02 [-0.03, 0.08]	0.5	0.15 [0.02, 0.28]	0.03
	RH	0.53	0.70	0.72	0.19 [0.02, 0.35]	0.02	0.02 [-0.05, 0.08]	0.6
	Mean LH&RH	0.66	0.66	0.73	0.08 [-0.02, 0.17]	0.1	0.07 [-0.03, 0.18]	0.2

LH - left hemisphere, RH - right hemisphere.

5.4.5 The effect of age at onset on visual ratings in AD

5.4.5.1 Atrophy patterns in EOAD and LOAD

Both EOAD and LOAD showed significantly higher MTA scores compared with younger and older controls, respectively, with MTA scores being significantly higher in LOAD than EOAD ($p=0.02$ for right, $p=0.04$ for mean left and right, Table 5.8). In addition, EOAD showed significantly greater PA scores compared with younger controls ($p=0.0001$), whereas no significant difference in PA scores between LOAD and older controls was found.

Dichotomizing MTA and PA scores into normal and abnormal revealed that over one third of EOAD patients (33%) had PA only, whereas almost half of the LOAD patients (46%) had MTA only (Table 5.9). The majority of the younger controls (81%) had no atrophy, whereas over half of the older controls (57%) had either MTA, PA or both MTA and PA. These data suggest that abnormal PA scores may only have diagnostic implications in younger patients and are less specific in elderly people.

Table 5.8: Group differences between EOAD, LOAD and younger and older controls. Shown are the means and SDs of MTA and PA scores in younger and older controls, EOAD and LOAD, as well as p values for differences between groups.

Group and comparison		**MTA**			**PA**		
		LH	RH	Mean LH&RH	LH	RH	Mean LH&RH
Younger controls (N=33)	Mean (SD)	0.38 (0.53)	0.29 (0.43)	0.33 (0.44)	0.65 (0.58)	0.71 (0.56)	0.68 (0.53)
EOAD (N=33)	Mean (SD)	1.29 (1.04)	1.05 (0.95)	1.17 (0.92)	1.42 (0.79)	1.45 (0.81)	1.44 (0.76)
Younger controls vs. EOAD	p	0.0002	0.001	0.0001	0.0001	0.0001	0.0001
Older controls (N=14)	Mean (SD)	0.68 (0.67)	0.64 (0.77)	0.66 (0.69)	1.14 (0.66)	1.07 (0.85)	1.11 (0.72)
LOAD (N=11)	Mean (SD)	1.86 (1.12)	1.82 (0.87)	1.84 (0.88)	1.32 (0.96)	1.45 (0.85)	1.39 (0.84)
Older controls vs. LOAD	p	0.01	0.003	0.002	0.7	0.3	0.5
EOAD vs. LOAD	p	0.1	0.02	0.04	0.7	0.8	0.7

LH - left hemisphere, RH - right hemisphere

Table 5.9: Atrophy patterns in younger and older controls, EOAD and LOAD. Shown are proportion of subjects in percent who had no atrophy, MTA only, PA only, and both MTA and PA.

	Younger controls	Older controls	EOAD	LOAD
No atrophy	81%	43%	24%	0%
MTA only	3%	14%	9%	46%
PA only	12%	36%	33%	18%
MTA & PA	3%	7%	33%	36%

5.4.5.2 Classification analysis

Combining MTA and PA ratings significantly improved the separation of EOAD from younger controls to 0.89 (mean left and right, Table 5.10). In contrast, adding the PA to the MTA scale did not significantly improve separation of LOAD from older controls (p=0.5), whereas adding the MTA to the PA scale did result in a greater separation (p=0.01). Discriminatory ability of the MTA scale was higher for the separation of LOAD from older controls than EOAD from younger controls. In contrast, the PA scale showed a better discrimination for the EOAD from younger control classification than LOAD vs. older controls. Whilst these differences were not statistically significant, the magnitude of these differences, in particularly for the PA scale, was relatively high.

Table 5.10: Classification analysis for EOAD and LOAD, as well as younger and older controls. AUCs for each group for single and combined rating scales, as well as differences in AUCs between combined and single rating scales, 95% confidence intervals (CI) and p values.

Group	**Side**	**MTA**	**PA**	**MTA & PA**	**Adding PA to MTA**		**Adding MTA to PA**	
		AUC	AUC	AUC	Difference (95% CI)	p	Difference (95% CI)	p
Younger controls vs. EOAD	LH	0.75	0.77	0.86	0.11 [0.02, 0.21]	0.02	0.09 [0.01, 0.17]	0.03
	RH	0.74	0.77	0.84	0.10 [0.00, 0.20]	0.05	0.07 [-0.01, 0.14]	0.07
	Mean LH&RH	0.77	0.78	0.89	0.11 [0.02, 0.21]	0.02	0.10 [0.01, 0.20]	0.03
Older controls vs. LOAD	LH	0.81	0.55	0.89	0.07 [-0.06, 0.21]	0.3	0.34 [0.09, 0.60]	0.01
	RH	0.85	0.61	0.87	0.02 [-0.10, 0.14]	0.8	0.26 [0.04, 0.48]	0.02
	Mean LH&RH	0.87	0.58	0.91	0.04 [-0.07, 0.14]	0.5	0.33 [0.09, 0.57]	0.01
EOAD vs. LOAD	LH	0.65	0.54	0.65	-0.01 [-0.12, 0.10]	0.9	0.11 [-0.10, 0.32]	0.3
	RH	0.73	0.52	0.76	0.03 [-0.07, 0.13]	0.5	0.24 [0.02, 0.46]	0.03
	Mean LH&RH	0.71	0.54	0.69	-0.02 [-0.10, 0.07]	0.7	0.15 [-0.06, 0.36]	0.2

LH - left hemisphere, RH - right hemisphere

5.5 Discussion

This study demonstrates that in addition to medial temporal lobe atrophy being a feature of AD, prominent atrophy in posterior regions of the brain is also frequently found. Furthermore, in a subset of patients with pathologically-proven AD, posterior atrophy may be present in the absence of marked atrophy in the medial temporal lobes, particularly in younger AD patients. MTA is also common in FTLD whereas PA is less common. The presence of posterior atrophy therefore helps to distinguish AD from FTLD, and also early-onset AD patients (onset <65 years) from younger controls. This study, with the strength of pathological confirmation in all patients, therefore suggests that the presence of posterior atrophy may be a useful additional marker of AD pathology, over and above MTA. This investigation further presents and establishes a tool with which posterior atrophy can be easily and reliably assessed in a clinical setting.

Non-memory related deficits such as visuospatial problems are increasingly recognized as being a feature of AD (van der Flier et al., 2010). It is perhaps therefore not surprising that an anatomical correlate of visuospatial deficits, namely posterior atrophy, is useful in distinguishing AD from FTLD. The involvement of posterior brain regions in AD seen in this study is in accordance with previous reports showing that AD is not only characterized by atrophy of the medial temporal lobe, but also of posterior regions such precuneus and posterior cingulate gyrus (Barnes et al., 2007a; Frisoni et al., 2007; Galton et al., 2000). Posterior hypometabolism has long been recognized to be characteristic of AD (Ishii et al., 2005b; Minoshima et al., 1997). Posterior regions have also been shown to have higher levels of amyloid deposition early in AD (Kemppainen et al., 2007; Klunk et al., 2004). Functional imaging studies have further shown that the default-mode network, which includes medial temporal lobe regions and posterior regions, is also affected early in AD (Greicius et al., 2004; Zhang et al., 2010).

Both the MTA and PA scales showed reasonable inter- and intra-rater kappa scores. Higher MTA scores corresponded to smaller hippocampal volumes on manual measurements, similar to previous studies (Bresciani et al., 2005; Scheltens et al., 1992; Wahlund et al., 2000). The difference in hippocampal volumes between normal and abnormal MTA score was relatively high, with 21.0% in the left and 17.5% in the right hemisphere, with on average a 1 point rise in MTA score being equivalent to around 12% reduction of hippocampal volume. It should be noted, however, that this difference is determined by the cut-off score used to define normal and abnormal MTA. It has been shown that this cut-off score is age-dependent, with a score of >1 being considered abnormal below the age of 75, whereas in patients >75 years of age a score of >2 would be required to identify abnormal MTA (Scheltens et al., 1992). Duara et al. showed that a mean MTA score of 1.33 produced optimal sensitivities and specificities to separate patients with AD and MCI from healthy controls (Duara et al., 2008). Using post-mortem MRI of very old AD patients (>85years), Barkhof et al. showed that a cut-

off score of 2 correctly excluded subjects with no or borderline Alzheimer-type pathology (Barkhof et al., 2007). Since the AD group in the current study was relatively young (mean age 58 years), a cut-off score of >1 was used to define abnormal MTA. The same cut-off score was used for the novel PA scale. Further work in larger numbers of subjects is needed to determine if this is optimum. Higher PA scores only roughly corresponded to smaller volumes of the posterior cingulate gyrus, probably because the PA scale reflects more than just posterior cingulate atrophy. Although there was only evidence of an association in the right hemisphere, a test for interaction showed no evidence that the association differs by hemisphere (p=0.1).

The presence of MTA in the FTLD group underlines the fact that hippocampal atrophy is not exclusive to AD, but has been widely described in FTLD as well, particularly anteriorly (Chan et al., 2001b; Galton et al., 2001; Mesulam, 2001; Thompson et al., 2003). Posterior atrophy scores, on the other hand, were significantly higher in the AD group compared with FTLD. This difference was driven by significantly higher PA ratings in the right hemisphere in AD compared with FTLD. It is perhaps surprising that a proportion of FTLD cases have quite prominent posterior atrophy in the left hemisphere. This is likely to be due to the language cases in this group where left-sided atrophy can spread posteriorly as the disease progresses. Higher PA ratings in the right hemisphere in AD significantly improved the distinction of AD from FTLD. It should be noted, however, that average scores of two raters were used in this study. Classification accuracies therefore may not necessarily reflect performance of a single rater.

Interestingly, 30% of AD subjects in this study had marked PA in the absence of an abnormal MTA rating, whereas only 18% showed the opposite pattern. However, these results are based on arbitrarily chosen cut-off scores. Whilst optimal cut-off scores for different age groups have been investigated for the MTA (see above), further studies are required to identify optimal cut-off scores for the PA scale. The AD patients with PA only tended to be younger (in terms of age and onset) than patients with MTA only. Splitting the AD group into early and late-onset patients further revealed that PA ratings significantly improved the classification of EOAD from younger controls, whereas it did not improve the separation between LOAD and older controls. This suggests that atrophy in posterior regions of the brain is particularly important to consider when making a diagnosis in early-onset patients. However, this segregation with age is not exclusive; some younger AD patients may present with mostly MTA, while some LOAD may have mostly PA.

One potential limitation is the variety in image acquisition. It is unclear how MTA and PA ratings are affected by different scan acquisition protocols and quality. However, it has been shown that MTA ratings are comparable using MRI and CT (Wattjes et al., 2009). Furthermore, the fact that strong patterns were still detected in different groups suggests that

visual rating tools are relatively robust to varying image quality. It should further be noted that only sporadic AD and FTLD cases were included in the group comparison and classification analyses. This was motivated by the fact that the familial AD cases were significantly younger than the sporadic AD cases (mean age 47.7 (SD 6.4) for familial AD and 62.3 (SD 8.9) for sporadic AD), and previous studies suggesting that familial AD patients can have a different clinical phenotype and different patterns of amyloid accumulation than sporadic AD cases (Knight et al., 2011; Ryan and Rossor, 2010). The exclusion of the familial cases therefore resulted in more homogenous groups for the group comparison analysis. Whilst some of these AD patients had non-amnestic clinical presentations during life and may therefore be considered as 'atypical', all of these patients had pathological confirmation of disease. Since pathological confirmation remains the gold standard to establish a definite diagnosis of AD, and since potential interventional treatments are likely to specifically target AD pathology, the main objective of the current study was to assess visual ratings in patients with AD pathology irrespective of clinical diagnosis. Further investigations assessing the relative utility of the visual assessment tools presented in this study should be performed in clinically-diagnosed older sporadic AD patients.

5.6 Chapter conclusion

In conclusion, the current study demonstrates pronounced atrophy in posterior cerebral regions in the absence of clear atrophy in the medial temporal lobe in patients with pathologically-confirmed AD. Since MTA is currently a proposed diagnostic marker for AD, these findings may suggest that some AD patients may not receive a diagnosis of AD if only MTA is considered. The presence of posterior atrophy may be a helpful additional marker for AD, especially in younger patients. This study further presents a tool with which posterior cerebral atrophy can be easily and reliably assessed in a clinical setting. Visual ratings of PA may improve diagnostic accuracy for distinguishing AD from FTLD, and may be valuable in distinguishing early-onset AD from younger controls.

The findings from this and the previous chapter suggest that PA is an important feature of AD. This is further demonstrated by the presence of marked posterior atrophy in individuals with PCA. Patients with PCA therefore represent a disease population in which we can further characterize the mechanisms underlying the marked involvement of posterior regions in AD. Specifically, studying PCA will improve our understanding of how atrophy patterns vary between this presentation and other focal variants of AD, such as typical amnestic AD, how atrophy progresses over time, and how these structural changes relate to cognitive deficits. A better understanding of the neuroimaging and neuropsychological features of PCA may pave the way to address fundamental questions such as which factors drive the heterogeneity of phenotypes in AD.

6. CROSS-SECTIONAL DIFFERENCES IN CORTICAL THICKNESS AND GREY MATTER VOLUME IN PCA AND TYPICAL AD

6.1 Chapter introduction

Whilst the posterior atrophy of PCA (chapter 1, section 1.2.2) may often be evident from visual assessment of structural MR images (chapter 1, Figure 1.1), a number of image analysis tools have been developed with which the patterns of atrophy can be more precisely quantified and localized. Automated image analysis tools such as VBM can be used to assess differences in patterns of cerebral atrophy over the whole brain between different groups (chapter 2, section 2.2.1.3.3). VBM in typical AD has demonstrated grey matter loss mainly in the medial temporal lobe that extends into the posterior cingulate gyrus, precuneus, insula, temporal-parietal association cortex and prefrontal gyrus (Baron et al., 2001; Boxer et al., 2003; Good et al., 2002; Karas et al., 2004; chapter 2, section 2.5.2). Only one study has assessed atrophy patterns in PCA compared with controls and typical AD using VBM (Whitwell et al., 2007a). The study revealed distinct patterns of grey matter loss in both the PCA and typical AD group compared with controls, however, the direct comparison between PCA and typical AD did not show any statistically significant differences after multiple comparison correction. Differential patterns of cortical thickness between PCA and typical AD have not been investigated.

The aim of this study was to assess patterns of cortical thickness and grey matter loss in well-characterized individuals with PCA, and compare these with typical, amnestic AD and with healthy controls.

6.2 Methods

6.2.1 Subjects

The study involved 48 patients with PCA, 30 patients with typical AD (tAD) and 50 age- and gender-matched healthy controls. All subjects were identified retrospectively from a clinical database. Subjects had to fulfil stringent inclusion criteria as described in chapter 3, section 3.4, and had to have at least one MRI scan. Demographics and clinical data of the subjects are summarized in Table 6.1.

6.2.2 MRI acquisition

Images were acquired as described in chapter 3 (section 3.5.1) and Appendix 5.

6.2.3 Image processing

Cortical thickness measurements were made using FreeSurfer version 4.0.3 (chapter 3, section 3.5.3.2.2), and grey matter volumes were measured using SPM5 and DARTEL (chapter 3, section 3.5.3.2.1).

6.2.4 Statistical analysis

Regional variations in cortical thickness and grey matter volumes between the patient groups and the control group were assessed using a vertex-by-vertex GLM (chapter 3, section 3.5.4.2.3). Atrophy A (cortical thickness or grey matter volume) was modelled as a function of group, controlling for age (mean-centred), gender, scanner and TIV, using estimated TIV (eTIV) from the FreeSurfer processing stream which was shown to be a reasonable estimate for TIV (Buckner et al., 2004), by their inclusion as covariates: $A = \beta1\ PCA + \beta2\ tAD + \beta3$ controls $+ \beta4$ age $+ \beta5$ gender $+ \beta6$ scanner $+ \beta7$ eTIV $+ \varepsilon$. The contrasts of interest were calculated using t-tests (two-tailed for FreeSurfer, one-tailed for VBM) between the estimates of the group parameters, i.e. β1 and β3 (PCA vs. controls), β2 and β3 (tAD vs. controls), and β1 and β2 (PCA vs. tAD). Cortical thickness and VBM maps show statistically-significant differences between the groups (FDR-corrected). Differences in cortical thickness between PCA and tAD are further presented as percent differences.

Thickness values were obtained for individual regions using FreeSurfer's Desikan parcellation (Desikan et al., 2006). Differences between groups were assessed on a descriptive level for each region by expressing mean thickness in PCA and tAD as percentage of mean control thickness. Differences were further assessed on a statistical level by using the same statistical analysis as described above (adjusting for the same covariates). This was applied to larger regions, namely frontal lobe, medial and lateral temporal lobes, precuneus and posterior parietal lobe, occipital lobe, and anterior and posterior cingulate gyri. Thickness estimates for these regions were obtained by averaging the thickness values of a number of smaller regions provided by FreeSurfer, details of which are shown in Table 6.3.

6.3 Results

6.3.1 Subjects

The groups were comparable in gender distribution ($p=0.5$), and the PCA group was matched in age to the control group ($p=0.6$). However, the tAD group was older ($p<0.005$ for an effect of age across all groups), and there was a marked difference in MMSE between PCA and tAD ($p<0.001$), with the tAD group having, on average, a lower MMSE score than the PCA group despite similar disease durations (~5 years, $p=0.3$) at time of scan. Pathological confirmation was available for 5 PCA patients (4 AD, 1 AD with Lewy Bodies), 5 tAD patients (all showing AD pathology), and 1 control (showing a normal brain).

Table 6.1: Subjects demographics and clinical data.

	Controls	PCA	tAD	p value
N	50	48	30	N/A
Gender % male	34%	40%	47%	0.5 [§]
Age in years, mean (SD)	63.7 (9.6)	63.0 (6.7) [†]	69.2 (8.9)	<0.005 [¶]
MMSE, mean (SD)	29.3 (1.0) [¥]	21.2 (4.6)	18.4 (4.6)	<0.0001 [¶]
Disease duration in years, mean (range)	-	4.8 (1.0, 12.0)	5.4 (1.0, 11.0)	0.3 [¶]

[§] Fisher's exact test; [¶] ANOVA; [†] age of PCA group matched to age of control group; p=0.6; [¥] available in 32 controls.

6.3.2 Cortical thickness

Table 6.2 shows the adjusted differences in cortical thickness between groups which were obtained from the GLM. Both PCA and tAD group showed significantly lower cortical thickness compared with controls in most regions across the cortex except in the anterior cingulate gyrus. Interestingly, the PCA group showed reduced thickness in the frontal lobe compared with controls, which is comparable to the reductions found for the tAD-control comparison. Compared with tAD, the PCA group showed significantly lower thicknesses bilaterally in the posterior parietal lobe, precuneus and occipital lobe. There was some evidence for significantly lower cortical thickness in the medial temporal lobe in the tAD group compared with PCA.

Table 6.2: Adjusted differences in cortical thickness between groups, 95% confidence intervals, and significance level.

Region	Side	PCA-C		tAD-C		PCA-tAD	
		Diff	**95% CI**	**Diff**	**95% CI**	**Diff**	**95% CI**
Frontal lobe							
	LH	-0.17	[-0.24 to -0.11] ***	-0.17	[-0.24 to -0.10] ***	-0.01	[-0.08 to 0.07]
	RH	-0.18	[-0.24 to -0.13] ***	-0.15	[-0.22 to -0.09] ***	-0.03	[-0.09 to 0.04]
Temporal lobe							
medial	LH	-0.32	[-0.41 to -0.23] ***	-0.42	[-0.52 to -0.32] ***	**0.10**	**[-0.001 to 0.21] ***
	RH	-0.32	[-0.41 to -0.24] ***	-0.34	[-0.45 to -0.24] ***	0.02	[-0.08 to 0.12]
lateral	LH	-0.28	[-0.34 to -0.21] ***	-0.31	[-0.38 to -0.23] ***	0.03	[-0.05 to 0.11]
	RH	-0.27	[-0.34 to -0.20] ***	-0.25	[-0.33 to -0.18] ***	-0.02	[-0.10 to 0.06]
Parietal lobe							
posterior	LH	-0.39	[-0.46 to -0.32] ***	-0.28	[-0.36 to -0.20] ***	**-0.11**	**[-0.19 to -0.03] ****
	RH	-0.41	[-0.47 to -0.36] ***	-0.23	[-0.30 to -0.16] ***	**-0.18**	**[-0.25 to -0.11] *****
precuneus	LH	-0.35	[-0.42 to -0.28] ***	-0.24	[-0.32 to -0.15] ***	**-0.12**	**[-0.20 to -0.03] ****
	RH	-0.41	[-0.47 to -0.34] ***	-0.25	[-0.33 to -0.18] ***	**-0.15**	**[-0.23 to -0.07] *****
Occipital lobe							
	LH	-0.29	[-0.34 to -0.24] ***	-0.17	[-0.23 to -0.10] ***	**-0.12**	**[-0.19 to -0.06] *****
	RH	-0.31	[-0.36 to -0.25] ***	-0.17	[-0.23 to -0.10] ***	**-0.14**	**[-0.20 to -0.08] *****
Cingulate gyrus							
anterior	LH	-0.03	[-0.13 to 0.07]	-0.07	[-0.18 to 0.04]	0.04	[-0.07 to 0.16]
	RH	-0.08	[-0.17 to 0.0004] *	-0.07	[-0.16 to 0.03]	-0.02	[-0.12 to 0.08]
posterior	LH	-0.30	[-0.38 to -0.23] ***	-0.28	[-0.37 to -0.19] ***	-0.02	[-0.11 to 0.07]
	RH	-0.33	[-0.40 to -0.25] ***	-0.27	[-0.36 to -0.18] ***	-0.05	[-0.14 to 0.04]

* p≤0.05; ** p≤0.01; *** p≤0.005, LH - left hemisphere, RH - right hemisphere

6.3.2.1 Comparison of PCA and controls

The PCA group showed widespread differences in cortical thickness, with parts of the orbitofrontal cortex being the only region not showing a significantly thinner cortex (Figure 6.1A). The maps further illustrate a posterior-anterior gradient, with posterior regions showing greater reductions in cortical thickness than anterior regions. As shown in Table 6.3, the superior parietal cortex showed the greatest reduction: on average 20% lower than controls on the left and 22% lower on the right.

6.3.2.2 Comparison of tAD and controls

In the tAD group, lower cortical thickness was found in many regions across the whole brain, only sparing regions around the central sulcus, and small parts of the occipital lobe (Figure 6.1B). Cortical thickness was thinnest in regions of the temporal lobes as well as parietal lobes and precuneus, followed by regions in the frontal lobe. The entorhinal cortex showed lowest cortical thickness compared with mean control thickness (30% reduced in the left and 25% in the right hemisphere, Table 6.3). Reductions in cortical thickness appear to be marginally more marked in the left hemisphere than the right.

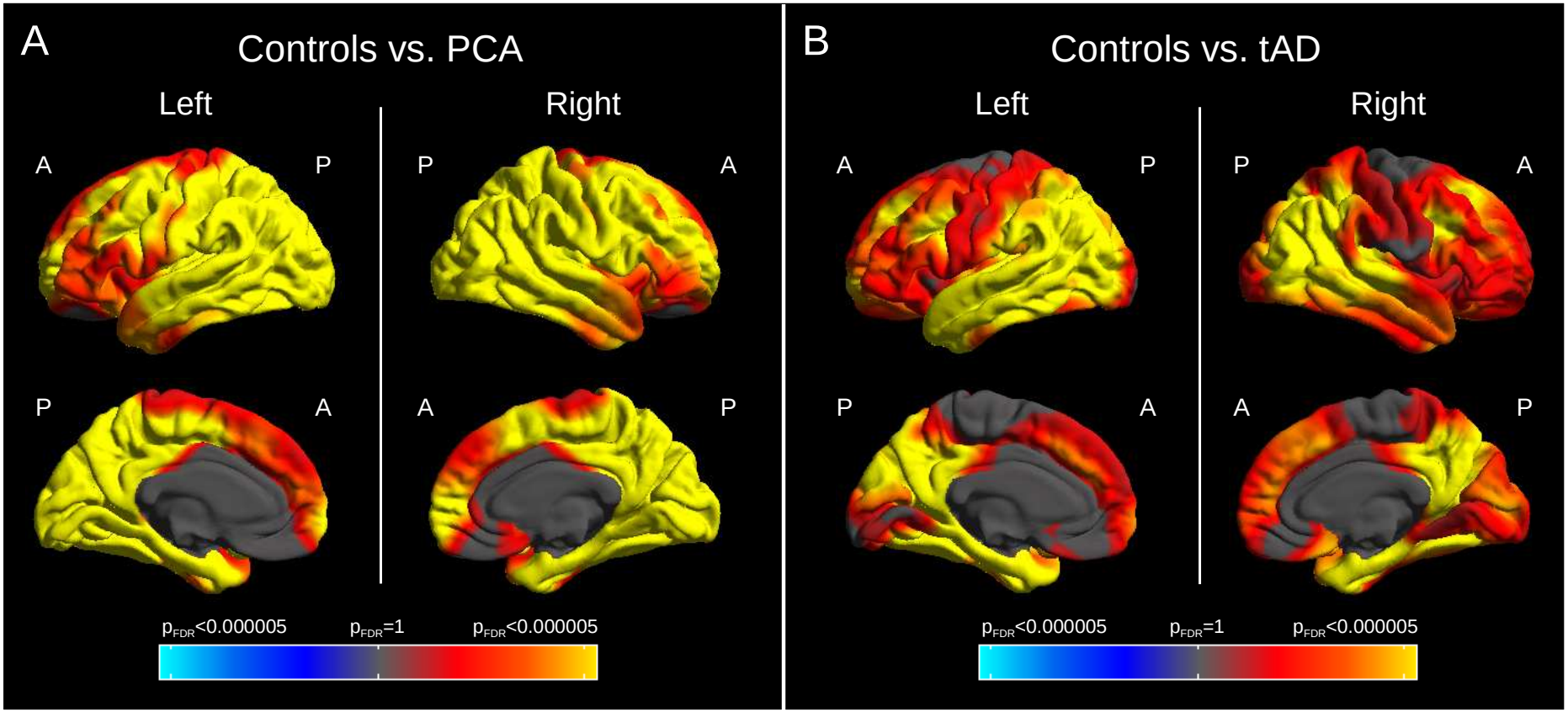

Figure 6.1: Differences in reduced cortical thickness in PCA and tAD compared with controls. A) PCA compared with controls; **B)** tAD compared with controls, for the left and right hemisphere. The colour scale for statistical difference represents FDR-corrected p values at a 0.05 significance level. Red and yellow (positive values) represent lower cortical thickness in the patients groups (PCA and tAD) compared with controls, whereas dark and light blue (negative values) represent greater cortical thickness (which yielded no statistically significant results). A - anterior, P - posterior.

6.3.2.3 Comparison of PCA and tAD

The statistical difference maps for the direct comparison between the patient groups revealed lower cortical thickness predominantly in the superior parietal cortex in the PCA group, and reduced thickness in the entorhinal cortex in the tAD group (Figure 6.2). As shown in Table 6.3, the superior parietal lobes were reduced by 7% in the left, and 12% in the right hemisphere in the PCA group, whereas the entorhinal cortex was reduced by 14% in the left, and 10% in the right hemisphere in the tAD group.

Percent difference maps further revealed lower cortical thickness in the occipital lobes, precuneus, posterior cingulate gyrus, and fusiform gyrus in PCA compared with tAD. In contrast, the tAD group showed lower cortical thickness in the medial temporal lobes as well as lateral temporal lobe regions. However, this difference did not survive FDR correction in the statistical difference maps. In the PCA group cortical thickness showed marginally greater reductions in the right hemisphere compared with the left, whereas in the tAD group thickness was slightly more reduced in the left hemisphere.

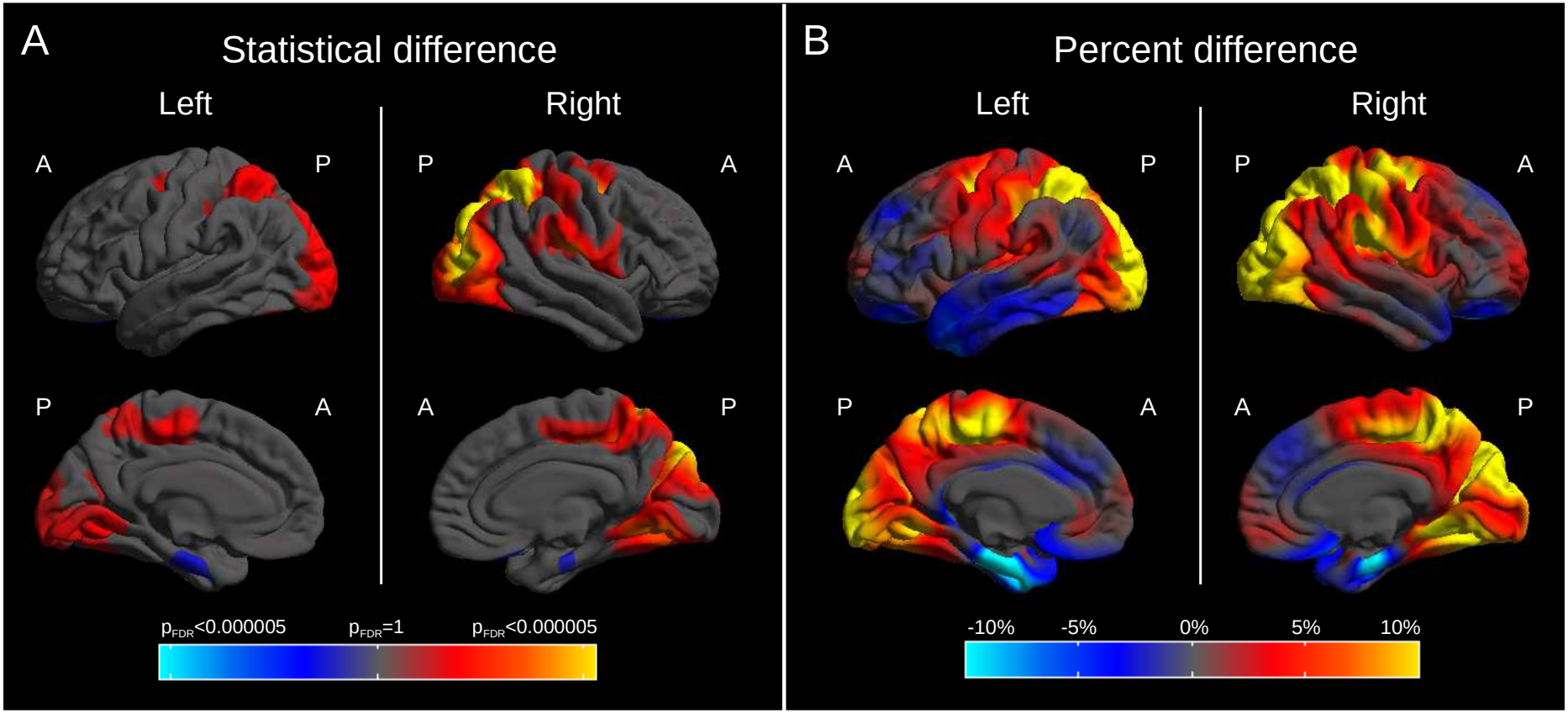

Figure 6.2: Differences in reduced cortical thickness in PCA compared with tAD. The colour scale for statistical difference **(A)** represents FDR-corrected p values at a 0.05 significance level, whereas the colour bar for percent difference **(B)** represents magnitude of cortical thickness difference. Red and yellow (positive values) represent lower cortical thickness in PCA compared with tAD, whereas dark and light blue (negative values) represent lower cortical thickness in tAD compared with PCA. A - anterior, P - posterior.

Table 6.3: Differences in cortical thickness in PCA and tAD. Cortical thickness values for PCA, tAD and difference between PCA and tAD are represented as percentage of mean control thickness in the regions automatically parcellated by FreeSurfer according to Desikan et al. (Desikan et al., 2006).

Region	%PCA/Controls mean (SD)	%tAD/Controls mean (SD)	% (PCA-AD) /Controls
Frontal lobe left hemisphere			
Frontal pole	88.1 (13.9)	88.0 (13.9)	0.1
Orbitofrontal gyrus [1]	96.0 (8.5)	93.3 (6.6)	2.7
Inferior frontal gyrus [2]	94.2 (9.3)	91.8 (6.0)	2.4
Middle frontal gyrus [3]	90.6 (9.0)	90.4 (7.3)	0.2
Superior frontal gyrus	92.8 (7.8)	92.1 (7.6)	0.7
Precentral gyrus	88.7 (9.8)	90.4 (7.6)	-1.7
Frontal lobe right hemisphere			
Frontal pole	88.7 (13.5)	90.6 (9.7)	-1.9
Orbitofrontal gyrus [1]	95.8 (7.5)	93.5 (7.6)	2.3
Inferior frontal gyrus [2]	93.7 (7.6)	92.7 (6.6)	1.0
Middle frontal gyrus [3]	90.3 (7.6)	92.1 (7.5)	-1.8
Superior frontal gyrus	92.5 (7.2)	91.9 (7.5)	0.6
Precentral gyrus	87.4 (8.8)	92.2 (8.2)	-4.8
Temporal lobe left hemisphere			
Medial temporal lobe			
Entorhinal cortex	84.6 (15.2)	70.4 (16.5)	14.2
Parahippocampal gyrus	91.3 (13.6)	85.5 (11.4)	5.8
Fusiform gyrus	87.0 (8.0)	87.8 (9.5)	9.2
Lateral temporal lobe			
Transverse temporal gyrus	88.0 (8.9)	86.6 (8.5)	1.4
Banks of superior temporal sulcus	84.1 (10.5)	85.2 (10.8)	-1.1
Superior temporal gyrus	91.7 (8.1)	86.8 (6.9)	4.9
Middle temporal gyrus	90.9 (9.8)	86.9 (7.9)	4.0
Inferior temporal gyrus	90.5 (10.3)	87.9 (7.8)	2.6
Temporal pole	88.5 (14.5)	82.3 (17.9)	6.2
Temporal lobe right hemisphere			
Medial temporal lobe			
Entorhinal cortex	85.5 (15.0)	75.1 (19.6)	10.4
Parahippocampal gyrus	88.3 (12.3)	87.6 (13.3)	0.7
Fusiform gyrus	87.0 (8.1)	89.3 (8.0)	-2.3
Lateral temporal lobe			
Transverse temporal gyrus	89.7 (11.4)	90.2 (9.2)	-0.5
Banks of superior temporal sulcus	84.9 (9.9)	88.1 (10.1)	-3.2
Superior temporal gyrus	91.1 (9.2)	88.6 (7.5)	2.5
Middle temporal gyrus	90.4 (8.0)	89.5 (9.5)	0.9
Inferior temporal gyrus	91.4 (9.0)	91.8 (8.0)	-0.4
Temporal pole	89.2 (12.0)	83.3 (17.9)	5.9

Table 6.3 continued.

Region	%PCA/Controls mean (SD)	%tAD/Controls mean (SD)	% (PCA-AD) /Controls
Parietal lobe left hemisphere			
Postcentral gyrus	91.2 (9.0)	91.2 (7.2)	0
Supramarginal gyrus	85.7 (9.5)	87.1 (7.0)	-1.4
Precuneus	83.4 (9.0)	88.4 (8.8)	-5.0
Posterior parietal lobe			
Inferior parietal lobe	83.7 (9.4)	84.9 (8.6)	-1.2
Superior parietal lobe	79.6 (10.9)	87.0 (8.0)	-7.4
Parietal lobe right hemisphere			
Postcentral gyrus	88.9 (8.6)	92.1 (7.8)	-3.2
Supramarginal gyrus	84.6 (8.0)	90.0 (8.2)	-5.4
Precuneus	80.7 (8.8)	87.8 (8.1)	-7.1
Posterior parietal lobe			
Inferior parietal lobe	82.5 (6.9)	87.7 (8.7)	-5.2
Superior parietal lobe	77.6 (9.5)	89.6 (7.1)	-12.0
Occipital lobe left hemisphere			
Lateral occipital gyrus	83.0 (11.3)	89.4 (7.4)	-6.4
Cuneus	84.6 (11.5)	88.5 (7.1)	-3.9
Lingual gyrus	86.0 (8.2)	91.0 (6.6)	-5.0
Occipital lobe right hemisphere			
Lateral occipital gyrus	81.3 (10.3)	89.7 (7.1)	-8.4
Cuneus	82.2 (11.3)	89.2 (8.7)	-7.0
Lingual gyrus	85.3 (10.3)	91.7 (7.2)	-6.4
Cingulate gyrus left hemisphere			
Anterior cingulate gyrus			
Rostral anterior cingulate gyrus	98.8 (13.7)	97.5 (10.4)	1.3
Caudal anterior cingulate gyrus	99.4 (12.0)	95.8 (12.0)	3.6
Posterior cingulate gyrus			
Posterior posterior cingulate gyrus	91.3 (9.4)	93.3 (7.8)	-2.0
Isthmus posterior cingulate gyrus	83.0 (11.4)	82.7 (7.5)	0.3
Cingulate gyrus right hemisphere			
Anterior cingulate gyrus			
Rostral anterior cingulate gyrus	96.1 (11.1)	97.2 (10.7)	-1.1
Caudal anterior cingulate gyrus	98.1 (11.7)	96.7 (11.9)	1.4
Posterior cingulate gyrus			
Posterior posterior cingulate gyrus	89.6 (10.6)	92.7 (7.9)	-3.1
Isthmus posterior cingulate gyrus	82.0 (10.8)	83.2 (9.6)	-1.2

[1] average of lateral and medial orbitofrontal regions, [2] average of pars opercularis, pars orbitalis and pars triangularis, [3] average of caudal and rostral midfrontal regions

6.3.3 Voxel-based morphometry

6.3.3.1 Comparison of PCA and controls

In the PCA group widespread grey matter differences were shown compared with controls, with the most significant reductions found in regions of the occipital and parietal lobe, followed by regions in the temporal lobe (Figure 6.3 left, Table 6.4). No significant reductions in grey matter volume were observed for the reverse contrast.

6.3.3.2 Comparison of tAD and controls

In the tAD group, grey matter reductions were shown across the whole brain, with the most significant grey matter loss found in the parietal and temporal regions (Figure 6.3 right, Table 6.4). No significant reductions in grey matter volume were found in the control group compared with tAD.

6.3.3.3 Comparison of PCA and tAD

Direct comparison between PCA and tAD revealed lower grey matter volume in bilateral posterior parietal regions and parts of the occipital lobe (Figure 6.4, Table 6.4). Unthresholded maps further revealed lower grey matter volumes in the medial temporal lobe in the tAD group compared with PCA, however, this reduction did not reach statistical significance following correction for multiple comparisons.

6.3.3.4 Posterior-anterior gradient

A clear posterior-anterior gradient was shown in the PCA group compared with controls and tAD (Figure 6.5). Regions in the temporal and frontal lobes showed similar levels of grey matter differences in both PCA and tAD compared with controls and therefore these were not found to be significantly different in the direct PCA<tAD comparison.

Table 6.4: Location of cluster maximum for each group comparison.

Comparison	Region	Hemisphere	MNI coordinates			T value	Cluster size	p_{FDR} value
			x	*y*	*z*			
PCA < Control	Occipital lobe	Left	-33	-64	-1	13.6	254462	<0.0001
tAD < Control	Temporal lobe	Left	-47	-36	-6	9.8	142790	<0.0001
PCA < tAD	Occipital lobe	Right	29	-78	-0	6.2	43421	<0.0001

Voxel coordinates are in millimetres after conversion from DARTEL into MNI stereotactic space. Results are corrected for multiple comparisons ($p<0.05$).

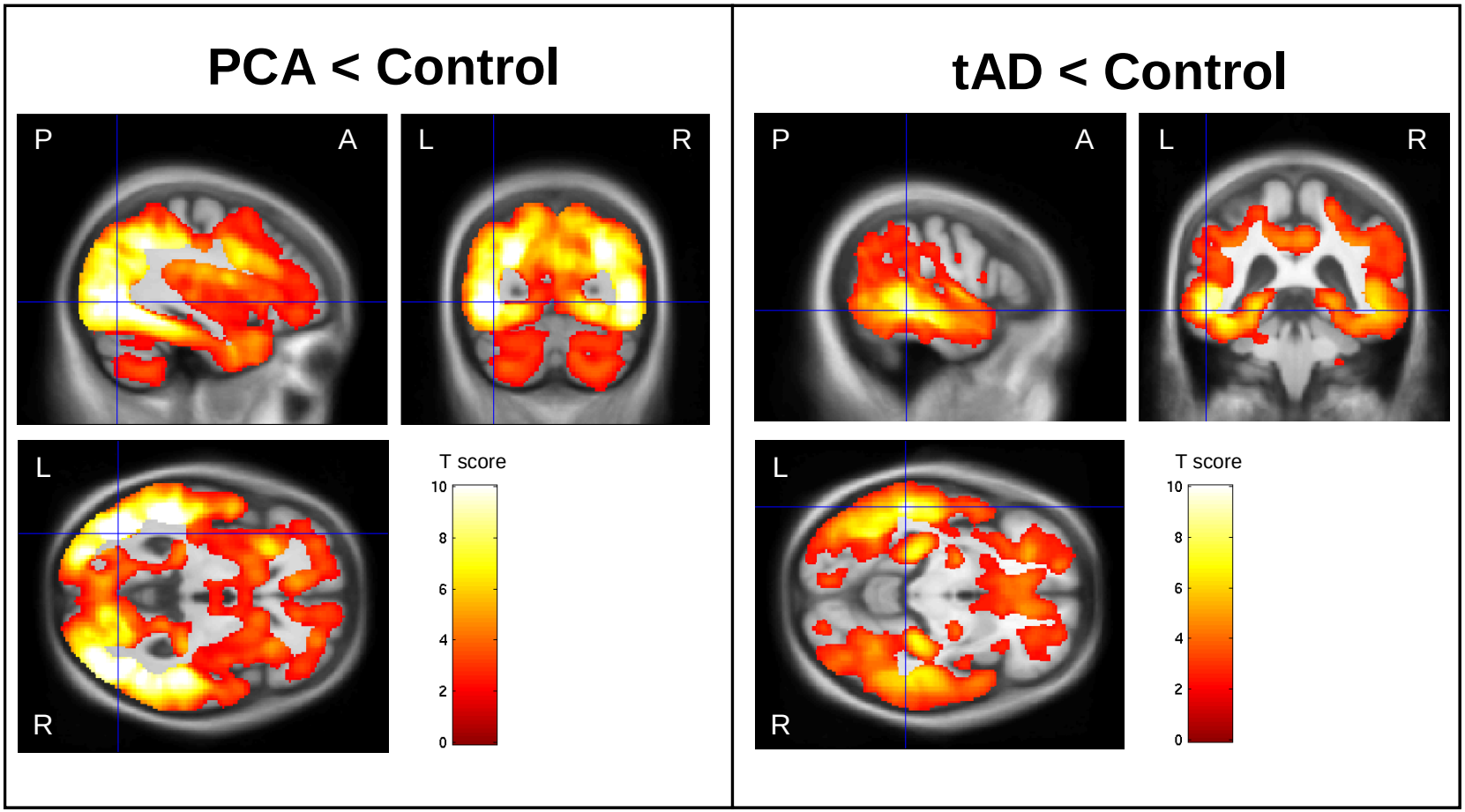

Figure 6.3: Differences in reduced grey matter in PCA and tAD compared with controls. Maps show t-scores (FDR-corrected at $p<0.05$), with warmer colours indicating statistically lower grey matter volumes in the PCA group (left) and the tAD group (right) compared with controls. The crosshair in each contrast is set to the global maximum, which is in the left occipital lobe in the PCA group, and in the left temporal in the tAD group. L - left hemisphere, R - right hemisphere, A - anterior, P - posterior.

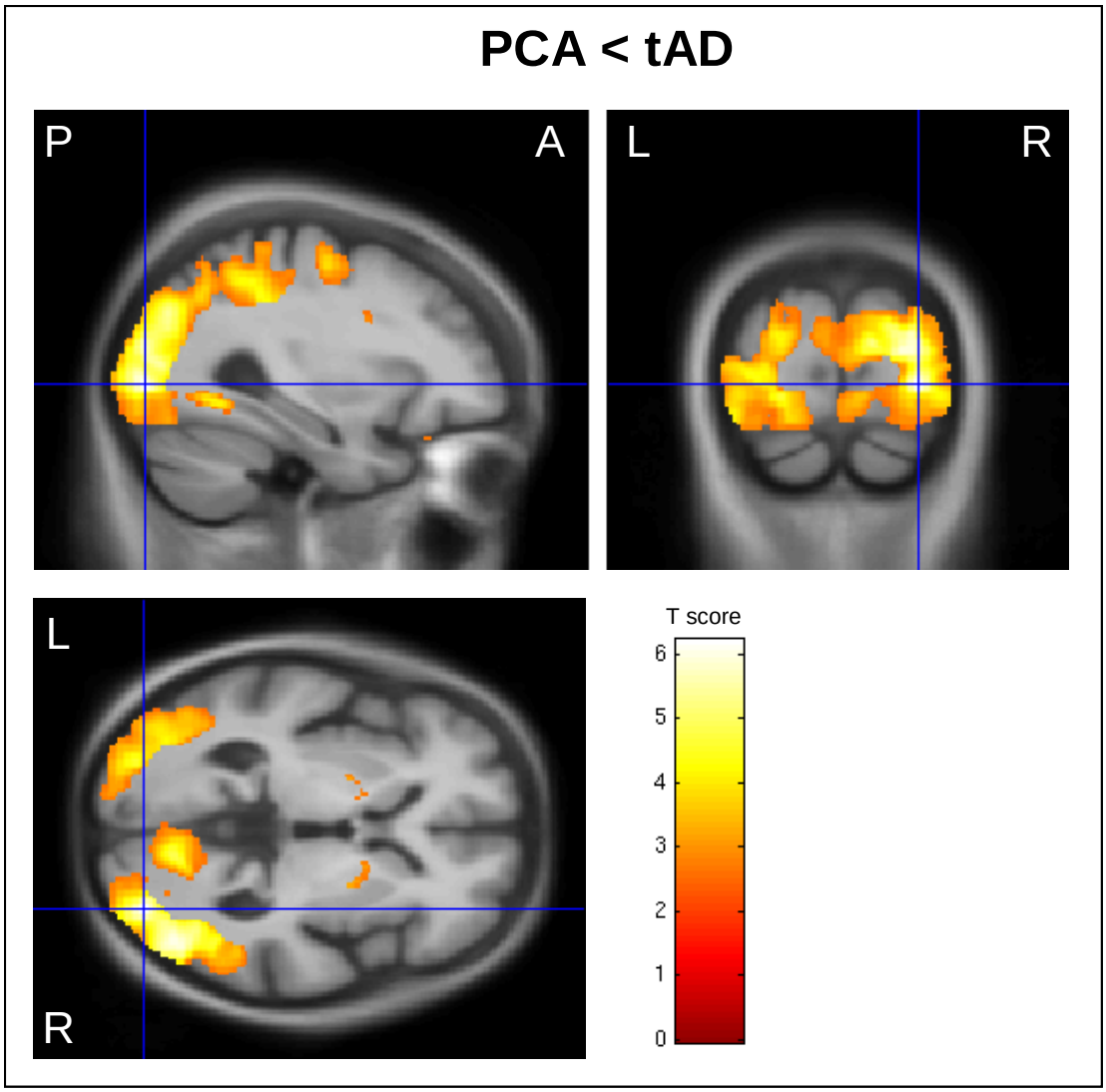

Figure 6.4: Differences in grey matter volume in the PCA group compared with tAD. Map shows t-scores (FDR-corrected at $p<0.05$), with warmer colours indicating statistically lower grey matter volumes in the PCA group compared with tAD. The crosshair is set to the global maximum in the right occipital lobe. L - left hemisphere, R - right hemisphere, A - anterior, P - posterior.

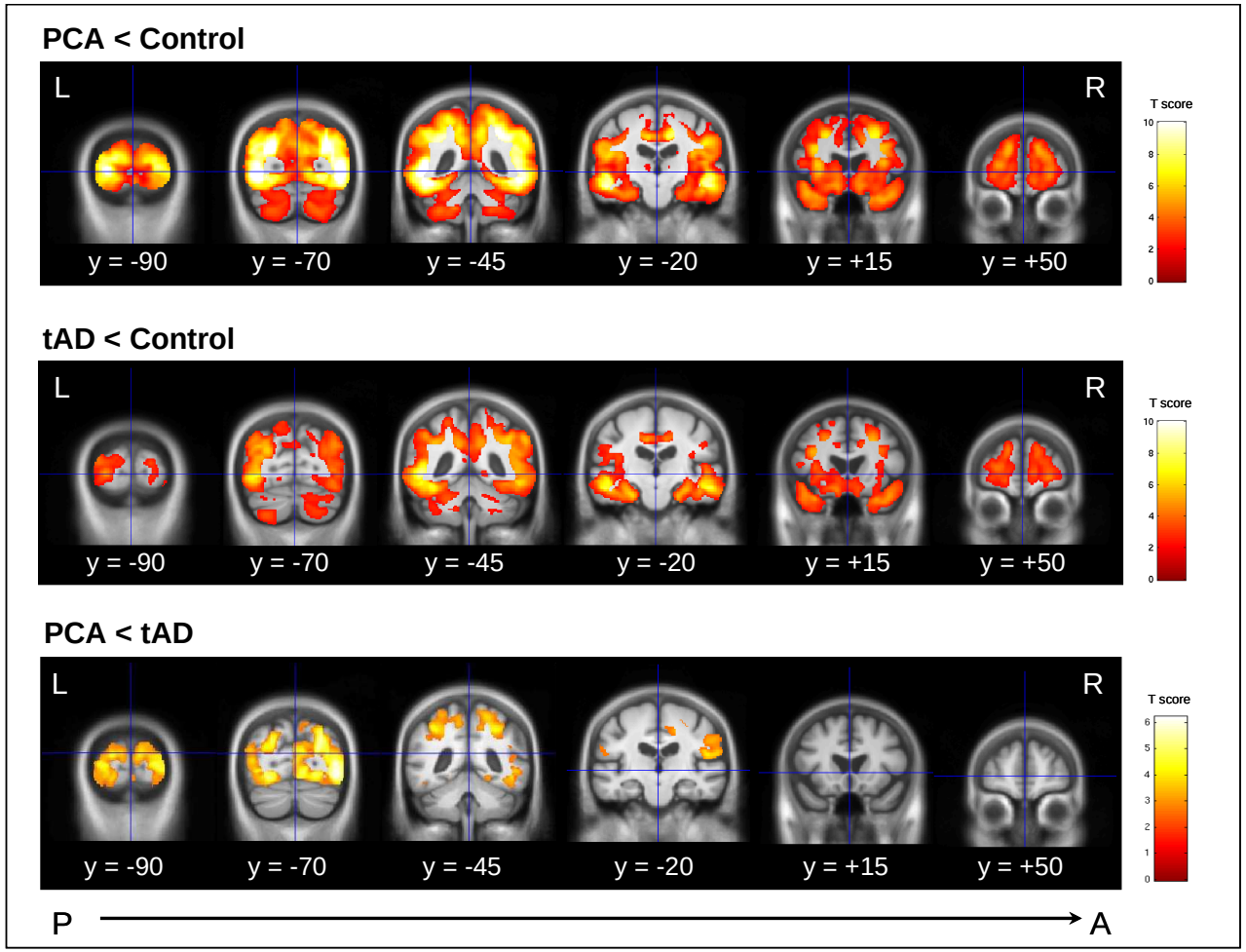

Figure 6.5: Posterior-anterior gradient for each group comparison. Presented are coronal slices from posterior (P) to anterior (A) for differences in grey matter volume in PCA compared with controls (upper panel), tAD compared with controls (middle panel), and PCA compared with tAD (lower panel). Scale bars represent t-values, with warmer colours representing statistically greater differences between groups. Note that y-coordinates here relate to the DARTEL average template, not to MNI space. L - left hemisphere, R - right hemisphere.

6.4 Discussion

This study reports patterns of grey matter loss and cortical thinning in a large series of PCA patients. Cortical thickness and grey matter volumes were compared with tAD patients and healthy controls. Distinct and dissociated patterns of loss were seen in PCA and tAD. The PCA group showed thinner cortex predominantly in occipital and posterior parietal regions compared with controls, whereas the tAD group showed a thinner cortex mainly in medial temporal lobe regions. A direct comparison between PCA and tAD further revealed significantly thinner cortex most marked in the right superior parietal lobe in the PCA group compared with tAD, and the left entorhinal cortex in the tAD group compared with PCA. These results indicate an interesting greater involvement of the right hemisphere in the PCA group compared with tAD which might be driven by the relatively high proportion of patients with predominantly right hemisphere deficits in the PCA group. It would be important to see if this is just a feature of the PCA group in this study (e.g. an artefact of inclusion criteria) or if this reflects a true difference in cerebral vulnerability of the right hemisphere in PCA.

The VBM analysis revealed similar patterns of differences in grey matter volume to those observed in cortical thickness. A direct comparison between PCA and tAD showed significant differences in grey matter volume in occipital lobe and posterior parietal regions in the PCA group compared with tAD, with the right hemisphere being marginally more affected than the left. However, there were no areas where grey matter volume was significantly lower in the tAD group compared with PCA.

These findings are in accordance with a previous volumetric imaging study using VBM. Whitwell et al. found greater grey matter atrophy in primary visual and visual association cortices in PCA compared with controls, and reduced grey matter in the medial temporal lobe in the typical AD group compared with controls (Whitwell et al., 2007a). However, no significant FDR-corrected differences in grey matter were found for the direct comparison between PCA and typical AD. The stronger differences between the disease groups shown in our study may be due to the larger size of the PCA group as well as to differences in the inclusion criteria applied to the PCA and tAD group. Therefore the current study strengthens the evidence base suggesting not only a clinical but also a neuroimaging distinction between these typical and atypical presentations of AD when assessing a single time point. This study also validates the use of cortical thickness measures as a method for quantifying and localising cortical loss in PCA. The posterior pattern of grey matter loss and cortical thinning is further in accordance with PET and SPECT studies showing marked hypoperfusion and hypometabolism in posterior regions in PCA (Bokde et al., 2001; Freedman et al., 1991; Nestor et al., 2003; Ross et al., 1996; Wakai et al., 1994).

Strengths of the current study include the size of the PCA group as well as the well-defined inclusion criteria for both the PCA group and the tAD group (chapter 3, section 3.4). Unlike

some previous studies where patients were selected purely on clinical grounds, the PCA subjects in this study conformed to specific behavioural criteria and in particular were clearly distinguished from tAD patients on the basis of relatively intact episodic memory functions. By only including individuals who met these selection criteria the potential overlap between groups was reduced. Many patients with tAD also show parietal deficits and episodic memory can be impaired in PCA patients later in the disease course. In addition, only PCA patients with AD as the most probable diagnosis were included, since patients with clinical features suggesting DLB, CBD or prion disease at presentation may have non-AD pathology. It should be noted that the tAD group reflects the most common amnestic presentation of AD and did not include any atypical (such as frontal or language) AD presentations.

It is generally difficult to match PCA and tAD groups for disease severity as disease progression and duration in PCA are still not very well understood. In this study, both disease groups showed similar ranges of disease duration, suggesting that both groups included patients with mild to severe impairments. As expected, mean MMSE scores differed between the two disease groups owing to the weighting of questions towards memory and orientation. Furthermore, pathological confirmation was only available in five PCA patients (at time of writing) which represents a limitation to this study since some PCA patients may have other, non-AD pathologies as the underlying cause (Tang-Wai et al., 2004; Victoroff et al., 1994).

Atrophy patterns were analysed using two computational image analysis tools which assessed differences in thickness and grey matter volume across the whole brain without making any *a priori* assumptions about which regions may or may not be affected by the disease. Each technique gives complementary information regarding brain structures in both patient groups. Whilst VBM provides grey matter volumes for subcortical regions for which no cortical thickness estimates are available, cortical thickness measures provided by FreeSurfer are more easily interpretable than the probabilistic grey matter volumes in VBM. The retrospective nature of this study meant that scans were obtained from different scanners, though these were all the same field strength and model, and statistical models were adjusted for scanner type.

Although techniques such as cortical thickness offer a measure of cortical rather than whole brain atrophy, they inevitably lack the resolution to identify changes in cell structure integrity at anything more than a regional level. Nevertheless, the evidence presented here of very significant occipital cortex thinning extending into the striate cortex, provides justification for further studies investigating the specific cognitive phenomena in PCA (e.g. prolonged colour after-images, visual crowding) and regional atrophy patterns (Chan et al., 2001a; Crutch and Warrington, 2007).

6.5 Chapter conclusion

This chapter presents significant cross-sectional differences in cortical thickness and grey matter volume in PCA compared with typical amnestic AD. Regions showing lower cortical thickness and grey matter volumes in the PCA group compared with tAD include the superior parietal lobe and areas of the visual cortex. In contrast, cortical thickness was lower in the entorhinal cortex in the typical AD group compared with PCA. These distinct patterns of atrophy may have diagnostic utility and may help identify posterior variants of AD. This means that in the appropriate clinical context AD should not be discounted simply because of relatively preserved medial temporal lobes and the presence of parietal lobe atrophy. Whilst cross-sectional imaging studies are useful in revealing characteristic patterns of atrophy which may aid clinical diagnosis, it is only through longitudinal studies that progression of atrophy in these patients can be assessed. Longitudinal changes in atrophy patterns in PCA and typical AD will be described in the next chapter.

7. LONGITUDINAL CHANGES IN GREY MATTER VOLUMES AND CORTICAL THICKNESS IN PCA

7.1 Chapter introduction

Longitudinal image analysis is particularly useful in assessing the progression of atrophy over time within an individual, and may increase power by allowing adjustment of tissue loss by initial volume (chapter 2, section 2.2.2). In particular, longitudinal investigations are needed to assess whether the focal cross-sectional patterns of atrophy (as presented in the previous chapter) remain confined to these regions or whether they become more global. Areas of greatest change may not be the areas that are most atrophied initially. The anatomical extent and amount of change in grey matter volume and cortical thickness in PCA is not well understood. Results from longitudinal studies of PCA may allow for a better understanding of the natural history of both PCA and AD.

The aim of the current study was to assess longitudinal changes in whole brain volume, grey matter volume, and cortical thickness in PCA, and compare these with structural changes over time in groups of typical amnestic AD (tAD) patients and healthy controls. Specifically, two possible outcomes were predicted: patterns of atrophy progression are either i) focal, with PCA showing greater atrophy changes in posterior regions compared with controls and tAD, and tAD showing greater atrophy changes in medial temporal lobe regions compared with controls and PCA, leading to significantly different patterns of atrophy changes between PCA and tAD, or ii) atrophy changes are global, with PCA and tAD showing widespread changes of atrophy compared with controls, and only subtle differences in the direct comparison of PCA and tAD. Understanding the progression of atrophy in PCA may improve diagnosis and the quality of prognostic information given to patients.

7.2 Methods

7.2.1 Subjects

The study included 17 PCA and 16 tAD patients, and 18 healthy controls. All subjects were identified retrospectively from a clinical database. Demographics and clinical data of the subjects are summarized in Table 7.1. Subjects had to fulfil specific inclusion criteria as described in chapter 3, section 3.4, and had to have at least two MRI scans on the same scanner approximately 1 year apart. All PCA and tAD patients (100%) as well as 12 control subjects (67%) were included in the cross-sectional study described in the previous chapter. The clinical notes of all PCA patients were reviewed by a clinician to identify initial symptoms and clinical findings (Table 7.2). All patients underwent comprehensive clinical and neuropsychological assessment. An overview of the proportion of PCA and tAD patients showing impaired performance (<5th %ile) on neuropsychological tests of memory,

arithmetic, naming, spelling, speed (letter cancellation), and visuospatial and visuoperceptual processing is provided in Table 7.3.

7.2.2 MRI acquisition

Images were acquired as described in chapter 3 (section 3.5.1) and Appendix 5. Scans of all subjects were acquired on the same scanner, and scan acquisition was consistent between time points for each subject.

7.2.3 Registration of repeat to baseline image

Both baseline and repeat brain regions were delineated (chapter 3, section 3.5.2.1) and the repeat brain images were registered to baseline images using 12dof registration (Woods et al., 1998). A differential bias correction (DBC) was applied to the registered baseline and repeat images using a kernel radius of 5 voxels, in order to correct for differences in intensity inhomogeneity artefacts between the two images (Lewis and Fox, 2004).

7.2.4 BSI

The registered and DBC-corrected scan pairs were used to calculate volume changes using the BSI algorithm (KN-BSI, Leung et al., 2010).

7.2.5 Fluid-registration

The registered and DBC-corrected scan pairs were cropped using subject-specific masks to exclude non-brain regions (e.g. neck and eye), whilst including lateral ventricular CSF, grey matter, white matter and a layer of brain-surface CSF. Fluid registrations (chapter 2, section 2.2.2.2) were run until a stopping criterion based on the derivative of the cost function of the registration was reached (Barnes et al., 2007b). The amount of voxel-level expansion or contraction was extracted from each resulting deformation field by computing the determinant of the Jacobian at each voxel (i.e. the determinant of the gradient of the deformation field). The Jacobian-determinants were then log-transformed, and the resulting ‘voxel-compression map’ for each subject was stored.

7.2.6 Longitudinal VBM

The voxel-compression maps as well as the baseline images were converted to NIFTI format in order to process them using SPM8. The baseline images were first processed in the standard way (chapter 3, section 3.5.3.2.1). The transformation parameters required to warp the original segments to the final template (i.e. rigid alignment plus DARTEL warping) were applied to the grey matter segments, as well as to the voxel-compression map images in order to normalise them to the group-wise average template. The warped grey matter segments were then thresholded at a value of 0.5 to produce binary masks that were then used to multiply the voxel-compression map images to generate separate grey matter voxel-

compression maps for each subject. These grey matter voxel-compression maps were smoothed using an isotropic Gaussian kernel of 6mm FWHM.

7.2.7 Longitudinal cortical thickness

Images were first processed using the standard cross-sectional FreeSurfer pipeline, version 4.5.0 (chapter 3, section 3.5.3.2.2). Baseline and repeat images were then processed using the longitudinal FreeSurfer processing stream (chapter 2, section 2.2.2.2). Cortical thickness was smoothed to approximate a 20mm FWHM Gaussian kernel. All images were visually inspected and editing was performed on the cross-sectional baseline and repeat images, as well as on the template images.

7.2.8 Statistical analysis

Differences in measures of atrophy between groups were analysed using a GLM with a three-level group factor, and adjusting for age, gender as well as interval between time points.

7.2.8.1 BSI

BSI measures were annualised and differences in rates of atrophy between groups were analysed using a GLM with age and gender included as covariates.

7.2.8.2 Longitudinal VBM

Longitudinal volume changes were analysed using a GLM, adjusting for age, gender and interval between time points. Statistical significance of the group differences was tested using FDR-correction at $p<0.05$. Results are displayed as overlays on a study-specific template which was created by normalizing all original images using the DARTEL transformations and calculating the average of the warped brain images. Group differences are presented either as statistical difference maps (FDR-corrected) or as effect size maps (using Pearson correlation coefficients).

7.2.8.3 Longitudinal cortical thickness

Longitudinal differences were assessed by producing thickness change values at each vertex by subtracting the baseline from the repeat. A linear regression model was then applied to assess group differences, adjusting for age, gender and interval between time points. Statistical significance was tested using an FDR-correction at $p<0.05$. Non-significant results are displayed as raw differences between groups in mm.

7.2.8.4 SVM

An SVM (chapter 3, section 3.5.4.2.6) was used in order to assess how well patterns of grey matter volume derived from the VBM analysis and patterns of cortical thickness data obtained from FreeSurfer can separate the three groups (controls, PCA and tAD).

7.2.8.5 Relative variability of changes

A post-hoc analysis was performed in order to assess the variability relative to mean changes over time within specific regions of grey matter. The motivation for this was to establish whether the lack of significant differences in cortical thickness changes between subject groups was owing to a relatively high variance or relatively low mean changes. Seven regions were selected from the FreeSurfer processing stream based on regions that showed the greatest differences in the VBM and FreeSurfer analyses between PCA/tAD and controls. These regions were the entorhinal cortex, fusiform gyrus, inferior and superior parietal cortex, precuneus, isthmus of cingulate gyrus and cuneus, all in both hemispheres. We assessed fluid-derived grey matter volume change alongside FreeSurfer-derived volume and thickness changes in these regions. Grey matter volume changes were measured by importing the FreeSurfer regions into the same space as the Jacobian voxel-compression maps, and calculating mean grey matter volume change in mm^3 within these regions by integrating the Jacobians. Cortical thickness and volume changes were measured by extracting thicknesses (in mm) and volumes (in mm^3) directly from FreeSurfer and subtracting the repeat thickness/volume from the baseline thickness/volume. Mean (SD) differences in volume and thickness changes between subject groups together with their ratio (mean difference/SD) were assessed. For this comparison a pooled SD was used derived from the GLM which was weighted according to the subject groups.

7.3 Results

7.3.1 Subjects demographics

As shown in Table 7.1, there was no evidence of a difference in gender distribution or age between the PCA and control group ($p>0.8$, both tests). However, the tAD group was older compared with controls and PCA (both $p<0.001$). As expected there was a significant difference in baseline and follow-up MMSE between PCA and controls ($p<0.0001$), and tAD and controls ($p<0.0001$), however, no significant difference was found between PCA and tAD ($p=0.2$ at baseline, $p=0.3$ at follow-up). Both PCA and tAD showed a similar decline in MMSE from baseline to follow-up (2.6 points in PCA, 2.4 points in tAD with similar, ~1-year, intervals between time points). Furthermore, no significant differences were found for TIV ($p=0.8$ across groups, $p>0.5$ between groups). Whole brain volume at baseline and follow-up, adjusted for TIV, was significantly different across groups ($p<0.0001$ for both baseline and follow-up) and between patient groups and controls ($p<0.001$ for both PCA and tAD), with both patient groups having significantly lower brain volumes (12-15%) than the controls. No significant differences in baseline and follow-up whole brain volume were found between PCA and tAD ($p=0.7$ at baseline, $p=0.8$ at follow-up).

Table 7.1: Subject demographics.

	Controls	PCA	tAD	p [¶]
N	18	17	16	N/A
Gender male / female	7 / 11	6 / 11	7 / 9	0.9 [§]
Age in years at baseline, mean (SD)	64.0 (5.0)	64.3 (4.7)	72.6 (7.1)[†‡]*	<0.001
Interval between time points in months, mean (SD)	12.4 (0.6)	12.0 (1.1)	11.6 (0.9)	0.06
Disease duration in years at baseline, mean (SD)	N/A	5.1 (2.4)	4.7 (3.1)	0.7
MMSE at baseline, mean (SD)	29.4 (0.7)[#]	21.4 (5.2)[†]**	19.3 (3.8)[†]**	<0.0001
MMSE at follow-up, mean (SD)	29.3 (1.1)[#]	18.8 (5.9)[†]**	16.9 (4.0)[†]**	<0.0001
Total intracranial volume at baseline in ml, mean (SD)	1477.9 (131.9)	1466.7 (153.3)	1448.5 (140.1)	0.8
Whole brain volume at baseline in ml, mean (SD)	1118.7 (103.1)	983.2 (121.4)[†]*	965.4 (96.2)[†]*	<0.0001 [¥]
Whole brain volume at follow-up in ml, mean (SD)	1120.3 (98.3)	966.1 (129.2)[†]*	949.0 (98.2)[†]*	<0.0001 [¥]

[¶] ANOVA (except gender); [§] Fischer's exact test; [#] available for 10 controls; [†] compared with controls; [‡] compared with PCA; * p<0.001; ** p<0.0001; [¥] adjusted for TIV

7.3.2 Clinical and neuropsychology data

The most commonly reported initial symptoms (Table 7.2) in the PCA group were difficulties with arithmetic (71%) as well as spelling (41%) and locating objects (41%). Whilst a high proportion of PCA patients also reported difficulties with 'memory' (47%), a much lower proportion showed impaired performance on memory tasks on formal neuropsychological testing at visit 1 (29%, Table 7.3). The most commonly reported clinical feature in the PCA group was difficulties handling objects (praxis, 47%)), followed by visual disorientation (24%).

Table 7.2: Frequency of first reported symptoms and clinical features in PCA group.

INITIAL SYMPTOMS	% DEFICITS PRESENT
Calculation	71%
Memory	47%
Spelling	41%
Locating objects	41%
Reading	35%
Perceiving distances/depth	35%
Word-finding	35%
Writing	24%
Facial recognition	18%
Identifying objects	12%
CLINICAL FEATURES	
Praxis	47%
Visual disorientation	24%
Myoclonus	6%
Extrapyramidal signs	6%

Neuropsychological testing (Table 7.3) revealed that all PCA patients showed impaired performance on the letter cancellation task (100%), and the majority of PCA patients also showed visuospatial (88% at visit 1) and visuoperceptual difficulties (82% at visit 1). In the tAD group, besides impaired performance on visual and verbal memory tasks (as defined by inclusion criteria), patients showed difficulties with visuoperceptual processing (81%) and arithmetic (81%). The PCA group showed a decline in performance on all tests, with a particularly marked drop in performance on the verbal memory task. A decline in performance was also revealed in the tAD group except on visual memory, letter cancellation, arithmetic and visuoperceptual processing tests. Formal statistical testing (chi-square test) of changes in performance between visit 1 and visit 2 in each group did not reveal significant differences. However, comparing performance at visit 1 between PCA and tAD revealed that the PCA group performed significantly better on the verbal memory task ($p<0.001$) and arithmetic ($p=0.01$), whereas performance in the PCA group was significantly worse on tasks of visuospatial processing ($p=0.01$) and the letter cancellation task ($p=0.02$) compared with tAD.

Table 7.3: Proportion of PCA and tAD patients showing deficits on neuropsychological tests.

COGNITIVE DEFICITS [¶]	PCA		tAD	
	VISIT 1 [‡]	VISIT 2	VISIT 1	VISIT 2
Memory (verbal) [1]	29% ***	47%	100%	100%
Memory (visual) [1]	-	-	100%	94%
Visuospatial [2]	88% **	94%	44%	81%
Visuoperceptual [3]	82%	88%	81%	81%
Naming [4]	59%	71%	56%	81%
Arithmetic [5]	35% **	41%	81%	75%
Speed [6]	100% *	100%	69%	63%
Spelling [†7]	50%	60%	-	-

[¶] Proportion (%) of subjects performing <5th %ile; [‡] Chi-square test comparing baseline assessments between PCA and tAD; * p≤0.05; ** p≤0.01; *** p≤0.001; [1] Short Recognition Memory Test (Warrington, 1996) or Easy Recognition Memory Test for words (Clegg and Warrington, 1994); [2] VOSP Number location test (Warrington and James, 1991); [3] VOSP Object Decision or VOSP Silhouettes test (Warrington and James, 1991); [4] Graded Naming test, verbal version of this test in 10 PCA patients (Warrington, 1997); [5] Graded Difficulty Arithmetic test (Jackson and Warrington, 1986); [6] Letter cancellation test (Willison and Warrington, 1992); [7] Graded Difficulty Spelling test (Baxter and Warrington, 1994); [†] available in 10 PCA subjects

7.3.3 BSI

Table 7.4 shows the means and SDs of the annualized brain atrophy rates in controls, PCA and tAD as well as adjusted group differences and significance levels. BSI is reported in ml as well as percent of whole brain volume at baseline. TIV was not significant when included as a covariate in this model (p=0.3 for ml, and p=0.7 for percentage BSI). Atrophy rates were significantly different between the patient groups and controls (p<0.0001 for both PCA and tAD), and across all groups (p<0.0001). The PCA group showed higher atrophy rates compared with tAD, however, this difference was not statistically significant (p=0.08).

Table 7.4: Overview atrophy rates (BSI) in controls, PCA and tAD.

		BSI annualized, in ml	BSI annualized, % of whole brain volume at baseline
Means and SD	**Controls (N=18)**	4.0 (4.5)	0.3 (0.4)
	PCA (N=17)	22.3 (6.0)	2.3 (0.7)
	tAD (N=16)	18.1 (7.4)	1.9 (0.8)
Adjusted differences and confidence intervals	**Controls vs. PCA**	18.4 [14.4, 22.3]*	2.0 [1.6, 2.4]*
	Controls vs. tAD	16.8 [12.0, 21.6]*	1.8 [1.3, 2.3]*
	PCA vs. tAD	1.6 [-3.2, 6.4]	0.2 [-0.3, 0.7]
p (across all groups)		<0.0001	<0.0001

* p<0.0001

7.3.4 Controls vs. PCA longitudinal changes

The longitudinal grey matter change analysis revealed global grey matter loss in PCA compared with controls (Figure 7.1A, Figure 7.2A, Figure 7.3A), with the most significant atrophy progression in temporal and parietal lobe regions, as well as areas in the frontal lobe. The cortical thickness analysis also showed global thinning in the PCA group, however, thinning in most areas did not survive FDR-correction. Cortical thickness maps therefore show raw differences in mm (Figure 7.4).

7.3.5 Controls vs. tAD longitudinal changes

The VBM analysis revealed global grey matter volume loss in tAD compared with controls (Figure 7.1B, Figure 7.2B, Figure 7.3B), with the most significant atrophy progression found in temporal and parietal lobe regions in tAD. Widespread cortical thinning was also found in the longitudinal cortical thickness comparison, none of which, however, survived FDR-correction (Figure 7.4).

7.3.6 PCA vs. tAD longitudinal changes

The direct comparison of longitudinal changes in grey matter volume and cortical thickness between PCA and tAD did not return statistically significant results after FDR-correction. Differences in grey matter volume change are therefore presented as effect size (Pearson correlation coefficient, Figure 7.1C, Figure 7.2C, Figure 7.3C), and differences in cortical thinning are shown in mm (Figure 7.4). The PCA group showed greater grey matter volume losses in the left medial temporal lobe, as well as bilaterally in the supramarginal and inferior parietal lobe, head of the caudate nucleus and frontal lobe regions compared with tAD. In contrast, the tAD group showed greater grey matter volume losses bilaterally in anterior, middle and superior temporal lobe regions, frontal lobe regions including the frontal pole,

precuneus, superior parietal lobe, and thalamus compared with PCA. Similarly, the cortical thickness difference maps show greater cortical thinning bilaterally in the medial temporal and medial frontal lobe regions, as well as right parietal lobe regions in PCA compared with tAD, and greater thinning bilaterally in anterior and lateral temporal lobe regions as well as left superior parietal lobe in tAD compared with PCA. However, the size of these effects was small and statistically non-significant.

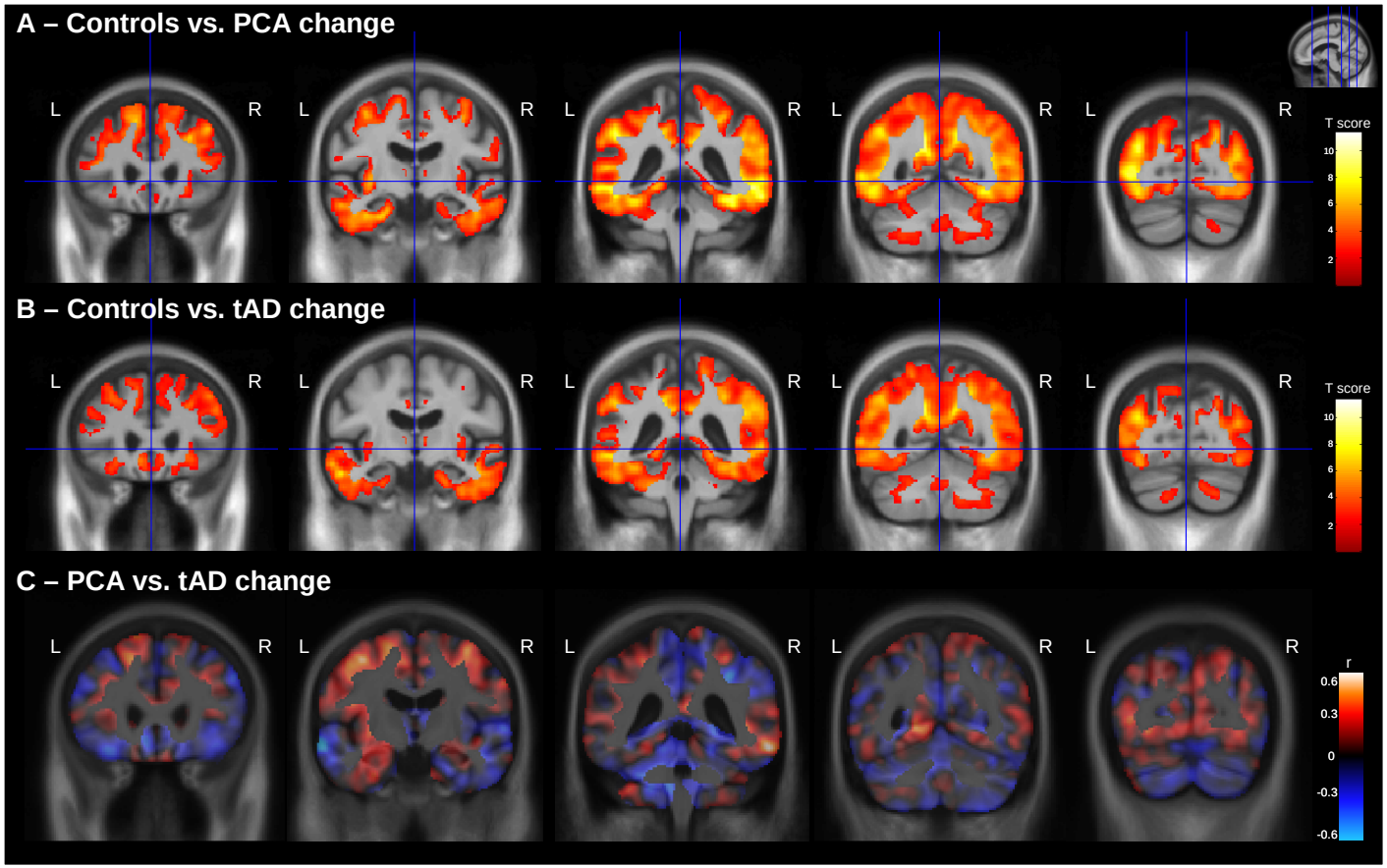

Figure 7.1: Longitudinal changes in grey matter volume, coronal view. Differences in grey matter atrophy are shown for A) PCA compared with controls, B) tAD compared with controls, and C) PCA compared with tAD. The colour bar for the control comparisons (A and B) show t-values for FDR-corrected results ($p<0.05$) with warmer colours indicating greater volume loss in PCA and tAD compared with controls, whereas the colour bar for the PCA vs. tAD comparison (C) shows correlation coefficients, with warmer colours indicating greater volume loss in PCA compared with tAD, and cooler colours representing the reverse contrast. DARTEL coordinates for the slices shown are (from left to right): y=20, y=-15, y=-45, y=-60, y=-80.

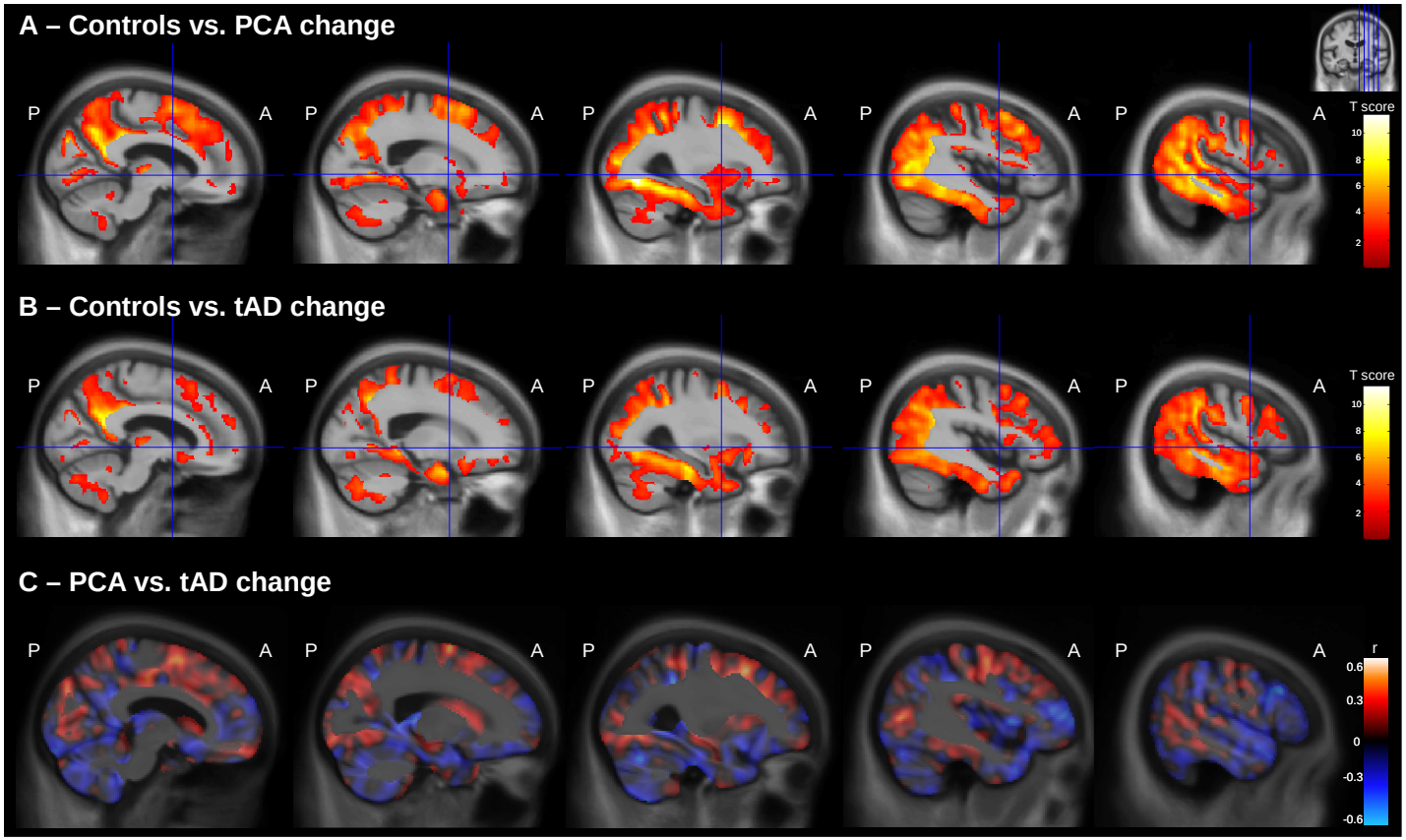

Figure 7.2: Longitudinal changes in grey matter volume, sagittal view. Differences in grey matter atrophy are shown for A) PCA compared with controls, B) tAD compared with controls, and C) PCA compared with tAD. The colour bar for the control comparisons (A and B) show t-values for FDR-corrected results ($p<0.05$) with warmer colours indicating greater volume loss in PCA and tAD compared with controls, whereas the colour bar for the PCA vs. tAD comparison (C) shows correlation coefficients, with warmer colours indicating greater volume loss in PCA compared with tAD, and cooler colours representing the reverse contrast. DARTEL coordinates for the slices shown are (from left to right): x=10, x=20, x=30, x=40, x=50.

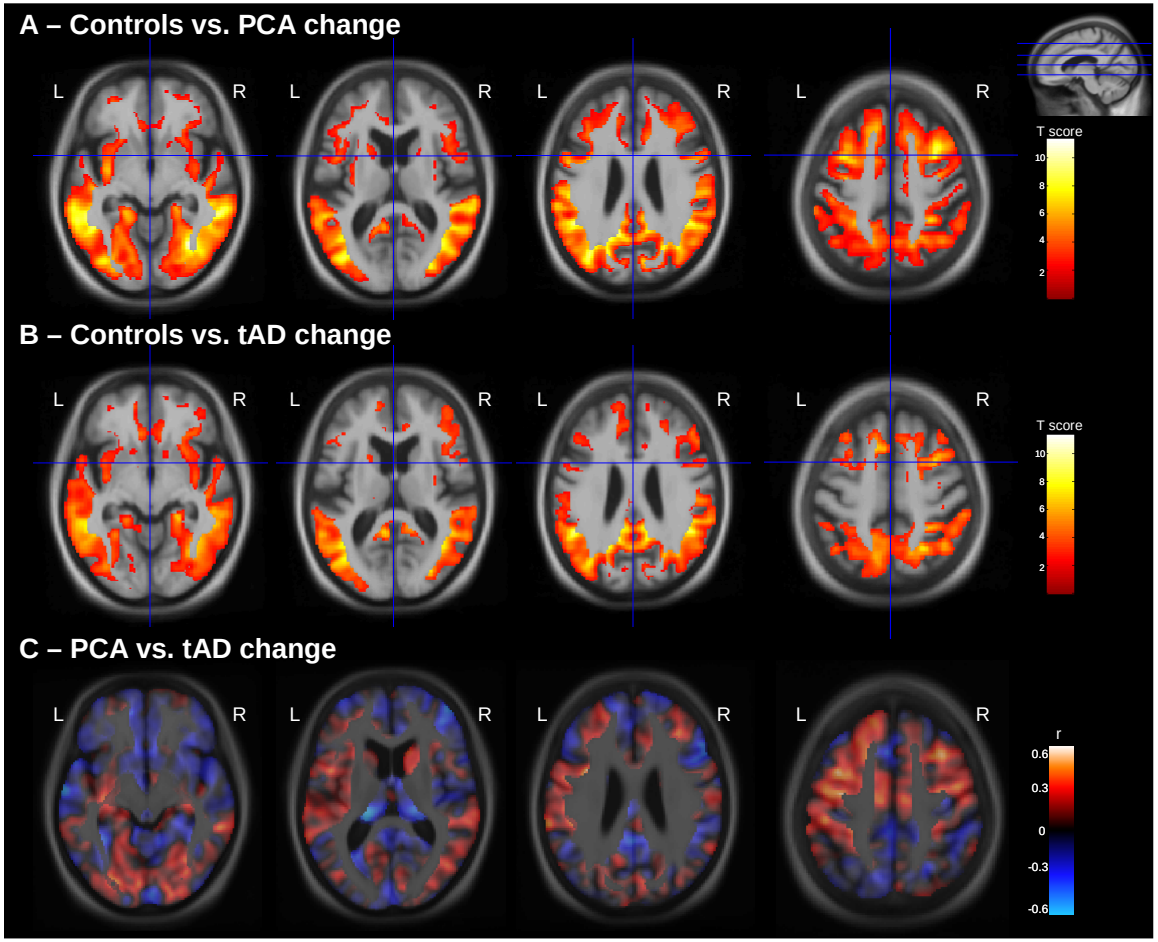

Figure 7.3: Longitudinal changes in grey matter volume, axial view. Differences in grey matter atrophy are shown for **A)** PCA compared with controls, **B)** tAD compared with controls, and **C)** PCA compared with tAD. The colour bar for the control comparisons (A and B) show t-values for FDR-corrected results ($p<0.05$) with warmer colours indicating greater volume loss in PCA and tAD compared with controls, whereas the colour bar for the PCA vs. tAD comparison (C) shows correlation coefficients, with warmer colours indicating greater volume loss in PCA compared with tAD, and cooler colours representing the reversed contrast. DARTEL coordinates for slices shown are (from left to right): z=-5, z=10, z=25, z=45.

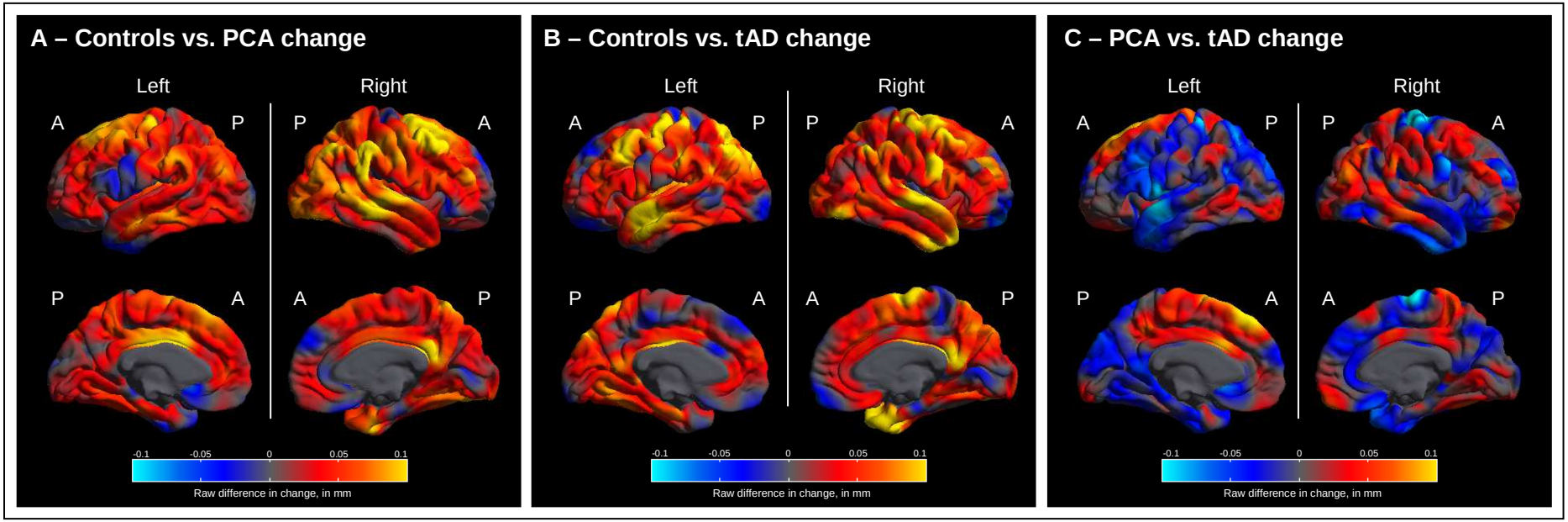

Figure 7.4: Longitudinal changes in cortical thickness. Differences in cortical thinning is shown for **A)** PCA compared with controls, **B)** tAD compared with controls, and **C)** PCA compared with tAD. The colour bar represents raw differences in mm, with warmer colours indicating greater cortical thinning in PCA and tAD compared with controls (A and B), and PCA compared with tAD (C), whereas cooler colours represent the reversed contrast.

7.3.7 Support vector machine

The results of the classification analysis (accuracies, sensitivities and specificities) are presented in Table 7.5. Using the cortical thickness change data from FreeSurfer, the SVM produced accuracies of 65.7% for classifying PCA from controls, and 73.5% for classifying tAD from controls, whereas using grey matter volume loss data from the VBM analysis classification accuracies for PCA and tAD from controls were 97.1% and 94.1%, respectively. The direct classification of PCA and tAD gave mixed results. Classification accuracy using cortical thickness was 63.6% [95% CI 45.1, 79.6]. The confidence intervals indicate that this accuracy is not significantly different from chance. In contrast, accuracy using grey matter volumes was 72.7% [95% CI 54.5, 86.7], which represents a reasonable classification accuracy which was significantly different from chance.

Furthermore, regions in which loss of grey matter and cortical thickness contributed most to the classification of PCA and tAD (Figure 7.5) are very similar to those found in the difference maps (Figure 7.1C, Figure 7.2C, Figure 7.3C and Figure 7.4C). These results may suggest that, although structural differences between PCA and tAD are subtle and statistically non-significant, using a voxel-by-voxel VBM analysis they are sufficiently strong to train a machine learning algorithm and provide reasonable classification accuracy between the two groups.

Table 7.5: **Classification analysis.** Shown are accuracies, specificities and sensitivities with 95% confidence intervals in percent for each group comparison and method.

Groups	Method	Accuracy	Specificity	Sensitivity
Controls vs. PCA	**FreeSurfer**	65.7 [47.8, 80.1]	72.2 [46.5, 90.3]	58.8 [32.9, 81.6]
	VBM	97.1 [85.1, 99.9]	100.0 [81.5, 100.0]	94.1 [71.3, 99.9]
Controls vs. tAD	**FreeSurfer**	73.5 [55.6, 87.1]	77.8 [52.4, 93.6]	68.8 [41.3, 89.0]
	VBM	94.1 [80.3, 99.3]	100.0 [81.5, 100.0]	87.5 [61.7, 98.5]
PCA vs. tAD	**FreeSurfer**	63.6 [45.1, 79.6]	64.7 [38.3, 85.8]	62.5 [35.4, 84.8]
	VBM	72.7 [54.5, 86.7]	70.6 [44.0, 89.7]	75.0 [47.6, 92.7]

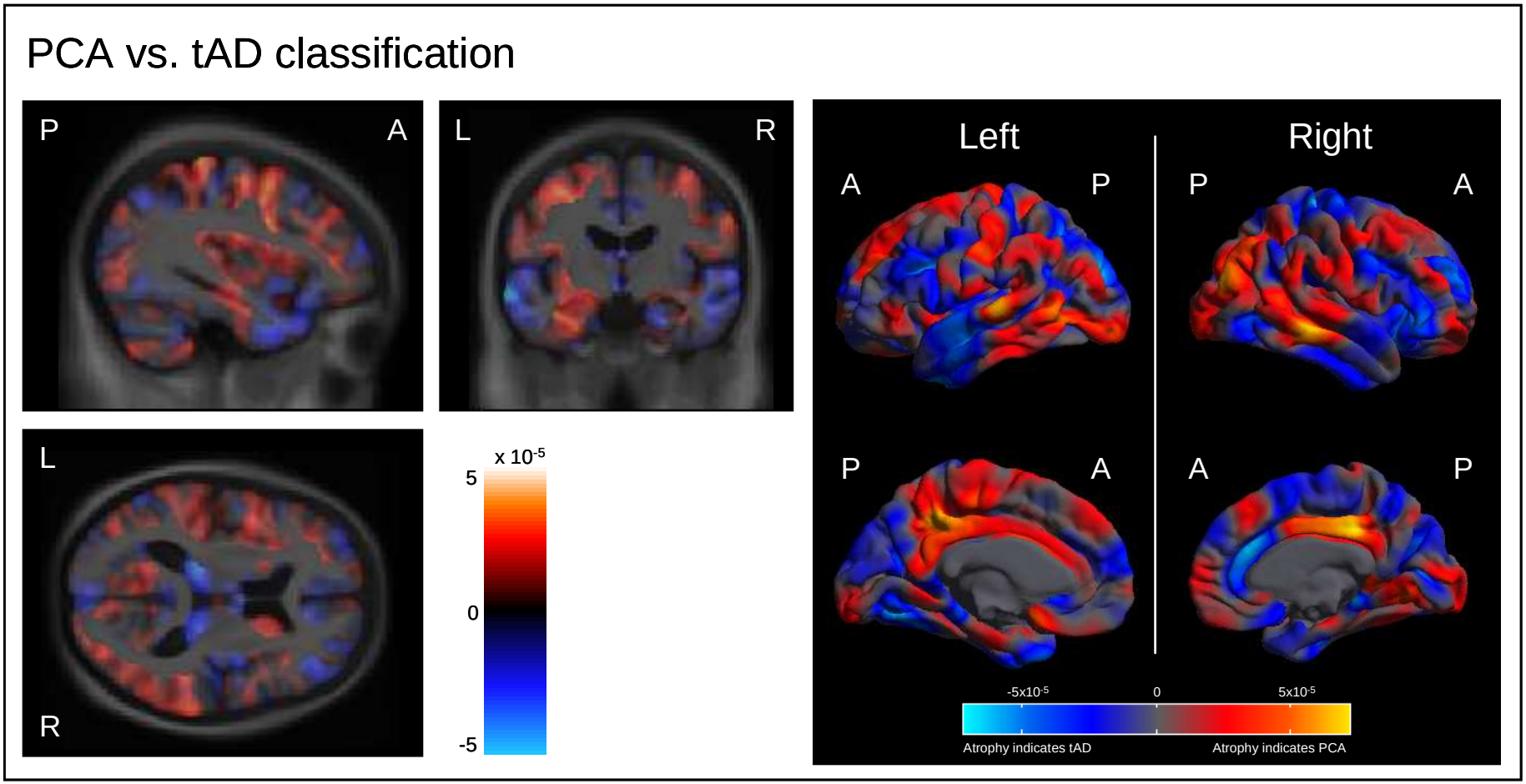

Figure 7.5: **VBM and cortical thickness maps for classification of PCA vs. tAD.** The classification maps show regions that were most influential in making a classification between the two groups, using grey matter volumes (left) and cortical thickness (right). Red represents areas where grey matter volume loss and cortical thinning indicates PCA, whereas blue shows areas where grey matter volume loss and cortical thinning indicates tAD.

7.3.8 Relative variability of changes

Table 7.6 presents the mean differences between patient group (PCA and tAD) and controls, as well as pooled SD and ratios of mean difference divided by pooled SD. Ratios were higher for the grey matter volume data from the fluid registration method (average ratio 2.6 and 1.9 for PCA and tAD, respectively) than the ratios for the cortical volume (average ratio 0.3 and 0.5 for PCA and tAD, respectively) and cortical thickness (average ratio 0.7 for both PCA and tAD). This may indicate that although FreeSurfer measures greater mean changes in patient groups than controls, this difference is also relatively more variable.

Table 7.6: Variability of fluid and FreeSurfer measures. Presented are mean differences, pooled SDs and ratios of difference/pooled SD for grey matter volume, cortical volume and cortical thickness between PCA and controls, and tAD and controls.

Region	Left / Right	PCA - Controls									tAD - Controls								
		Fluid - volume			FS - volume			FS - thickness			Fluid - volume			FS - volume			FS - thickness		
		diff in mm^3	SD	diff / SD	diff in mm^3	SD	diff / SD	diff in mm	SD	diff / SD	diff in mm^3	SD	diff / SD	diff in mm^3	SD	diff / SD	diff in mm	SD	diff / SD
Entorhinal	**L**	41.5	20.4	**2.0**	54.4	205.6	**0.3**	30.0	188.4	**0.2**	29.5	15.2	**1.9**	148.8	415.6	**0.4**	20.1	170.5	**0.1**
	R	39.4	20.4	**1.9**	-12.8	237.6	**-0.1**	81.9	67.0	**1.2**	19.5	35.3	**0.6**	360.4	432.1	**0.8**	128.8	172.6	**0.7**
Fusiform	**L**	241.8	75.4	**3.2**	99.6	360.4	**0.3**	18.7	63.1	**0.3**	188.0	60.2	**3.1**	124.9	370.4	**0.3**	30.7	63.6	**0.5**
	R	212.6	58.9	**3.6**	238.9	269.0	**0.9**	43.4	75.4	**0.6**	191.7	65.8	**2.9**	346.1	325.4	**1.1**	60.5	70.3	**0.9**
Inferiorparietal	**L**	261.4	82.6	**3.2**	184.1	464.2	**0.4**	36.9	50.0	**0.7**	218.0	68.9	**3.2**	38.2	463.2	**0.1**	45.7	42.2	**1.1**
	R	313.5	97.2	**3.2**	223.4	463.0	**0.5**	54.8	56.1	**1.0**	254.3	137.2	**1.9**	336.4	360.1	**0.9**	39.7	46.8	**0.8**
Superiorparietal	**L**	235.0	93.0	**2.5**	3.7	684.4	**<0.1**	32.9	42.6	**0.8**	188.7	94.0	**2.0**	219.9	387.9	**0.6**	45.3	46.2	**1.0**
	R	217.7	83.7	**2.6**	161.2	452.1	**0.4**	53.8	46.3	**1.2**	194.6	110.8	**1.8**	374.5	463.8	**0.8**	55.2	46.2	**1.2**
Precuneus	**L**	175.0	45.9	**3.8**	135.7	233.1	**0.6**	44.5	46.8	**0.9**	161.4	74.9	**2.2**	58.3	227.8	**0.3**	29.6	44.4	**0.7**
	R	181.9	55.7	**3.3**	141.0	237.2	**0.6**	27.9	49.4	**0.6**	123.4	78.2	**1.6**	154.9	224.1	**0.7**	32.2	42.9	**0.8**
Isthmuscingulate	**L**	43.6	24.9	**1.8**	-5.4	143.8	**<-0.1**	28.1	54.4	**0.5**	35.6	17.1	**2.1**	105.8	156.9	**0.7**	9.9	65.2	**0.2**
	R	23.1	21.1	**1.1**	7.5	172.3	**<0.1**	75.0	65.3	**1.1**	28.8	23.4	**1.2**	28.0	172.2	**0.2**	39.1	68.2	**0.6**
Cuneus	**L**	35.5	18.7	**1.9**	17.4	211.8	**0.1**	36.8	72.0	**0.5**	30.4	17.2	**1.8**	81.3	244.6	**0.3**	29.4	59.3	**0.5**
	R	35.1	18.8	**1.9**	3.9	203.5	**<0.1**	38.2	67.0	**0.6**	26.1	24.9	**1.0**	17.0	234.7	**0.1**	44.2	71.3	**0.6**
Mean ratio				**2.6**			**0.3**			**0.7**			**1.9**			**0.5**			**0.7**

7.4 Discussion

This study investigates the progression of atrophy in PCA compared with typical AD and healthy controls. Compared with controls, at 5 years disease duration both PCA and tAD showed widespread grey matter loss including changes in medial temporal and frontal lobe regions in PCA, and posterior regions in tAD. Differences between PCA and tAD were subtle, reaching statistical significance only when using a multi-variate classification approach.

Cross-sectional studies have shown marked focal patterns of atrophy in PCA and tAD (chapter 6 and Whitwell et al., 2007a) suggesting that at some point during the disease atrophy changes are confined to posterior regions in PCA, and medial temporal lobe regions in tAD. The widespread pattern of grey matter loss in the PCA and tAD groups compared with controls may therefore suggest that initial focal patterns of atrophy changes become more global as the diseases progress. This is in accordance with previous reports showing that anterograde memory functions, linguistic skills and frontal lobe functions, which are sometimes strikingly preserved in the earlier stages of PCA, gradually deteriorate as some patients progress to a more global dementia state (Levine et al., 1993) making their presentation ultimately indistinguishable from that found in typical AD (DellaSala et al., 1996).

Whilst differences in grey matter volume changes and cortical thinning between PCA and tAD were small with respect to size of effect and non-significant in the VBM and FreeSurfer analyses, the patterns of atrophy are interesting. As atrophy progression spreads across the cortex, the PCA group shows slightly greater rates of atrophy in medial temporal lobe areas than tAD, and conversely, tAD showed slightly more atrophy progression in lateral parts of the temporal lobe compared with PCA. Whilst the involvement of individual regions in this comparison may provide useful information about the progression of structural changes in these groups, differences between PCA and tAD have to be interpreted with caution since they are very small and non-significant using the mass-univariate VBM and FreeSurfer approach. Statistically significant global changes in grey matter volume in both disease groups compared with controls, however, suggest that, whilst regions of greatest total tissue loss in both groups remain those typically associated with these diseases (i.e. posterior regions in PCA, medial temporal lobe regions in tAD), atrophy becomes more global as the diseases progress.

Whole brain atrophy rates, as measured using the BSI, were approximately 5 times higher in both PCA and tAD than in controls. Atrophy rates in the PCA group were slightly higher than in the tAD group, however, the age- and gender-adjusted difference of 0.2 percentage points was not statistically significant. The mean volume loss found in the tAD group was comparable with those found in previous studies of around 2% per year (Evans et al., 2010; Freeborough and Fox, 1997; Schott et al., 2005).

Although subject numbers in this study are relatively high given the rarity of PCA, it is possible that this study was not sufficiently powered to detect statistically significant longitudinal differences between the PCA and tAD groups using the mass-univariate VBM and FreeSurfer approach. However, the global patterns of atrophy changes in PCA and tAD compared with controls point to a global progression of atrophy in these disease groups. Studies including milder cases of PCA are required to fully understand the evolution of PCA from the very earliest symptomatic stages. The recruitment of milder PCA patients closer to symptom onset is often difficult since early visual symptoms are often mistaken as being ophthalmological rather than neurological. To date, only one study has assessed early structural changes in an individual with PCA who volunteered as a healthy control subject in a longitudinal study investigating subjective memory complaints (Kennedy et al., 2011). During the 5 year follow-up, this patient showed a gradual decline in posterior cortical functions including visuoperceptual, visuospatial and literacy impairments in the context of intact verbal episodic memory. The imaging data (presented in Appendix 3) revealed atrophy which was initially most marked in inferior temporal and posterior parietal cortices before spreading to occipital cortices and subsequently to more anterior regions.

Although most baseline images selected for both patient groups (77% for PCA, 75% for tAD) were the first scan available for each subject, the mean disease durations were already 5 years. Disease durations reported in this study are comparable with those reported in previous cross-sectional studies of PCA where posterior atrophy patterns have been shown, e.g. Mendez et al. (2002): PCA 4.5 years, AD 4.2 years; Whitwell et al. (2007a): PCA 4.0 years, AD 4.7 years; Schott et al. (2006): PCA 3.8 years, AD 4.4 years; and McMonagle et al. (2006): PCA 4.5 years. It would also be interesting to study progression of atrophy over multiple time points. This may reveal areas which atrophy earlier vs. later in the disease as well as whether atrophy accelerates or slows down selectively across the brain. Larger group studies will also permit more detailed assessment of the variance within the wider PCA population and in particular whether a small number of individuals retain a truly focal pattern of atrophy until late in the disease.

The cognitive and clinical features of the PCA patients included in this study are consistent with those typically reported in PCA studies (see chapter 1, section 1.2.2.6). A large proportion of PCA subjects showed visuospatial and visuoperceptual deficits, as well as dyscalculia, dysgraphia, dyspraxia and visual disorientation. A number of patients also reported difficulties with their memory as initial symptom. It should be noted, however, that these subjective memory complaints may not necessarily reflect difficulties with episodic memory per se, but rather may indicate other non-amnestic cognitive symptoms which are difficult for the patient to articulate (Kennedy et al., 2011). This may explain the relatively smaller proportion of individuals with PCA who showed impaired memory performance on formal neuropsychological testing 5 years after symptom onset.

Only the VBM analysis returned statistically significant results for the patient group (PCA and tAD) vs. control comparisons. The lack of significant results in the FreeSurfer analysis appears to be due to a higher variability of mean changes in cortical thickness over time relative to the analogous statistic for grey matter volume changes. To test this hypothesis a post-hoc analysis was performed which assessed the variability of grey matter volumes from the fluid-registration method, and cortical thickness and cortical volume from FreeSurfer in a specific set of regions. Variability in grey matter volume was found to be lower than that of cortical thickness changes, which could be due to the different metrics used here (volume vs. thickness). However, both cortical thickness and cortical volume (both derived from FreeSurfer) show higher relative variabilities compared with changes in grey matter volume measured using Jacobian integration from the voxel-compression maps which may suggest a more fundamental difference between the two methods. The fluid-based method used in this study is a 'direct' measure of change, i.e. change is measured 'directly' from the two registered serial scans. In contrast, FreeSurfer represents a less 'direct' approach which measures cortical thickness changes by subtracting two measured thicknesses. A previous study has shown that the variability in 'direct' estimates of whole brain volume change is smaller than that in 'indirectly' estimated differences calculated by brain volume subtraction (Frost et al., 2004).

Although studies have shown that AD is the underlying pathology in the majority of PCA patients (Hof et al., 1997; Levine et al., 1993), a small number of patients may be attributable to non-AD pathologies. In this study, pathological confirmation was only available in 1 PCA patient (AD with additional Lewy Body pathology) and 4 tAD patients (all AD pathology). Future studies using datasets of pathologically proven AD with PCA and typical presentations would be helpful in informing us of the different degenerative trajectories of patients with typical and atypical AD phenotypes.

7.5 Chapter conclusions

In conclusion, these data show that although PCA and tAD are known to have different cross-sectional atrophy patterns (as presented in the previous chapter), at 5 years symptom duration atrophy progression is widespread throughout the cortex including medial temporal lobe areas in PCA and posterior regions in tAD when compared with controls. Whilst differences in patterns of tissue loss between PCA and tAD were small and non-significant, the fact that these were sufficient to enable a multivariate classification analysis to achieve statistically significant group separation may encourage further studies which assess longitudinal structural changes in larger subject groups. Future studies using potentially milder patients may further elucidate differences in the natural history of PCA and tAD and may provide early markers of change for PCA. Finally, in the current study the fluid-VBM approach was more sensitive in detecting longitudinal changes than the relatively novel longitudinal

processing stream in FreeSurfer, probably due to the relatively higher inter-subject variability of the cortical thickness measures, which greatly reduced the power to detect significant differences.

Whilst understanding the neuroimaging signature of PCA in relation to normal ageing and typical AD is a crucial step towards characterizing atypical variants of AD, structural changes need to be examined in relation to cognitive changes in these patients. Although PCA is often regarded as being relatively homogeneous in terms of atrophy and cognitive symptoms, some studies have suggested the existence of different subtypes in PCA, each showing different deficits. However, the existence of these variants of PCA is disputed. This will be investigated in the next chapter.

8. HETEROGENEITY OF VISUAL DEFICITS AND CORTICAL THICKNESS PATTERNS IN PCA

8.1 Chapter introduction

Although PCA is often considered a relatively homogeneous syndrome, clinical experience indicates that a degree of heterogeneity exists in the behavioural and neuroimaging profiles of PCA patients. It has been suggested that separate parietal (dorsal), occipitotemporal (ventral), and primary visual (striate cortex; caudal) forms of PCA exist (Galton et al., 2000; Ross et al., 1996, see chapter 1, section 1.2.2.1). However, these claims are based upon the observation of patterns of impairment in single cases. Furthermore, the most detailed neuropsychological study of PCA to date found evidence of object perception deficits, faces and colours in a proportion of the patients tested, but overall the pattern of impairments was suggestive of greater deficits of the dorsal than ventral visual processing streams as no pure ventral stream syndromes were detected (McMonagle et al., 2006).

One limitation in understanding PCA and evaluating the relationship between PCA and typical AD is that very few studies have assessed the integrity of fundamental, basic visual processes supported by striate and extrastriate occipital cortices (e.g. basic form, colour, motion and location processing). Without testing these basic visual functions, it is difficult to determine whether higher-order object and space perception deficits are attributable to parietotemporal tissue loss, or in fact result from a more fundamental deafferentation of such areas owing to occipital lobe disease. A second limitation is that no studies reported to date have systematically evaluated both neuropsychological deficits and patterns of brain atrophy using quantitative, unbiased methods in a large group of patients.

The current study was designed to address these limitations with the motivation to more precisely characterize AD-associated syndromes such as PCA in order to identify factors driving the distribution and spread of pathology underpinning typical and atypical clinical presentations of AD. The study investigated a relatively large sample of patients with PCA using detailed neuropsychological evaluation and systematic measurement of cortical thickness. The primary hypothesis was that higher-order visual deficits in PCA are associated with specific and separable patterns of basic visual processing impairments. The secondary hypothesis was that different patterns of posterior behavioural dysfunction are associated with distinct patterns of atrophy. These hypotheses were addressed by: i) characterizing the basic visual, space and object perceptual processing abilities of patients with PCA; ii) identifying associations between specific basic visual functions and measures of higher-order object and space perception; and iii) assessing whether PCA patients with predominant object and space perception impairments show greater cortical thinning in dorsal (superior parietal) and ventral (occipitotemporal) regions.

8.2 Methods

8.2.1 Subjects

The behavioural part of the study involved 21 patients with PCA. Demographics and clinical data of the subjects are summarized in Table 8.1. For the imaging part of the study, 20 PCA patients were included (11 female, 9 male, mean (SD) age: 63.0 (8.5) years), as well as a group of 20 healthy control subjects for comparison (11 female, 9 male, mean (SD) age: 61.9 (10.6) years). The groups (20 PCA vs. controls) were matched for gender (p=1), age (p=0.7) and scanner distribution (p=0.7). All subjects fulfilled the inclusion criteria described in chapter 3 (section 3.4.1).

8.2.2 Background neuropsychological assessment

Each patient completed a background neuropsychological battery at the time of the current experimental investigations, including tests of general cognitive function (Folstein et al., 1975), verbal recognition memory (Warrington, 1996), word comprehension (Warrington et al., 1998), naming from verbal description (Randlesome (unpublished)), cognitive estimates (Shallice and Evans, 1978), calculation (Crutch (unpublished)), spelling (Baxter and Warrington, 1994), gesture production (Crutch (unpublished)), and auditory-verbal short term memory (digit span, Wechsler, 1987). In addition, patients were administered tests of visual acuity (Cortical Visual Screening Test (CORVIST), James et al., 2001), space perception (Warrington and James, 1991, Appendix 4), and object perception (Warrington, 1996; Warrington and James, 1988, Appendix 4).

8.2.3 Experimental investigations of basic visual processing

The following detailed experimental investigations were administered in order to assess the contribution of basic form, colour, motion and location processing to the object and space perception deficits observed in the PCA cohort (see Appendix 4 for example items for each test).

Form I: Form detection: VOSP Shape Detection test (Warrington and James, 1991) examining figure-ground discrimination. Stimuli (N=20) were random black patterns, half with a degraded 'X' superimposed. Patients were requested to state whether an 'X' was present.

Form II: Form coherence: Adapted from Braddick et al., the stimuli (N=80) consisted of static arrays of 3000 randomly oriented short line segments (Braddick et al., 2000). In half the arrays, a percentage of the line segments in an 11.8° central region were coherently oriented tangentially to concentric circles. In the remaining arrays, all line segments were arranged randomly. There were 4 levels of difficulty: 90%, 70%, 50% and 30% coherence. Patients were requested to state whether a 'circle' was present in each stimulus.

Form III: Form discrimination: The stimuli (N=60) for this boundary detection task, adapted from Efron, were a square (50 x 50mm) or an oblong matched for total flux (Efron, 1968). There were 3 levels of difficulty: oblong edge ratio 1:1.63 (Level I), 1:1.37 (Level II), and

1:1.20 (Level III). The task was to discriminate whether each shape presented was a square or an oblong.

Colour discrimination: The stimuli (N=60) were pairs of matte colour chips presented adjacently. The colours were selected from the Munsell colour system and had a fixed value and chroma (6/6). There were 3 difficulty levels based on varying the distance between hue-pairs on the Munsell hue scale. The task was to determine whether the hues in each pair were the same or different.

Motion coherence: Using the same experimental paradigm as the form coherence task, the stimuli (N=80) were arrays of 3000 0.1° high contrast dots drifting in random linear directions (5.12°/s). In half the arrays, the direction of motion of a percentage of dots in an 11.8° central region was coherently circular. In the remaining arrays, all the dots moved in random directions. There were 4 levels of difficulty: 90%, 70%, 50% and 30% coherence. Patients were requested to state whether a 'moving circle' was present in each stimulus.

Point localisation: The stimuli (N=8) were A3 laminated white cards with a single, randomly positioned black dot (5mm diameter). The position of each dot was revealed for 3s before the stimulus was covered by a second blank A3 card, and participants were requested to mark the position of the dot on the blank sheet using a pen in their dominant hand. Target-response discrepancy was measured.

8.2.4 Neuropsychological data analysis

8.2.4.1 Correlations

Performance on each level of each experimental task was recorded as a raw score, and a total score calculated for multi-level tasks. In the calculation of total scores, performance at untestable levels and scores of <10 were assigned a chance score of 10/20. Correlations were based on total scores.

8.2.4.2 Syndrome subgroups

Two behavioural subgroups were generated on the basis of object perception and space perception composite scores which were obtained from the mean performance across the Fragmented letters/Object decision and Number location/Dot counting scores, respectively, transformed onto linear scales of 0-100 representing minimum and maximum values of the range of PCA group performance. The Object subgroup (N=11) showed lower object than space perception composite scores, whilst the Space subgroup showed the reverse tendency (Figure 8.1). Pair-wise comparisons between the Object and Space subgroups on each of the demographic and behavioural measures were conducted using Wilcoxon-Mann-Whitney ranksum statistics.

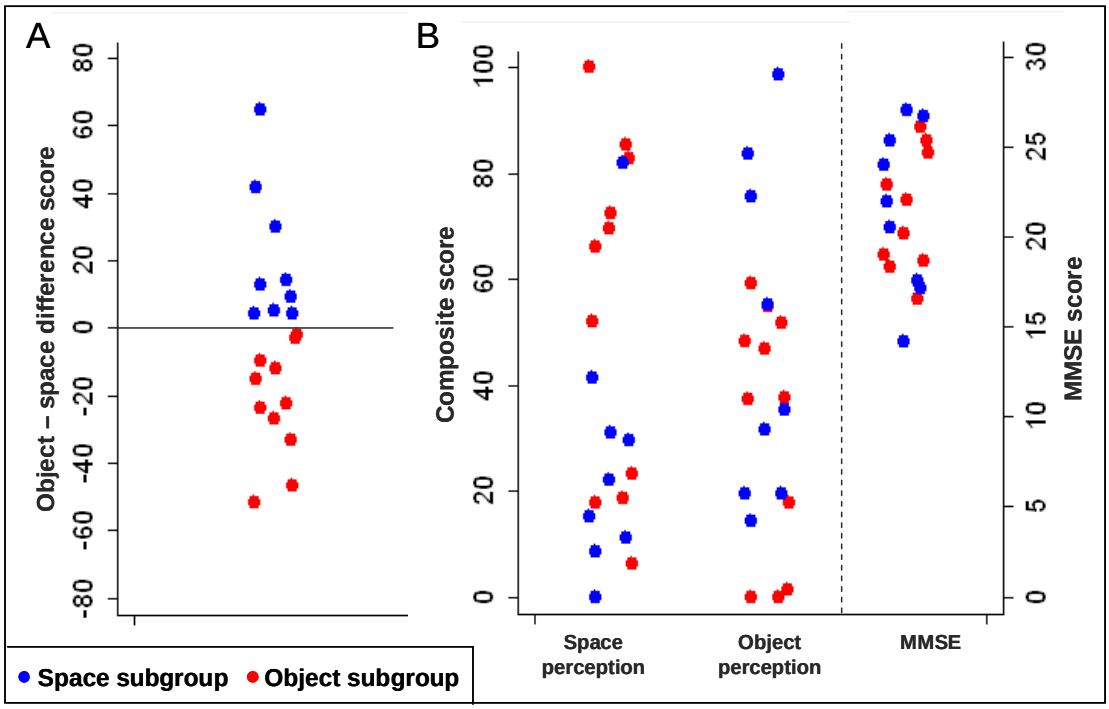

Figure 8.1: Classification of behavioural subgroups. Illustrated are **A)** split between Space and Object subgroups, and **B)** range of scores for each subgroup for each composite score and MMSE. Blue - Space subgroup; red - Object subgroup. Composite scores were generated for space perception (VOSP Number Location and Dot Counting) and object perception (VOSP Fragmented Letters and Object Decision) by transforming raw scores proportionally onto a linear scale of 0-100, where 0 and 100 represent the minimum and maximum values of the range of PCA group performance on a given task. Composite scores are means of the transformed scores.

8.2.5 Image acquisition and analyses

Images were acquired from all patients and controls, however, one PCA patient (Space subgroup) had to be excluded due to an artefact on the scan. Therefore 20 patients and 20 control subjects were included for the imaging analysis. Scans were acquired at two different scanners (chapter 3, section 3.5.1, and Appendix 5). Controls and patients were matched for scanner: 14 patients and 14 controls were scanned on a 1.5T GE Signa scanner, and 6 patients and 6 controls were scanned on a Siemens Trio TIM 3T. The average time between psychological assessment and scan was 27.7 days (SD 72.2 days). In the subgroup analysis, 8/9 scans in the Space subgroup and 6/11 scans in the Object subgroup were acquired on the 1.5T scanner.

8.2.5.1 Cortical thickness

Cortical thickness measurements were made using FreeSurfer version 4.3.0 (chapter 3, section 3.5.3.2.2).

8.2.5.2 Statistical analysis

Regional cortical thickness variations between controls and the two syndrome subgroups were assessed using a vertex-by-vertex GLM (chapter 3, section 3.5.4.2.3). Cortical thickness (C) was modelled as a function of group, controlling for age (mean-centred), gender, and scanner: $C = \beta1$ (Controls) + $\beta2$ (Space) + $\beta3$ (Object) + $\beta4$ age + $\beta5$ gender + $\beta6$ scanner + ε. The comparisons between individual PCA subgroups were further corrected for average cortical thickness (mean-centred) by inclusion as covariate. Statistical difference maps for comparisons with controls show FDR-corrected p values thresholded at a 0.05 significance level, whereas maps for the comparisons between individual subgroups present uncorrected statistical differences ($p<0.05$) and percent differences.

8.2.5.3 Support vector machine

An SVM (chapter 3, section 3.5.4.2.6) was trained to classify the controls and PCA subjects, and the resultant SVM scores were subsequently labelled according to Space (dorsal) and Object (ventral) PCA subgroups. A second SVM was trained directly to separate Space and Object subgroups.

8.3 Results

8.3.1 Neuropsychological analysis

Details of background neuropsychological test scores as well as percentage of patients failing each task are shown in Table 8.1. Verbal recognition memory (short RMT) and verbal comprehension (concrete synonyms) were generally well preserved, but the majority of patients showed deficits in calculation, praxis and short-term memory (digit span). In particular, 95% of patients failed one or both space perception tasks, and 100% of patients failed at least two object perception tasks.

Means and standard deviations for the performance on each experimental task of basic visual processing are shown in Table 8.2. All 21 patients (100%) failed at least 1 of the 6 experimental tests of basic visual processing (with 90% failing at least 2 tasks, and 81% failing at least 3 tasks). Therefore, there was not a single case of higher-order object or space agnosia in the current sample to which a basic visual processing deficit did not potentially contribute.

Table 8.1: **Overview scores of background neuropsychological assessment.** Mean and SD scores are presented for the PCA patient group as well as number of subjects scoring <5th %ile.

	PCA Mean(SD)	**N below 5th %ile**	**Normative** Mean(SD)
Age	63.5 (7.7)	-	-
Gender male / female	9 / 12	-	-
Disease duration (years)	5.0 (2.6)	-	-
GENERAL FUNCTION			
MMSE (/30)	21.5 (3.4)	-	-
Short RMT (words; /25)	20.1 (2.8)	5 (24%)	23.5 (2.1)
Concrete synonyms (/25)	21.3 (3.1)	1 (5%)	20.8 (3.0)
Naming (/20)	13.6 (5.1)	12 (57%)	18.9 (1.5)
Cognitive estimates	12.0 (6.6)	15 (71%)	3.6 (1.9)
DOMINANT PARIETAL			
Calculation (/20)	11.9 (3.6)	18 (86%)	20.7 (3.1)
Spelling (/20)	10.5 (6.6)	6 (29%)	-
Gesture production (/15)	12.2 (3.0)	14 (67%)	15.0 (0.0)
Digit span (N forwards)	5.7 (1.4)	15 (71%) †	Range 5-9
SPACE PERCEPTION			
Number location (/10)	3.1 (3.2)	19 (90%)	9.4 (1.1)
Dot counting (/10)	4.8 (3.2)	17 (81%)	9.9 (0.2)
OBJECT PERCEPTION			
Fragmented letters (/20)	5.1 (4.8)	21 (100%)	18.8 (1.4)
Object decision (/20)	11.6 (4.8)	15 (71%)	17.7 (1.9)
Unusual views (/20)	2.7 (3.0)	21 (100%)	17.1 (3.0)
Usual views (/20)	11.5 (6.2)	18 (86%)	19.7 (0.5)

† Below mean normal performance.

Table 8.2: Experimental assessment of basic visual processing skills. Mean and SD scores are presented for the PCA patient group as well as number of subjects scoring <5th %ile and relevant control samples.

	PCA Mean (SD)	**N below 5th %ile**	**Normative** Mean(SD)
FORM DETECTION			
Score (/20)	17.2 (2.3)	14 (67%)	19.9 (0.3)[a]
FORM COHERENCE			
90% coherence (/20)	19.1 (1.8)	8 (38%)	20.0 (0.0)
70% coherence (/20)	19.3 (1.3)	7 (33%)	19.9 (0.3)
50% coherence (/20)	17.9 (2.3)	11 (52%)	19.9 (0.4)
30% coherence (/20)	14.0 (3.1)	18 (86%)	19.4 (0.9)
Total score (/80)	69.3 (8.5)	18 (86%)	79.9 (0.9)[b]
FORM DISCRIMINATION			
Level 1 (/20)	18.2 (3.5)	-	-
Level 2 (/20)	17.2 (2.9)	-	-
Level 3 (/20)	12.3 (5.4)	14 (67%)	19.1 (2.1)[c]
Total score (/60)	48.0 (8.6)	-	-
COLOUR			
Level 1 (/16)	15.4 (1.4)	5 (24%)	16.0 (0.2)
Level 2 (/16)	14.6 (2.0)	11 (52%)	16.0 (0.1)
Level 3 (/16)	13.7 (2.6)	13 (62%)	16.0 (0.0)
Total score (/48)	43.7 (5.5)	14 (67%)	47.9 (0.2)[d]
MOTION COHERENCE			
90% coherence (/20)	19.1 (1.8)	6 (29%)	20.0 (0.0)
70% coherence (/20)	18.2 (2.1)	14 (67%)	19.9 (0.3)
50% coherence (/20)	17.2 (2.5)	12 (57%)	19.7 (1.1)
30% coherence (/20)	13.5 (2.9)	18 (86%)	19.3 (0.9)
Total score (/80)	69.1 (6.1)	18 (86%)	78.9 (1.8)[e]
POINT LOCALISATION			
Mean error (cm)	2.6 (2.5)	12 (60%)	0.8 (0.3)[f]

Normative data samples: [a] Warrington and James (1991; N=60); Keilty (unpublished; [b]N=14; [c]N=39; [e]N=16); [d]Connell (unpublished; N=54); [f]Randlesome (unpublished; N=83).

8.3.1.1 Correlations

Pair-wise correlations and significance values between the 6 experimental tests of basic visual processing and tests of higher-order space and object perception as well as general cognition and tests of parietal, non-visual skills are shown in Table 8.3. Three basic visual tests (form detection, form coherence, colour) were significantly correlated with both higher-order object and space perception. However, form discrimination correlated significantly only with object perception, whilst point localisation correlated significantly only with space perception. Furthermore, none of the basic visual processing tasks correlated with non-visual parietal functions (calculation and spelling), or tests of memory and general cognition (with the exception of a spurious negative colour-MMSE correlation).

Table 8.3: Pair-wise correlations between basic visual processing and general cognition, parietal non-visual tasks, and higher-order object and space perception tasks.

		BASIC VISUAL PROCESSING					
		Form detection	Form coherence	Form discrimination	Colour	Motion	Location
GENERAL FUNCTION	MMSE	0.09	-0.26	0.13	**-0.44 ***	-0.05	-0.28
	Recognition memory	0.03	-0.01	0.02	-0.29	-0.01	-0.36
DOMINANT PARIETAL	Calculation	0.02	0.05	0.08	-0.06	-0.04	0.30
	Spelling	-0.18	0.06	0.28	-0.14	0	0.16
SPACE PERCEPTION	Number location	**0.64 *** **	**0.58**** **	0.31	**0.52 ***	0.26	**0.49 ***
	Dot counting	**0.68 **** **	**0.48 ***	0.3	**0.58 ****	0.28	**0.61 *** **
OBJECT PERCEPTION	Fragmented letters	**0.44 ***	0.34	**0.52 ***	0.36	0.10	0.37
	Object decision	0.26	0.41	**0.61 ****	**0.77 **** **	-0.18	0.36
	Unusual views	0.39	**0.47 ***	**0.45 ***	**0.47 ***	0.36	0.37
	Usual views	0.37	**0.58 ****	**0.74 **** **	**0.71 **** **	0.15	0.31

* p≤0.05; ** p≤0.01; *** p≤0.005 **** p≤0.001

8.3.1.2 Syndrome subgroups

There were no significant differences between the subgroups in terms of age (Object: 62.0 (7.4) years, Space: 64.3 (10.0) years), gender (Object: 46% male, Space: 44% male), MMSE (Object: 21.4 (2.8), Space: 21.8 (4.4)), disease duration (Object: 4.9 (2.7) years, Space: 4.6 (2.3) years) or on any of the individual neuropsychological tests.

8.3.2 Cortical thickness analysis

8.3.2.1 Syndrome subgroups (Object and Space) comparisons

Differences in cortical thickness between the two putative PCA subgroups (Space and Object) and controls are shown in Figure 8.2. The Space (dorsal) subgroup compared with controls showed significantly lower cortical thickness predominantly bilaterally in the occipital lobe and the posterior parietal lobe, as well as the precuneus, occipitotemporal gyrus and medial temporal lobe, with relative sparing of the orbitofrontal gyrus (Figure 8.2A). Similar results were shown in the Object (ventral) subgroup versus controls comparison, however, cortical thinning showed more focal differences, including thinner cortex bilaterally in the inferior parietal lobe and fusiform gyrus, with relative sparing of medial occipital lobe and frontal lobe regions (Figure 8.2B). Figure 8.3 presents differences in cortical thickness for the direct comparison between Object and Space subgroups. The Space subgroup compared with the Object subgroup showed reduced cortical thickness in the right occipital and medial temporal lobe, and bilaterally in the inferior and superior parietal lobe (Figure 8.3A). However, these differences did not survive FDR-correction. No statistically significant differences were found in the Object subgroup compared with the Space subgroup.

The less widespread reduction in cortical thickness in the Object subgroup, despite matching for age and disease duration, suggested that this group overall had a relatively thick cortex (possibly owing to premorbid differences and/or lesser disease severity). This motivated the use of correction for average cortical thickness for the direct comparison between Object and Space subgroup. Figure 8.3B shows percent differences in cortical thickness over and above global thinning between the two subgroups. The Space subgroup compared with the Object subgroup showed reduced cortical thickness bilaterally in the occipital, inferior parietal and medial temporal lobe. In contrast, the Object subgroup showed reduced cortical thickness in the right fusiform gyrus, right lateral inferior temporal lobe and frontal lobe regions.

These cortical thickness maps provide some evidence that thickness of the cortex varies in a predictable manner between the two behaviourally-defined subgroups, as seen most clearly in the right lateral percentage map in Figure 8.3B. More specifically, there was an indication of greater thinning in occipital and superior parietal (dorsal) regions in patients with greater impairment of Space perception, and greater thinning of inferior temporal (ventral) regions in patients with greater impairment of Object perception. However, putting issues of statistical power to one side, the scarcity of regions showing significant thickness differences between

the two subgroups suggests substantial anatomical overlap, making a separation into distinct subgroups less clear.

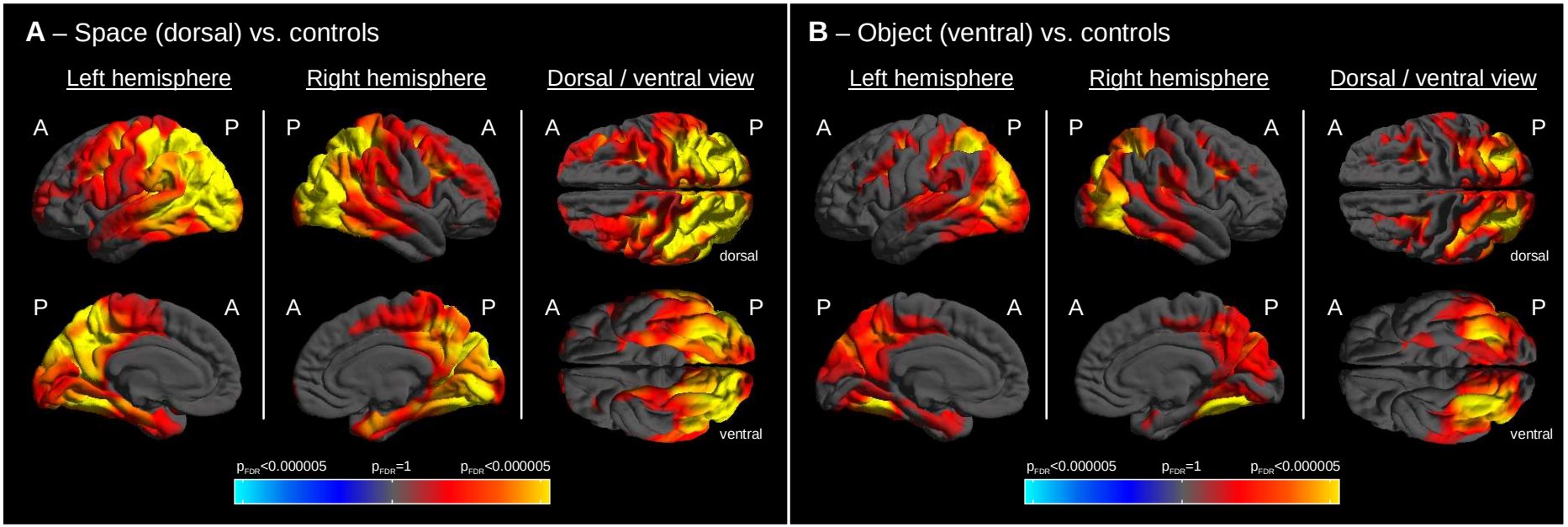

Figure 8.2: Differences in cortical thickness between controls and PCA subgroups. Regional variation in cortical thickness shown in **A)** Space subgroup compared with controls, and **B)** Object subgroup compared with controls. The colour scale represents FDR-corrected p values at a 0.05 significance level. Red and yellow (positive values) represent lower cortical thickness in the PCA subgroups compared with controls whereas dark and light blue (negative values) represent the reverse contrasts. A - anterior, P - posterior.

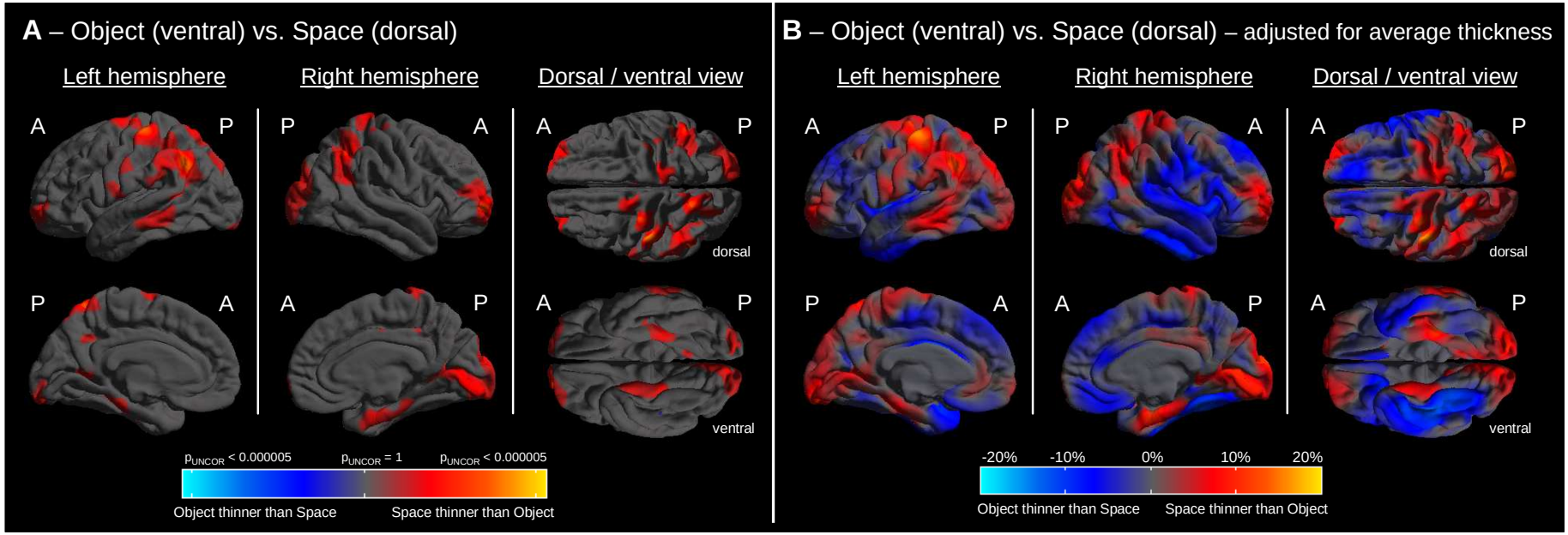

Figure 8.3: **Difference in cortical thickness between Space and Object subgroups. A)** shows uncorrected p values at a 0.05 significance level, and **B)** shows percent difference maps after correcting for average cortical thickness. Warmer colours show regions thinner in the Space subgroup compared with the Object subgroup whereas cooler colours represent the opposite comparison. A - anterior, P - posterior.

8.3.2.2 Support vector machine:

The classification analysis produced a near complete separation between the controls and the PCA patients (Figure 8.4), with 97.5% accuracy [95% CI 86.8 - 99.9%]. In contrast, no clear separation into the two putative subgroups was found, with the SVM-weighted scores showing great overlap between subgroups. The SVM trained specifically to separate Object and Space subgroups yielded a low accuracy with confidence interval spanning chance performance.

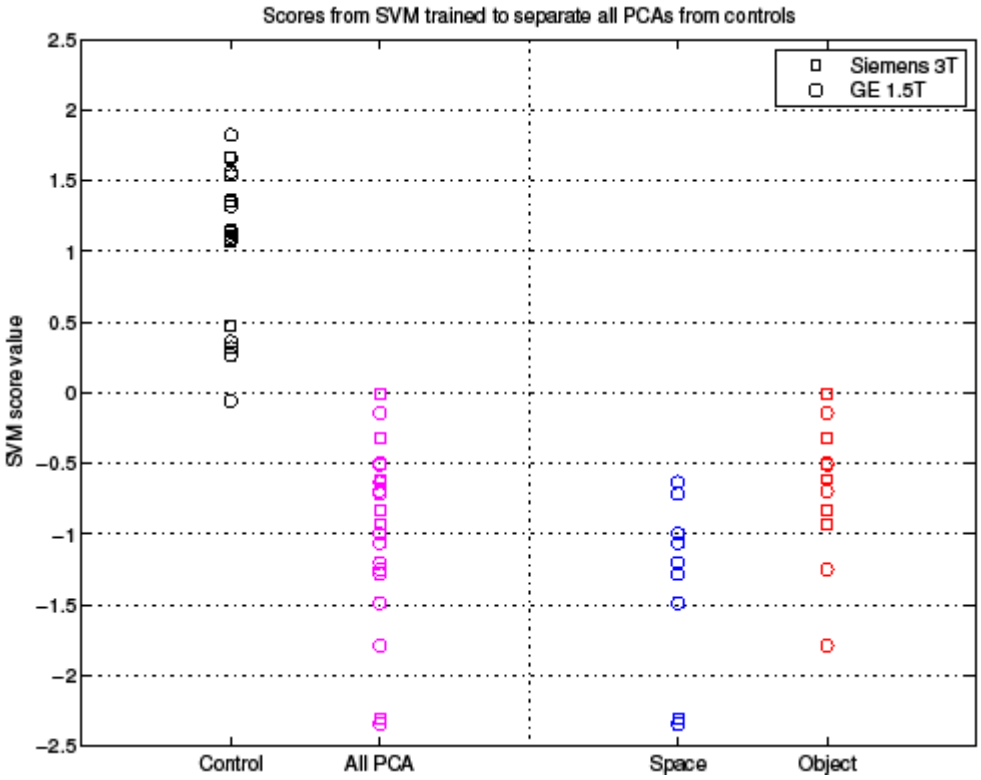

Figure 8.4: **SVM-weighted scores for each subject.** Left: Illustration of separation between the controls and PCA group; right: no separation between the two putative PCA subgroups (Space and Object).

8.4 Discussion

This study investigated basic and higher-order visual function in a relatively large sample of patients with PCA using both detailed neuropsychological assessments and quantitative measures of cortical thickness. Considering that the primary deficits in PCA are visual, it is, perhaps, surprising that previous studies have failed to examine the nature of basic visual deficits in more detail or to consider their influence upon higher-order visual processing. In this study it is shown that basic visual functions are affected in the vast majority of PCA patients, and that the severity of deficit in these basic visual skills predicts the pattern of higher-order object and space perception observed. The current study also demonstrates that

the severity of space and object perception difficulties can partially predict the degree of cortical thinning in dorsal and ventral posterior cortical regions, however, the neuroimaging evidence garnered from the current study is insufficient to justify the specification of distinct PCA subtypes.

8.4.1 Basic visual deficits predict the nature of higher-order perceptual deficits in PCA

The first hypothesis addressed in the current study was that higher-order visual deficits in PCA are associated with specific and separable patterns of basic visual processing. Object and space perception problems are reported commonly in PCA and yet it is unknown whether these problems constitute true visual agnosias or result from impaired sensory processing, because the integrity of basic visual processes (e.g. form, colour, motion and location) have not been assessed systematically in previous neuropsychological studies of PCA. Furthermore, although atrophy and pathological changes have been found in striate and extrastriate occipital cortex, it is unknown whether mechanisms supporting these fundamental components of vision are uniformly affected in PCA or can be selectively disrupted in line with models of the human visual system (e.g. Deyoe et al., 1996; Goodale and Milner, 1992; Ungerleider and Mishkin, 1982; Wandell et al., 2007).

The neuropsychological data revealed that every PCA patient was impaired on at least one basic visual processing task. Thus, no evidence of 'pure' visual agnosia was found, with the data suggesting that basic visual processing deficits contribute to the object and space agnosias commonly reported in PCA patients. The correlation analysis further revealed that basic visual processing impairments have a significant impact upon the nature of higher-order visual dysfunctions: whilst form detection, form coherence and colour performance were correlated with both object and space perception, form discrimination predicted object but not space perception, and point localisation predicted only space but not object perception. Together, these findings provide the first evidence that higher-order visual deficits in PCA are associated with different patterns of basic visual processing impairment. Furthermore in contrast to their influence on higher-order perceptual functions, basic visual processing dysfunction had no significant impact upon non-visual parietal functions (e.g. calculation, spelling), despite the equivalent proximity of the critical cortical regions. Models of the evolution of AD and related disorders contrast pathological proliferation between contiguous brain regions with network-based progression, in which functional and anatomical connections between non-contiguous brain areas play an important role in determining the spread and development of tissue pathology (e.g. Palop et al., 2006; Seeley et al., 2009). The current evidence of associations between occipital dysfunction and some but not other forms of parietal dysfunction may therefore support network models, and reflect network dysfunction and disconnection. Basic visual processing deficits also did not correlate with recognition memory, MMSE or disease duration, providing some evidence that involvement of basic visual processing, considered to be mediated primarily by more posterior occipital regions,

may reflect a different locus of pathology in some individuals rather than merely greater disease severity.

8.4.2 Variation in patterns of cortical thinning

The study further assessed the hypothesis that different types of behavioural dysfunction are associated with distinct patterns of structural change in posterior cortical regions. More specifically, it was hypothesised that PCA patients with predominant spatial perception problems (Space subgroup) would be associated with greater posterior parietal cortical thinning, and that patients with predominant object perception problems (Object subgroup) would be associated with greater inferior temporal cortical thinning. In line with this hypothesis, the Space subgroup showed thinning particularly in the occipital and inferior parietal lobes, and the Object subgroup showed particular thinning in the fusiform gyrus and inferior temporal lobe. Trends toward lower cortical thickness in ventral (Object Subgroup) and dorsal (Space subgroup) regions were apparent in independent subgroup-controls comparisons (Figure 8.2) and between-subgroup comparisons (Figure 8.3).

However, whilst these neuroimaging findings provide some evidence for differential patterns of tissue loss in the dorsal and ventral regions of different PCA patients, the majority of differences detected between subgroups were only found as percent differences. Furthermore, the indirect comparisons between each subgroup and the control population (Figure 8.2) showed multiple common areas of tissue loss across the subgroups. This observation was confirmed by the SVM analysis, with SVM-weighted scores showing considerable overlap between subgroups (Figure 8.4), while almost perfectly separating controls from patients. Thus overall the neuroimaging findings are indicative of a degree of heterogeneity within the PCA population but do not motivate a clinical characterisation of distinct PCA subtypes.

Previous neuropsychological analyses of PCA have claimed good evidence to support the description of caudal (occipital) and dorsal (parietal) subtypes of PCA, but have failed to find convincing evidence for a ventral (occipito-temporal) subtype (McMonagle et al., 2006). In the current study, individual examples of a ventrally-focussed syndrome have been found, for example one patient failed all object perception tests and passed all space perception tests. However, this patient's cognitive profile constituted merely the most extreme value on a continuous range of object-space difference scores, with several patients showing moderate, mild or no differences between object and space perception tasks (see Figure 8.1). Clinical experience suggests that the majority of PCA patients complain of or exhibit both space and object processing difficulties from early in the disease course, but as demonstrated in Figure 8.1 the relative severity of these deficits can be quite variable.

8.4.3 Continuous variation within PCA

The current study yields evidence of both similarities and differences amongst the PCA patients. At one level, the PCA cohort is collectively quite different from individuals with typical AD: relatively preserved memory, impaired perceptual skills and predominant posterior deficits and atrophy (chapter 6). At a more fine-grain level, detailed assessment reveals that PCA patients differ in the severity of their basic visual, object and space perception deficits and the extent to which occipital, superior parietal and inferior temporal cortical regions are affected. However, these more fine-grain differences do not reflect discrete, definable syndromic subtypes of PCA. Rather, the manual classification of neuropsychological profiles (Figure 8.1) and the automated classification of cortical thickness patterns (Figure 8.4) are more suggestive of continuous variation within the syndrome of PCA. The data in the present study are insufficient to support the existence of discrete dorsal and ventral sub-syndromes within PCA, although patients at the outer limits of such continuous variability can indeed possess markedly different phenotypes (Galton et al., 2000). Instead, those putative subtypes are more likely to represent points in a continuously varying topological distribution of cortical dysfunction, which may in turn reflect the distribution of underlying pathology. A similar notion has recently been expressed in a study of progressive PNFA to describe the relationship between putative PNFA subtypes such as progressive apraxia of speech and LPA; namely that individual patients with such phenotypes represent 'points at the edges of a space of continuous variability within PNFA' (Knibb et al., 2009, p2744).

If PCA phenotypes do represent different points in a space of continuous variation, this has implications for studies investigating the factors which drive the variation both within and between the different 'typical' and 'atypical' presentations of AD and related disorders. It may be more appropriate to consider how a population of patients varies on a particular continuous marker of topology (e.g. measures of basic visual function as a marker of occipital cortical loss) rather than dichotomising the population into symptomatic categories (e.g. 'typical AD', PCA), the boundaries of which may be poorly defined. Such continuous rather than categorical techniques may be used to determine the role of molecular and environmental factors in driving the topological focus of pathology (e.g. anterior-posterior, superior-inferior, unilateral-bilateral) and their interaction with other structural and physiological constraints. It should also be noted that the anterior-posterior and dorsal-ventral distinctions considered to date also fail to capture the pronounced asymmetry apparent in the neuropsychological and neuroimaging profiles of many individuals with PCA (e.g. Freedman et al., 1991; Snowden et al., 2007b). Without considering this lateral dimension of pathological distribution, it will also be difficult to establish the relationship between PCA and atypical variants of AD and related disorders such as LPA which is characterised by highly asymmetric atrophy of the dominant hemisphere (Gorno-Tempini et al., 2004).

8.4.4 Limitations of the current study

With regard to the neuropsychological aspects of the study several possible limitations should be considered. Firstly, visual fields were not tested formally in the PCA patients. Many showed problems on informal clinical field assessment, but clinical experience of PCA suggests that an inability to detect the presence or movement of a stimulus in the periphery during clinical examination is often more accurately attributed to visual disorientation and attentional problems rather than a field defect per se. Secondly, the division between visual processes labelled 'basic' and 'higher' is relative rather than absolute; it cannot be denied that for example that the boundary detection skills critical to the 'basic' form detection task are also necessary for the 'higher'-order fragmented letter task. Thirdly, whilst the space and object perception tests (mainly from the VOSP) employed in the current study are routinely used in clinical and research practice, there is little direct evidence to demonstrate differential dependence upon dorsal and ventral visual streams. Therefore alternative tasks with greater or more demonstrable localising power may yield a more accurate classification of 'dorsal' and 'ventral' subgroups.

From the neuroimaging and diagnostic perspectives, one limitation of this study is that scans were obtained from two different scanners with different field strengths which may have an effect on thickness measures (Han et al., 2006). Statistical models were therefore adjusted for scanner type. Furthermore, subject numbers, particularly in the subgroup analysis, were relatively small leading to a lack of power to detect statistically significant results after correcting for multiple comparisons. Replication of this study with a larger cohort of patients may increase the power to detect differences between the behaviourally-defined subgroups. Although all the patients in the current study have a clinical diagnosis of probable AD, another limitation is the lack of pathological confirmation. A further issue which applies to most studies of degenerative disease relates to controlling for the variable of disease severity when conducting between-group comparisons. There were no significant differences between the two behaviourally-defined subgroups on measures of general cognitive function, although measures such as the MMSE are of limited utility in this population of patients. Furthermore, cortical thickness comparisons were corrected for mean cortical thickness in order to adjust for potential premorbid differences and/or differences in disease severity.

8.5 Chapter conclusion

This study aimed to investigate the nature of visual impairments in PCA, in particular the contribution of deficits of basic visual processing to higher-order object and space processing impairments. The neuropsychological data revealed specific correlations between basic and higher-order visual deficits, however, no correlations were found with non-visual parietal skills suggesting the specific involvement of visual networks in PCA. Furthermore, the cortical thickness analysis revealed trends towards lower cortical thickness in occipitotemporal (ventral) and occipitoparietal (dorsal) regions in patients with visuoperceptual and visuospatial

deficits, respectively. However, there was also great overlap in the patterns of cortical thinning in these two subgroups of PCA.

The great heterogeneity of the visual deficits in PCA and the overlap in patterns of cortical thickness therefore provide only limited support for the existence of distinct phenotypical subtypes in PCA. Rather it may be more appropriate to consider different presentations of PCA as points on a continuum of phenotypical variation. This conclusion may be applicable to AD as a whole, with different phenotypes, including amnestic, visual and aphasic phenotypes, representing points in a space of continuous variation, rather than distinct subtypes of AD. For the purpose of most research studies, including the studies presented in this thesis, the inclusion criteria chosen to define groups such as PCA and typical amnestic AD are designed to minimize the overlap between these groups, i.e. to maximize the separation between them, allowing the identification of those features that are most characteristic for each group. Future studies, however, need to address the degree of overlap between different variants of AD in order to understand the nature of the heterogeneity of phenotypical presentations in AD.

9.THESIS CONCLUSIONS

9.1 Chapter introduction

With ageing populations, AD is a growing health and socio-economic problem, greatly affecting the quality of life for the patient and the carers. Increasing international efforts therefore aim to identify markers which may aid diagnosis and track disease progression. Structural neuroimaging techniques have become widely used tools to diagnose dementia, discriminate neurodegeneration from normal ageing, differentiate between degenerative diseases, and track the progression of disease by providing detailed, quantitative and increasingly automated measures of whole and regional brain volume as an index of neurodegeneration. Imaging markers may therefore provide sensitive outcome measures for testing the efficacy of drugs aimed at slowing disease progression.

AD is most commonly associated with memory loss and atrophy in the medial temporal lobes (chapter 1, section 1.2.1). The prominence of these two markers in AD is reflected by their inclusion in proposed research diagnostic criteria for AD (Dubois et al., 2007), which argue that the presence of memory loss and medial temporal lobe atrophy is sufficient to make a diagnosis of prodromal AD. However, atrophy in the medial temporal lobe is also present in other neurodegenerative diseases, such as FTLD (chapter 2, section 2.5.4), and normal ageing (chapter 2, section 2.5.1). In addition increasing numbers of studies have stressed the importance of atrophy, and metabolic and pathological changes in posterior regions in typical AD (chapter 2, section 2.5.2). Furthermore, atypical clinical presentations have been highlighted in AD, in which memory is not the primary deficit and which tend to have a younger age at onset (van der Flier et al., 2010), such as PCA and LPA (chapter 1, section 1.2.1.3).

This thesis aimed to investigate the nature of the heterogeneity of different phenotypes in AD by using two different approaches: a) by studying atrophy patterns in patients with pathological confirmation of AD with different clinical presentations during life, and b) by characterizing patterns of atrophy and visual deficits in a form of atypical AD: PCA. With both these approaches comparisons were made with healthy controls and additionally for PCA comparisons were made with amnestic, typical AD.

Increasing the clinical and scientific community's knowledge of atypical variants in particular is important in order to help identify the biological factors which drive this heterogeneity in AD, which may lead to a better understanding of AD as a whole. Better understanding should also improve the support, care and education that can be given to the patients, carers and healthcare professionals.

9.2 Posterior atrophy is a common finding in patients with AD pathology

This thesis first investigated patterns of cortical thickness in patients with AD pathology with different clinical diagnoses during life (including typical amnestic, visual, aphasic and behavioural phenotypes) (chapter 4). Regions with reduced cortical thickness in patients with AD pathology compared with controls were found to be the medial temporal lobe, as well as posterior regions such as posterior cingulate gyrus, precuneus and the posterior parietal cortex. Lower cortical thickness was also shown in the frontal pole. Compared with patients with FTLD pathology, subjects with AD pathology who had a clinical presentation of FTD during life also showed lower cortical thickness in posterior regions (precuneus, posterior parietal lobe, and posterior cingulate gyrus), frontal pole and superior temporal lobe. The involvement of these regions in patients with AD pathology despite different clinical presentations and diagnoses during life may suggest that atrophy in these regions is indicative of AD pathology, at least when compared with normal ageing and patients with FTLD pathology. Interestingly, these areas greatly overlap with regions commonly associated with the default-mode network which is a highly active network, even at rest, and has been shown to be strongly involved in the processing of memories. It has also been found to be affected early in AD. The cortical thickness findings presented here therefore support models of AD affecting functional networks leading to atrophy in the regions described above.

The posterior involvement in patients with AD is in accordance with previous reports, and has been further demonstrated by using visual rating scales (chapter 5). In this study, two visual ratings scales were used to assess atrophy in medial temporal and posterior regions in pathologically-confirmed AD and FTLD. It was demonstrated that a significant proportion of AD subjects showed prominent posterior atrophy in the absence of significant medial temporal lobe involvement. Ratings of posterior atrophy also improved accuracy for separating AD from FTLD, and proved valuable for distinguishing early-onset AD from younger controls. These findings stress the need to consider atrophy in posterior regions when making a diagnosis of AD, especially in younger patients. This is particularly important considering that proposed diagnostic criteria for AD (Dubois et al., 2007) include medial temporal lobe atrophy as a diagnostic marker, however, not posterior atrophy, which might mean that AD patients with prominent posterior atrophy in the absence of medial temporal lobe atrophy might not be given a diagnosis of AD during early disease stages.

Whilst growing evidence points to a number of key regions commonly affected in patients with AD pathology, largely matching areas typically associated with the default-mode network, there are forms of AD which show strong involvement in other areas as well, such as visual areas in patients with PCA, and language areas in patients with LPA. Although these patient populations can also have other, non-AD pathologies as their underlying cause, studying these different phenotypes will provide insights into the nature of the heterogeneity in AD. Specifically, studying PCA, which is characterized by marked posterior atrophy with only

minimal medial temporal lobe involvement, will provide insights into the mechanisms underlying the marked involvement of posterior regions in AD.

9.3 Characteristic cross-sectional and longitudinal patterns of atrophy in PCA

Whilst the posterior atrophy of PCA may often be evident from visual inspection of structural MR images (chapter 1, Figure 1.1), using automated image analysis tools allows the exact localization and quantification of atrophy in PCA. Using VBM and FreeSurfer to measure cross-sectional (chapter 6) and longitudinal differences (chapter 7) in grey matter volume and cortical thickness, respectively, revealed some interesting results about the natural history of the disease in PCA and typical amnestic AD. The cross-sectional data revealed significantly lower grey matter volumes and cortical thickness in posterior regions in PCA compared with typical amnestic AD as expected. In contrast, amnestic AD showed significantly lower cortical thickness in the entorhinal cortex compared with PCA. Assuming that the majority of the patients included in this study have AD pathology, these findings of prominent posterior atrophy with minimal atrophy in the medial temporal lobes are in accordance with the patterns of atrophy in pathologically-confirmed AD subjects presented in chapter 4 and 5. Furthermore, the significant differences in grey matter volume and cortical thickness in the direct comparison between PCA and typical AD provide evidence that different behaviourally-defined AD phenotypes are associated with significantly different brain atrophy patterns.

However, despite these striking cross-sectional differences between PCA and typical amnestic AD, the longitudinal results demonstrated global changes in grey matter loss and cortical thinning in PCA and typical AD compared with controls over the course of 1 year, with only subtle differences in the direct patient group comparison. Since both disease groups had a disease duration of approximately 5 years, these findings suggest that initial focal patterns of atrophy (as demonstrated by the cross-sectional results in chapter 6) become more widespread as the diseases progress. These results may encourage future studies to investigate disease progression in prodromal and presymptomatic cases of PCA and typical AD to identify the processes which result in different AD phenotypes. These data may also point to a common path of AD progression, a theory which will need further support from studies investigating atrophy progression in patients with pathology-confirmation and studies investigating earlier disease stages. This study further demonstrated the advantage of using multiple techniques to analyse imaging data, particularly when a number of different outcomes are possible and a number of hypotheses have been posed. As has been demonstrated in previous studies, combining a fluid-registration approach with VBM represents a powerful tool to assess longitudinal changes in a disease group. The relatively novel longitudinal processing stream in FreeSurfer, however, did not return any statistically significant results. This is possibly due to the higher inter-subject variability of the cortical thickness measures, which greatly reduced the power to detect significant differences. The reason why the variability of the VBM data was lower might be due to the fact that the fluid-

based method is a ‘direct’ measure of change, i.e. change is measured ‘directly’ from the two registered serial scans. In contrast, FreeSurfer represents a less ‘direct’ approach which measures cortical thickness changes by subtracting two measured thicknesses.

9.4 PCA and AD as continuums of varying phenotypical presentations

In addition to the heterogeneity of different phenotypes in AD, it has been suggested that different phenotypes also exist within PCA. Studies which have investigated the presence of different clinical subtypes in PCA have returned mixed results. The study presented in chapter 8 therefore aimed to investigate further the existence of these subtypes in PCA using behavioural and cortical thickness measures at a single time point. The behavioural data revealed heterogeneous patterns of basic and higher-order visual deficits in PCA. The cortical thickness analysis further revealed trends towards lower cortical thickness in occipitotemporal (ventral) and occipitoparietal (dorsal) regions in PCA patients with visuoperceptual and visuospatial deficits, respectively. However, there was also great overlap in the patterns of cortical thinning in these two subgroups of PCA. Furthermore, classifying PCA patients on the basis of their cortical thickness patterns did not return a clear separation into subgroups. These findings therefore provide only limited support for the existence of very distinct subtypes in PCA; rather they suggest a spectrum of varying phenotypical presentations in PCA. Considering different presentations of PCA as points on a continuum of phenotypical variation may also have implications for how we view the variation of different phenotypes in AD as whole. The variation within and between typical and atypical presentations of AD may therefore also represent a spectrum rather than distinct categories.

9.5 Clinical implications

An increasing number of studies emphasize the importance of posterior atrophy in AD, a finding supported by the studies presented in this thesis. Atrophy in posterior regions may therefore be a useful additional marker for AD and certainly should not be ignored in the clinical and radiological assessment of patients with cognitive decline. Growing awareness of the posterior involvement as well as the presence of atypical, non-amnestic phenotypes in AD is reflected by renewed suggestions for a revision of the AD diagnostic criteria (Dubois et al., 2010), acknowledging non-memory related deficits (e.g. visuospatial problems) as being a feature of AD.

Furthermore, the characterisation of the structural and cognitive features of specific atypical variants of AD, such as PCA, should lead to a better understanding of the nature of the heterogeneity in AD. As importantly this should also help to raise awareness amongst scientists, medical practitioners and society in general of the existence of these unusual syndromes. This is particularly important in under-diagnosed variants such as PCA in which initial visual symptoms are often mistaken as being of ophthalmological rather than neurological origin resulting in a great delay or even a complete lack of diagnosis in these

patients. This is not only frustrating for the patients and their carers, but also means that treatments which might be available might be missed because patients are already too severely impaired. Understanding the evolution of the disease in different variants of AD may further improve diagnosis and the quality and accuracy of prognosis given to patients and their carers. Finally, it is important to develop tools which allow the characterisation of the cognitive deficits and the structural damage in patients on a routine basis in a clinical setting. Visual rating scales have been shown to represent a convenient method to assess atrophy in a clinical environment.

9.6 Future directions

Whilst this thesis aimed to improve our understanding and characterisation of atypical variants of AD, it has also revealed a number of issues and questions which remain to be addressed in future studies. For example, it is currently unknown which factors drive the heterogeneity of different phenotypes in AD. It has been suggested that the default-mode network, which is affected early in AD, is particularly vulnerable to AD pathology due to its high metabolic activity throughout life (Buckner et al., 2005). This and its strong involvement in memory processing might explain the great prevalence of the amnestic phenotype in AD. However, it remains unclear how the default-mode network is affected in non-amnestic variants of AD, and what makes other networks, such as visual and language networks, more vulnerable to pathology and atrophy in some people but not others. Factors driving the selective vulnerability of visual and language networks in PCA and LPA, respectively, may include genetic predisposition, higher vascular burden or even developmental damage or predisposition as has been suggested in patients with PPA who were shown to have a high rate of developmental language disorders (Rogalski et al., 2008).

Another question which remains is how disease progresses in different variants of AD. It has been suggested that the sites of earliest change in AD includes posterior regions such as the posterior cingulate cortex, retrosplenial and lateral parietal cortex (Buckner et al., 2005; Migliaccio et al., 2009). It may even be that these regions are affected as early or even earlier than the medial temporal lobe. The common involvement of posterior regions in patients with AD pathology, as presented in chapter 4 and 5 in this thesis, might support this theory. Further studies, however, are needed to address the question of the sites of earliest involvement. There is of course no fundamental reason for suggesting that all variants of AD have common areas of disease origin in terms of increased pathology, decreased metabolism or increased atrophy. In fact, it is likely that in this regard, like in so many others, AD demonstrates heterogeneity.

The study of early disease in some variants of AD remains problematic: the inclusion of milder cases of PCA is difficult since early visual symptoms are often not recognized as being of neurological origin. Furthermore, since potential therapeutic drugs are likely to target specific

pathological processes such as amyloid, it is also important to identify possible markers which may help to distinguish between PCA subjects with different pathological causes, such as AD, CBD and DLB. The utility of amyloid imaging and cerebrospinal markers of pathology remains to be fully explored in this disease presentation.

9.7 Chapter conclusion

The studies described in this thesis contribute to the growing interest in characterising and understanding atypical variants of AD. Atrophy in posterior regions is common to many variants of AD and is particularly striking in patients with PCA. This brain region therefore needs to be considered when making a diagnosis of AD, particularly in younger patients. Studying atypical presentations such as PCA is important in order to understand the nature of the heterogeneity of clinical phenotypes in AD. Moreover, their study may shed light on issues relevant to AD more generally.

PUBLICATIONS

This section documents published (or submitted) papers based on the results in this thesis, as well as other publications which I authored or contributed to during my PhD. I would like to thank everyone who was involved in generating and analysing these data and their contributions are stated below.

Chapter 4

Lehmann M., Rohrer J.D., Clarkson M.J., Ridgway G.R., Scahill R.I., Modat M., Warren J.D., Ourselin S., Barnes J., Rossor M.N., Fox N.C. (2010). Reduced cortical thickness in the posterior cingulate gyrus is characteristic of both typical and atypical Alzheimer's disease. Journal of Alzheimer's disease. 20(2):587-98.

Participants for this study were selected by Rachael Scahill and me. Jonathan Rohrer and Jason Warren reviewed notes for all patients. Image processing and analysis was conducted by me, with guidance from Matthew Clarkson. Statistical advice was provided by Ged Ridgway. The paper was drafted by me with all other co-authors contributing. Supervision and guidance was provided by Josephine Barnes, Nick Fox and Martin Rossor.

Chapter 5

Koedam E.L.G.E., **Lehmann M.**, van der Flier, W.M., Scheltens P., Pijnenburg, Y.A.L., Fox N.C., Barkhof F., Wattjes M. (2011). Visual assessment of posterior atrophy: Development of a MRI rating scale, European Radiology, doi:10.1007/s00330-011-2205-4.

The posterior atrophy (PA) scale was developed by Esther Koedam and me under supervision of Wiesje van der Flier, Philip Scheltens, Yolande Pijnenburg, Frederik Barkhof and Mike Wattjes. Scans were rated by Esther Koedam, Mike Wattjes and me. The paper was drafted by Esther Koedam and me, with all co-authors contributing.

Lehmann M., Koedam E.L.G.E., Barnes J., Bartlett J., Ryan N.S., Pijnenburg Y.A.L., Barkhof F., Wattjes M.P., Scheltens P., Fox N.C. (2011). Posterior cerebral atrophy in the absence of medial temporal lobe atrophy in pathologically-confirmed Alzheimer's disease. Neurobiology of Aging, doi:10.1016/j.neurobiolaging.2011.04.003.

Subjects were selected by me. Visual ratings were performed by Esther Koedam and me. Jonathan Bartlett gave statistical advice. Natalie Ryan reviewed patient notes for clinical details. The paper was drafted by me and all co-authors contributed. Supervision and guidance was provided by Josephine Barnes, Philip Scheltens and Nick Fox.

Chapter 6

Lehmann M., Crutch S.J., Ridgway G.R., Ridha B.H., Barnes J., Warrington E.K., Rossor M.N., Fox N.C. (2009). Cortical thickness and voxel-based morphometry in posterior cortical

atrophy and typical Alzheimer's disease. Neurobiology of Aging, doi:10.1016/j.neurobiolaging.2009.08.017.

Patients were recruited and data were collected by Basil Ridha, Sebastian Crutch, Elizabeth Warrington and me as part of a wider PCA project. Patients to be included in this study were selected by me with guidance from Sebastian Crutch. The selection process also included the review of patient notes which was done by me. Ged Ridgway gave statistical advice. Image processing and analysis was conducted by me. The paper was drafted by me with all co-authors contributing. Guidance was given by Martin Rossor and Nick Fox, Josephine Barnes and Sebastian Crutch.

Chapter 7

Lehmann M., Barnes J., Ridgway G.R., Ryan N.S., Warrington E.K., Crutch S.J., Fox N.C. (2010). Global grey matter changes in posterior cortical atrophy: a serial imaging study. Alzheimer's and Dementia, *in press*.

Patients were recruited and data collected by Sebastian Crutch, Elizabeth Warrington and me as part of a wider project on PCA. Patients included in this study were selected by me. Images were processed and analysed by me. Ged Ridgway gave advice on the image processing and statistical analyses. Natalie Ryan reviewed patient notes for clinical details. The paper was drafted by me and all co-authors contributed. Guidance and supervision was given by Nick Fox, Josephine Barnes and Sebastian Crutch.

Chapter 8

Lehmann M., Barnes J., Ridgway G.R., Wattam-Bell J., Warrington E.K., Fox N.C., Crutch S.J. (2010). Basic visual function and cortical thickness patterns in Posterior Cortical Atrophy. Cerebral Cortex, *in press*, doi:10.1093/cercor/bhq287.

Patients were recruited and data collected by Sebastian Crutch, Elizabeth Warrington and me. Ged Ridgway gave statistical advice. Image processing and analysis were conducted by me. Behavioural data were analysed by Sebastian Crutch and me. The paper was drafted by Sebastian Crutch and me, with all co-authors contributing. Guidance was given by Nick Fox, Josephine Barnes and Sebastian Crutch.

Appendix 3

Kennedy J., **Lehmann M.**, Sokolska M.J., Archer H., Warrington E.K., Fox N.C., Crutch S.J. (2011). Visualising the emergence of posterior cortical atrophy. Neurocase, *in press.*

Annual neuropsychological assessments of the patient were performed by Sebastian Crutch, me and other research assistants. Clinical investigations were performed by Jonathan Kennedy and Hilary Archer. Image analysis was conducted by Magda Sokolska and me. The paper was drafted by John Kennedy, Sebastian Crutch and me. Guidance was provided by Nick Fox.

Other publications:

Barnes J., Ridgway G.R., Bartlett J., Henley S.M., **Lehmann M.**, Hobbs N., Clarkson M.J., MacManus D.G., Ourselin S., Fox N.C. (2010). Head size, age and gender adjustment in MRI studies: a necessary nuisance? Neuroimage, 53(4), 1244-1255.

Crutch S.J., **Lehmann M.**, Gorgoraptis N., Kaski D., Ryan N., Husain M., Warrington E.K. (2010). Abnormal visual phenomena in posterior cortical atrophy: static motion, after-image, reverse size and room tilt illusion effects. Neurocase, *in press*, doi:10.1080/13554794.2010.504729.

Barnes J., Mitchell L.A., Kennedy J., Barker S., **Lehmann M.**, Nordstrom R.C., Frost C., Smith J.R., Garde E., Rossor M.N., Fox N.C. (2010). Does registration of serial MRI improve diagnosis of dementia? Neuroradiology 52(11), 987-995.

Lehmann, M., Douiri, A., Barnes, J., Chan, D., Rossor, M.N., Fox, N.C. (2010). Atrophy patterns in Alzheimer's disease and semantic dementia: A comparison of FreeSurfer and manual measurements. Neuroimage 49 (3), 2264-2274.

Gutiérrez-Galve L., **Lehmann M.**, Hobbs, N.Z., Clarkson M.J., Ridgway, G.R., Crutch, S.J., Ourselin S., Schott, J.M., Fox, N.C., Barnes, J. (2009). Patterns of cortical thickness according to ApoE genotype in Alzheimer's disease. Dementia and Geriatric Cognitive Disorders 28 (5), 476-485.

Modat M., Ridgway G.R., Taylor Z.A., **Lehmann M.**, Barnes J., Hakwes D.J., Fox N.C., Ourselin S. (2010). Fast free-form deformation using graphics processing units. Computer Methods and Programs in Biomedicine 98 (3), 278-284.

ACKNOWLEDGMENTS

I am extremely thankful for the time given by all patients and their partners and carers to take part in research studies at the Dementia Research Centre. Their dedication, often under extremely difficult circumstances, made this work possible. I would like to extend my thanks to those people who have helped scan these subjects, at St Mary's Hospital, the National Hospital for Neurology and Neurosurgery (main site and Queen Square Imaging Centre), and the Institute of Neurology.

This thesis would have not been possible without the support, expertise and help of numerous people within the Dementia Research Centre. In particular I would like to thank my supervisors Nick Fox, Sebastian Crutch and Josephine Barnes for the excellent support they have provided during my PhD. I would also like to thank other members of the Dementia Research team who have provided valuable contributions to this thesis, namely Natalie Ryan, Ged Ridgway, Jonathan Bartlett, Kelvin Leung, Matt Clarkson, Jason Warren, Elizabeth Warrington, Rachael Scahill, and Martin Rossor. Thanks also to all people at work with whom I have discussed various issues, whether or not they are related to work: Imaging Team: Liz Gordon, Laila Ahsan, Kate MacDonald, Emily Manning, Raivo Kittus, Ian Malone, and Shona Clegg; Psychology Team: Aisling Buckley, Jo Goll, and Julia Hailstone; Medical Staff: Colin Mahoney and Basil Ridha. I would also like to express my thanks to the Support and Administrative Staff for arranging supervisions, hunting patient notes, handling administrative issues and fixing computers: Gillian Barley, Claire Bloomfield, Suzie Barker, Anne Parnell, Carolyn Andersen, Ayesha Khatun, and Stuart Luscombe.

I would also like to thank the research team at the VU Medical Centre in Amsterdam for their warm welcome during my stay at their research facility and for their support in publishing the research conducted during my visit: Esther Koedam, Yolande Pijnenburg, Wiesje van der Flier, Mike Wattjes, Frederik Barkhof, and Philip Scheltens.

Funding for this work was provided by the Alzheimer's Society.

Last but no means least, I would like to thank my family: my mum whose encouragements to move and study abroad has greatly shaped my scientific career and life, and my sisters Cindy and Sandra for their continued moral support.

APPENDIX 1 - NINCDS-ADRDA CRITERIA FOR AD

Criteria for probable Alzheimer's disease given by the National Institute of Neurological and Communicative Disorders and the Alzheimer's Disease and Related Disorders Association (NINCDS-ADRDA) (McKhann et al., 1984).

I) The diagnosis of PROBABLE Alzheimer's disease include:

a) Dementia established by clinical examination and documented by the Mini-Mental Test; Blessed Dementia Scale, or some similar examination, and confirmed by neuropsychological tests

b) Deficits in two or more areas of cognition

c) Progressive worsening of memory and other cognitive functions

d) No disturbance of consciousness

e) Onset between 40 and 90, most often after age 65

f) Absence of systemic disorders or other brain diseases that in and of themselves could account for the progressive deficits in memory and cognition

II) The diagnosis of PROBABLE Alzheimer's disease is supported by:

a) Progressive deterioration of specific cognitive functions such as language (aphasia), motor skills (apraxia), and perceptions (agnosia)

b) Impaired activities of daily living and altered patterns of behaviour

c) Family history of similar disorders, particularly if confirmed neuropathologically

d) Normal lumbar puncture as evaluated by standard techniques

e) Normal pattern or non-specific changes in EEG, such as increased slow-wave activity

f) Evidence of cerebral atrophy on CT with progression documented by serial observation

III) Other clinical features consistent with the diagnosis of PROBABLE Alzheimer's disease, after exclusion of causes of dementia other than Alzheimer's disease, include:

a) Plateaus in the course of progression of the illness

b) Associated symptoms of depression, insomnia, incontinence, delusions, illusions, hallucinations, catastrophic verbal, emotional, or physical outbursts, sexual disorders, and weight loss

c) Other neurologic abnormalities in some patients, especially with more advanced disease and including motor signs such as increased muscle tone, myoclonus, or gait disorder

d) Seizures in advanced disease

e) CT normal for age

IV) Features that make the diagnosis of PROBABLE Alzheimer's disease uncertain or unlikely include:

a) Sudden, apoleptic onset

b) Focal neurologic findings such as hemiparesis, sensory loss, visual field deficits, and incoordination early in the course of the illness

c) Seizures or gait disturbance at the onset or very early in the course of the illness

V) Clinical diagnosis of POSSIBLE Alzheimer's disease:

a) May be made on the basis of the dementia syndrome, in the absence of other neurologic, psychiatric, or systemic disorders sufficient to cause dementia, in the presence of variations in the onset, in the presentation, or in clinical course

b) May be made in the presence of a second systemic or brain disorder sufficient to produce dementia, which is not considered to be the cause of the dementia

c) Should be used in research studies when a single, gradually progressive severe cognitive deficit is identified in the absence of other identifiable cause

VI Criteria for the diagnosis of DEFINITE Alzheimer's disease are:

a) The clinical criteria for probable Alzheimer's disease

b) Histopathological evidence obtained from biopsy or autopsy

APPENDIX 2 - PROPOSED DIAGNOSTIC CRITERIA FOR PCA

I Proposed clinical diagnostic criteria for PCA (Mendez et al., 2002)

1) Core diagnostic features (all must be present)

a) Insidious onset and gradual progression

b) Presentation with visual complaints with intact primary visual functions

c) Evidence of predominant complex visual disorder on examination; elements of Balint's syndrome; visual agnosia; dressing apraxia; environmental disorientation

d) Proportionally less impaired deficits in memory and verbal fluency

e) Relatively preserved insight with or without depression

2) Supportive diagnostic features

a) Presenile onset

b) Alexia

c) Elements of Gerstmann's syndrome

d) Ideomotor apraxia

e) Physical examination within normal limits

f) Investigations

- Neuropsychology: predominantly impaired perceptual deficits
- Brain imaging: predominantly occipitoparietal abnormality (especially on functional neuroimaging) with relative sparing of frontal and mesiotemporal regions

II Proposed clinical diagnostic criteria for PCA (Tang-Wai et al., 2004)

1) Core features

a) Insidious onset and gradual progression

b) Presentation of visual complaints in the absence of significant primary ocular disease explaining the symptoms

c) Relative preservation of anterograde memory and insight early in the disorder

d) Disabling visual impairment throughout the disorder

e) Absence of stroke or tumor

f) Absence of early parkinsonism and hallucinations

g) Any of the following findings:

- Simultanagnosia with or without optic ataxia or ocular apraxia
- Constructional dyspraxia
- Visual field defect
- Environmental disorientation

h) Any of the elements of Gerstmann syndrome

2) Supportive features

a) Alexia

b) Presenile onset

c) Ideomotor or dressing apraxia

d) Prosopagnosia

e) Investigations

- Neuropsychological deficits referable to parietal and/or occipital regions
- Focal or asymmetric atrophy in parietal and/or occipital regions on structural imaging
- Focal or asymmetric hypoperfusion/hypometabolism in parietal and/or occipital regions on functional imaging

APPENDIX 3 - VISUALIZING THE EMERGENCE OF PCA

Diagnosis of PCA is often delayed because of poor general knowledge of the syndrome's existence, and because early visual symptoms are often mistaken as being of ophthalmological rather than neurological origin. Therefore, little is known about the earliest cognitive and structural changes in PCA. Studying the early stages of PCA is, however, crucial to fully understand the evolution of this disease. In a single case study, a patient with PCA who volunteered as a healthy control subject in a longitudinal study investigating subjective memory complaints was assessed. Over the course of 5 years the participant underwent extensive investigations including clinical, neuropsychological and neuroimaging assessments. Each assessment included a clinical interview with the patient and his informant, a standardised neuropsychological battery, and a volumetric T1-weighted MRI brain scan with additional T2-weighted images which were obtained on a 1.5T GE Signa scanner. This case has been described in detail in Kennedy et al., 2011. A summary of the imaging findings is presented below, which represent a good example of the application of fluid registration to visualize structural changes over multiple time points in an individual patient.

Imaging findings

During the first three years of this study, the patient's serial MR imaging was reviewed by the same neuroradiologist and individually felt to be normal. After viewing registered scan pairs of visit 4 and 5, the neuroradiologist suggested that a progressive neurodegenerative disease may be present. For the purpose of this study, MR images were segmented (chapter 3, section 3.5.2.1, Freeborough et al., 1997) and each time point was registered to the baseline using the fluid algorithm described in chapter 2, section 2.2.2.2 (Freeborough and Fox, 1998). The resulting voxel-compression maps are shown in Figure A-1. The neuroimaging data revealed a marked posterior-anterior gradient of atrophy, with early changes occurring predominantly in inferior temporal and superior parietal regions at visit 2. Atrophy then spread affecting inferior parietal and occipital lobe areas at visit 3. This continued to be the focus of progressive atrophy but by visit 6 atrophy in anterior regions also appeared.

Annualised whole brain atrophy rates (% loss per year) were also calculated using the KN-BSI (chapter 2, section 2.2.2.2, Leung et al., 2010): -0.28% (Baseline-Visit 2), 0.83% (Visit 2-3), 1.69% (Visit 3-4), 1.45% (Visit 4-5) and 0.99% (Visit 5-6). The initial apparent increase in brain volume between baseline and Visit 2 is at odds with subsequent atrophy, however, this is not beyond the change in volume between same day scans (Boyes et al., 2006). The mean atrophy rate thereafter is 0.93% which is approximately three times what would be expected for a healthy man of this age (chapter 2, section 2.5.1). Whilst normal variation and artefacts can make it difficult to interpret atrophy rates on an individual basis, particularly on one year alone, the patient's rates were highly suggestive of pathological atrophy.

It is noteworthy that one of the regions affected early in the present case was the inferior temporal lobe, and continued to atrophy throughout the later stages. As discussed in chapter 8, different subtypes of PCA have been suggested (Galton et al., 2000; Ross et al., 1996), with some patients exhibiting a more dorsal (i.e. parieto-occipital) phenotype, and others a more ventral (i.e. temporo-occipital) presentation. According to this distinction, the present case may represent an example of a PCA patient with a ventral phenotype. There is some evidence to suggest that PCA often occurs more commonly in the absence of an ApoE ε4 allele and it has been postulated that this allows AD pathology to be directed more posteriorly. Our subject was an ApoE ε4 allele heterozygote which may account for the more ventral phenotype and striking inferior temporal lobe involvement, perhaps, suggesting that the present case lies somewhat between the two extremes of typical amnestic AD and typical visual AD (i.e. PCA).

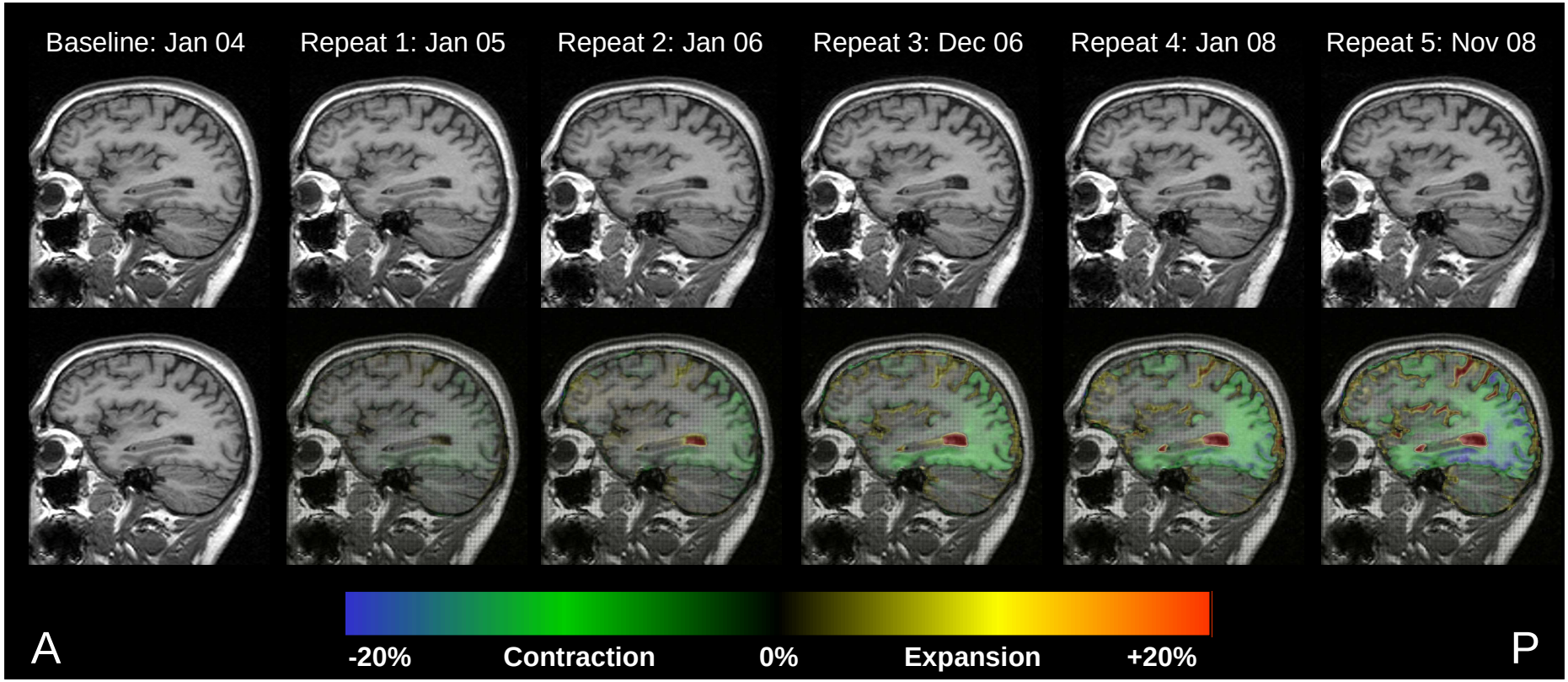

Figure A-1: Fluid-registered serial MR images of a PCA patient for 6 visits. Shown is a sagittal view of the patient's right hemisphere. Repeat scans were fluid-registered to the baseline image and colour-coded voxel-compression maps were produced. The scale shows the percentage volume change per voxel (-20% to 20%) with green and blue representing contraction and yellow and red representing expansion.

APPENDIX 4 - PCA NEUROPSYCHOLOGY TESTS

1) Basic visual processing

1.1) Form detection

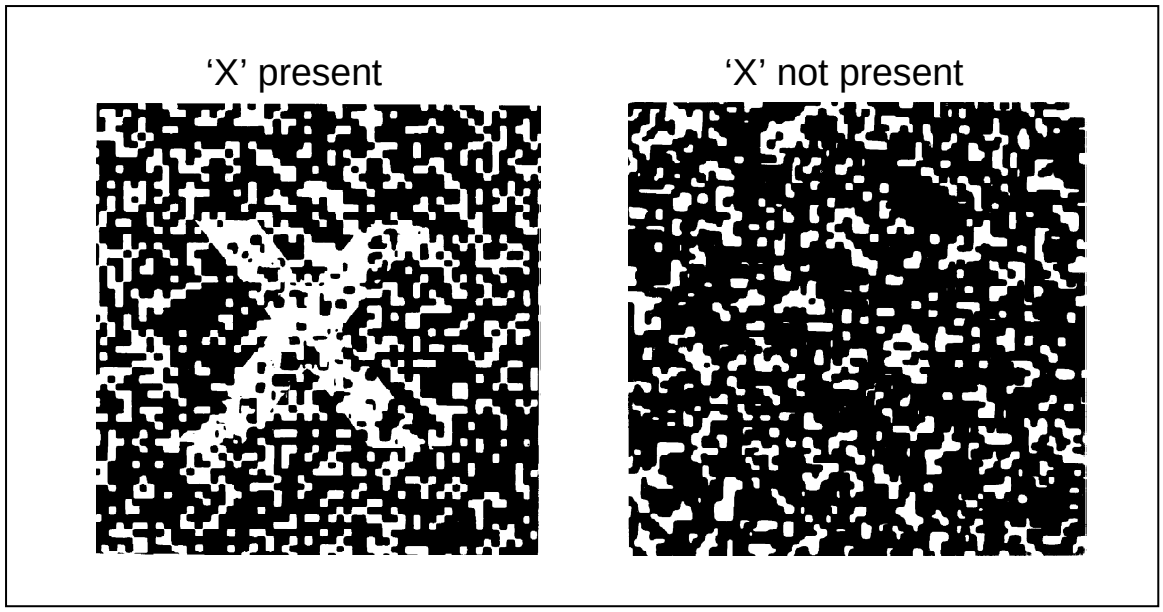

Figure A-2: VOSP Figure-ground discrimination task. Participants were shown random black patterns, half with a degraded 'X' superimposed. They were requested to state whether an 'X' was present.

1.2) Form discrimination

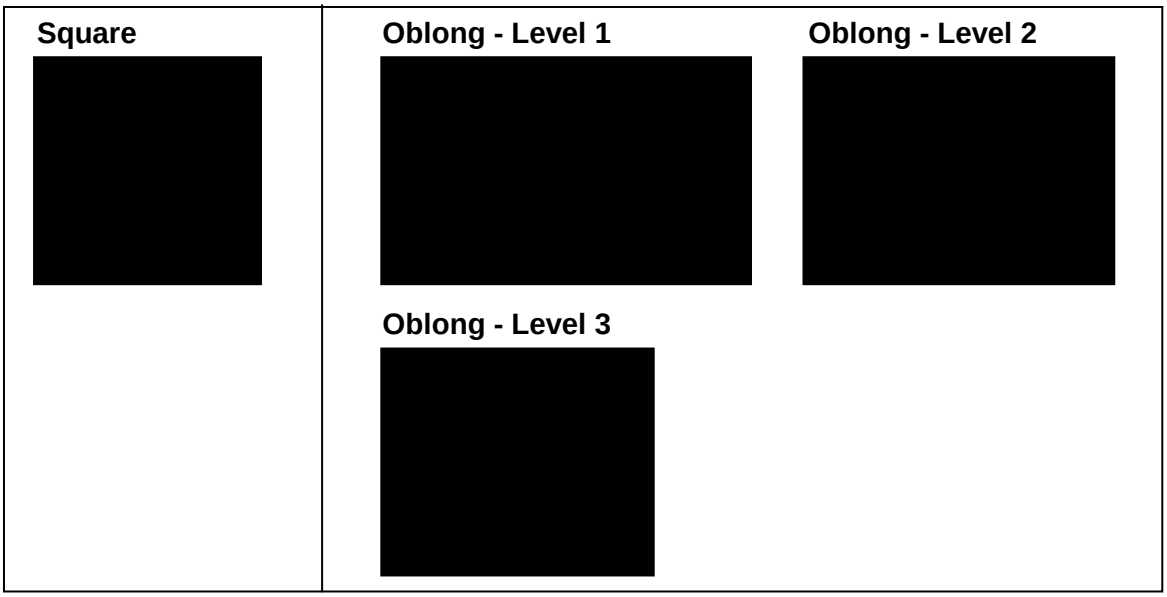

Figure A-3: Form discrimination task. The task was to discriminate whether a shape presented to the participant was a square or an oblong.

1.3) Form coherence

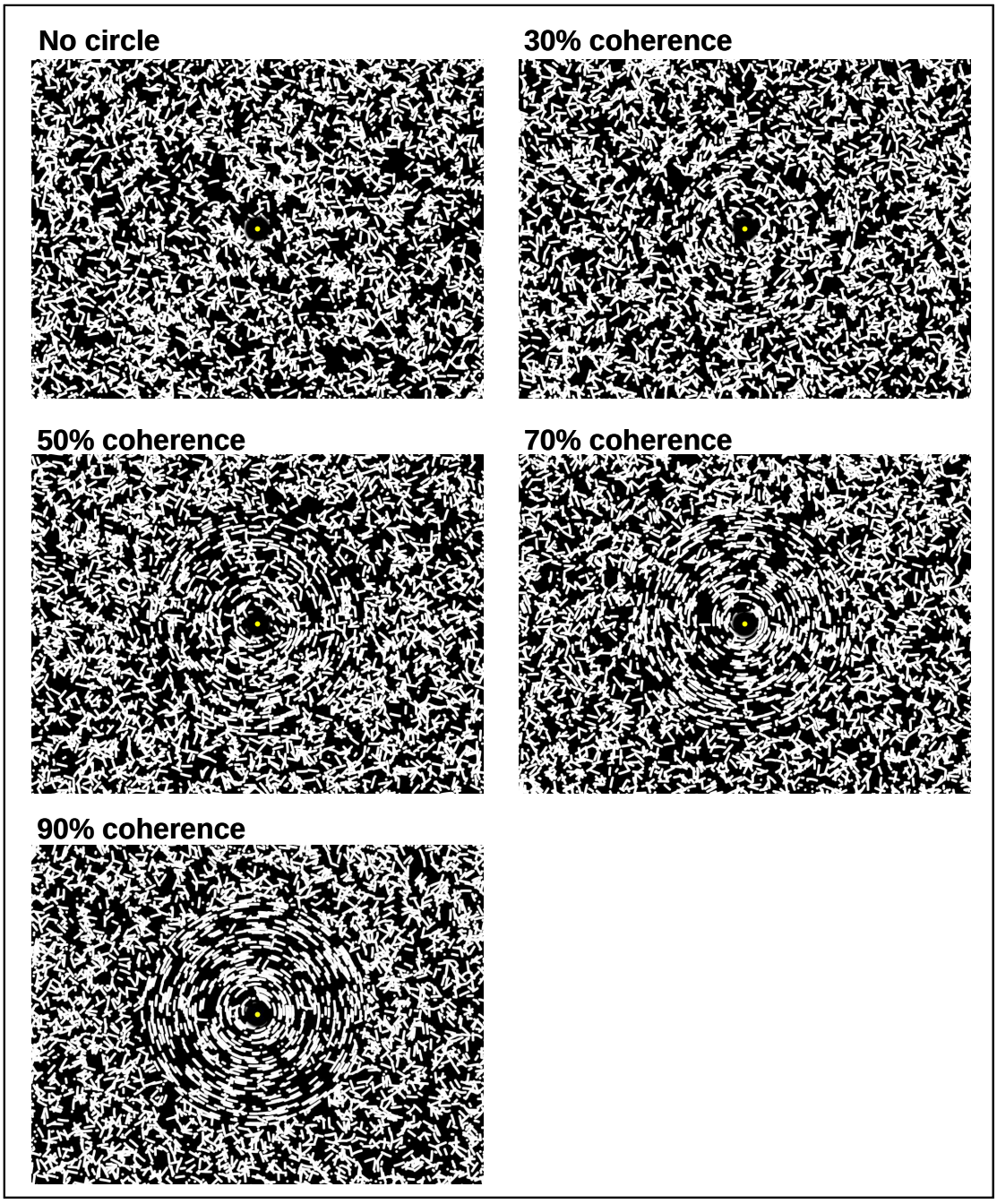

Figure A-4: Form coherence task. This and the motion coherence test were administered on a computer screen. In half the arrays, a percentage of the line segments in a central region were coherently oriented tangentially to concentric circles. In the remaining arrays, all line segments were arranged randomly. Patients were requested to state whether a 'circle' is present in each stimulus. The motion coherence task was similar, only difference being that the short line segments were dots moving around.

1.4) Colour discrimination

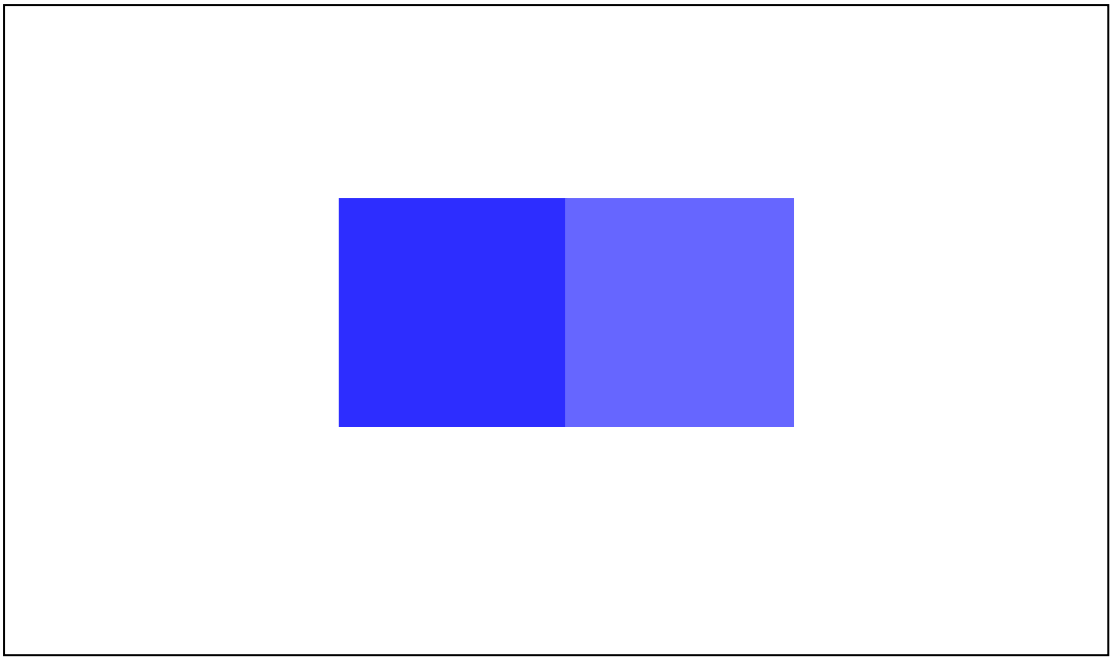

Figure A-5: Colour discrimination task. The stimuli were pairs of matte colour chips presented adjacently. The task was to determine whether the hues in each pair are the same or different. This example shows different colours.

1.5) Point localization

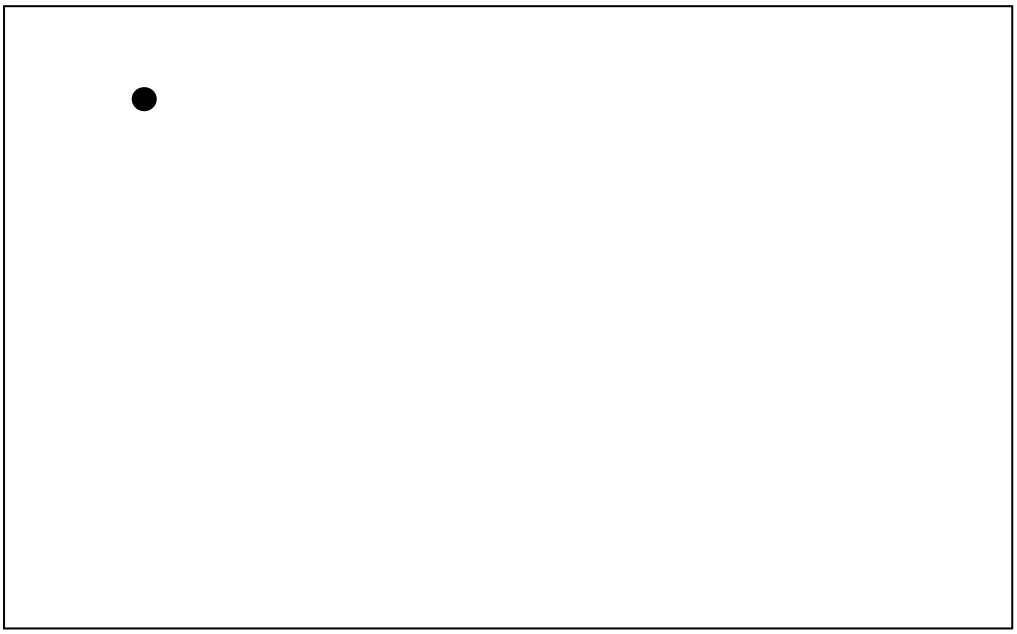

Figure A-6: Point localization task. Stimuli were A3 laminated white cards with a single, randomly-position black dot. The position of each dot was revealed for 3s before the stimulus was covered by a second blank A3 card, and participants were requested to mark the position of the dot on the blank sheet using a pen in their dominant hand.

2) Higher-order visual processing

2.1) Object perception - ventral processing

2.1.1) Object decision (VOSP)

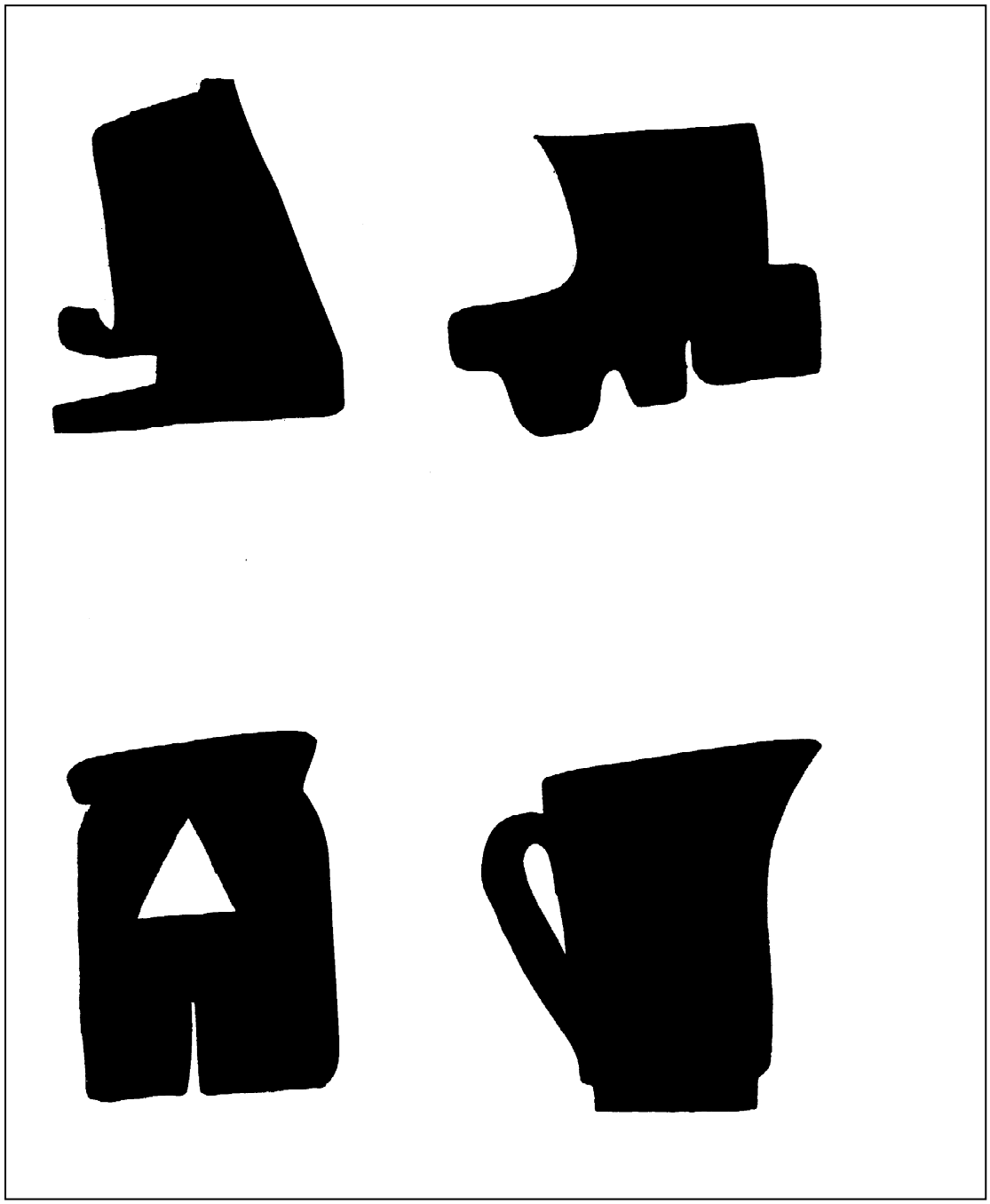

Figure A-7: VOSP Object decision task. Participants were shown 4 silhouettes. Only one of them was a silhouette of a real object, the other 3 were completely made up. Participants were asked to point to the one they think is real. In this example the correct answer is “jug” in the right bottom corner.

2.1.2) Fragmented letters (VOSP)

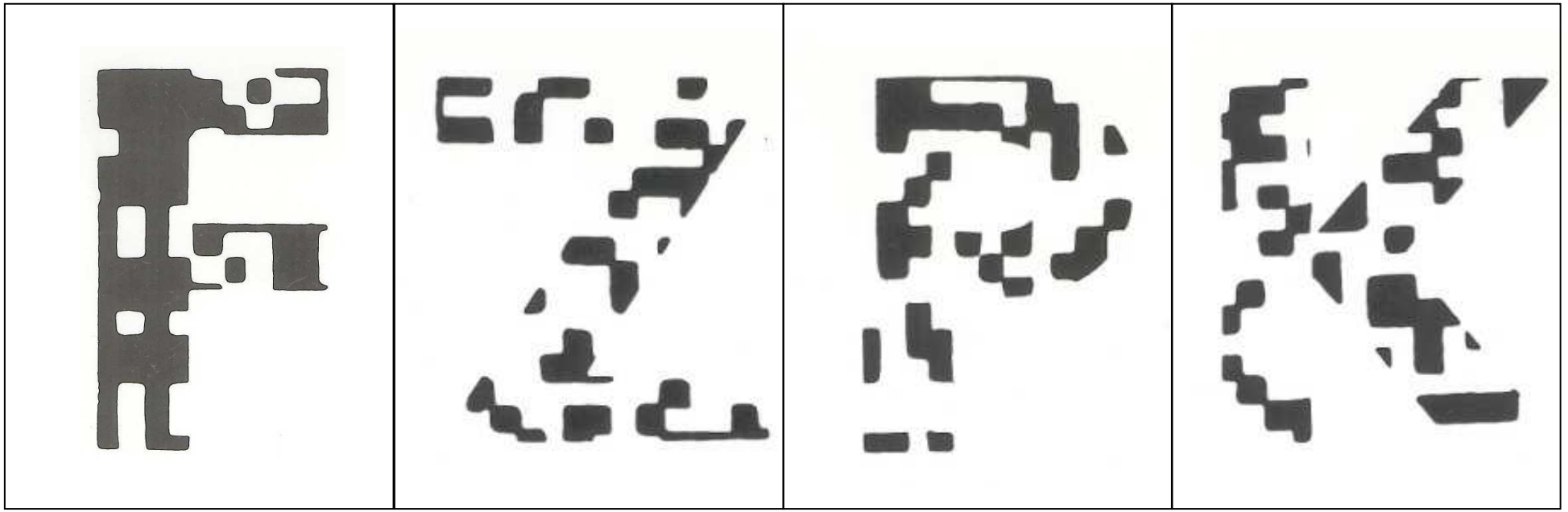

Figure A-8: VOSP Fragmented letters task. Subjects were shown incomplete letters and they were asked which letter they can see. In this example the letters are (from left to right): F, Z, P, K.

2.1.3) Unusual/usual views

Plug - unusual view **Plug - usual view**

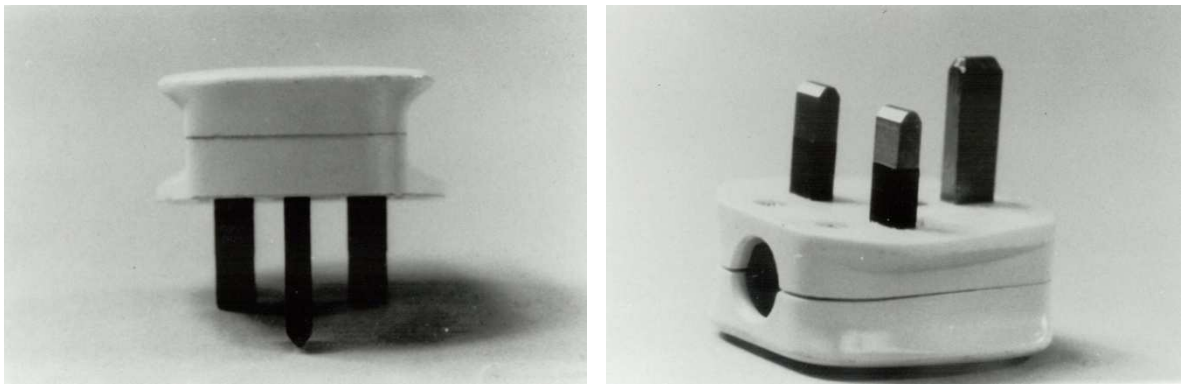

Figure A-9: Unusual/usual views. Participants were shown a number of photos of household objects, taken from odd angles (unusual views) and they were asked what object they can see. If they did not recognize the object, they were shown another photograph of the same object from a 'usual' angle. The example shown here is a "plug".

2.2) Space perception - dorsal processing

2.2.1) Number location (VOSP)

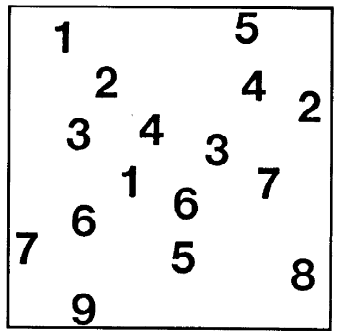

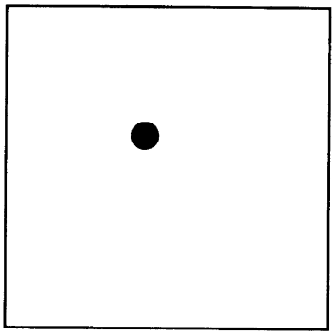

Figure A-10: VOSP Number location task. Participants were shown two boxes. One box contained a black dot, the other box above it contained numbers. Participants were asked which number corresponded to the position of the dot. In the example shown here, the correct answer is "4".

2.2.2) Dot counting (VOSP)

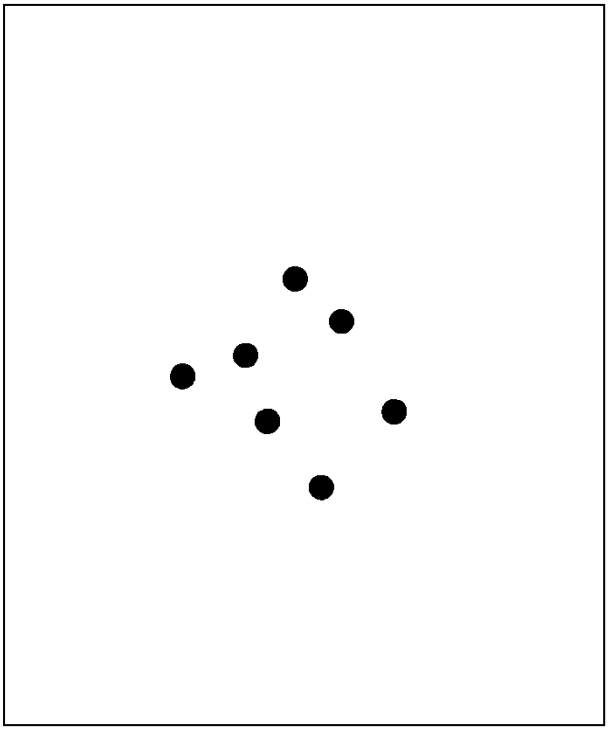

Figure A-11: VOSP Dot counting task. Subjects were presented a number of black dots and were asked to say, as quickly as they could, how many dots they can see. In this example the correct answer is “7”.

APPENDIX 5 - IMAGE ACQUISITION PROTOCOLS

The majority of scans were acquired on one of four 1.5T Signa MRI scanners (General Electric, Milwaukee, Wisconsin, USA) as 124 contiguous 1.5mm coronal slices. The 4 scan sites were as follows:

1) Dave MacManus' scanner, NMR group, Queen Square:

This protocol was an inversion recovery (IR)-prepared fast SPGR sequence with a 256x256 image matrix and a 24cm field of view. This scanner underwent a software upgrade in April 2004 which consisted of new gradient drivers, a new computer operating system (Linux platform) and a scanner operating software upgrade from v5.8 to v11.0. Scans acquired prior to the upgrade have the following parameters: readout interval repetition time TR=15ms; echo time TE=5.4ms; inversion time TI=650ms; flip angle=15°. Scans obtained after the upgrade have the following parameters: readout interval TR=12ms; TE=5.2ms; TI=650ms; flip angle=13°.

2) St Mary's hospital, Paddington and Queen Square Imaging Centre:

The scans were taken using a 256x126 image matrix with the field of view being 24cm; acquisition parameters: TE=5.4ms; readout interval TR=12ms; flip angle=15°; TI=650ms.

3) Queen Square Imaging Centre:

Scans were taken using a 256x224 image matrix with the field of view being 24cm. The scanning protocol used the following acquisition parameters: TE=2.3ms; readout interval TR=20ms; flip angle=20°; TI=450ms.

4) National Hospital for Neurology and Neurosurgery:

4.1) 1.5T scanner: This scanner used an IR-prepared SPGR with a 256x256 image matrix and a field of view of 24cm; acquisition parameters: TE=6.3ms; readout interval TR=14.2ms; flip angle=15°; TI=650ms.

4.2) 3T scanner: A small number of scans were acquired on a Siemens Trio TIM 3T scanner using an MPRAGE sequence with a 256x256 acquisition matrix and 28.2-cm field of view to provide 208 contiguous 1.1-mm-thick slices in the sagittal plane; acquisition parameters: TE=2.9ms, inversion interval TR=2200ms, TI=900ms.

GLOSSARY

AD: Alzheimer's disease
ApoE: Apolipoprotein E
AUC: Area under the curve
BSI: Boundary-shift integral
bvFTD: behavioural variant frontotemporal dementia
CBD: Corticobasal degeneration
CI: Confidence intervals
CJD: Creutzfeld Jakob disease
CORVIST: Cortical Visual Screening Test
CSF: Cerebrospinal fluid
CT: Computed tomography
DLB: Dementia with Lewy Bodies
DLDH: Dementia lacking distinctive histology
dof: degrees-of-freedom
DTI: Diffusion tensor imaging
EOAD: Early-onset Alzheimer's disease
FDR: False discovery rate
FTLD: Frontotemporal lobar degeneration
FTD: Frontotemporal dementia
FWHM: full-width at half-maximum
GLM: General linear model
LOAD: Late-onset Alzheimer's disease
LPA: Logopenic progressive aphasia
MCI: Mild cognitive impairment
MIDAS: Medical information display and analysis system
MMSE: Mini-mental state examination
MNI: Montreal Neurological Institute
MPRAGE: magnetization-prepared rapid acquisition with gradient echo
MRI: Magnetic resonance imaging
MTA: Medial temporal lobe atrophy
NINCDS-ADRDA: National Institute of Neurological and Communicative Disorders and Stroke and the Alzheimer's Disease and Related Disorders Association
PA: Posterior atrophy
PCA: Posterior cortical atrophy
PET: Positron emission tomography
PNFA: Progressive non-fluent aphasia
PPA: Primary progressive aphasia
PSP: Progressive supranuclear palsy

RMT: Recognition Memory Test

ROC: Receiver operating characteristic

ROI: Region of interest

SemD: Semantic dementia

SD: Standard deviation

SPECT: Single photon emission computed tomography

SPGR: Spoiled gradient echo

SPM: Statistical parametric mapping

SVM: Support vector machine

tAD: typical Alzheimer’s disease

TIV: Total intracranial volume

VBM: Voxel-based morphometry

VOSP: Visual Object and Space Perception Battery

BIBLIOGRAPHY

1. Agdeppa, E.D., Kepe, V., Liu, J., Flores-Torres, S., Satyamurthy, N., Petric, A., Cole, G.M., Small, G.W., Huang, S.C., Barrio, J.R., 2001. Binding characteristics of radiofluorinated 6-dialkylamino-2-naphthylethylidene derivatives as positron emission tomography imaging probes for beta-amyloid plaques in Alzheimer's disease. Journal of Neuroscience 21, RC189.

2. Aharon-Peretz, J., Israel, O., Goldsher, D., Peretz, A., 1999. Posterior cortical atrophy variants of Alzheimer's disease. Dementia and Geriatric Cognitive Disorders 10, 483-487.

3. Aizenstein, H.J., Nebes, R.D., Saxton, J.A., Price, J.C., Mathis, C.A., Tsopelas, N.D., Ziolko, S.K., James, J.A., Snitz, B.E., Houck, P.R., Bi, W.Z., Cohen, A.D., Lopresti, B.J., Dekosky, S.T., Halligan, E.M., Klunk, W.E., 2008. Frequent amyloid deposition without significant cognitive impairment among the elderly. Archives of Neurology 65, 1509-1517.

4. Alladi, S., Xuereb, J., Bak, T., Nestor, P., Knibb, J., Patterson, K., Hodges, J.R., 2007. Focal cortical presentations of Alzheimer's disease. Brain 130, 2636-2645.

5. Allen, J.S., Bruss, J., Brown, C.K., Damasio, H., 2005. Normal neuroanatomical variation due to age: The major lobes and a parcellation of the temporal region. Neurobiology of Aging 26, 1245-1260.

6. Anderson, V.M., Bartlett, J.W., Fox, N.C., Fisniku, L., Miller, D.H., 2007. Detecting treatment effects on brain atrophy in relapsing remitting multiple sclerosis: Sample size estimates. Journal of Neurology 254, 1588-1594.

7. Andrade, K., Samri, D., Sarazin, M., de Souza, L.C., Cohen, L., Thiebaut de, S.M., Dubois, B., Bartolomeo, P., 2010. Visual neglect in posterior cortical atrophy. BMC Neurology 10, 68.

8. Arnold, S.E., Hyman, B.T., Flory, J., Damasio, A.R., Van Hoesen, G.W., 1991. The topographical and neuroanatomical distribution of neurofibrillary tangles and neuritic plaques in the cerebral cortex of patients with Alzheimer's disease. Cerebral Cortex 1, 103-116.

9. Ashburner, J., 2007. A fast diffeomorphic image registration algorithm. Neuroimage 38, 95-113.

10. Ashburner, J., Friston, K.J., 2000. Voxel-based morphometry - the methods. Neuroimage 11, 805-821.

11. Ashburner, J., Friston, K.J., 2005. Unified segmentation. Neuroimage 26, 839-851.

12. Bacskai, B.J., Frosch, M.P., Freeman, S.H., Raymond, S.B., Augustinack, J.C., Johnson, K.A., Irizarry, M.C., Klunk, W.E., Mathis, C.A., Dekosky, S.T., Greenberg, S.M., Hyman, B.T., Growdon, J.H., 2007. Molecular imaging with Pittsburgh compound B confirmed at autopsy - A case report. Archives of Neurology 64, 431-434.

13. Ball, M.J., Fisman, M., Hachinski, V., Blume, W., Fox, A., Kral, V.A., Kirshen, A.J., Fox, H., Merskey, H., 1985. A new definition of Alzheimer's disease: a hippocampal dementia. Lancet 1, 14-16.

14. Barkhof, F., Polvikoski, T.M., van Straaten, E.C., Kalaria, R.N., Sulkava, R., Aronen, H.J., Niinisto, L., Rastas, S., Oinas, M., Scheltens, P., Erkinjuntti, T., 2007. The significance of medial temporal lobe atrophy: a postmortem MRI study in the very old. Neurology 69, 1521-1527.

15. Barnes, J., Bartlett, J.W., van de Pol, L.A., Loy, C.T., Scahill, R.I., Frost, C., Thompson, P., Fox, N.C., 2009. A meta-analysis of hippocampal atrophy rates in Alzheimer's disease. Neurobiology of Aging 30, 1711-1723.

16. Barnes, J., Godbolt, A.K., Frost, C., Boyes, R.G., Jones, B.F., Scahill, R.I., Rossor, M.N., Fox, N.C., 2007a. Atrophy rates of the cingulate gyrus and hippocampus in AD and FTLD. Neurobiology of Aging 28, 20-28.

17. Barnes, J., Lewis, E.B., Scahill, R.I., Bartlett, J.W., Frost, C., Schott, J.M., Rossor, M.N., Fox, N.C., 2007b. Automated measurement of hippocampal atrophy using fluid-registered serial MRI in AD and controls. Journal of Computer Assisted Tomography 31, 581-587.

18. Barnes, J., Mitchell, L.A., Kennedy, J., Bastos-Leite, A.J., Barker, S., Lehmann, M., Nordstrom, R.C., Frost, C., Smith, J.R., Garde, E., Rossor, M.N., Fox, N.C., 2010. Does registration of serial MRI improve diagnosis of dementia? Neuroradiology 52, 987-995.

19. Baron, J.C., Chetelat, G., Desgranges, B., Perchey, G., Landeau, B., De La Sayette, V., Eustache, F., 2001. *In vivo* mapping of gray matter loss with voxel-based morphometry in mild Alzheimer's disease. Neuroimage 14, 298-309.

20. Basso, M., Yang, J., Warren, L., MacAvoy, M.G., Varma, P., Bronen, R.A., van Dyck, C.H., 2006. Volumetry of amygdala and hippocampus and memory performance in Alzheimer's disease. Psychiatry Research - Neuroimaging 146, 251-261.

21. Baumann, T.P., Duyar, H., Sollberger, M., Kuhle, J., Regeniter, A., Gomez-Mancilla, B., Schmidtke, K., Monsch, A.U., 2010. CSF-tau and CSF-Abeta(1-42) in posterior cortical atrophy. Dementia and Geriatric Cognitive Disorders 29, 530-533.

22. Baxter, D.M., Warrington, E.K., 1994. Measuring dysgraphia: A graded-difficulty spelling test. Behavioural Neurology 7, 107-116.

23. Benson, F., Davis, J., Snyder, B.D., 1988. Posterior Cortical atrophy. Archives of Neurology 45, 789-793.

24. Bokde, A.L.W., Pietrini, P., Ibanez, V., Furey, M.L., Alexander, G.E., Graff-Radford, N.R., Rapoport, S.I., Schapiro, M.B., Horwitz, B., 2001. The effect of brain atrophy on cerebral hypometabolism in the visual variant of Alzheimer disease. Archives of Neurology 58, 480-486.

25. Bookstein, F.L., 2001. "Voxel-based morphometry" should not be used with imperfectly registered images. Neuroimage 14, 1454-1462.

26. Boxer, A.L., Rankin, K.P., Miller, B.L., Schuff, N., Weiner, M., Gorno-Tempini, M.L., Rosen, H.J., 2003. Cinguloparietal atrophy distinguishes Alzheimer disease from semantic dementia. Archives of Neurology 60, 949-956.

27. Boyes, R.G., Rueckert, D., Aljabar, P., Whitwell, J., Schott, J.M., Hill, D.L., Fox, N.C., 2006. Cerebral atrophy measurements using Jacobian integration: comparison with the boundary shift integral. Neuroimage 32, 159-169.

28. Braak, H., Braak, E., 1991. Neuropathological staging of Alzheimer-related changes. Acta Neuropathologica 82, 239-259.

29. Braak, H., Braak, E., 1995. Staging of Alzheimer's disease related neurofibrillary changes. Neurobiology of Aging 16, 271-278.

30. Braddick, O.J., O'Brien, J.M.D., Wattam-Bell, J., Atkinson, J., Turner, R., 2000. Form and motion coherence activate independent, but not dorsal/ventral segregated, networks in the human brain. Current Biology 10, 731-734.

31. Bradley, K.M., Bydder, G.M., Budge, M.M., Hajnal, J.V., White, S.J., Ripley, B.D., Smith, A.D., 2002. Serial brain MRI at 3-6 month intervals as a surrogate marker for Alzheimer's disease. British Journal of Radiology 75, 506-513.

32. Brayne, C., Richardson, K., Matthews, F.E., Fleming, J., Hunter, S., Xuereb, J.H., Paykel, E., Mukaetova-Ladinska, E.B., Huppert, F.A., O'Sullivan, A., Dening, T., 2009. Neuropathological correlates of dementia in over-80-year-old brain donors from

the population-based Cambridge city over-75s cohort (CC75C) study. Journal of Alzheimer's disease 18, 645-658.

33. Bresciani, L., Rossi, R., Testa, C., Geroldi, C., Galluzzi, S., Laakso, M.P., Beltramello, A., Soininen, H., Frisoni, G.B., 2005. Visual assessment of medial temporal atrophy on MR films in Alzheimer's disease: comparison with volumetry. Aging Clinical and Experimental Research 17, 8-13.

34. Bresjanac, M., Smid, L.M., Vovko, T.D., Petric, A., Barrio, J.R., Popovic, M., 2003. Molecular-imaging probe 2-(1-[6-[(2-fluoroethyl)(methyl) amino]-2-naphthyl]ethylidene) malononitrile labels prion plaques in vitro. Journal of Neuroscience 23, 8029-8033.

35. Broe, M., Hodges, J.R., Schofield, E., Shepherd, C.E., Kril, J.J., Halliday, G.M., 2003. Staging disease severity in pathologically confirmed cases of frontotemporal dementia. Neurology 60, 1005-1011.

36. Buckner, R.L., Andrews-Hanna, J.R., Schacter, D.L., 2008. The brain's default network - Anatomy, function, and relevance to disease. Year in Cognitive Neuroscience 2008 1124, 1-38.

37. Buckner, R.L., Head, D., Parker, J., Fotenos, A.F., Marcus, D., Morris, J.C., Snyder, A.Z., 2004. A unified approach for morphometric and functional data analysis in young, old, and demented adults using automated atlas-based head size normalization: reliability and validation against manual measurement of total intracranial volume. Neuroimage 23, 724-738.

38. Buckner, R.L., Snyder, A.Z., Shannon, B.J., LaRossa, G., Sachs, R., Fotenos, A.F., Sheline, Y.I., Klunk, W.E., Mathis, C.A., Morris, J.C., Mintun, M.A., 2005. Molecular, structural, and functional characterization of Alzheimer's disease: evidence for a relationship between default activity, amyloid, and memory. Journal of Neuroscience 25, 7709-7717.

39. Busatto, G.E., Garrido, G.E.J., Almeida, O.P., Castro, C.C., Camargo, C.H.P., Cid, C.G., Buchpiguel, C.A., Furuie, S., Bottino, C.M., 2003. A voxel-based morphometry study of temporal lobe gray matter reductions in Alzheimer's disease. Neurobiology of Aging 24, 221-231.

40. Cairns, N.J., Bigio, E.H., Mackenzie, I.R., Neumann, M., Lee, V.M., Hatanpaa, K.J., White, C.L., III, Schneider, J.A., Grinberg, L.T., Halliday, G., Duyckaerts, C., Lowe, J.S., Holm, I.E., Tolnay, M., Okamoto, K., Yokoo, H., Murayama, S., Woulfe, J., Munoz, D.G., Dickson, D.W., Ince, P.G., Trojanowski, J.Q., Mann, D.M., 2007. Neuropathologic diagnostic and nosologic criteria for frontotemporal lobar

degeneration: consensus of the Consortium for Frontotemporal Lobar Degeneration. Acta Neuropathologica 114, 5-22.

41. Campion, D., Dumanchin, C., Hannequin, D., Dubois, B., Belliard, S., Puel, M., Thomas-Anterion, C., Michon, A., Martin, C., Charbonnier, F., Raux, G., Camuzat, A., Penet, C., Mesnage, V., Martinez, M., Clerget-Darpoux, F., Brice, A., Frebourg, T., 1999. Early-onset autosomal dominant Alzheimer disease: prevalence, genetic heterogeneity, and mutation spectrum. American Journal of Human Genetics 65, 664-670.

42. Cardenas, V.A., Du, A.T., Hardin, D., Ezekiel, F., Weber, P., Jagust, W.J., Chui, H.C., Schuff, N., Weiner, M.W., 2003. Comparison of methods for measuring longitudinal brain change in cognitive impairment and dementia. Neurobiology of Aging 24, 537-544.

43. Chan, D., Anderson, V., Pijnenburg, Y., Whitwell, J., Barnes, J., Scahill, R., Stevens, J.M., Barkhof, F., Scheltens, P., Rossor, M.N., Fox, N.C., 2009. The clinical profile of right temporal lobe atrophy. Brain 132, 1287-1298.

44. Chan, D., Crutch, S.J., Warrington, E.K., 2001a. A disorder of colour perception associated with abnormal colour after-images: a defect of the primary visual cortex. Journal of Neurology Neurosurgery and Psychiatry 71, 515-517.

45. Chan, D., Fox, N., Scahill, R., Crum, W., Whitwell, J., Cipolotti, L., Rossor, M.N., 2001b. Patterns of temporal lobe atrophy in semantic dementia and Alzheimer's disease. Journal of Neurology Neurosurgery and Psychiatry 70, 276.

46. Chan, D., Fox, N.C., Jenkins, R., Scahill, R.I., Crum, W.R., Rossor, M.N., 2001c. Rates of global and regional cerebral atrophy in AD and frontotemporal dementia. Neurology 57, 1756-1763.

47. Chan, D., Janssen, J.C., Whitwell, J.L., Watt, H.C., Jenkins, R., Frost, C., Rossor, M.N., Fox, N.C., 2003. Change in rates of cerebral atrophy over time in early-onset Alzheimer's disease: longitudinal MRI study. Lancet 362, 1121-1122.

48. Chang, C.C., Lin, C.J., 2001. Training nu-support vector classifiers: Theory and algorithms. Neural Computation 13, 2119-2147.

49. Charles, R.F., Hillis, A.E., 2005. Posterior cortical atrophy: clinical presentation and cognitive deficits compared to Alzheimer's disease. Behavioural Neurology 16, 15-23.

50. Chumbley, J., Worsley, K., Flandin, G., Friston, K., 2010. Topological FDR for neuroimaging. Neuroimage 49, 3057-3064.

51. Chumbley, J.R., Friston, K.J., 2009. False discovery rate revisited: FDR and topological inference using Gaussian random fields. Neuroimage 44, 62-70.

52. Clark, K.A., Woods, R.P., Rottenberg, D.A., Toga, A.W., Mazziotta, J.C., 2006. Impact of acquisition protocols and processing streams on tissue segmentation of TI weighted MR images. Neuroimage 29, 185-202.

53. Clegg, F., Warrington, E.K., 1994. Four easy memory tests for older adults. Memory 2, 167-182.

54. Coffey, C.E., Wilkinson, W.E., Parashos, I.A., Soady, S.A., Sullivan, R.J., Patterson, L.J., Figiel, G.S., Webb, M.C., Spritzer, C.E., Djang, W.T., 1992. Quantitative cerebral anatomy of the aging human brain: a cross-sectional study using magnetic resonance imaging. Neurology 42, 527-536.

55. Cogan, D.G., 1985. Visual disturbances with focal progressive dementing disease. American Journal of Ophthalmology 100, 68-72.

56. Cohen, J., 1968. Weighted kappa - Nominal scale agreement with provision for scaled disagreement or partial credit. Psychological Bulletin 70, 213-220.

57. Cohen, M.L., Burtis, B., Kwon, J.C., Williamson, J., Heilman, K.M., 2010. Action-intentional spatial bias in a patient with Posterior Cortical Atrophy. Neurocase, 1-6.

58. Cosentino, S., Scarmeas, N., Helzner, E., Glymour, M.M., Brandt, J., Albert, M., Blacker, D., Stern, Y., 2008. APOE epsilon 4 allele predicts faster cognitive decline in mild Alzheimer disease. Neurology 70, 1842-1849.

59. Crutch, S.J., Warrington, E.K., 2007. Foveal crowding in posterior cortical atrophy: a specific early-visual-processing deficit affecting word reading. Cognitive Neuropsychology 24, 843-866.

60. Dale, A.M., Fischl, B., Sereno, M.I., 1999. Cortical surface-based analysis - I. Segmentation and surface reconstruction. Neuroimage 9, 179-194.

61. Davatzikos, C., Resnick, S.M., Wu, X., Parmpi, P., Clark, C.M., 2008. Individual patient diagnosis of AD and FTD via high-dimensional pattern classification of MRI. Neuroimage 41, 1220-1227.

62. De Renzi, E., 1986. Slowly progressive visual agnosia or apraxia without dementia. Cortex 22, 171-180.

63. de Souza, L.C., Lamari, F., Belliard, S., Jardel, C., Houillier, C., De, P.R., Dubois, B., Sarazin, M., 2011. Cerebrospinal fluid biomarkers in the differential diagnosis of

Alzheimer's disease from other cortical dementias. Journal of Neurology Neurosurgery and Psychiatry 82, 240-246.

64. DellaSala, S., Spinnler, H., Trivelli, C., 1996. Slowly progressive impairment of spatial exploration and visual perception. Neurocase 2, 299-323.

65. Desikan, R.S., Segonne, F., Fischl, B., Quinn, B.T., Dickerson, B.C., Blacker, D., Buckner, R.L., Dale, A.M., Maguire, R.P., Hyman, B.T., Albert, M.S., Killiany, R.J., 2006. An automated labeling system for subdividing the human cerebral cortex on MRI scans into gyral based regions of interest. Neuroimage 31, 968-980.

66. Devanand, D.P., Mikhno, A., Pelton, G.H., Cuasay, K., Pradhaban, G., Kumar, J.S.D., Upton, N., Lai, R., Gunn, R.N., Libri, V., Liu, X.H., van Heertum, R., Mann, J.J., Parsey, R.V., 2010. Pittsburgh Compound B (C-11-PIB) and Fluorodeoxyglucose (F-18-FDG) PET in patients with Alzheimer disease, mild cognitive impairment, and healthy controls. Journal of Geriatric Psychiatry and Neurology 23, 185-198.

67. Deyoe, E.A., Carman, G.J., Bandettini, P., Glickman, S., Wieser, J., Cox, R., Miller, D., Neitz, J., 1996. Mapping striate and extrastriate visual areas in human cerebral cortex. Proceedings of the National Academy of Sciences of the United States of America 93, 2382-2386.

68. Diehl-Schmid, J., Grimmer, T., Drzezga, A., Bornschein, S., Perneczky, R., Forstl, H., Schwaiger, M., Kurz, A., 2006. Longitudinal changes of cerebral glucose metabolism in semantic dementia. Dementia and Geriatric Cognitive Disorders 22, 346-351.

69. Drzezga, A., Grimmer, T., Henriksen, G., Stangier, I., Pemeczky, R., Diehl-Schmid, J., Mathis, C.A., Klunck, W.E., Price, J., DeKosky, S., Wester, H.J., Schwaiger, M., Kurz, A., 2008. Imaging of amyloid plaques and cerebral glucose metabolism in semantic dementia and Alzheimer's disease. Neuroimage 39, 619-633.

70. Du, A.T., Schuff, N., Amend, D., Laakso, M.P., Hsu, Y.Y., Jagust, W.J., Yaffe, K., Kramer, J.H., Reed, B., Norman, D., Chui, H.C., Weiner, M.W., 2001. Magnetic resonance imaging of the entorhinal cortex and hippocampus in mild cognitive impairment and Alzheimer's disease. Journal of Neurology Neurosurgery and Psychiatry 71, 441-447.

71. Du, A.T., Schuff, N., Kramer, J.H., Ganzer, S., Zhu, X.P., Jagust, W.J., Miller, B.L., Reed, B.R., Mungas, D., Yaffe, K., Chui, H.C., Weiner, M.W., 2004. Higher atrophy rate of entorhinal cortex than hippocampus in AD. Neurology 62, 422-427.

72. Du, A.T., Schuff, N., Kramer, J.H., Rosen, H.J., Gorno-Tempini, M.L., Rankin, K., Miller, B.L., Weiner, M.W., 2007. Different regional patterns of cortical thinning in Alzheimer's disease and frontotemporal dementia. Brain 130, 1159-1166.

73. Du, A.T., Schuff, N., Zhu, X.P., Jagust, W.J., Miller, B.L., Reed, B.R., Kramer, J.H., Mungas, D., Yaffe, K., Chui, H.C., Weiner, M.W., 2003. Atrophy rates of entorhinal cortex in AD and normal aging. Neurology 60, 481-486.

74. Duara, R., Loewenstein, D.A., Potter, E., Appel, J., Greig, M.T., Urs, R., Shen, Q., Raj, A., Small, B., Barker, W., Schofield, E., Wu, Y., Potter, H., 2008. Medial temporal lobe atrophy on MRI scans and the diagnosis of Alzheimer disease. Neurology 71, 1986-1992.

75. Dubois, B., Feldman, H.H., Jacova, C., Cummings, J.L., Dekosky, S.T., Barberger-Gateau, P., Delacourte, A., Frisoni, G., Fox, N.C., Galasko, D., Gauthier, S., Hampel, H., Jicha, G.A., Meguro, K., O'Brien, J., Pasquier, F., Robert, P., Rossor, M., Salloway, S., Sarazin, M., de Souza, L.C., Stern, Y., Visser, P.J., Scheltens, P., 2010. Revising the definition of Alzheimer's disease: a new lexicon. Lancet Neurology 9, 1118-1127.

76. Dubois, B., Feldman, H.H., Jacova, C., Dekosky, S.T., Barberger-Gateau, P., Cummings, J., Delocourte, A., Galasko, D., Gauthier, S., Jicha, G., Meguro, K., O'Brien, J., Pasquier, F., Robert, P., Rossor, M., Solloway, S., Stern, Y., Visser, P.J., Scheltens, P., 2007. Research criteria for the diagnosis of Alzheimer's disease: revising the NINCDS-ADRDA criteria. Lancet Neurology 6, 734-746.

77. Duning, T., Warnecke, T., Mohammadi, S., Lohmann, H., Schiffbauer, H., Kugel, H., Knecht, S., Ringelstein, E.B., Deppe, M., 2009. Pattern and progression of white-matter changes in a case of posterior cortical atrophy using diffusion tensor imaging. Journal of Neurology Neurosurgery and Psychiatry 80, 432-436.

78. Efron, R., 1968. What is perception? In: Cohen, R.S., Wartofsky, M.W. (Eds.), Boston Studies in the Philosophy of Science. D. Reidel, Dordrecht, The Netherlands, pp. 137-173.

79. Evans, J.J., Heggs, A.J., Antoun, N., Hodges, J.R., 1995. Progressive prosopagnosia associated with selective right temporal lobe atrophy - A new syndrome? Brain 118, 1-13.

80. Evans, M.C., Barnes, J., Nielsen, C., Kim, L.G., Clegg, S.L., Blair, M., Leung, K.K., Douiri, A., Boyes, R.G., Ourselin, S., Fox, N.C., 2010. Volume changes in Alzheimer's disease and mild cognitive impairment: cognitive associations. European Radiology 20, 674-682.

81. Farrer, L.A., Cupples, L.A., Haines, J.L., Hyman, B., Kukull, W.A., Mayeux, R., Myers, R.H., Pericakvance, M.A., Risch, N., vanDuijn, C.M., 1997. Effects of age, sex, and ethnicity on the association between apolipoprotein E genotype and Alzheimer disease - A meta-analysis. Journal of the American Medical Association 278, 1349-1356.

82. Fennema-Notestine, C., Mcevoy, L.K., Hagler, D.J., Jr., Jacobson, M.W., Dale, A.M., The Alzheimer's Disease Neuroimaging Initiative, 2009. Structural neuroimaging in the detection and prognosis of pre-clinical and early AD. Behavioural Neurology 21, 3-12.

83. Ferri, C.P., Prince, M., Brayne, C., Brodaty, H., Fratiglioni, L., Ganguli, M., Hall, K., Hasegawa, K., Hendrie, H., Huang, Y., Jorm, A., Mathers, C., Menezes, P.R., Rimmer, E., Scazufca, M., 2005. Global prevalence of dementia: a Delphi consensus study. Lancet 366, 2112-2117.

84. Fischl, B., Salat, D.H., Busa, E., Albert, M., Dieterich, M., Haselgrove, C., van der, K.A., Killiany, R., Kennedy, D., Klaveness, S., Montillo, A., Makris, N., Rosen, B., Dale, A.M., 2002. Whole brain segmentation: automated labeling of neuroanatomical structures in the human brain. Neuron 33, 341-355.

85. Fischl, B., Sereno, M.I., Dale, A.M., 1999. Cortical surface-based analysis - II: Inflation, flattening, and a surface-based coordinate system. Neuroimage 9, 195-207.

86. Fjell, A.M., Walhovd, K.B., Fennema-Notestine, C., Mcevoy, L.K., Hagler, D.J., Holland, D., Brewer, J.B., Dale, A.M., 2009. One-year brain atrophy evident in healthy aging. Journal of Neuroscience 29, 15223-15231.

87. Folstein, M.F., Folstein, S.E., Mchugh, P.R., 1975. Mini-mental state - Practical method for grading cognitive state of patients for clinician. Journal of Psychiatric Research 12, 189-198.

88. Foster, N.L., Heidebrink, J.L., Clark, C.M., Jagust, W.J., Arnold, S.E., Barbas, N.R., DeCarli, C.S., Turner, R.S., Koeppe, R.A., Higdon, R., Minoshima, S., 2007. FDG-PET improves accuracy in distinguishing frontotemporal dementia and Alzheimer's disease. Brain 130, 2616-2635.

89. Fox, N.C., Black, R.S., Gilman, S., Rossor, M.N., Griffith, S.G., Jenkins, L., Koller, M., 2005. Effects of Abeta immunization (AN1792) on MRI measures of cerebral volume in Alzheimer disease. Neurology 64, 1563-1572.

90. Fox, N.C., Freeborough, P.A., 1997. Brain atrophy progression measured from registered serial MRI: validation and application to Alzheimer's disease. Journal of Magnetic Resonance Imaging 7, 1069-1075.

91. Fox, N.C., Freeborough, P.A., Rossor, M.N., 1996a. Visualisation and quantification of rates of atrophy in Alzheimer's disease. Lancet 348, 94-97.

92. Fox, N.C., Scahill, R.I., Crum, W.R., Rossor, M.N., 1999. Correlation between rates of brain atrophy and cognitive decline in AD. Neurology 52, 1687-1689.

93. Fox, N.C., Schott, J.M., 2004. Imaging cerebral atrophy: normal ageing to Alzheimer's disease. Lancet 363, 392-394.

94. Fox, N.C., Warrington, E.K., Stevens, J.M., Rossor, M.N., 1996b. Atrophy of the hippocampal formation in early familial Alzheimer's disease. A longitudinal MRI study of at-risk members of a family with an amyloid precursor protein 717Val-Gly mutation. Annals of the New York Academy of Sciences 777, 226-232.

95. Freeborough, P.A., Fox, N.C., 1997. The boundary shift integral: An accurate and robust measure of cerebral volume changes from registered repeat MRI. Ieee Transactions on Medical Imaging 16, 623-629.

96. Freeborough, P.A., Fox, N.C., 1998. Modeling brain deformations in Alzheimer disease by fluid registration of serial 3D MR images. Journal of Computer Assisted Tomography 22, 838-843.

97. Freeborough, P.A., Fox, N.C., Kitney, R.I., 1996. Accurate segmentation of 3D brain scans: Interactive software and algorithms. In: Raby, R., Vicars, D. (Eds.), Proceedings of the Eurographics 14th Annual Conference (UK Chapter), pp. 261-270.

98. Freeborough, P.A., Fox, N.C., Kitney, R.I., 1997. Interactive algorithms for the segmentation and quantitation of 3-D MRI brain scans. Computer Methods and Programs in Biomedicine 53, 15-25.

99. Freedman, L., Selchen, D.H., Black, S.E., Kaplan, R., Garnett, E.S., Nahmias, C., 1991. Posterior cortical dementia with alexia: neurobehavioural, MRI, and PET findings. Journal of Neurology Neurosurgery and Psychiatry 54, 443-448.

100. Frisoni, G.B., Beltramello, A., Geroldi, C., Weiss, C., Bianchetti, A., Trabucchi, M., 1996. Brain atrophy in frontotemporal dementia. Journal of Neurology Neurosurgery and Psychiatry 61, 157-165.

101. Frisoni, G.B., Pievani, M., Testa, C., Sabattoli, F., Bresciani, L., Bonetti, M., Beltramello, A., Hayashi, K.M., Toga, A.W., Thompson, P.M., 2007. The topography of grey matter involvement in early and late onset Alzheimer's disease. Brain 130, 720-730.

102. Frost, C., Kenward, M.G., Fox, N.C., 2004. The analysis of repeated 'direct' measures of change illustrated with an application in longitudinal imaging. Statistics in Medicine 23, 3275-3286.

103. Galton, C.J., Patterson, K., Graham, K., Lambon-Ralph, M.A., Williams, G., Antoun, N., Sahakian, B.J., Hodges, J.R., 2001. Differing patterns of temporal atrophy in Alzheimer's disease and semantic dementia. Neurology 57, 216-225.

104. Galton, C.J., Patterson, K., Xuereb, J.H., Hodges, J.R., 2000. Atypical and typical presentations of Alzheimer's disease: a clinical, neuropsychological, neuroimaging and pathological study of 13 cases. Brain 123, 484-498.

105. Gee, J., Ding, L.J., Xie, Z.Y., Lin, M., DeVita, C., Grossman, M., 2003. Alzheimer's disease and frontotemporal dementia exhibit distinct atrophy-behavior correlates: A computer-assisted imaging study. Academic Radiology 10, 1392-1401.

106. Genovese, C.R., Lazar, N.A., Nichols, T., 2002. Thresholding of statistical maps in functional neuroimaging using the false discovery rate. Neuroimage 15, 870-878.

107. Goethals, M., Santens, P., 2001. Posterior cortical atrophy. Two case reports and a review of the literature. Clinical Neurology and Neurosurgery 103, 115-119.

108. Good, C.D., Johnsrude, I.S., Ashburner, J., Henson, R.N.A., Friston, K.J., Frackowiak, R.S.J., 2001. A voxel-based morphometric study of ageing in 465 normal adult human brains. Neuroimage 14, 21-36.

109. Good, C.D., Scahill, R.I., Fox, N.C., Ashburner, J., Friston, K.J., Chan, D., Crum, W.R., Rossor, M.N., Frackowiak, R.S.J., 2002. Automatic differentiation of anatomical patterns in the human brain: validation with studies of degenerative dementias. Neuroimage 17, 29-46.

110. Goodale, M.A., Milner, A.D., 1992. Separate visual pathways for perception and action. Trends in Neurosciences 15, 20-25.

111. Gordon, E., Rohrer, J.D., Kim, L.G., Omar, R., Rossor, M.N., Fox, N.C., Warren, J.D., 2010. Measuring disease progression in frontotemporal lobar degeneration: a clinical and MRI study. Neurology 74, 666-673.

112. Gorno-Tempini, M.L., Brambati, S.M., Ginex, V., Ogar, J., Dronkers, N.F., Marcone, A., Perani, D., Garibotto, V., Cappa, S.F., Miller, B.L., 2008. The logopenic/phonological variant of primary progressive aphasia. Neurology 71, 1227-1234.

113. Gorno-Tempini, M.L., Dronkers, N.F., Rankin, K.P., Ogar, J.M., Phengrasamy, L., Rosen, H.J., Johnson, J.K., Weiner, M.W., Miller, B.L., 2004. Cognition and anatomy in three variants of primary progressive aphasia. Annals of Neurology 55, 335-346.

114. Grady, C.L., Springer, M.V., Hongwanishkul, D., McIntosh, A.R., Winocur, G., 2006. Age-related changes in brain activity across the adult lifespan. Journal of Cognitive Neuroscience 18, 227-241.

115. Greicius, M.D., Krasnow, B., Reiss, A.L., Menon, V., 2003. Functional connectivity in the resting brain: A network analysis of the default mode hypothesis. Proceedings of the National Academy of Sciences of the United States of America 100, 253-258.

116. Greicius, M.D., Srivastava, G., Reiss, A.L., Menon, V., 2004. Default-mode network activity distinguishes Alzheimer's disease from healthy aging: evidence from functional MRI. Proceedings of the National Academy of Sciences of the United States of America 101, 4637-4642.

117. Grossman, M., McMillan, C., Moore, P., Ding, L.J., Glosser, G., Work, M., Gee, J., 2004. What's in a name: voxel-based morphometric analyses of MRI and naming difficulty in Alzheimer's disease, frontotemporal dementia and corticobasal degeneration. Brain 127, 628-649.

118. Gutierrez-Galve, L., Lehmann, M., Hobbs, N.Z., Clarkson, M.J., Ridgway, G.R., Crutch, S., Ourselin, S., Schott, J.M., Fox, N.C., Barnes, J., 2009. Patterns of cortical thickness according to APOE genotype in Alzheimer's disease. Dementia and Geriatric Cognitive Disorders 28, 476-485.

119. Hammers, A., Allom, R., Koepp, M.J., Free, S.L., Myers, R., Lemieux, L., Mitchell, T.N., Brooks, D.J., Duncan, J.S., 2003. Three-dimensional maximum probability atlas of the human brain, with particular reference to the temporal lobe. Human Brain Mapping 19, 224-247.

120. Han, X., Jovicich, J., Salat, D., van der Kouwe, A., Quinn, B., Czanner, S., Busa, E., Pacheco, J., Albert, M., Killiany, R., Maguire, P., Rosas, D., Makris, N., Dale, A., Dickerson, B., Fischl, B., 2006. Reliability of MRI-derived measurements of human cerebral cortical thickness: The effects of field strength, scanner upgrade and manufacturer. Neuroimage 32, 180-194.

121. Harvey, R.J., Skelton-Robinson, M., Rossor, M.N., 2003. The prevalence and causes of dementia in people under the age of 65 years. Journal of Neurology Neurosurgery and Psychiatry 74, 1206-1209.

122. Hashimoto, M., Kazui, H., Matsumoto, K., Nakano, Y., Yasuda, M., Mori, E., 2005. Does donepezil treatment slow the progression of hippocampal atrophy in patients with Alzheimer's disease? American Journal of Psychiatry 162, 676-682.

123. Hashimoto, M., Yasuda, M., Tanimukai, S., Matsui, M., Hirono, N., Kazui, H., Mori, E., 2001. Apolipoprotein E epsilon 4 and the pattern of regional brain atrophy in Alzheimer's disease. Neurology 57, 1461-1466.

124. Hebert, L.E., Scherr, P.A., Bienias, J.L., Bennett, D.A., Evans, D.A., 2003. Alzheimer disease in the US population - Prevalence estimates using the 2000 census. Archives of Neurology 60, 1119-1122.

125. Henley, S.M.D., Frost, C., MacManus, D.G., Warner, T.T., Fox, N.C., Tabrizi, S.J., 2006. Increased rate of whole-brain atrophy over 6 months in early Huntington disease. Neurology 67, 694-696.

126. Hodges, J.R., Davies, R.R., Xuereb, J.H., Casey, B., Broe, M., Bak, T.H., Kril, J.J., Halliday, G.M., 2004. Clinicopathological correlates in frontotemporal dementia. Annals of Neurology 56, 399-406.

127. Hodges, J.R., Patterson, K., 2007. Semantic dementia: a unique clinicopathological syndrome. Lancet Neurology 6, 1004-1014.

128. Hof, P.R., Archin, N., Osmand, A.P., Dougherty, J.H., Wells, C., Bouras, C., Morrison, J.H., 1993. Posterior cortical atrophy in Alzheimer's disease - Analysis of a new case and reevaluation of a historical report. Acta Neuropathologica 86, 215-223.

129. Hof, P.R., Bouras, C., Constantinidis, J., Morrison, J.H., 1989. Balint's syndrome in Alzheimer's disease: specific disruption of the occipito-parietal visual pathway. Brain Research 493, 368-375.

130. Hof, P.R., Bouras, C., Constantinidis, J., Morrison, J.H., 1990. Selective disconnection of specific visual association pathways in cases of Alzheimer's disease presenting with Balint's syndrome. Journal of Neuropathology and Experimental Neurology 49, 168-184.

131. Hof, P.R., Vogt, B.A., Bouras, C., Morrison, J.H., 1997. Atypical form of Alzheimer's disease with prominent posterior cortical atrophy: a review of lesion distribution and circuit disconnection in cortical visual pathways. Vision Research 37, 3609-3625.

132. Holm, I.E., Isaacs, A.M., Mackenzie, I.R.A., 2009. Absence of FUS-immunoreactive pathology in frontotemporal dementia linked to chromosome 3 (FTD-3) caused by mutation in the CHMP2B gene. Acta Neuropathologica 118, 719-720.

133. Hort, J., O'Brien, J.T., Gainotti, G., Pirttila, T., Popescu, B.O., Rektorova, I., Sorbi, S., Scheltens, P., 2010. EFNS guidelines for the diagnosis and management of Alzheimer's disease. European Journal of Neurology 17, 1236-1248.

134. Ikonomovic, M.D., Klunk, W.E., Abrahamson, E.E., Mathis, C.A., Price, J.C., Tsopelas, N.D., Lopresti, B.J., Ziolko, S., Bi, W.Z., Paljug, W.R., Debnath, M.L., Hope, C.E., Isanski, B.A., Hamilton, R.L., Dekosky, S.T., 2008. Post-mortem correlates of in vivo PiB-PET amyloid imaging in a typical case of Alzheimer's disease. Brain 131, 1630-1645.

135. Insausti, R., Juottonen, K., Soininen, H., Insausti, A.M., Partanen, K., Vainio, P., Laakso, M.P., Pitkanen, A., 1998. MR volumetric analysis of the human entorhinal, perirhinal, and temporopolar cortices. American Journal of Neuroradiology 19, 659-671.

136. Ishii, K., Kawachi, T., Sasaki, H., Kono, A.K., Fukuda, T., Kojima, Y., Mori, E., 2005a. Voxel-based morphometric comparison between early- and late-onset mild Alzheimer's disease and assessment of diagnostic performance of Z score images. American Journal of Neuroradiology 26, 333-340.

137. Ishii, K., Sasaki, H., Kono, A.K., Miyamoto, N., Fukuda, T., Mori, E., 2005b. Comparison of gray matter and metabolic reduction in mild Alzheimer's disease using FDG-PET and voxel-based morphometric MR studies. European Journal of Nuclear Medicine and Molecular Imaging 32, 959-963.

138. Jack, C.R., Jr., 1994. MRI-based hippocampal volume measurements in epilepsy. Epilepsia 35 Suppl 6, S21-S29.

139. Jack, C.R., Jr., Petersen, R.C., O'Brien, P.C., Tangalos, E.G., 1992. MR-based hippocampal volumetry in the diagnosis of Alzheimer's disease. Neurology 42, 183-188.

140. Jack, C.R., Jr., Petersen, R.C., Xu, Y., O'Brien, P.C., Smith, G.E., Ivnik, R.J., Boeve, B.F., Tangalos, E.G., Kokmen, E., 2000. Rates of hippocampal atrophy correlate with change in clinical status in aging and AD. Neurology 55, 484-489.

141. Jack, C.R., Jr., Petersen, R.C., Xu, Y., O'Brien, P.C., Smith, G.E., Ivnik, R.J., Tangalos, E.G., Kokmen, E., 1998. Rate of medial temporal lobe atrophy in typical aging and Alzheimer's disease. Neurology 51, 993-999.

142. Jack, C.R., Petersen, R.C., Xu, Y.C., O'Brien, P.C., Smith, G.E., Ivnik, R.J., Boeve, B.F., Waring, S.C., Tangalos, E.G., Kokmen, E., 1999. Prediction of AD with MRI-based hippocampal volume in mild cognitive impairment. Neurology 52, 1397-1403.

143. Jack, C.R., Jr., Petersen, R.C., Xu, Y.C., Waring, S.C., O'Brien, P.C., Tangalos, E.G., Smith, G.E., Ivnik, R.J., Kokmen, E., 1997. Medial temporal atrophy on MRI in normal aging and very mild Alzheimer's disease. Neurology 49, 786-794.

144. Jack, C.R., Jr., Shiung, M.M., Gunter, J.L., O'Brien, P.C., Weigand, S.D., Knopman, D.S., Boeve, B.F., Ivnik, R.J., Smith, G.E., Cha, R.H., Tangalos, E.G., Petersen, R.C., 2004. Comparison of different MRI brain atrophy rate measures with clinical disease progression in AD. Neurology 62, 591-600.

145. Jack, C.R., Jr., Shiung, M.M., Weigand, S.D., O'Brien, P.C., Gunter, J.L., Boeve, B.F., Knopman, D.S., Smith, G.E., Ivnik, R.J., Tangalos, E.G., Petersen, R.C., 2005. Brain atrophy rates predict subsequent clinical conversion in normal elderly and amnestic MCI. Neurology 65, 1227-1231.

146. Jackson, M., Warrington, E.K., 1986. Arithmetic skills in patients with unilateral cerebral lesions. Cortex 22, 611-620.

147. James, M., Plant, G.T., Warrington, E.K., 2001. Cortical vision screening test. Manual. Thames Valley Test Company Limited, Bury St. Edmunds, England.

148. Janes, H., Longton, G., Pepe, M.S., 2009. Accommodating covariates in receiver operating characteristic analysis. Stata Journal 9, 17-39.

149. Jellinger, K.A., 2006. Clinicopathological analysis of dementia disorders in the elderly - an update. Journal of Alzheimer's disease 9, 61-70.

150. Jellinger, K.A., Attems, J., 2005. Prevalence and pathogenic role of cerebrovascular lesions in Alzheimer disease. Journal of Neurological Sciences 229-230, 37-41.

151. Jellinger, K.A., Attems, J., 2008. Prevalence and impact of vascular and Alzheimer pathologies in Lewy body disease. Acta Neuropathologica 115, 427-436.

152. Johnson, J.K., Head, E., Kim, R., Starr, A., Cotman, C.W., 1999. Clinical and pathological evidence for a frontal variant of Alzheimer disease. Archives of Neurology 56, 1233-1239.

153. Johnson, K.A., Jones, K., Holman, B.L., Becker, J.A., Spiers, P.A., Satlin, A., Albert, M.S., 1998. Preclinical prediction of Alzheimer's disease using SPECT. Neurology 50, 1563-1571.

154. Jones, B.F., Barnes, J., Uylings, H.B.M., Fox, N.C., Frost, C., Witter, M.P., Scheftens, P., 2006. Differential regional atrophy of the cingulate gyrus in Alzheimer disease: A volumetric MRI study. Cerebral Cortex 16, 1701-1708.

155. Jorm, A.F., Jolley, D., 1998. The incidence of dementia: a meta-analysis. Neurology 51, 728-733.

156. Josephs, K.A., Whitwell, J.L., Parisi, J.E., Petersen, R.C., Boeve, B.F., Jack, C.R., Dickson, D.W., 2010. Caudate atrophy on MRI is a characteristic feature of FTLD-FUS. European Journal of Neurology 17, 969-975.

157. Juottonen, K., Laakso, M.P., Insausti, R., Lehtovirta, M., Pitkanen, A., Partanen, K., Soininen, H., 1998. Volumes of the entorhinal and perirhinal cortices in Alzheimer's disease. Neurobiology of Aging 19, 15-22.

158. Juottonen, K., Laakso, M.P., Partanen, K., Soininen, H., 1999. Comparative MR analysis of the entorhinal cortex and hippocampus in diagnosing Alzheimer disease. American Journal of Neuroradiology 20, 139-144.

159. Kambe, T., Motoi, Y., Ishii, K., Hattori, N., 2010. Posterior cortical atrophy with [C-11] Pittsburgh compound B accumulation in the primary visual cortex. Journal of Neurology 257, 469-471.

160. Karas, G., Scheltens, P., Rombouts, S., van Schijndel, R., Klein, M., Jones, B., van der Flier, W., Vrenken, H., Barkhof, F., 2007. Precuneus atrophy in early-onset Alzheimer's disease: A morphometric structural MRI study. Neuroradiology 49, 967-976.

161. Karas, G.B., Scheltens, P., Rombouts, S.A.R.B., Visser, P.J., van Schijndel, R.A., Fox, N.C., Barkhof, F., 2004. Global and local gray matter loss in mild cognitive impairment and Alzheimer's disease. Neuroimage 23, 708-716.

162. Kemppainen, N.M., Aalto, S., Wilson, I.A., Nagren, K., Helin, S., Bruck, A., Oikonen, V., Kailajarvi, M., Scheinin, M., Viitanen, M., Parkkola, R., Rinne, J.O., 2007. PET amyloid ligand [C-11]PIB uptake is increased in mild cognitive impairment. Neurology 68, 1603-1606.

163. Kennedy, J., Lehmann, M., Sokolska, M.J., Archer, H., Warrington, E.K., Fox, N.C., Crutch, S.J., 2011. Visualising the emergence of posterior cortical atrophy. Neurocase in press.

164. Killiany, R.J., Gomez-Isla, T., Moss, M., Kikinis, R., Sandor, T., Jolesz, F., Tanzi, R., Jones, K., Hyman, B.T., Albert, M.S., 2000. Use of structural magnetic resonance

imaging to predict who will get Alzheimer's disease. Annals of Neurology 47, 430-439.

165. Killiany, R.J., Moss, M.B., Albert, M.S., Sandor, T., Tieman, J., Jolesz, F., 1993. Temporal lobe regions on magnetic resonance imaging identify patients with early Alzheimer's disease. Archives of Neurology 50, 949-954.

166. Kitagaki, H., Mori, E., Yamaji, S., Ishii, K., Hirono, N., Kobashi, S., Hata, Y., 1998. Frontotemporal dementia and Alzheimer disease: Evaluation of cortical atrophy with automated hemispheric surface display generated with MR images. Radiology 208, 431-439.

167. Klauschen, F., Goldman, A., Barra, V., Meyer-Lindenberg, A., Lundervold, A., 2009. Evaluation of automated brain MR image segmentation and volumetry methods. Human Brain Mapping 30, 1310-1327.

168. Kloppel, S., Stonnington, C.M., Chu, C., Draganski, B., Scahill, R.I., Rohrer, J.D., Fox, N.C., Jack, C.R., Jr., Ashburner, J., Frackowiak, R.S., 2008. Automatic classification of MR scans in Alzheimer's disease. Brain 131, 681-689.

169. Klunk, W.E., Engler, H., Nordberg, A., Wang, Y.M., Blomqvist, G., Holt, D.P., Bergstrom, M., Savitcheva, I., Huang, G.F., Estrada, S., Ausen, B., Debnath, M.L., Barletta, J., Price, J.C., Sandell, J., Lopresti, B.J., Wall, A., Koivisto, P., Antoni, G., Mathis, C.A., Langstrom, B., 2004. Imaging brain amyloid in Alzheimer's disease with Pittsburgh Compound-B. Annals of Neurology 55, 306-319.

170. Knibb, J.A., Woollams, A.M., Hodges, J.R., Patterson, K., 2009. Making sense of progressive non-fluent aphasia: an analysis of conversational speech. Brain 132, 2734-2746.

171. Knibb, J.A., Xuereb, J.H., Patterson, K., Hodges, J.R., 2006. Clinical and pathological characterization of progressive aphasia. Annals of Neurology 59, 156-165.

172. Knight, W.D., Okello, A.A., Ryan, N.S., Turkheimer, F.E., de Llano, S.R.M., Edison, P., Douglas, J., Fox, N.C., Brooks, D.J., Rossor, M.N., 2011. Carbon-11-Pittsburgh compound B positron emission tomography imaging of amyloid deposition in presenilin 1 mutation carriers. Brain 134, 293-300.

173. Knopman, D.S., Dekosky, S.T., Cummings, J.L., Chui, H., Corey-Bloom, J., Relkin, N., Small, G.W., Miller, B., Stevens, J.C., 2001. Practice parameter: diagnosis of dementia (an evidence-based review). Report of the Quality Standards Subcommittee of the American Academy of Neurology. Neurology 56, 1143-1153.

174. Knopman, D.S., Jack, C.R., Jr., Kramer, J.H., Boeve, B.F., Caselli, R.J., Graff-Radford, N.R., Mendez, M.F., Miller, B.L., Mercaldo, N.D., 2009. Brain and ventricular volumetric changes in frontotemporal lobar degeneration over 1 year. Neurology 72, 1843-1849.

175. Korf, E.S.C., Wahlund, L.O., Visser, P.J., Scheltens, P., 2004. Medial temporal lobe atrophy on MRI predicts dementia in patients with mild cognitive impairment. Neurology 63, 94-100.

176. Laakso, M.P., Frisoni, G.B., Kononen, M., Mikkonen, M., Beltramello, A., Geroldi, C., Bianchetti, A., Trabucchi, M., Soininen, H., Aronen, H.J., 2000. Hippocampus and entorhinal cortex in frontotemporal dementia and Alzheimer's disease: A morphometric MRI study. Biological Psychiatry 47, 1056-1063.

177. Lehericy, S., Baulac, M., Chiras, J., Pierot, L., Martin, N., Pillon, B., Deweer, B., Dubois, B., Marsault, C., 1994. Amygdalohippocampal MR volume measurements in the early stages of Alzheimer disease. American Journal of Neuroradiology 15, 929-937.

178. Lehmann, M., Douiri, A., Kim, L.G., Modat, M., Chan, D., Ourselin, S., Barnes, J., Fox, N.C., 2010. Atrophy patterns in Alzheimer's disease and semantic dementia: a comparison of FreeSurfer and manual volumetric measurements. Neuroimage 49, 2264-2274.

179. Lerch, J.P., Pruessner, J., Zijdenbos, A.P., Collins, D.L., Teipel, S.J., Hampel, H., Evans, A.C., 2008. Automated cortical thickness measurements from MRI can accurately separate Alzheimer's patients from normal elderly controls. Neurobiology of Aging 29, 23-30.

180. Lerch, J.P., Pruessner, J.C., Zijdenbos, A., Hampel, H., Teipel, S.J., Evans, A.C., 2005. Focal decline of cortical thickness in Alzheimer's disease identified by computational neuroanatomy. Cerebral Cortex 15, 995-1001.

181. Leung, K.K., Clarkson, M.J., Bartlett, J.W., Clegg, S., Jack, C.R., Weiner, M.W., Fox, N.C., Ourselin, S., 2010. Robust atrophy rate measurement in Alzheimer's disease using multi-site serial MRI: Tissue-specific intensity normalization and parameter selection. Neuroimage 50, 516-523.

182. Levine, D.N., Lee, J.M., Fisher, C.M., 1993. The visual variant of Alzheimer's disease: a clinicopathologic case study. Neurology 43, 305-313.

183. Lewis, E.B., Fox, N.C., 2004. Correction of differential intensity inhomogeneity in longitudinal MR images. Neuroimage 23, 75-83.

184. Likeman, M., Anderson, V.M., Stevens, J.M., Waldman, A.D., Godbolt, A.K., Frost, C., Rossor, M.N., Fox, N.C., 2005. Visual assessment of atrophy on magnetic resonance imaging in the diagnosis of pathologically confirmed young-onset dementias. Archives of Neurology 62, 1410-1415.

185. Lustig, C., Snyder, A.Z., Bhakta, M., O'Brien, K.C., McAvoy, M., Raichle, M.E., Morris, J.C., Buckner, R.L., 2003. Functional deactivations: change with age and dementia of the Alzheimer type. Proceedings of the National Academy of Sciences of the United States of America 100, 14504-14509.

186. MacDonald, D., Kabani, N., Avis, D., Evans, A.C., 2000. Automated 3-D extraction of inner and outer surfaces of cerebral cortex from MRI. Neuroimage 12, 340-356.

187. Mackenzie, I.R.A., Baborie, A., Pickering-Brown, S., Du Plessis, D., Jaros, E., Perry, R.H., Neary, D., Snowden, J.S., Mann, D.M.A., 2006. Heterogeneity of ubiquitin pathology in frontotemporal lobar degeneration: classification and relation to clinical phenotype. Acta Neuropathologica 112, 539-549.

188. Mackenzie, I.R.A., Neumann, M., Bigio, E.H., Cairns, N.J., Alafuzoff, I., Kril, J., Kovacs, G.G., Ghetti, B., Halliday, G., Holm, I.E., Ince, P.G., Kamphorst, W., Revesz, T., Rozemuller, A.J.M., Kumar-Singh, S., Akiyama, H., Baborie, A., Spina, S., Dickson, D.W., Trojanowski, J.Q., Mann, D.M.A., 2010. Nomenclature and nosology for neuropathologic subtypes of frontotemporal lobar degeneration: an update. Acta Neuropathologica 119, 1-4.

189. Marra, C., Bizzarro, A., Daniele, A., De Luca, L., Ferraccioli, M., Valenza, A., Brahe, C., Tiziano, F.D., Gainotti, G., Masullo, C., 2004. Apolipoprotein E epsilon 4 allele differently affects the patterns of neuropsychological presentation in early- and late-onset Alzheimer's disease patients. Dementia and Geriatric Cognitive Disorders 18, 125-131.

190. Matsuda, H., 2001. Cerebral blood flow and metabolic abnormalities in Alzheimer's disease. Annals of Nuclear Medicine 15, 85-92.

191. Mazziotta, J.C., Toga, A.W., Evans, A., Fox, P., Lancaster, J., 1995. A probabilistic atlas of the human brain - Theory and rationale for its development. Neuroimage 2, 89-101.

192. McKeith, I.G., Galasko, D., Kosaka, K., Perry, E.K., Dickson, D.W., Hansen, L.A., Salmon, D.P., Lowe, J., Mirra, S.S., Byrne, E.J., Lennox, G., Quinn, N.P., Edwardson, J.A., Ince, P.G., Bergeron, C., Burns, A., Miller, B.L., Lovestone, S., Collerton, D., Jansen, E.N.H., Ballard, C., Devos, R.A.I., Wilcock, G.K., Jellinger, K.A., Perry, R.H., 1996. Consensus guidelines for the clinical and pathologic diagnosis of dementia with

Lewy bodies (DLB): Report of the consortium on DLB international workshop. Neurology 47, 1113-1124.

193. McKhann, G., Drachman, D., Folstein, M., Katzman, R., Price, D., Stadlan, E.M., 1984. Clinical diagnosis of Alzheimer's disease: report of the NINCDS-ADRDA Work Group under the auspices of Department of Health and Human Services Task Force on Alzheimer's Disease. Neurology 34, 939-944.

194. McMonagle, P., Deering, F., Berliner, Y., Kertesz, A., 2006. The cognitive profile of posterior cortical atrophy. Neurology 66, 331-338.

195. Mendez, M.F., Ghajarania, M., Perryman, K.M., 2002. Posterior cortical atrophy: Clinical characteristics and differences compared to Alzheimer's disease. Dementia and Geriatric Cognitive Disorders 14, 33-40.

196. Mesulam, M.M., 2001. Primary progressive aphasia. Annals of Neurology 49, 425-432.

197. Meyer, M.R., Tschanz, J.T., Norton, M.C., Welsh-Bohmer, K.A., Steffens, D.C., Wyse, B.W., Breitner, J.C., 1998. APOE genotype predicts when--not whether--one is predisposed to develop Alzheimer disease. Nature Genetics 19, 321-322.

198. Migliaccio, R., Agosta, F., Rascovsky, K., Karydas, A., Bonasera, S., Rabinovici, G.D., Miller, B.L., Gorno-Tempini, M.L., 2009. Clinical syndromes associated with posterior atrophy early age at onset AD spectrum. Neurology 73, 1571-1578.

199. Miller, S.L., Celone, K., DePeau, K., Diamond, E., Dickerson, B.C., Rentz, D., Pihlajamaki, M., Sperling, R.A., 2008. Age-related memory impairment associated with loss of parietal deactivation but preserved hippocampal activation. Proceedings of the National Academy of Sciences of the United States of America 105, 2181-2186.

200. Minoshima, S., Giordani, B., Berent, S., Frey, K.A., Foster, N.L., Kuhl, D.E., 1997. Metabolic reduction in the posterior cingulate cortex in very early Alzheimer's disease. Annals of Neurology 42, 85-94.

201. Morey, R.A., Petty, C.M., Xu, Y., Hayes, J.P., Wagner, H.R., Lewis, D.V., Labar, K.S., Styner, M., McCarthy, G., 2009. A comparison of automated segmentation and manual tracing for quantifying hippocampal and amygdala volumes. Neuroimage 45, 855-866.

202. Mosconi, L., 2005. Brain glucose metabolism in the early and specific diagnosis of Alzheimer's disease. FDG-PET studies in MCI and AD. European Journal of Nuclear Medicine and Molecular Imaging 32, 486-510.

203. Mungas, D., Harvey, D., Reed, B.R., Jagust, W.J., DeCarli, C., Beckett, L., Mack, W.J., Kramer, J.H., Weiner, M.W., Schuff, N., Chui, H.C., 2005. Longitudinal volumetric MRI change and rate of cognitive decline. Neurology 65, 565-571.

204. Neary, D., Snowden, J., 1996. Fronto-temporal dementia: Nosology, neuropsychology, and neuropathology. Brain and Cognition 31, 176-187.

205. Neary, D., Snowden, J.S., Gustafson, L., Passant, U., Stuss, D., Black, S., Freedman, M., Kertesz, A., Robert, P.H., Albert, M., Boone, K., Miller, B.L., Cummings, J., Benson, D.F., 1998. Frontotemporal lobar degeneration - A consensus on clinical diagnostic criteria. Neurology 51, 1546-1554.

206. Nestor, P.J., Caine, D., Fryer, T.D., Clarke, J., Hodges, J.R., 2003. The topography of metabolic deficits in posterior cortical atrophy (the visual variant of Alzheimer's disease) with FDG-PET. Journal of Neurology Neurosurgery and Psychiatry 74, 1521-1529.

207. Neumann, M., Rademakers, R., Roeber, S., Baker, M., Kretzschmar, H.A., Mackenzie, I.R.A., 2009a. A new subtype of frontotemporal lobar degeneration with FUS pathology. Brain 132, 2922-2931.

208. Neumann, M., Roeber, S., Kretzschmar, H.A., Rademakers, R., Baker, M., Mackenzie, I.R.A., 2009b. Abundant FUS-immunoreactive pathology in neuronal intermediate filament inclusion disease. Acta Neuropathologica 118, 605-616.

209. Neumann, M., Sampathu, D.M., Kwong, L.K., Truax, A.C., Micsenyi, M.C., Chou, T.T., Bruce, J., Schuck, T., Grossman, M., Clark, C.M., McCluskey, L.F., Miller, B.L., Masliah, E., Mackenzie, I.R., Feldman, H., Feiden, W., Kretzschmar, H.A., Trojanowski, J.Q., Lee, V.M.Y., 2006. Ubiquitinated TDP-43 in frontotemporal lobar degeneration and amyotrophic lateral sclerosis. Science 314, 130-133.

210. Ng, S.Y., Villemagne, V.L., Masters, C.L., Rowe, C.C., 2007. Evaluating atypical dementia syndromes using positron emission tomography with carbon 11 labeled Pittsburgh Compound B. Archives of Neurology 64, 1140-1144.

211. O'Brien, J.T., Paling, S., Barber, R., Williams, E.D., Ballard, C., McKeith, I.G., Gholkar, A., Crum, W.R., Rossor, M.N., Fox, N.C., 2001. Progressive brain atrophy on serial MRI in dementia with Lewy bodies, AD, and vascular dementia. Neurology 56, 1386-1388.

212. Okuizumi, K., Onodera, O., Tanaka, H., Kobayashi, H., Tsuji, S., Takahashi, H., Oyanagi, K., Seki, K., Tanaka, M., Naruse, S., 1994. ApoE-epsilon 4 and early-onset Alzheimer's. Nature Genetics 7, 10-11.

213. Otten, L.J., Rugg, M.D., 2001. When more means less: neural activity related to unsuccessful memory encoding. Current Biology 11, 1528-1530.

214. Palop, J.J., Chin, J., Mucke, L., 2006. A network dysfunction perspective on neurodegenerative diseases. Nature 443, 768-773.

215. Pantel, J., O'Leary, D.S., Cretsinger, K., Bockholt, H.J., Keefe, H., Magnotta, V.A., Andreasen, N.C., 2000. A new method for the in vivo volumetric measurement of the human hippocampus with high neuroanatomical accuracy. Hippocampus 10, 752-758.

216. Paviour, D.C., Price, S.L., Jahanshahi, M., Lees, A.J., Fox, N.C., 2006. Longitudinal MRI in progressive supranuclear palsy and multiple system atrophy: rates and regions of atrophy. Brain 129, 1040-1049.

217. Pellerin, L., Magistretti, P.J., 1994. Glutamate uptake into astrocytes stimulates aerobic glycolysis: a mechanism coupling neuronal activity to glucose utilization. Proceedings of the National Academy of Sciences of the United States of America 91, 10625-10629.

218. Pendleton, N., Payton, A., van den Boogerd, E.H., Holland, F., Diggle, P., Rabbitt, P.M.A., Horan, M.A., Worthington, J., Ollier, W.E.R., 2002. Apolipoprotein E genotype does not predict decline in intelligence in healthy older adults. Neuroscience Letters 324, 74-76.

219. Pfefferbaum, A., Mathalon, D.H., Sullivan, E.V., Rawles, J.M., Zipursky, R.B., Lim, K.O., 1994. A quantitative magnetic resonance imaging study of changes in brain morphology from infancy to late adulthood. Archives of Neurology 51, 874-887.

220. Pietrini, P., Furey, M.L., GraffRadford, N., Freo, U., Alexander, G.E., Grady, C.L., Dani, A., Mentis, M.J., Schapiro, M.B., 1996. Preferential metabolic involvement of visual cortical areas in a subtype of Alzheimer's disease: Clinical implications. American Journal of Psychiatry 153, 1261-1268.

221. Pihlajamaki, M., Depeau, K.M., Blacker, D., Sperling, R.A., 2008. Impaired medial temporal repetition suppression is related to failure of parietal deactivation in Alzheimer disease. American Journal of Geriatric Psychiatry 16, 283-292.

222. Pruessner, J.C., Li, L.M., Serles, W., Pruessner, M., Collins, D.L., Kabani, N., Lupien, S., Evans, A.C., 2000. Volumetry of hippocampus and amygdala with high-resolution MRI and three-dimensional analysis software: minimizing the discrepancies between laboratories. Cerebral Cortex 10, 433-442.

223. Rabinovici, G.D., Furst, A.J., O'Neil, J.P., Racine, C.A., Mormino, E.C., Baker, S.L., Chetty, S., Patel, P., Pagliaro, T.A., Klunk, W.E., Mathis, C.A., Rosen, H.J., Miller, B.L., Jagust, W.J., 2007. C-11-PIB PET imaging in Alzheimer disease and frontotemporal lobar degeneration. Neurology 68, 1205-1212.

224. Rabinovici, G.D., Jagust, W.J., 2009. Amyloid imaging in aging and dementia: testing the amyloid hypothesis in vivo. Behavioural Neurology 21, 117-128.

225. Raichle, M.E., MacLeod, A.M., Snyder, A.Z., Powers, W.J., Gusnard, D.A., Shulman, G.L., 2001. A default mode of brain function. Proceedings of the National Academy of Sciences of the United States of America 98, 676-682.

226. Ratnavalli, E., Brayne, C., Dawson, K., Hodges, J.R., 2002. The prevalence of frontotemporal dementia. Neurology 58, 1615-1621.

227. Raz, N., Gunning-Dixon, F., Head, D., Rodrigue, K.M., Williamson, A., Acker, J.D., 2004. Aging, sexual dimorphism, and hemispheric asymmetry of the cerebral cortex: replicability of regional differences in volume. Neurobiology of Aging 25, 377-396.

228. Renner, J.A., Burns, J.M., Hou, C.E., McKeel, D.W., Jr., Storandt, M., Morris, J.C., 2004. Progressive posterior cortical dysfunction: a clinicopathologic series. Neurology 63, 1175-1180.

229. Resnick, S.M., Goldszal, A.F., Davatzikos, C., Golski, S., Kraut, M.A., Metter, E.J., Bryan, R.N., Zonderman, A.B., 2000. One-year age changes in MRI brain volumes in older adults. Cerebral Cortex 10, 464-472.

230. Resnick, S.M., Pham, D.L., Kraut, M.A., Zonderman, A.B., Davatzikos, C., 2003. Longitudinal magnetic resonance imaging studies of older adults: a shrinking brain. Journal of Neuroscience 23, 3295-3301.

231. Richards, B.A., Chertkow, H., Singh, V., Robillard, A., Massoud, F., Evan, A.C., Kabani, N.J., 2009. Patterns of cortical thinning in Alzheimer's disease and frontotemporal dementia. Neurobiology of Aging 30, 1626-1636.

232. Ridgway, G.R., Henley, S.M., Rohrer, J.D., Scahill, R.I., Warren, J.D., Fox, N.C., 2008. Ten simple rules for reporting voxel-based morphometry studies. Neuroimage 40, 1429-1435.

233. Ridgway, G.R., Omar, R., Ourselin, S., Hill, D.L.G., Warren, J.D., Fox, N.C., 2009. Issues with threshold masking in voxel-based morphometry of atrophied brains. Neuroimage 44, 99-111.

234. Ridha, B.H., Anderson, V.M., Barnes, J., Boyes, R.G., Price, S.L., Rossor, M.N., Whitwell, J.L., Jenkins, L., Black, R.S., Grundman, M., Fox, N.C., 2008. Volumetric MRI and cognitive measures in Alzheimer disease: comparison of markers of progression. Journal of Neurology 255, 567-574.

235. Ridha, B.H., Barnes, J., Bartlett, J.W., Godbolt, A., Pepple, T., Rossor, M.N., Fox, N.C., 2006. Tracking atrophy progression in familial Alzheimer's disease: a serial MRI study. Lancet Neurology 5, 828-834.

236. Rocher, A.B., Chapon, F., Blaizot, X., Baron, J.C., Chavoix, C., 2003. Resting-state brain glucose utilization as measured by PET is directly related to regional synaptophysin levels: a study in baboons. Neuroimage 20, 1894-1898.

237. Rogalski, E., Johnson, N., Weintraub, S., Mesulam, M., 2008. Increased frequency of learning disability in patients with primary progressive aphasia and their first-degree relatives. Archives of Neurology 65, 244-248.

238. Rohrer, J.D., McNaught, E., Foster, J., Clegg, S.L., Barnes, J., Omar, R., Warrington, E.K., Rossor, M.N., Warren, J.D., Fox, N.C., 2008. Tracking progression in frontotemporal lobar degeneration: serial MRI in semantic dementia. Neurology 71, 1445-1451.

239. Rohrer, J.D., Warren, J.D., Modat, M., Ridgway, G.R., Douiri, A., Rossor, M.N., Ourselin, S., Fox, N.C., 2009. Patterns of cortical thinning in the language variants of frontotemporal lobar degeneration. Neurology 72, 1562-1569.

240. Rosen, H.J., Gorno-Tempini, M.L., Goldman, W.P., Perry, R.J., Schuff, N., Weiner, M., Feiwell, R., Kramer, J.H., Miller, B.L., 2002. Patterns of brain atrophy in frontotemporal dementia and semantic dementia. Neurology 58, 198-208.

241. Rosenbloom, M.H., Alkalay, A., Agarwal, N., Baker, S.L., Oneill, J.P., Janabi, M., Yen, I.V., Growdon, M., Jang, J., Madison, C., Miller, B.L., Jagust, W.J., Rabinovici, G.D., 2010. Distinct clinical and metabolic deficits in Alzheimer's disease and Posterior Cortical Atrophy are not related to amyloid distribution. Neurology 74, A301.

242. Ross, S.J., Graham, N., Stuart Green, L., Prins, M., Xuereb, J., Patterson, K., Hodges, J.R., 1996. Progressive biparietal atrophy: an atypical presentation of Alzheimer's disease. Journal of Neurology Neurosurgery and Psychiatry 61, 388-395.

243. Rossor, M., 1993. Alzheimer's disease. British Medical Journal 307, 779-782.

244. Rowe, C.C., Ng, S., Ackermann, U., Gong, S.J., Pike, K., Savage, G., Cowie, T.F., Dickinson, K.L., Maruff, P., Darby, D., Smith, C., Woodward, M., Merory, J., Tochon-Danguy, H., O'Keefe, G., Klunk, W.E., Mathis, C.A., Price, J.C., Masters, C.L., Villemagne, V.L., 2007. Imaging beta-amyloid burden in aging and dementia. Neurology 68, 1718-1725.

245. Rusinek, H., Endo, Y., De, S.S., Frid, D., Tsui, W.H., Segal, S., Convit, A., de Leon, M.J., 2004. Atrophy rate in medial temporal lobe during progression of Alzheimer disease. Neurology 63, 2354-2359.

246. Ryan, N.S., Rossor, M.N., 2010. Correlating familial Alzheimer's disease gene mutations with clinical phenotype. Biomarkers in Medicine 4, 99-112.

247. Salat, D.H., Buckner, R.L., Snyder, A.Z., Greve, D.N., Desikan, R.S.R., Busa, E., Morris, J.C., Dale, A.M., Fischl, B., 2004. Thinning of the cerebral cortex in aging. Cerebral Cortex 14, 721-730.

248. Salloway, S., Sperling, R., Gilman, S., Fox, N.C., Blennow, K., Raskind, M., Sabbagh, M., Honig, L.S., Doody, R., van Dyck, C.H., Mulnard, R., Barakos, J., Gregg, K.M., Liu, E., Lieberburg, I., Schenk, D., Black, R., Grundman, M., 2009. A phase 2 multiple ascending dose trial of bapineuzumab in mild to moderate Alzheimer disease. Neurology 73, 2061-2070.

249. Saunders, A.M., Strittmatter, W.J., Schmechel, D., George-Hyslop, P.H., Pericak-Vance, M.A., Joo, S.H., Rosi, B.L., Gusella, J.F., Crapper-MacLachlan, D.R., Alberts, M.J., 1993. Association of apolipoprotein E allele epsilon 4 with late-onset familial and sporadic Alzheimer's disease. Neurology 43, 1467-1472.

250. Savva, G.M., Wharton, S.B., Ince, P.G., Forster, G., Matthews, F.E., Brayne, C., 2009. Age, neuropathology, and dementia. New England Journal of Medicine 360, 2302-2309.

251. Scahill, R.I., Frost, C., Jenkins, R., Whitwell, J.L., Rossor, M.N., Fox, N.C., 2003. A longitudinal study of brain volume changes in normal aging using serial registered magnetic resonance imaging. Archives of Neurology 60, 989-994.

252. Scahill, R.I., Schott, J.M., Rossor, M.N., Fox, N.C., Stevens, J.M., 2002. Mapping the evolution of regional atrophy in Alzheimer's disease: Unbiased analysis of fluid-registered serial magnetic resonance images. Neurobiology of Aging 23, S420-S421.

253. Scheltens, P., Launer, L.J., Barkhof, F., Weinstein, H.C., Vangool, W.A., 1995. Visual assessment of medial temporal lobe atrophy on magnetic resonance imaging - Interobserver reliability. Journal of Neurology 242, 557-560.

254. Scheltens, P., Leys, D., Barkhof, F., Huglo, D., Weinstein, H.C., Vermersch, P., Kuiper, M., Steinling, M., Wolters, E.C., Valk, J., 1992. Atrophy of medial temporal lobes on MRI in probable Alzheimer's disease and normal aging - Diagnostic value and neuropsychological correlates. Journal of Neurology Neurosurgery and Psychiatry 55, 967-972.

255. Scheltens, P., Pasquier, F., Weerts, J.G., Barkhof, F., Leys, D., 1997. Qualitative assessment of cerebral atrophy on MRI: inter- and intra-observer reproducibility in dementia and normal aging. European Neurology 37, 95-99.

256. Schott, J.M., Fox, N.C., Frost, C., Scahill, R.I., Janssen, J.C., Chan, D., Jenkins, R., Rossor, M.N., 2003. Assessing the onset of structural change in familial Alzheimer's disease. Annals of Neurology 53, 181-188.

257. Schott, J.M., Price, S.L., Frost, C., Whitwell, J.L., Rossor, M.N., Fox, N.C., 2005. Measuring atrophy in Alzheimer disease - A serial MRI study over 6 and 12 months. Neurology 65, 119-124.

258. Schott, J.M., Ridha, B.H., Crutch, S.J., Healy, D.G., Uphill, J.B., Warrington, E.K., Rossor, M.N., Fox, N.C., 2006. Apolipoprotein E genotype modifies the phenotype of Alzheimer disease. Archives of Neurology 63, 155-156.

259. Seelaar, H., Klijnsma, K.Y., de Koning, I., van der Lugt, A., Chiu, W.Z., Azmani, A., Rozemuller, A.J.M., Swieten, J.C., 2010a. Frequency of ubiquitin and FUS-positive, TDP-43-negative frontotemporal lobar degeneration. Journal of Neurology 257, 747-753.

260. Seelaar, H., Rohrer, J.D., Pijnenburg, Y.A., Fox, N.C., van Swieten, J.C., 2010b. Clinical, genetic and pathological heterogeneity of frontotemporal dementia: a review. Journal of Neurology Neurosurgery and Psychiatry in press.

261. Seeley, W.W., Bauer, A.M., Miller, B.L., Gorno-Tempini, M.L., Kramer, J.H., Weiner, M., Rosen, H.J., 2005. The natural history of temporal variant frontotemporal dementia. Neurology 64, 1384-1390.

262. Seeley, W.W., Crawford, R.K., Zhou, J., Miller, B.L., Greicius, M.D., 2009. Neurodegenerative diseases target large-scale human brain networks. Neuron 62, 42-52.

263. Shallice, T., Evans, M.E., 1978. Involvement of frontal lobes in cognitive estimation. Cortex 14, 294-303.

264. Shiino, A., Watanabe, T., Kitagawa, T., Kotani, E., Takahashi, J., Morikawa, S., Akiguchi, I., 2008. Different atrophic patterns in early- and late-onset Alzheimer's disease and evaluation of clinical utility of a method of regional z-score analysis using voxel-based morphometry. Dementia and Geriatric Cognitive Disorders 26, 175-186.

265. Shin, J., Lee, S.Y., Kim, S.J., Kim, S.H., Cho, S.J., Kim, Y.B., 2010. Voxel-based analysis of Alzheimer's disease PET imaging using a triplet of radiotracers: PIB, FDDNP, and FDG. Neuroimage 52, 488-496.

266. Silbert, L.C., Quinn, J.F., Moore, M.M., Corbridge, E., Ball, M.J., Murdoch, G., Sexton, G., Kaye, J.A., 2003. Changes in premorbid brain volume predict Alzheimer's disease pathology. Neurology 61, 487-492.

267. Siri, A., Benaglio, I., Frigerio, A., Binetti, G., Cappa, S.F., 2001. A brief neuropsychological assessment for the differential diagnosis between frontotemporal dementia and Alzheimer's disease. European Journal of Neurology 8, 125-132.

268. Small, G.W., Kepe, V., Ercoli, L.M., Siddarth, P., Bookheimer, S.Y., Miller, K.J., Lavretsky, H., Burggren, A.C., Cole, G.M., Vinters, H.V., Thompson, P.M., Huang, S.C., Satyamurthy, N., Phelps, M.E., Barrio, J.R., 2006. PET of brain amyloid and tau in mild cognitive impairment. New England Journal of Medicine 355, 2652-2663.

269. Smith, S.M., De Stefano, N., Jenkinson, M., Matthews, P.M., 2001. Normalized accurate measurement of longitudinal brain change. Journal of Computer Assisted Tomography 25, 466-475.

270. Smith, S.M., Jenkinson, M., Woolrich, M.W., Beckmann, C.F., Behrens, T.E.J., Johansen-Berg, H., Bannister, P.R., De Luca, M., Drobnjak, I., Flitney, D.E., Niazy, R.K., Saunders, J., Vickers, J., Zhang, Y.Y., De Stefano, N., Brady, J.M., Matthews, P.M., 2004. Advances in functional and structural MR image analysis and implementation as FSL. Neuroimage 23, S208-S219.

271. Smith, S.M., Zhang, Y., Jenkinson, M., Chen, J., Matthews, P.M., Federico, A., De, S.N., 2002. Accurate, robust, and automated longitudinal and cross-sectional brain change analysis. Neuroimage 17, 479-489.

272. Snowden, J., Neary, D., Mann, D., 2007a. Frontotemporal lobar degeneration: clinical and pathological relationships. Acta Neuropathologica 114, 31-38.

273. Snowden, J.S., Stopford, C.L., Julien, C.L., Thompson, J.C., Davidson, Y., Gibbons, L., Pritchard, A., Lendon, C.L., Richardson, A.M., Varma, A., Neary, D., Mann, D.M.A., 2007b. Cognitive phenotypes in Alzheimer's disease and genetic risk. Cortex 43, 835-845.

274. Sowell, E.R., Peterson, B.S., Thompson, P.M., Welcome, S.E., Henkenius, A.L., Toga, A.W., 2003. Mapping cortical change across the human life span. Nature Neuroscience 6, 309-315.

275. Stopford, C.L., Snowden, J.S., Thompson, J.C., Neary, D., 2007. Distinct memory profiles in Alzheimer's disease. Cortex 43, 846-857.

276. Tae, W.S., Kim, S.S., Lee, K.U., Nam, E.C., Kim, K.W., 2008. Validation of hippocampal volumes measured using a manual method and two automated methods (FreeSurfer and IBASPM) in chronic major depressive disorder. Neuroradiology 50, 569-581.

277. Takahashi, R., Ishii, K., Miyamoto, N., Yoshikawa, T., Shimada, K., Ohkawa, S., Kakigi, T., Yokoyama, K., 2010. Measurement of gray and white matter atrophy in dementia with Lewy bodies using diffeomorphic anatomic registration through exponentiated lie algebra: A comparison with conventional voxel-based morphometry. AJNR Am.J.Neuroradiol. 31, 1873-1878.

278. Talairach, J., Tournoux, P., 1988. Co-planar stereotaxic atlas of the human brain: 3-dimensional proportional system - an approach to cerebral imaging. Thieme Medical Publishers, New York.

279. Tang-Wai, D., Mapstone, M., 2006. What are we seeing? Is posterior cortical atrophy just Alzheimer disease? Neurology 66, 300-301.

280. Tang-Wai, D.F., Graff-Radford, N.R., Boeve, B.F., Dickson, D.W., Parisi, J.E., Crook, R., Caselli, R.J., Knopman, D.S., Petersen, R.C., 2004. Clinical, genetic, and neuropathologic characteristics of posterior cortical atrophy. Neurology 63, 1168-1174.

281. Tang-Wai, D.F., Josephs, K.A., Boeve, B.F., Dickson, D.W., Parisi, J.E., Petersen, R.C., 2003a. Pathologically confirmed corticobasal degeneration presenting with visuospatial dysfunction. Neurology 61, 1134-1135.

282. Tang-Wai, D.F., Josephs, K.A., Boeve, B.F., Petersen, R.C., Parisi, J.E., Dickson, D.W., 2003b. Coexistent Lewy body disease in a case of "visual variant of Alzheimer's disease". Journal of Neurology Neurosurgery and Psychiatry 74, 389.

283. Taylor, K.I., Probst, A., Miserez, A.R., Monsch, A.U., Tolnay, M., 2008. Clinical course of neuropathologically confirmed frontal-variant Alzheimer's disease. Nature Clinical Practice Neurology 4, 226-232.

284. Teipel, S.J., Pruessner, J.C., Faltraco, F., Born, C., Rocha-Unold, M., Evans, A., Moller, H.J., Hampel, H., 2006. Comprehensive dissection of the medial temporal lobe in AD: measurement of hippocampus, amygdala, entorhinal, perirhinal and parahippocampal cortices using MRI. Journal of Neurology 253, 794-800.

285. Tenovuo, O., Kemppainen, N., Aalto, S., Nagren, K., Rinne, J.O., 2008. Posterior Cortical Atrophy: A rare form of dementia with in vivo evidence of amyloid-beta accumulation. Journal of Alzheimers Disease 15, 351-355.

286. Thompson, P.M., Mega, M.S., Woods, R.P., Zoumalan, C.I., Lindshield, C.J., Blanton, R.E., Moussai, J., Holmes, C.J., Cummings, J.L., Toga, A.W., 2001. Cortical change in Alzheimer's disease detected with a disease-specific population-based brain atlas. Cerebral Cortex 11, 1-16.

287. Thompson, S.A., Patterson, K., Hodges, J.R., 2003. Left/right asymmetry of atrophy in semantic dementia - Behavioral-cognitive implications. Neurology 61, 1196-1203.

288. Tzourio-Mazoyer, N., Landeau, B., Papathanassiou, D., Crivello, F., Etard, O., Delcroix, N., Mazoyer, B., Joliot, M., 2002. Automated anatomical labeling of activations in SPM using a macroscopic anatomical parcellation of the MNI MRI single-subject brain. Neuroimage 15, 273-289.

289. Ungerleider, L.G., Mishkin, M., 1982. Two cortical visual systems. MIT Press, Cambridge MA.

290. Urwin, H., Josephs, K.A., Rohrer, J.D., Mackenzie, I.R., Neumann, M., Authier, A., Seelaar, H., van Swieten, J.C., Brown, J.M., Johannsen, P., Nielsen, J.E., Holm, I.E., Dickson, D.W., Rademakers, R., Graff-Radford, N.R., Parisi, J.E., Petersen, R.C., Hatanpaa, K.J., White, C.L., Weiner, M.F., Geser, F., Van Deerlin, V.M., Trojanowski, J.Q., Miller, B.L., Seeley, W.W., van der Zee, J., Kumar-Singh, S., Engelborghs, S., De Deyn, P.P., Van Broeckhoven, C., Bigio, E.H., Deng, H.X., Halliday, G.M., Kril, J.J., Munoz, D.G., Mann, D.M., Pickering-Brown, S.M., Doodeman, V., Adamson, G., Ghazi-Noori, S., Fisher, E.M.C., Holton, J.L., Revesz, T., Rossor, M.N., Collinge, J., Mead, S., Isaacs, A.M., 2010. FUS pathology defines the majority of tau- and TDP-43-negative frontotemporal lobar degeneration. Acta Neuropathologica 120, 33-41.

291. van der Flier, W.M., Pijnenburg, Y.A.L., Fox, N.C., Scheltens, P., 2010. Early-onset versus late-onset Alzheimer's disease: the case of the missing APOE epsilon4 allele. Lancet Neurology in press.

292. van Swieten, J., Spillantini, M.G., 2007. Hereditary frontotemporal dementia caused by Tau gene mutations. Brain Pathology 17, 63-73.

293. Vance, C., Rogelj, B., Hortobagyi, T., De Vos, K.J., Nishimura, A.L., Sreedharan, J., Hu, X., Smith, B., Ruddy, D., Wright, P., Ganesalingam, J., Williams, K.L., Tripathi, V., Al-Saraj, S., Al-Chalabi, A., Leigh, P.N., Blair, I.P., Nicholson, G., de Belleroche, J., Gallo, J.M., Miller, C.C., Shaw, C.E., 2009. Mutations in FUS, an RNA processing protein, cause familial amyotrophic lateral sclerosis type 6. Science 323, 1208-1211.

294. Vapnik, V., 1995. The nature of statistical learning theory. Springer, New York.

295. Vapnik, V., 1998. Statistical learning theory. John Wiley and Sons, New York.

296. Vemuri, P., Whitwell, J., Kantarci, K., Josephs, K., Parisi, J., Knopman, D., Boeve, B., Petersen, R., Dickson, D., Jack, C., 2008. Antemortem MRI based structural abnormality index (STAND)-scores correlate with postmortem Braak stages. Neurology 70, A447.

297. Victoroff, J., Ross, G.W., Benson, D.F., Verity, M.A., Vinters, H.V., 1994. Posterior cortical atrophy - Neuropathologic correlations. Archives of Neurology 51, 269-274.

298. Villain, N., Desgranges, B., Viader, F., De La Sayette, V., Mezenge, F., Landeau, B., Baron, J.C., Eustache, F., Chetelat, G., 2008. Relationships between hippocampal atrophy, white matter disruption, and gray matter hypometabolism in Alzheimer's disease. Journal of Neuroscience 28, 6174-6181.

299. Wahlund, L.O., Barkhof, F., Fazekas, F., Bronge, L., Augustin, M., Sjogren, M., Wallin, A., Ader, H., Leys, D., Pantoni, L., Pasquier, F., Erkinjuntti, T., Scheltens, P., 2001. A new rating scale for age-related white matter changes applicable to MRI and CT. Stroke 32, 1318-1322.

300. Wahlund, L.O., Julin, P., Johansson, S.E., Scheltens, P., 2000. Visual rating and volumetry of the medial temporal lobe on magnetic resonance imaging in dementia: a comparative study. Journal of Neurology Neurosurgery and Psychiatry 69, 630-635.

301. Wakai, M., Honda, H., Takahashi, A., Kato, T., Ito, K., Hamanaka, T., 1994. Unusual findings on PET study of a patient with posterior cortical atrophy. Acta neurologica Scandinavica 89, 458-461.

302. Waldemar, G., Dubois, B., Emre, M., Georges, J., McKeith, I.G., Rossor, M., Scheltens, P., Tariska, P., Winblad, B., 2007. Recommendations for the diagnosis and management of Alzheimer's disease and other disorders associated with dementia: EFNS guideline. European Journal of Neurology 14, e1-26.

303. Wandell, B.A., Dumoulin, S.O., Brewer, A.A., 2007. Visual field maps in human cortex. Neuron 56, 366-383.

304. Wang, D., Chalk, J.B., Rose, S.E., de, Z.G., Cowin, G., Galloway, G.J., Barnes, D., Spooner, D., Doddrell, D.M., Semple, J., 2002. MR image-based measurement of rates of change in volumes of brain structures. Part II: application to a study of Alzheimer's disease and normal aging. Magnetic Resonance Imaging 20, 41-48.

305. Warrington, E.K., 1984. Recognition memory test. NFER-Nelson, Windsor, UK.

306. Warrington, E.K., 1996. The Camden Memory Tests. Psychology Press (Erlbaum, Taylor & Francis), Hove, UK.

307. Warrington, E.K., 1997. The graded naming test: A restandardisation. Neuropsychological Rehabilitation 7, 143-146.

308. Warrington, E.K., James, M., 1988. Visual apperceptive agnosia - A clinico-anatomical study of 3 cases. Cortex 24, 13-32.

309. Warrington, E.K., James, M., 1991. The Visual Object and Space Battery Perception. Thames Valley Company, Bury St Edmunds, UK.

310. Warrington, E.K., McKenna, P., Orpwood, L., 1998. Single word comprehension: A concrete and abstract word synonym test. (vol 8, pg 143, 1998). Neuropsychological Rehabilitation 8, 472.

311. Watson, C., Andermann, F., Gloor, P., Jones-Gotman, M., Peters, T., Evans, A., Olivier, A., Melanson, D., Leroux, G., 1992. Anatomic basis of amygdaloid and hippocampal volume measurement by magnetic resonance imaging. Neurology 42, 1743-1750.

312. Wattjes, M.P., Henneman, W.J.P., van der Flier, W.M., de Vries, O., Traber, F., Geurts, J.J.G., Scheltens, P., Vrenken, H., Barkhof, F., 2009. Diagnostic imaging of patients in a memory clinic: Comparison of MR imaging and 64-detector row CT. Radiology 253, 174-183.

313. Wechsler, D., 1987. Manual for the Wechsler Memory Scale-Revised. The Psychological Corporation, San Antonio, TX.

314. Whitwell, J.L., Crum, W.R., Watt, H.C., Fox, N.C., 2001. Normalization of cerebral volumes by use of intracranial volume: Implications for longitudinal quantitative MR imaging. American Journal of Neuroradiology 22, 1483-1489.

315. Whitwell, J.L., Jack, C.R., Jr., 2005. Comparisons between Alzheimer disease, frontotemporal lobar degeneration, and normal aging with brain mapping. Topics in Magnetic Resonance Imaging 16, 409-425.

316. Whitwell, J.L., Jack, C.R., Kantarci, K., Weigand, S.D., Boeve, B.F., Knopman, D.S., Drubach, D.A., Tang-Wai, D.F., Petersen, R.C., Josephs, K.A., 2007a. Imaging correlates of posterior cortical atrophy. Neurobiology of Aging 28, 1051-1061.

317. Whitwell, J.L., Jack, C.R., Jr., Pankratz, V.S., Parisi, J.E., Knopman, D.S., Boeve, B.F., Petersen, R.C., Dickson, D.W., Josephs, K.A., 2008a. Rates of brain atrophy over time in autopsy-proven frontotemporal dementia and Alzheimer disease. Neuroimage 39, 1034-1040.

318. Whitwell, J.L., Jack, C.R., Jr., Parisi, J.E., Knopman, D.S., Boeve, B.F., Petersen, R.C., Ferman, T.J., Dickson, D.W., Josephs, K.A., 2007b. Rates of cerebral atrophy differ in different degenerative pathologies. Brain 130, 1148-1158.

319. Whitwell, J.L., Josephs, K.A., Murray, M.E., Kantarci, K., Przybelski, S.A., Weigand, S.D., Vemuri, P., Senjem, M.L., Parisi, J.E., Knopman, D.S., Boeve, B.F., Petersen, R.C., Dickson, D.W., Jack, C.R., Jr., 2008b. MRI correlates of neurofibrillary tangle pathology at autopsy: a voxel-based morphometry study. Neurology 71, 743-749.

320. Whitwell, J.L., Josephs, K.A., Rossor, M.N., Stevens, J.M., Revesz, T., Holton, J.L., Al Sarraj, S., Godbolt, A.K., Fox, N.C., Warren, J.D., 2005a. Magnetic resonance imaging signatures of tissue pathology in frontotemporal dementia. Archives of Neurology 62, 1402-1408.

321. Whitwell, J.L., Sampson, E.L., Watt, H.C., Harvey, R.J., Rossor, M.N., Fox, N.C., 2005b. A volumetric magnetic resonance imaging study of the amygdala in frontotemporal lobar degeneration and Alzheimer's disease. Dementia and Geriatric Cognitive Disorders 20, 238-244.

322. Willison, J.R., Warrington, E.K., 1992. Cognitive retardation in a patient with preservation of psychomotor speed. Behavioural Neurology 5, 113-116.

323. Wilson, S.M., Ogar, J.M., Laluz, V., Growdon, M., Jang, J., Glenn, S., Miller, B.L., Weiner, M.W., Gorno-Tempini, M.L., 2009. Automated MRI-based classification of primary progressive aphasia variants. Neuroimage 47, 1558-1567.

324. Woods, R.P., Grafton, S.T., Holmes, C.J., Cherry, S.R., Mazziotta, J.C., 1998. Automated image registration: I. General methods and intrasubject, intramodality validation. Journal of Computer Assisted Tomography 22, 139-152.

325. Xu, Y., Jack, C.R., O'Brien, P.C., Kokmen, E., Smith, G.E., Ivnik, R.J., Boeve, B.F., Tangalos, R.G., Petersen, R.C., 2000. Usefulness of MRI measures of entorhinal cortex versus hippocampus in AD. Neurology 54, 1760-1767.

326. Yoshida, T., Shiga, K., Yoshikawa, K., Yamada, K., Nakagawa, M., 2004. White matter loss in the splenium of the corpus callosum in a case of posterior cortical atrophy: A diffusion tensor imaging study. European Neurology 52, 77-81.

327. Zhang, H.Y., Wang, S.J., Liu, B., Ma, Z.L., Yang, M., Zhang, Z.J., Teng, G.J., 2010. Resting brain connectivity: changes during the progress of Alzheimer disease. Radiology 256, 598-606.